

# Late Palaeozoic lamprophyres and associated mafic subvolcanic rocks of the Sudetes (SW Poland): petrology, geochemistry and petrogenesis

Marek Awdankiewicz

*Wrocław University, Institute of Geological Sciences, Department of Mineralogy and Petrology, ul. Cybulskiego 30, 50-205 Wrocław, Poland, email: marek.awdankiewicz@ing.uni.wroc.pl*

**Key words:** lamprophyres, Sudetes, mineral chemistry, trace elements, Sr-Nd isotopes, petrogenesis.

**Abstract** Lamprophyric magmatism in the Sudetes, in the eastern part of the European Variscides, occurred during a period of post-collisional extension in the Carboniferous. The lamprophyres (minettes, vogesites, spessartites, kersantites) and associated mafic rocks (monzonites, micromonzodiorites) were emplaced as dyke swarms and as scattered veins that cut the crystalline basement and, locally, the overlying molasse deposits. The dyke swarms are adjacent to major regional dislocations, represent distinctive magmatic centres that are related to separate magmatic systems and each are characterized by specific parental melts that have undergone individualised shallow-level differentiation processes. The two largest dyke swarms are associated with the Karkonosze and Kłodzko–Złoty Stok granitoid massifs: these show the widest geochemical and petrographic variation, due to more advanced differentiation in long-lived magmatic systems. In contrast, a small dyke swarm emplaced in the SW part of the Orlica–Śnieżnik Dome, unrelated to granites, is strongly dominated by minettes only. Geochemical characteristics of the mafic rocks studied herein vary from (ultra)potassic in the minettes to calc-alkaline in the micromonzodiorites and from primitive ( $Mg\# = 80\text{--}60$  in many lamprophyres) to evolved ( $Mg\#$  down to 30 in some micromonzodiorites). Some richterite minettes show Nb-enriched trace element patterns, but negative Nb anomalies are more typical. Richterite minettes possess  $\epsilon Nd_{300}$  and  $^{87}Sr/^{86}Sr_{300}$  values that range from +1.9 to –8.3, and from 0.7037 to 0.715, respectively. The other rocks in this study show negatively correlated Nd and Sr isotopic ratios, between these extremes. The geochemical data suggest three types of mantle source for the lamprophyres and associated mafic rocks: (1) An asthenospheric, depleted and later re-enriched source; (2) A lithospheric source contaminated by subducted crustal rocks; (3) A lithospheric source metasomatized by subduction-related fluids. The richterite minette magmas originated from low degrees of partial melting, under high  $H_2O/CO_2$  conditions, of garnet-phlogopite-peridotites. The Nb-enriched and Nb-depleted minettes are derived from sources (1) and (2), respectively. Kersantite magmas originated from source (3). The factors of source mixing, variable depths and degrees of melting, and aggregation of melts all influenced the compositions of other primitive minette and vogesite magmas. The other rocks studied (spessartites, monzonites, micromonzodiorites) are variably differentiated. Zoning and other disequilibrium textures in phlogopite, biotite, amphibole and clinopyroxene phenocrysts, together with the presence of xenocrysts, xenoliths and enclaves (cognate, restitic, migmatitic) constrain several processes that were involved in the shallow-level evolution of magmas: mixing, fractional crystallization, assimilation of crustal rocks. However, post-magmatic replacement of the igneous phases by albite, chlorite, epidotes, actinolite, blue amphiboles, titanite, carbonates, prehnite, pumpellyite and grossularite-andradite partly obscures the magmatic assemblages and textures. There are four more general results of this study. First, there is evidence for a strong heterogeneity of the upper mantle and of the presence of subduction-modified mantle beneath the Sudetes during the Late Palaeozoic. Second, the lamprophyre magmas originated and evolved in spatially and petrologically distinct, vertically extensive magmatic systems that spanned the asthenospheric and lithospheric mantle and the lower/middle crust. Third, a broad spectrum of source-related and shallow-level magmatic processes gave rise to the emplacement of primitive, mantle-derived magmas and of variably evolved magmas. Fourth, close links existed between late Variscan tectonics, the location of lamprophyric magmatism, and the shallow-level emplacement processes of mafic dykes.

## INTRODUCTION

## SCOPE AND AIMS OF THIS STUDY

Lamprophyres are mafic hypabyssal (subvolcanic) rocks that are commonly found as dykes of various ages, different origins and in a wide variety of tectonic settings. The most common, foid-free lamprophyres are the minettes, kersantites, vogesites and spessartites, which are collectively known as the calc-alkaline lamprophyres. These rock types are widely distributed within the Palaeozoic orogenic belts of Europe – the Caledonian Belt and the Variscan Belt. The Variscan belt hosts many of the type-localities (e.g., Kersanton and the Vosges Mountains in France, Spessart in Germany) and it is here that lamprophyres were first distinguished and described (Gümbel, 1874; Rosenbush, 1897; *vide* Rock, 1991). Lamprophyres have continued to attract the attention of exploration geologists as well as igneous petrologists from the first classic petrographic studies of the 19<sup>th</sup> century. The significance of lamprophyres for both applied and academic research was highlighted in the comprehensive monograph by N. M. S. Rock (1991). Lamprophyre magmas, enriched in volatile components and several trace elements, are the source of, and participate in the formation of, precious metal deposits, including gold. Lamprophyres are also amongst the very few igneous rock types to carry macro-diamonds (Rock, 1991; Kramer & Seifert, 1993; Groves & Edgar, 1994; Mitchell, 1997; Müller & Groves, 2000; De Stefano *et al.*, 2006). Many lamprophyres represent primitive, mantle-derived melts which provide information on the lithosphere, deep mantle dynamics, and the metasomatic and contamination processes that affect the upper mantle. Primitive lamprophyre melts can also represent parental magmas and mafic end-members that have undergone shallow-level differentiation and mixing processes, including the formation of voluminous granitoid magmas

(e.g., Didier & Barbarin, 1991; Galan *et al.*, 1996; Bea *et al.*, 1999; Słaby & Götze, 2004; Müller *et al.*, 2005; Słaby *et al.*, 2006, 2007; Słaby & Martin, 2008). The specific, and often puzzling, petrographic, mineralogical and geochemical characteristics of lamprophyres make them both intriguing and difficult research objects. To this day, lamprophyres still prove controversial with respect to their systematic position, origin and petrogenetic significance (Rock, 1991; Groves & Edgar, 1994; Le Maitre *et al.*, 2002).

In the Sudetes mountain range, located in southwestern Poland in the eastern part of the Variscan Belt of Europe (Fig. 1), calc-alkaline lamprophyres are widespread (Fig. 2). Detailed geological maps (“Szczegółowa mapa geologiczna Sudetów 1:25 000”; several sheets issued by the Polish Geological Institute between 1954 and 1994) reveal that there may be ~150 lamprophyre veins here. There are also numerous small “melanocratic veins” not marked in the geological maps, many of which may represent lamprophyres (Dumicz, 1964; Wojciechowska, 1975; Wierchołowski, 1977). Based on the geological position, and by analogy with other parts of the European Variscides, the emplacement of the lamprophyres and associated mafic dykes in the Sudetes has been generally linked with Carboniferous–Permian, late- to post-orogenic magmatism (e.g., Wierchołowski, 1977; Muszyński, 1987).

The Sudetic lamprophyres belong to the calc-alkaline group and, judging from the published maps and papers, all the main members of this group are present. A petrographic study of lamprophyres and other mafic and felsic dykes within the Karkonosze intrusion was carried out by Berg (1923). Later research by Borkowska (1966), despite focusing on the granites, also described some mafic dykes and showed that a revision of the early classification schemes was necessary. More recently, the petrography, mineralogy and geochemistry of lamprophyre occurrences in the Góry Sowie and Złoty Stok areas were studied (Wierchołowski, 1977, 1979, 2000, 2003; Muszyński 1987), and Machowiak *et al.* (2004) characterized the kersantites that are associated with the Żelaźniak subvolcanic complex in the Kaczawa Mountains. Selected, preliminary results of geochemical, petrographic and mineralogical studies have also been published for lamprophyre and associated dykes in the Karkonosze, Góry Sowie, Orlica–Śnieżnik and Kłodzko–Złoty Stok Massifs (Awdankiewicz *et al.*, 2004, 2005 a, b; Awdankiewicz, 2007; Awdankiewicz & Awdankiewicz, 2007; Awdankiewicz *et al.*, 2007a; Mazur *et al.*, 2007). These studies together show that the Sudetes represent one of larger late Palaeozoic lamprophyre sub-provinces within the Variscan Belt of Europe, a sub-province characterized by substantial petrographic and mineralogical diversity in its lamprophyres and associated mafic rocks. Nevertheless, a comprehensive, regional petrological study of these rocks has not, to date, been undertaken.

The general problem attacked in this study is the petrogenesis of the Late Palaeozoic lamprophyres and associated mafic subvolcanic rocks in the Sudetes. More specifi-

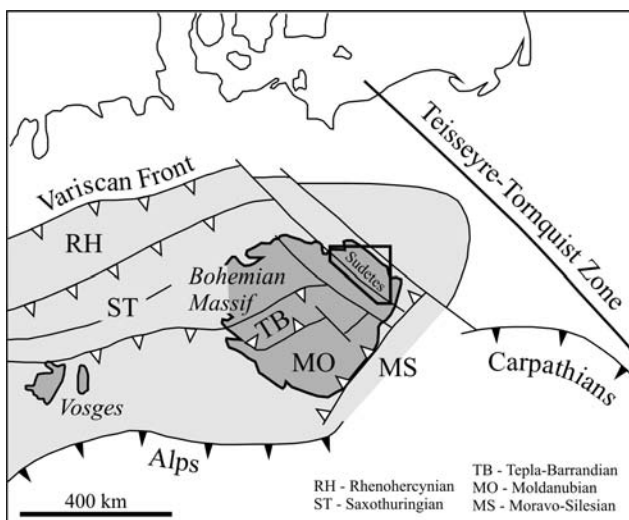
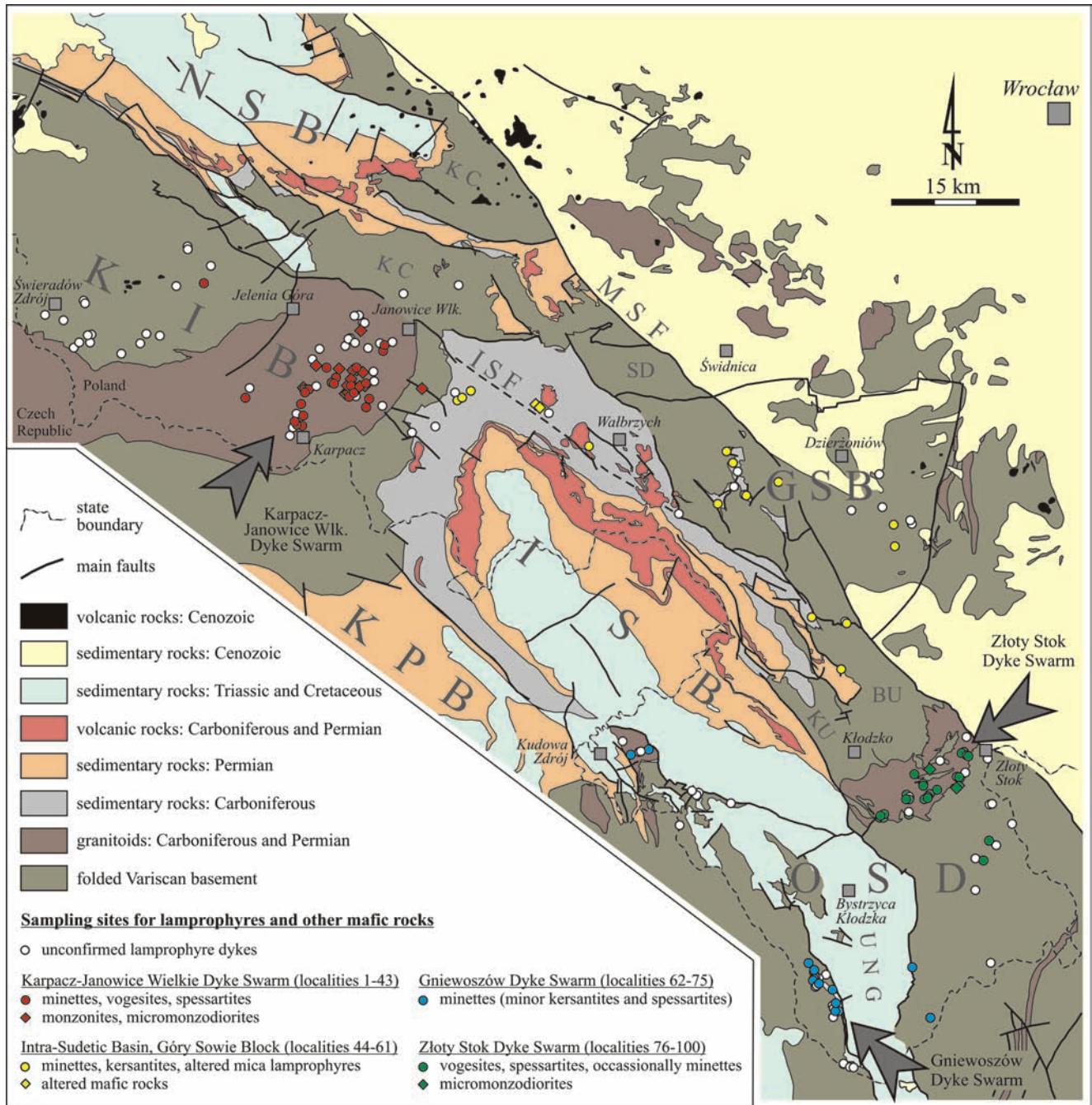


Fig. 1. Location of the Sudetes and the study area (black frame) in the context of the Variscan Belt of Europe (after Mazur *et al.*, 2006).



**Fig. 2.** Geological sketch map of the study area (Polish part modified from Bossowski *et al.*, 1981; Sawicki, 1988; and Milewicz *et al.*, 1989. Czech part modified after Kodym *et al.*, 1967). The map incorporates the distribution of lamprophyre and other mafic dykes (after Szczegółowa Mapa Geologiczna Sudetów 1: 25,000; Badura & Bossowski, 1987; Bossowski & Czernski, 1985; Bossowski *et al.*, 1994; Cwojdziański, 1976, 1979a, b, 1985; Cwojdziański & Kozdrój, 1995; Cymerman, 1992, 1995; Cymerman & Walczak-Augustyniak, 1988; Frąckiewicz & Teisseyre, 1976; Gawroński, 1959, 1961; Gierwielaniec, 1971; Gierwielaniec & Radwański, 1958; Kasza, 1967; Kozdrój, 1994a, b; Mastalerz *et al.*, 1995; Oberc *et al.*, 1994; Sawicki, 1959, 1968; Szałamacha J., 1960, 1972, 1973; Szałamacha & Szałamacha, 1971, 1984, 1991; Szałamacha & Tucholska, 1960; Szałamacha M., 1960; Teisseyre, 1976. Teisseyre & Sawicki, 1958; Trepka & Gawroński, 1961; Walczak-Augustyniak & Wroński, 1982; Wójcik, 1958). The full list of localities studied is given in Appendix 1. Geological units and faults: BU (Bardo Unit), GSB (Góry Sowie Block), ISB (Intra-Sudetic Basin), ISF (Intra-Sudetic Fault), KC (Kaczawa Complex), KIB (Karkonosze-Izera Block), KP B (Krkonoše Piedmont Basin), KU (Kłodzko Unit), MSF (Marginal Sudetic Fault), NSB (North-Sudetic Basin), OSD (Orlica-Śnieżnik Dome), SD (Świebodzice Depression), UNG (Upper Nysa Graben).

cally, attention is given to the distribution and geological setting of the lamprophyres and their associated mafic rocks; to the petrographic, mineralogical and geochemical characteristics of these rocks; to the origin of lamprophyre magmas, including the characterization of their mantle sources and shallow-level differentiation processes, such as fractional crystallization, hybridisation and magma mixing, crustal contamination; and to the genetic relationships between the various lamprophyres and the associated mafic subvolcanic rocks.

Herein, a petrogenetic model of lamprophyric magmatism in the Sudetes is given, and some general implications for the formation and differentiation of lamprophyre magmas are briefly discussed.

## METHODS USED

This paper provides a synthesis of the main results obtained from 2002 to 2007 under the research project "Petrologia i geochemia lamprofirów regionu sudeckiego", which was supported by the Polish Committee of Scientific Research (KBN grant 3 P04D 0255 22; Awdankiewicz *et al.*, 2007b). The field work was carried out in the Polish part of the Sudetes and covered the area from Świeradów Zdrój in the northwest, to Złoty Stok and Międzygórze in the southeast, together with selected areas of the Fore-Sudetic Block. The field work included the location, description and sampling of all lamprophyre outcrops marked on the "Detailed geological maps of the Sudetes 1:25 000" (Polish Geological Institute, 1954–1994; references are given in the caption to Fig. 2). In addition, selected outcrops of associated hypabyssal mafic rocks were also sampled. The general term "mafic rocks" is used in this paper for rocks rich in mafic minerals; "felsic rocks", such as various "porphyries", microgranites, aplites, and so on, were not studied. In total, 178 rock samples, including 136 lamprophyre samples, were collected from 100 localities. The location and basic topographic characterization of sampling sites, together with the list of samples used for laboratory studies, are given in Appendix 1.

Thin sections were prepared from all samples except for a few, strongly weathered specimens. Samples characterized by small-scale petrographic variation or containing xenoliths or enclaves were studied in 2–3 thin sections. Over 200 thin sections in total were investigated; modal compositions were determined by point counting in 20 of the most representative, freshest specimens (Table 1). Based on the petrographic characteristics, representative specimens were selected for more detailed mineralogical and geochemical studies.

The chemical composition of minerals was determined using CAMECA SX50 microprobe at Ruhr-Universität Bochum, Germany, and CAMECA SX100 microprobes at Université Blaise Pascal, Clermont-Ferrand, France, and at Warsaw University, Poland. The wavelength dispersive spectrometry (WDS) technique was used and most analyses were carried out under the following conditions: counting time 20 s; beam current 15 nA; accelerating voltage 15 kV; beam size 2  $\mu\text{m}$ ; ZAF (atomic number, absorp-

tion, fluorescence) correction. Albite and carbonates were analyzed using a defocused beam (5–7  $\mu\text{m}$ ). Supplementary analyses were also carried out using the Cambridge Microscan 5 microprobe at the Institute of Geological Sciences, Wrocław University, where the typical analytical conditions were as follows: counting time 20 s; beam current 50 nA; accelerating voltage 15 kV. In total, 1,969 quantitative mineral analyses were obtained from 36 thin sections. Selected analyses of minerals, their crystallochemical formulae and the recalculation methods that were applied, are given in Appendices 2 to 11. Back scattered electron (BSE) imaging was an integral part of the microprobe studies and several hundred BSE images were taken. Energy dispersive spectrometry (EDS) aided in the identification of groundmass minerals and in discerning micrometer-scale complex intergrowths.

Eighty-seven samples of lamprophyre and other mafic rocks were selected for whole-rock chemical analyses. These samples were collected from blocks a few kg in weight, from which the weathered parts were removed by hammer. The specimens were then cut with a diamond saw and the freshest pieces, ~0.3–0.5 kg from each sample, were selected for detailed analysis. Fragments containing xenoliths, veins or amygdalae were avoided. After washing in tap water and drying, the samples were crushed down to a <5 mm size fraction in a tungsten carbide jaw crusher. A subsample of this, ~100g, was pulverized in a tungsten carbide ring mill for 3–4 min. The ring mill was cleaned with quartz for ~2 min. after each sample and, in many cases, the mill was double cleaned to remove all contamination. Pulverization and milling were carried out at the Institute of Geological Sciences, Wrocław University.

The whole-rock major and trace element chemistry was determined using the inductively coupled plasma emission spectrometry (ICP-ES) and inductively coupled plasma mass spectrometry (ICP-MS) methods at ACME laboratories, Vancouver, Canada. The detection limits were as follows: 0.04% for  $\text{SiO}_2$ ,  $\text{Fe}_2\text{O}_3$ ,  $\text{K}_2\text{O}$ ; 0.03% for  $\text{Al}_2\text{O}_3$ ; 0.1% for other major elements; 0.5 ppm for Zr, Hf, Ba, Rb, Sr, Nb, La, Ce; 0.4 ppm for Nd; 0.05 ppm for Eu, Gd, Dy, Ho, Er, Tm, Yb; 0.01 ppm for Tb and Lu; and 0.1 ppm for the other trace elements. Chromium was determined as  $\text{Cr}_2\text{O}_3$  at the detection limit of 0.001%. The Góry Sowie kersantites and some altered mafic rocks of the Intra-Sudetic Basin were analyzed at Activation Laboratories Ltd (Actlabs), Canada, using the INAA (instrumental neutron activation analysis) and ICP-MS methods. The detection limits were similar to, or lower than, those for the methods at ACME laboratories. In general, the precision and accuracy are  $\pm 5\%$ ,  $\pm 10\%$  and  $\pm 100\%$  at the abundance levels of 100x, 10x and 1x the detection limit, respectively. Further details on the specific analytical procedures may be found on the web pages of the two laboratories in question. The chemical analyses of representative samples are given in Appendix 12.

The Sr and Nd isotopic ratios were determined for 16 representative samples of the mafic rocks. The analyses were carried out at the Activation Laboratories Ltd in Canada. Conventional cation-exchange techniques were used to separate Rb and Sr; the analyses were performed

on a Triton multi-collector mass-spectrometer in static mode; and the weighted average of fifteen SRM-987 Sr-standard runs yielded  $0.710262 \pm 11$  (2sigma) for  $^{87}\text{Sr}/^{86}\text{Sr}$ . Extraction chromatography on teflon powder covered by HDEHP [Bis-(2-Ethylhexyl) Phosphoric Acid] was used to separate Sm and Nd; the analysis was also performed on a Triton multi-collector mass-spectrometer in static mode.

The analyzed  $^{143}\text{Nd}/^{144}\text{Nd}$  ratios are relative to 0.511860 for the La Jolla standard. Results are given in Table 3.

The mafic rocks were dated using the Ar-Ar and sensitive high mass-resolution ion microprobe (SHRIMP) methods. However, these data will be published elsewhere and only some preliminary results are reported here.

## OUTLINE PETROLOGY OF THE CALC-ALKALINE LAMPROPHYRES

Within the broad spectrum of igneous rocks, lamprophyres are currently distinguished as one of nine "special" groups due to their specific geological and petrological characteristics (Rock, 1991; Le Maitre *et al.*, 2002). The most widespread lamprophyres, both worldwide and in the Variscan Belt of Europe, are the calc-alkaline lamprophyres (Rock, 1991). These comprise dark mica-rich minettes and kersantites, as well as amphibole-rich vogesites and spessartites. The dominant light-coloured minerals in minettes and vogesites are the alkali feldspars, while that in kersantites and spessartites is plagioclase. Foids are generally absent, being characteristic of the alkaline lamprophyres camptonite, monchiquite and sannaitite. Apart from the characteristic panidiomorphic, porphyritic textures with abundant, euhedral dark micas and/or amphiboles, the specific petrographic characteristics of the calc-alkaline lamprophyres that distinguish them from more common rocks of similar bulk composition (e.g., andesites and diorites) include the lack of feldspar phenocrysts, the lack of orthopyroxene, the association of MgO-rich mafic minerals with alkali feldspars and quartz, and the abundance of various xenoliths and enclaves. In terms of bulk-rock chemical composition, lamprophyres are distinguished by a high content of volatile components ( $\text{H}_2\text{O}$ , Cl, F), high magnesium numbers (Mg#), high Cr, Ni and V contents, and a particularly strong enrichment in the large ion lithophile elements (LILE) and the light rare earth elements (LREE) over the high-field strength elements (HFSE).

The calc-alkaline lamprophyres occur in most geotectonic settings except oceanic intra-plate environments and mid-ocean ridges. These lamprophyres are most characteristic of convergent, Andean-type continental margins and orogenic belts, where they are often found in dyke swarms associated with late- to post-orogenic granitoids (Rock, 1991). The origin of lamprophyric magmas has been much debated, and an overview and discussion of the older concepts is given by Rock (1991). Significant advances have been achieved over the last couple of decades thanks to the extensive use of detailed trace element and isotopic studies (Macdonald *et al.*, 1985; Esperança & Holloway, 1987; Leat *et al.*, 1987; Turpin *et al.*, 1988; Stille *et al.*, 1989; Béziat *et al.*, 1993; Meyer *et al.*, 1994; Mitchell, 1994; Peterson *et al.*, 1994; Shand *et al.*, 1994; Carmichael *et al.*, 1996; Carlier *et al.*, 1997; Hegner *et al.*, 1998; Elburg & Foden, 1999; Feldstein & Lange, 1999; Hoch *et al.*, 2001; Prelević *et al.*, 2004). The main results from the modern-era research can be generalized into six major conclusions. First, calc-alkaline lamprophyric magmatism may be directly related in space and time to contemporaneous subduction

processes or, in many cases, can be linked to younger extension processes over ancient subduction zones. Second, lamprophyres represent volatile-rich magmas (often primary) that possess primitive chemical compositions rich in Mg, Cr, Ni, V, high magnesium numbers, and often without evidence of shallow level differentiation. Third, lamprophyric magmas originate from low degrees of partial melting of lithospheric mantle peridotites. Fourth, the mantle sources of lamprophyres underwent enrichment in the incompatible elements due to the subduction-related processes of metasomatism and infiltration by fluids and melts, and contamination of the mantle by subducted sediments. Fifth, lamprophyre magmas may form due to the mixing/hybridisation of mantle and crustal melts. Sixth, fractional crystallization and crystal accumulation appear to be important petrogenetic factors in many calc-alkaline lamprophyre suites.

The petrogenetic models proposed in the papers cited above, however, differ in several important respects. These include the mantle source characteristics and the melting processes. As a consequence, the petrogenesis of calc-alkaline lamprophyres is still far from being completely understood. Notably, the causes of the petrographic variation of the calc-alkaline lamprophyres and their genetic relationship are unclear. Rock (1991) considered that the kersantites, spessartites, minettes and vogesites show a similar chemical composition and that the differences in their modal composition are due to heteromorphism, i.e., for a magma of a given composition, crystallization conditions alone can produce different mineral assemblages. However, Rock (1991) does not specify the conditions that are necessary for the crystallization of particular mineral assemblages but suggests the presence of at least two genetically different types of calc-alkaline lamprophyre magmas. Other authors suggest that the petrographic variation of the calc-alkaline lamprophyres is of a more essential nature. Turpin *et al.* (1988) link the differences between minettes and kersantites from several Variscan massifs in France with some unspecified differences in partial melting processes of their mantle sources. Similarly, Carmichael *et al.* (1996) explain the differences between Quaternary minettes and spessartites from Mexico as the result of variable degrees of partial melting of their mantle sources. Macdonald *et al.* (1985) studied Caledonian mica lamprophyres of northern England and suggested that the variation in their bulk-rock chemical and modal composition can be related to a variable  $\text{CO}_2/(\text{CO}_2 + \text{H}_2\text{O})$  ratio in the mantle, and partly to a polybaric fractional crystallization. Based on data on

post-Caledonian lamprophyres from Scotland and reviews of earlier work, Shand *et al.* (1994) propose that the various types of calc-alkaline lamprophyres represent magmas that originated at various depths in the mantle. Mica-rich lamprophyric magmas (e.g., minettes) formed at deeper levels and at higher pressures that stabilized garnet and phlogopite in the mantle peridotites; amphibole-rich lamprophyric magmas (e.g., spessartites) formed at shallower levels and at lower pressures that stabilized hornblende. A similar model was proposed by von Seckendorff *et al.* (2004) who argued that the minette–kersantite–spessartite suite in the Saxothuringian Zone of the Variscan Orogen in Germany resulted from an increasing degree of partial melting of progressively shallower mantle sources: from <2.5% partial melting of a garnet lherzolite for minette magmas, to ~7% partial melting of a spinel lherzolite for spessartite magmas.

Although the models outlined above provide detailed solutions for individual lamprophyre suites, their applicability to lamprophyre petrogenesis in general remains to be demonstrated.

The calc-alkaline lamprophyres show variable transitions and gradations towards other volcanic, hypabyssal and plutonic rocks. However, the terminology used for these transitional rock types is complex and confusing. Many rock names, although not strictly discarded, are also not strictly defined nor included in the recommended IUGS classification (see Glossary in Le Maitre *et al.*, 2002). Some more important varieties and relatives of the calc-alkaline lamprophyres are briefly discussed below.

The plutonic equivalents of the amphibole lamprophyres are appinites. Appinites usually occur as pipes, vents and dykes that can be massive or brecciated. Appinites are coarse-grained rocks that show a great variation in modal composition and colour index, from ultramafic to leucocratic. A common feature of appinites, as well as spessartites and vogesites, apart from similarities in bulk chemistry and modal composition, is the abundance of euhedral, zoned pargasitic amphiboles. Most appinite

occurrences are known from the British Isles (Rock, 1991). There are also plutonic equivalents of the mica lamprophyres – vaugnerites, durbachites and redwitzites. Despite sharing generally similar chemical and mineralogical characteristics with the minettes and kersantites (Rock, 1991, chapter 7), the coarse-grained plutonic equivalents show significant variation in their petrographic features: some of them contain feldspar phenocrysts, and most have been reported only from the European Hercynides (Rock, 1991, p. 117).

The calc-alkaline lamprophyres often represent the mafic end-members in rock suites that comprise mafic to intermediate to felsic hypabyssal rocks. Such rock suites are particularly characteristic of dyke swarms that are related to late- and post-collisional calc-alkaline granitoids (Rock, 1991). The intermediate and felsic lithologies include rocks known as malchites, semilamprophyres, porphyrites and porphyries. In general, these subvolcanic rocks are distinguished from the associated lamprophyres by their lower colour index and the presence of feldspar phenocrysts. Many of them may represent differentiates of lamprophyre magmas that originated from hybridization of mantle and crustal melts as well as from fractionation and contamination processes (Rock, 1991, chapter 8).

The amphibole lamprophyres (spessartites and vogesites) show gradations towards shoshonites, andesites and diorites. However, the amphibole lamprophyres can be recognized by their lack of orthopyroxene, lack of plagioclase phenocrysts, and the particular chemical composition of the clinopyroxenes and the amphiboles themselves (Rock, 1991, Table 1.4). The petrographic differences between the lamprophyres and the more common calc-alkaline to shoshonitic igneous rocks may be primarily linked with specific magma composition, in particular the high H<sub>2</sub>O content of lamprophyre melts. It is this high water content that facilitates the crystallization of dark micas and amphiboles, and inhibits early feldspar crystallization and feldspar phenocryst growth.

## GEOLOGY OF THE LAMPROPHYRES AND ASSOCIATED MAFIC ROCKS IN THE SUDETES

### REGIONAL CONTEXT AND AGE OF THE LAMPROPHYRIC MAGMATISM

The Sudetes are located in Lower Silesia in south-west Poland, at the north-eastern margin of the Bohemian Massif (Figs. 1 and 2). The NW-trending Sudetic Marginal Fault represents a long-recognized regional dislocation that separates the hilly lowlands of the Fore-Sudetic Block to the north-east and the uplifted Sudetes range to the south-west. The downthrown Fore-Sudetic Block is largely covered with Cenozoic sediments, there being only relatively rare outcrops of older crystalline basement rocks. Pre-Cenozoic rock complexes, however, extensively crop out in the uplifted Sudetic block. These latter

complexes represent an eastern segment of the Variscan Belt of Europe and comprise a deformed, and usually metamorphosed, Upper Proterozoic to Lower Carboniferous rock series intruded with Late Palaeozoic granitoids; and also some Carboniferous–Permian volcano-sedimentary molasse deposits, overlain by Upper Triassic and Upper Cretaceous sedimentary rocks of the epi-Variscan platform cover. The detailed geological relationships in this region are complex, with numerous fault-bounded geological units that themselves are characterized by their own individual structures, rock assemblages and origins (Franke & Żelaźniewicz, 2002; Mazur *et al.*, 2006).

The Variscan Orogen of Europe developed due to the oblique collision of the palaeocontinents Gondwana and

Laurussia, and the accretion of Gondwana-derived terranes onto the Laurussian margin (e.g., Ziegler & Dezes, 2006). The main phases of the Variscan orogeny in Late Devonian and Carboniferous times included a major crustal shortening and the subduction of oceanic and continental lithosphere. Subsequent dextral translation between Laurussia and Gondwana resulted in wrench tectonics and the collapse and disruption of the orogen. The late- to post-orogenic processes included the formation of intracontinental sedimentary basins across the decaying orogen, as well as several episodes of magmatism in the Carboniferous and Permian. The origin of this Late Palaeozoic magmatic activity has been genetically linked with the detachment of subducted lithospheric slabs, mantle upwelling, and the interaction of mantle-derived and crustal melts (Ziegler & Dezes, 2006).

Modern research on the evolution of the Sudetic segment of the Variscan Belt has been published by Johnston *et al.* (1994), Cymerman *et al.* (1997), Aleksandrowski *et al.* (1998), Franke & Żelaźniewicz (2002) and Mazur *et al.* (2006). Similar to other parts of the Variscides, the pre-Permian crystalline rock complexes of the Sudetes provide a record of the late Proterozoic (Cadomian) orogeny; a record of Cambro-Ordovician and Devonian rifting and basin opening, with related magmatism and sedimentation; and a record of late Devonian to early Carboniferous basin closure, collision and orogeny, which juxtaposed variably deformed and metamorphosed terranes along major suture zones. The Sudetic segment of the Variscides was also strongly affected by Late Palaeozoic lateral displacements along NW- and NE-trending regional strike-slip shear zones, which further reworked the orogenic collage of terranes.

Throughout the Sudetes region during the Carboniferous and Permian late- to post-orogenic extension, there were several episodes of intramontane basin development and intense magmatism (Borkowska, 1966; Majerowicz, 1972; Puziewicz, 1990; Duthou *et al.*, 1991; Lorenc, 1994; Dziedzic, 1996; Awdankiewicz, 1999a, b, 2004, 2006; Oberc-Dziedzic, 1999; Machowiak *et al.*, 2004; Słaby & Götze, 2004; Ulrych *et al.*, 2006; Słaby *et al.*, 2006, 2007; Bachliński & Bagiński, 2007; Kozłowski & Wiszniewska, 2007; Mazur *et al.*, 2007; Mierzejewski, 2007; Słaby & Martin 2008). The late Palaeozoic igneous rocks of the Sudetes fall into two broad categories. First, volcanic complexes that are interstratified within the molasse successions of the intramontane basins, i.e., the North-Sudetic and the Intra-Sudetic Basins, and the Krkonoše Piedmont Basin in the Bohemian part of the Sudetes. Second, plutonic to subvolcanic complexes that comprise granitoid plutons, mafic to felsic dykes and other subvolcanic intrusions cropping out within the uplifted crystalline basement blocks.

In essence, the lamprophyres and related hypabyssal rocks represent the mafic members of the plutonic-subvolcanic complexes. Most of the lamprophyre dykes cut granitoids and so generally postdate granite plutonism. Some dykes, however, are found within crystalline basement rocks away from granite intrusions. A few lamprophyre dykes and sills occur in the Carboniferous sedimen-

tary rocks (Viséan to Namurian) of the Central Sudetes and accompany the much more widespread volcanic complexes. No lamprophyre veins are found in the Permian (or younger) sedimentary rocks of the Sudetes.

The age of granite plutonism in the Sudetes is reasonably well constrained by radiometric age determinations. These ages indicate two distinct Carboniferous magmatic phases: one at ~340–330 Ma, and the other at ~320–300 Ma (Mazur *et al.*, 2007). The volcanic rocks in the intramontane basins have not been radiometrically dated, but geological evidence suggests two stages of Carboniferous volcanism, followed by a climax of activity in the early Permian (Awdankiewicz, 1999a, b; 2006).

Radiometric age determinations of the mafic dykes in the Sudetes are scarce. An age of  $314 \pm 6$  Ma was determined from a minette dyke in the South Krkonoše Complex using the  $^{40}\text{Ar}$ - $^{39}\text{Ar}$  method (Marheine *et al.*, 2002). A similar age of ~318 Ma was obtained from a microzonodiorite dyke in the Karkonosze granite using the SHRIMP method (Awdankiewicz *et al.*, 2007a). An older age of  $326 \pm 6$  Ma was reported for a post-tectonic biotite-hornblende syenite dyke in gneisses of the western part of the Orlica-Śnieżnik Dome using the SHRIMP method (Żelaźniewicz *et al.*, 2006). In addition, preliminary  $^{40}\text{Ar}$ - $^{39}\text{Ar}$  dating of phlogopite and kaersutite, using separates from four lamprophyre samples from the Karkonosze, Góry Sowie and Orlica-Śnieżnik massifs, range from 296 to 330 Ma (Marek Awdankiewicz and Martin Timmerman, unpublished). In summary, the geological constraints, together with the available radiometric data, indicate that the lamprophyric magmatism in the Sudetes occurred predominantly during the Carboniferous, probably in the late Early Carboniferous–Late Carboniferous.

## DISTRIBUTION OF THE LAMPROPHYRES AND ASSOCIATED MAFIC VEINS

The distribution of lamprophyres in the Sudetes is shown in Figure 2. This map gives the location of all lamprophyre veins (~150) indicated in several sheets of the “Szczegółowa mapa geologiczna Sudetów 1:25 000” (“Detailed Geological Map of the Sudetes 1:25 000”; references are given in the caption to Fig. 2). However, many of these veins could not be identified in the field: neither exposures nor loose blocks of lamprophyres, nor other mafic hypabyssal igneous rocks could be found within a few hundred meters of the supposed locations. Such problematic veins are marked in Figure 2 as “unconfirmed lamprophyre dykes”. It is possible that some of these unconfirmed dykes were originally mapped from trench cuttings, or were identified in small, currently overgrown exposures, or represent very thin dykes (only centimetres wide?) that were not found during the new field work undertaken here. However, at some locations it seems clear that outcrops of weathered fine-grained amphibolites, and possibly even some granitoids south-east of Świeradów Zdrój, were erroneously mapped as “lamprophyres”.

Mafic hypabyssal igneous rocks occur at many other sites in the Sudetes, but their classification too must be

considered insufficient or incorrect. For example, in the eastern part of the Karkonosze–Izera Block some “lamprophyre” dykes can be more precisely classified as vogesites or spessartites; all “kersantites” are, in fact, minettes; and several “lamprophyres” are micromonzodiorites. Similarly, sampling and petrographic determination of selected dykes of other mafic rocks in this area reveals inconsistencies: many “syenites” appear to be monzonites.

The confirmed and sampled occurrences of lamprophyres and associated mafic rocks included in this study are listed in Appendix 1 (lamprophyres from 75 sites; other mafic rocks from 25 sites), together with detailed location, rock classification and summary of analytical procedures. Nearly half of the sampled sites are natural exposures or old quarries; the other sites are from loose blocks that presumably reflect subcrops.

Although detailed mapping was beyond the scope of this study, the verification of the existing geological data, summarized in Figure 2, highlights the inhomogeneous distribution of lamprophyres in the Sudetes: there are a few large groups with at least 10–25 larger lamprophyre dykes, some smaller clusters, and some single, isolated dykes. There is a notable scarcity of lamprophyre dykes in the Fore-Sudetic Block and in the low-grade metamorphic complexes of the Sudetes, such as the Kaczawa, Rudawy Janowickie and Kłodzko Complexes. And although not included in the present study, kersantites associated with the Żelaźniak intrusion have been described from the Kaczawa Complex (Zimmermann & Berg, 1932; Machowiak *et al.*, 2004), and vaugnerites have been reported from the Niemcza Zone in the Fore-Sudetic Block by Puziewicz (1988). In some areas, particularly in the Karkonosze and Kłodzko–Złoty Stok plutons, lamprophyres show considerable petrographic variation and there is a spatial association with other types of mafic to felsic dykes.

Based on the relationships discussed above, the three largest groups of mafic dykes in the Sudetes are distinguished herein as the Karpacz–Janowice Wielkie Dyke Swarm (KJWDS), the Złoty Stok Dyke Swarm (ZSDS) and the Gniewoszów Dyke Swarm (GDS). The other, more scattered occurrences in the area between the swarms are here termed the Central Sudetic dykes.

## MAFIC DYKE SWARMS AND STRUCTURES OF THE DYKES

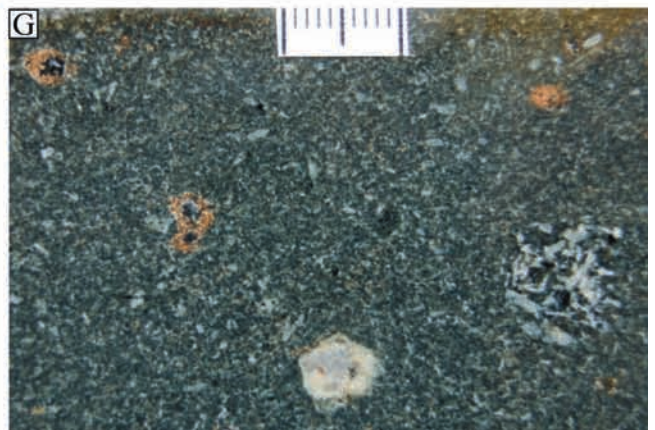
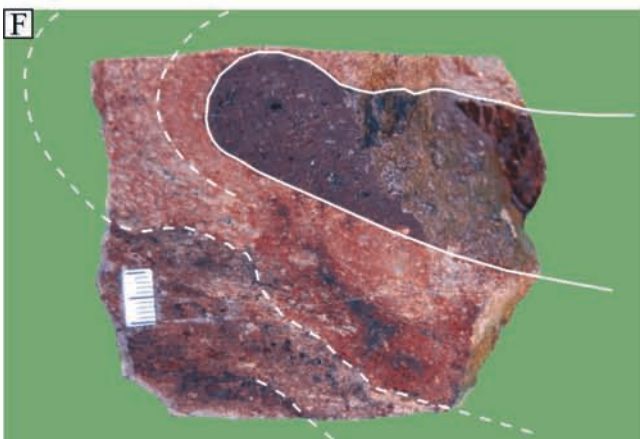
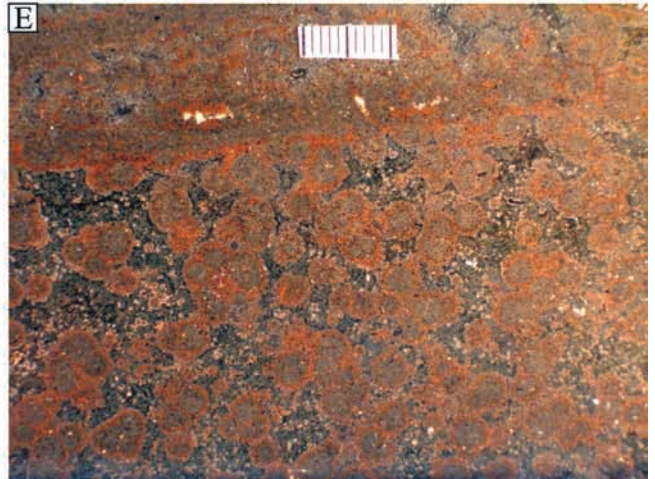
### Karpacz–Janowice Wielkie Dyke Swarm (KJWDS)

The Karpacz–Janowice Wielkie Dyke Swarm (KJWDS) cuts the eastern part of the Karkonosze granite pluton. The mafic and felsic dykes concentrate in a NE-aligned area ~20 x 10 km in size. Individual dykes strike mainly NNE, slightly oblique to the whole swarm. The location of the KJWDS coincides with a major feeder zone of the granitic magma defined by the arrangement of schlieren and phenocrysts (Cloos 1925; Borkowska, 1966; Mierzejewski, 2007). The swarm also parallels the south-eastern margin of the Karkonosze–Izera Block where, within the eastern metamorphic cover of the Karkonosze intrusion, the Teplá/Saxothuringian suture is located (Aleksandrowski & Mazur, 2002; Mazur *et al.*, 2006). This suture experienced Late Devonian to Early Carboniferous NW-directed thrusting that was followed by an ESE-directed extensional collapse during the Early Carboniferous (e.g., Mazur *et al.*, 2006).

The KJWDS comprises minette, vogesite, and spessartite lamprophyres; monzonite and micromonzodiorite mafic rocks; and microgranite, aplite and “porphyries” as the felsic component. There are a greater number of evolved mafic and felsic dykes than lamprophyre dykes, and the felsic dykes show a wider geographical distribution, with many veins cropping out further to the west in the central part of the Karkonosze Pluton (Figure 1 in Borkowska, 1966). Isolated mafic dykes are also found in the northern and eastern metamorphic cover of the Karkonosze granite. Because of petrographic and geochemical similarities, these latter dykes are discussed together with the KJWDS.

The lamprophyre and other mafic dykes of the KJWDS are up to few kilometres long and over 10 metres wide, but typical dimensions are an order of magnitude smaller. The minette dykes show flow foliations and platy joints defined by subparallel alignments of the dark micas; these planar structures are parallel to the strike of the dykes (Fig. 3A). Dykes of other mafic rocks are typically

**Fig. 3.** Mafic dykes of the Karpacz–Janowice Wielkie Dyke Swarm. Locality numbers refer to Appendix 1. Scale bar in (E), (F) and (G) is 1 cm long. (A) Subvertical minette dyke with well defined flow foliation from locality 42, Mysłakowice. (B) Gently inclined, thin vogesite dyke which is nearly massive, with indistinct flow foliation from locality 43, Mysłakowice. (C) A central part of ~2 m thick, subvertical, spessartite dyke with platy to irregular joints from locality 2, near Trzczańsko. This dyke interdigitates with host granites in the form of subparallel veins/wedges: Granite intercalation inside vogesite can be seen in the central part of this photo. (D) Flow banding in a vogesite block from a composite, minette–vogesite dyke from locality 42, Mysłakowice. (E) Spheroidal structures in a minette from locality 36, Bukowiec. A gradation from felsitic veinlet into felsitic ‘globules’ dispersed in a more mafic matrix can be seen in the upper part of photo. (F) Flow-folded felsic inclusion in a micromonzodiorite sample from locality 31, Głębock. The lines show the outline of the flow fold. The contact of the mafic and felsic components varies from sharp (solid line) to gradational (broken lines). The outer part of the inclusion is partly mingled with the host, and the texture of this felsic rock confirms a partly melted state during the interaction with the host micromonzodiorite magma (cf. Fig. 7B). (G) Micromonzodiorite sample from locality 7, Bukowiec, with numerous microphenocrysts of altered plagioclase and of less distinctive clinopyroxene. Visible inclusions are the following: pink-coloured, alkali feldspar-rich ocellae; a mafic cognate enclave composed of altered plagioclase and clinopyroxene, located near the lower right corner of photo (cf. Fig. 7A); and a feldspar xenocryst, near the lower edge of photo, likely derived from the host Karkonosze granite.



more massive (Fig. 3B), with well developed chilled margins in the thicker dykes. The contacts of the dykes with their host granites are sharp and usually planar at outcrop scale, which can be up to several metres. In places where non-weathered samples were collected directly from the contact of a dyke and its host granite, the latter shows signs of hydrothermal alteration (chloritization of biotite, sericitization of plagioclase) as well as some cataclasis. Millimetre- to centimetre-sized xenoliths and xenocrysts derived from the host granite may locally be included in the dyke rocks, and wedge-shaped veinlets of chilled mafic rock may penetrate the granite. Rarely, some dykes split into subparallel/wedge-shaped veins separated by granite (Fig. 3C).

The majority of the KJWDS dykes are homogeneous in terms of the main petrographic characteristics, though there is a limited textural variation as a result of chilled margins. Inhomogeneous lamprophyre dykes are very rare. In a series of exposures near Mysłakowice, south of Jelenia Góra (localities 42–43, Appendix 1), there are a few cm- to dm-thick dykes of minette and vogesite, as well as 5–10 m thick composite dyke (Zagożdżon & Zagożdżon, 2003). The outer parts of the composite dyke are ~1 m thick and are of a flow-foliated minette; the interior is of massive to banded vogesite (Fig. 3D). The bands in the vogesite result from differences in the proportions of Fe-Mg silicates and feldspars. The boundaries between minette and vogesite in the composite dyke, and between the dark and light bands in vogesite itself are sharp and vary from planar to wavy. Some minette dykes in the vicinity of Bukowiec (e.g., locality 6) show the presence of rare, mm-cm thick, leucocratic veins in the form of a loose network, and rarely there are dykes of spheroidal minettes (Fig. 3E). Petrographic inhomogeneities such as flow banding or felsic veinlets are rarely found in the other mafic rocks of the KJWDS. But many specimens of the KJWDS micromonzodiorites carry variable inclusions, i.e., ocellae, enclaves, clusters of crystals and single crystals (Fig. 3F and G).

### Złoty Stok Dyke Swarm (ZSDS)

The Złoty Stok Dyke Swarm (ZSDS) comprises dykes cropping out within the Kłodzko–Złoty Stok granitoids and, locally, within the country rocks of this intrusion. The Kłodzko–Złoty Stok Pluton, and the ZSDS, were emplaced between the Bardo and Kłodzko Units to the north-west and the Śnieżnik Massif to the south-east, and abut against the Skrzyńska Dislocation Zone at the northern margin of the Śnieżnik Massif (Fig. 2). The Skrzyńska Zone is a Late Palaeozoic strike-slip dislocation, possibly equivalent to the Niemcza Zone in the Fore-Sudetic Block (e.g., Mazur *et al.*, 2006). The mylonitization of the south-eastern margin of the Kłodzko–Złoty Stok intrusion suggests that the latest stages of shearing along the Skrzyńska Zone post-dated the emplacement of the granitoids (Mazur *et al.*, 2006).

Mafic dykes of the ZSDS crop out in a NE-aligned area 15 x 6 km in size, mainly in the eastern and southern parts of the Kłodzko–Złoty Stok Pluton, and are variable in strike orientation. The lamprophyres comprise

vogesites and spessartites and there are associated mafic to felsic dykes of variable petrographic characteristics, including fine-grained dioritoids, syenitoids and granitoids (Wojciechowska 1975; Wierchołowski 1977).

The mafic dykes in the Złoty Stok swarm are up to a few hundred metres long and usually only tens of centimetres wide (Fig. 4A). The dykes are typically massive to flow-foliated, without any significant internal petrographic variation except for well-developed chilled margins. Indistinct flow folds are locally observed. Contacts with the host granitoids are sharp and the granitoids may show local cataclasis. However, one well-exposed dyke shows some offset and bending (Fig. 4B), and another may interdigitate with the granitoids in the form of subparallel veins (Fig. 4C). In contrast to the KJWDS, the ZSDS dykes are more homogeneous and typically contain very few inclusions, excepting some vogesites which may host small igneous enclaves, crystal aggregates and xenocrysts.

### Gniewoszków Dyke Swarm (GDS)

The Gniewoszków Dyke Swarm (GDS) occurs within metamorphic rocks in the eastern part of the Orlica Massif. The swarm trends to the NNW and comprises NNW-aligned lamprophyre dykes cropping out in an area of ~7 x 4 km. The lamprophyres here are minettes and, very rarely, spessartites; there is an apparent absence of associated mafic or felsic dykes. The lamprophyre dykes cut mica schists and, locally, some marbles and amphibolites that are intercalated with the schists. The dykes strike parallel to the foliation and to small faults in the country rocks and also strike parallel to a larger dislocation zone that defines the western margin of the Cretaceous Upper Nysa Graben to the east. The NNW trend of the GDS, which is the same as the structures in the metamorphic host rocks, can also be linked with a major tectonic boundary in the south-western margin of the Orlica Massif, ~10 km to the south-west. Mazur *et al.* (2006) consider that the boundary between the Orlica Massif and the Nové Město Unit further southwest represents the Teplá–Barrandian/Moldanubian suture zone that developed during the Early Carboniferous as a thrust but that later became a dextral ductile fault.

Isolated dykes of mica lamprophyres (minette and kersantite) crop out in scattered localities in the Śnieżnik Massif area between the GDS and the ZSDS (Fig. 2). Minettes from two dykes cutting the granitoids of the Kudowa Massif to the north-west of the GDS were also sampled, though most lamprophyre dykes reported to be adjacent to the Kudowa Massif remain unconfirmed. Because of their similar geological position and petrographic characteristics, lamprophyres from these scattered localities are considered together as part of the GDS.

The minette dykes of the GDS are relatively short (less than 200 m), but some of them attain a thickness of over 10 m. One of the best exposed and thickest dykes occurs near Gniewoszków (Fig. 4D) and consists of a fine- to medium-grained minette that shows well developed magmatic foliation and platy joints defined by the alignment of dark mica plates, which are subparallel to the strike of the dyke. The chilled margins of this dyke, observable



**Fig. 4.** Lamprophyre and other mafic dykes of the Złoty Stok Dyke Swarm, the Gniewoszów Dyke Swarm and the Bardo Unit. Locality numbers refer to Appendix 1. **(A)** Spessartite dyke with well developed flow foliation, chilled margins, and joints perpendicular to contact with granites from locality 96, Chwalisław. **(B)** Thin (~ 5 cm), deformed vogesite dyke, possibly displaced along a shallow-lying shear zone in the host granitoid, also from locality 96. **(C)** Steeply inclined vogesite dyke in granitoids, from locality 82, Jaskowa Górna. The dyke, which is outlined and dips to the left in this photo, shows densely spaced joints perpendicular to the contact with the granitoids. Chilled margins are well developed against the contacts with the granitoids. A 0.5 m long granite inclusion (also outlined) in the central part of the dyke may reflect some interdigitation of the vogesites with the granitoids. **(D)** An outcrop of ~ 10 m thick richterite minette dyke from locality 70, Gniewoszów, shows steeply inclined flow foliation and platy joints that are parallel to the margins of the dyke and dipping to the right in this photo. **(E)** Pegmatite vein in a minette dyke from locality 66, Gniewoszów. **(F)** The contact of altered mafic dyke (?kersantite, left part of photo) with bedded, steeply inclined shales (to the right) at locality 51, near Wojbórz. The contact is locally non-planar, with dm-scale offsets.

only from loose blocks, are fine-grained to aphanitic and massive. The minette in places contains leucocratic, coarse-grained (pegmatitic) veins and patches that show some folding and disruption. Similar features are common in other minette exposures near Gniewoszków (Fig. 4E) and in minettes from other scattered locations around the GDS. A specific feature of the minette dykes emplaced in the marbles in the vicinity of Różanka (southern part of the GDS) is their strong alteration, which can generally be linked with enhanced post-magmatic, fluid-related reactions at the contact between the minettes and the carbonate host rocks. In contrast to the minettes of the KJWDS, composite dykes or flow banding are not found in the GDS.

### The dykes and sills of the Central Sudetes

Lamprophyres and related mafic rocks are found in the Central Sudetes at several widely distributed sites in the Intra-Sudetic Basin, in the Góry Sowie Block and, at one locality, in the Bardo Unit (Fig. 2). These rocks occur as veins that comprise minettes, kersantites, altered mafic rocks or, rarely, spessartites. The mafic rocks form dykes and sills in Viséan to Namurian sedimentary rocks where they are associated with widespread, mostly acidic, volcanic to subvolcanic rocks (Awdankiewicz, 1999a, b; Łapot, 1986; Kryza *et al.*, 2007). Although the individual dykes and sills probably reflect some local tectonic controls, most of these mafic veins concentrate in a NW-SE aligned zone that broadly follows the Intra-Sudetic Fault, one of the major Late Palaeozoic strike-slip zones of the Sudetes (e.g., Mazur *et al.*, 2006). Compared with the dykes emplaced in the crystalline basement rocks (the KJWDS, KZSDS and GDS), the mafic veins found in the Carboniferous sedimentary rocks in the Central Sudetes are, with few exceptions, poorly exposed and strongly altered. There follows brief characteristics of intrusions from selected localities.

A poorly exposed minette dyke crops out north of Kamienna Góra in a field road (locality 48). The dyke occurs within bedded conglomerates and sandstones whose bedding strikes to the NNE and whose dips are very steep to vertical. The dyke is ~5–10 m thick and is roughly parallel or slightly oblique to bedding. The contacts of the minette with the sedimentary rocks are not exposed. The minette shows flow foliation, presumably parallel to the

margins of the dyke. Some specimens from this dyke, and from other veins in the Kamienna Góra area, contain small leucocratic and ultramafic enclaves composed of alkali feldspars and phlogopite, respectively.

A well exposed altered mica lamprophyre occurs in a quarry adjacent to the Chełmiec rhyodacite laccolith west of Wałbrzych (locality 47). The outcrop shape of this lamprophyre intrusion is oval, ~250 × 80 m in size (Bosowski & Czerski, 1985) and probably represents a short dyke. In the quarry, there occur crags of altered lamprophyre that are composed of monotonous, massive rocks with irregular to blocky joints. Locally, there are ~5–15 mm thick leucocratic veins in a variety of orientations. Contacts of the lamprophyre with the host clastic sedimentary rocks are not exposed.

A strongly altered mafic dyke (?kersantite) is exposed in a quarry near Wojbórz in the Bardo Unit (locality 51), south of the Góry Sowie Block. The country rocks of this dyke are most probably Lower Carboniferous shales (Oberc, 1957, p. 161; however, these rocks have also been considered to be Permian sediments by Oberc *et al.*, 1994). The dyke is subvertical, strikes NWW and is probably ~20–30 m thick. The dyke's southern contact is sharp and well exposed against steeply inclined, well-bedded shales (Fig. 4F), though occasionally tending to be uneven or with irregular steps. According to Oberc (1957, p.161), this contact is largely tectonic. The dyke locally shows vesicles, and Oberc (1957) noted abundant xenoliths of shales. Petrographic variations within this mafic dyke are difficult to discern due to the high degree of alteration. Similar, but much thinner and less altered, dykes were exposed in trench cuttings in the Wojbórz area (Bolesław Wajsprych, personal communication, 2007).

Another definable group of intrusions are the Góry Sowie kersantites (Muszyński, 1987). These intrusions comprise sills, up to ~50 m thick, emplaced in sandstones and conglomerates. Although the relevant outcrops are now overgrown, conformable contacts and short offshoots (apophyses) of the sills have been locally observed (Muszyński, 1987). The kersantites at Ostrzew Hill (locality 52) are distinguished by abundant and variable inclusions, such as magmatic enclaves, crystal aggregates, xenocrysts and megacrysts (Muszyński, 1987; Awdankiewicz *et al.*, 2004).

## PETROGRAPHY

### CLASSIFICATIONS AND TERMINOLOGY

According to Le Maitre *et al.* (2002; chapter 3), lamprophyres are "... strongly porphyritic in mafic minerals, typically biotite, amphiboles and pyroxenes, with any feldspars being confined to the groundmass. They commonly occur as dykes or small intrusions and often show signs of hydrothermal alteration". The recommended classification of the foid-free lamprophyres (the calc-alkaline

lamprophyres of Rock, 1991) is based on the relative volumetric abundance of feldspars, dark micas and amphiboles (Table 1).

In practice, the identification and classification of lamprophyres may be problematic because petrographic gradations exist between lamprophyres and other igneous rocks and because post-magmatic alteration can obscure original igneous characteristics. These problems were discussed by Rock (1991, Chapter 1), who proposed some ad-

Table 1

The petrographic classification of calc-alkaline lamprophyres (based on table 2.9 of Le Maitre *et al.*, 2002, and on Rock, 1991)

LIGHT-COLOURED COMPONENTS	DOMINANT MAFIC MINERALS	
	biotite > hornblende ± diopsidic augite (± olivine)	biotite > hornblende ± diopsidic augite (± olivine)
alkali feldspar > plagioclase	minette	vogesite
plagioclase > alkali feldspar	kersantite	spessartite

ditional petrographic and mineralogical criteria to facilitate rock classification, e.g., the common occurrence of crustal enclaves and ocellar textures in lamprophyres (rare in dioritic to andesitic rocks); the lack of orthopyroxene in lamprophyres (common in andesites); and pargasitic and tschermakitic amphibole composition in lamprophyres (hornblende in andesites and diorites).

However, the current study of lamprophyres in the Sudetes reveals that the International Union of Geological Sciences (IUGS) definition does not, perhaps, take sufficient account of textural variations. For instance, the textures of the minettes in the GDS range from strongly phlogopite-phyric, to inequigranular poikilitic (numerous euhedral dark micas enclosed in much larger, subhedral alkali feldspars). If the IUGS definition were strictly applied, then the porphyritic rocks would be classified as minettes, whereas the non-porphyritic, poikilitic rocks might be described as phlogopite melasyenites (based on the *QAP* triangle). However, all these rocks are similar in modal composition, in mineral chemistry, and in bulk-rock chemistry. Making a distinction between minettes and melasyenites, based on the textural differences alone, would seem artificial and misleading. Apparently, all these phlogopite-alkali feldspar rocks crystallized from magmas of similar composition and the textural variation is a second-order feature, possibly related to such factors as different cooling rates and the interplay between nucleation and growth rates of the minerals involved (the origin of porphyritic and poikilitic textures in the igneous rocks are discussed by Shelley, 1993, chapters 3 and 4). It would seem better to use the term for lamprophyres (e.g., minettes) rather than that for the more common igneous rocks (e.g., syenites), because the GDS rocks lack the feldspar phenocrysts that are characteristic of many common igneous rocks, including syenites. Consequently, the IUGS lamprophyre definition given above is used here with some caution, and it is extended to include not only “strongly porphyritic”, but also any related textural modifications such as weakly porphyritic, euhedral-granular, or inequigranular poikilitic.

The modal composition of the Sudetic lamprophyres forms the basis for the petrographic classification, and these modes were determined by point counting 20 representative samples that preserve primary igneous minerals. The results are shown in Table 2. In each specimen, 500–600 points were counted, and repeated counting in one specimen indicated that the precision of the results was within 1–2%. Nevertheless, even in these relatively fresh specimens there are significant amounts of post-magmatic

minerals (often 10–20%, but up to 38% in one specimen). The most abundant alteration products are chlorites and carbonates which, together with intergrowths of other minerals (e.g., epidotes, titanite), replace olivine and other primary Fe–Mg silicates. The textural relationships of these post-magmatic minerals statistically justify their inclusion into the mafic component count. The calculation of the colour index is 100% minus the felsic components, i.e., quartz and feldspars (Table 2).

Feldspar alteration is also common. In several specimens sericitized plagioclase can easily be distinguished from fresh alkali feldspars. In lamprophyres such as the kersantites of the Góry Sowie Block, micrometer-scale feldspar intergrowths make point counting specific feldspars not possible and only general relationships can be determined (e.g., Pl > Afs). However, even such semi-quantitative determinations are sufficient to classify a lamprophyre (Table 1).

The other subvolcanic rocks of the Sudetes included in this study were classified following the IUGS suggestions (Le Maitre *et al.*, 2002; chapter 2.11) based on the *QAP* triangle for plutonic rocks (Fig. 5; lamprophyres plotted for comparison). The preferred names are given in Table 2. Some of the mafic rocks actually plot in the quartz monzonite field but, for the simplicity of terminology, they are classified here more generally as monzonites. Other mafic rocks – rich in plagioclase, altered, but determined as anorthite-poor in some relics preserved – plot in

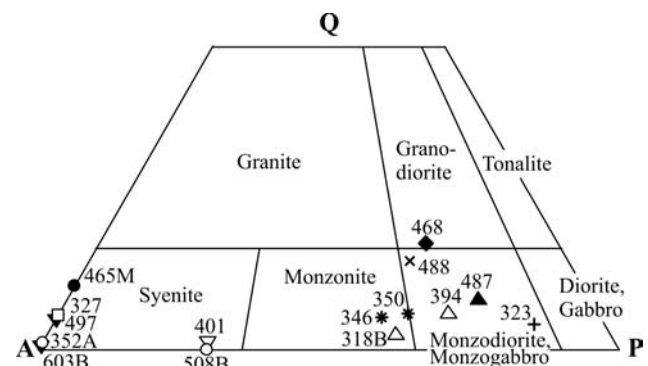


Fig. 5. Classification of the mafic rocks of this study as plotted in a QAP diagram (simplified from Le Maitre *et al.*, 2002) and based on data from Table 2. Lamprophyres are plotted for comparison, except samples where feldspars were determined only semi-quantitatively. Q – quartz, A – alkali feldspar, P – plagioclase.

Table 2

The modal composition and classification of representative samples of the mafic rocks

Location	Sample	Rock type	Qtz	Fs tot	Afs	Pl	Cpx	Am	PB	Opq	Ap	Chl	Cal	other	fel	M'
KJWDS	327	rm	4	47	47	-	4	20	15	6	3	-	-	3	54	46
	352A	m	<1	46	46	-	25	-	8	10	-	10	-	-	47	53
	401	v	1	56	40	16*	1	31	-	1	<1	6	<1	4	57	43
	318B	s	2	53	20	33	5	21	-	4	1	9	-	7	56	44
	394	s	4	52	17	35	1	26	-	4	-	9	1	3	56	44
	350	mn	4	57	20	37*	4	4	4	3	2	11	3	8	63	37
	346	mn	4	66	26	40*	3	-	-	3	-	20	2	3	70	30
	323	mmd	3	52	7	45*	14	-	-	9	-	18	1	3	55	45
ISB	508B	m	-	34	24	10	-	-	33	6	5	8	13	-	39	61
GSB	250D	k	5	65	Pl**>Afs		7	3	10	4	<1	4	-	3	70	30
	251	k	6	65	Pl**>Afs		10	<1	10	2	<1	4	-	1	71	29
	305	k	3	59	Pl**>Afs		13	7	8	2	-	2	-	5	62	38
	425	k	4	56	Pl*>Afs		-	-	32	2	<1	-	1	5	60	40
GDS	465A	rm	7	48	48	-	-	18	19	1	3	-	-	4	58	42
	468	k	7	27	8	19	1	-	21	5	1	Chl+ Cal=38	-	-	35	65
ZSDS	492A	s	-	57	Pl**>Afs		-	16	-	<1	-	-	-	26	57	43
	487	s	6	53	11	42*	-	27	-	3	<1	8	1	3	59	41
	497	v	3	45	45	-	1	28	-	<1	2	10	4	6	50	50
	603B	v	<1	43	43	-	2	34	-	1	<1	-	-	19	44	56
	488	mmd	12	56	19	38*	-	12	9	-	1	4	-	5	69	31

In some specimens, the proportions of alkali feldspar and plagioclase were only semi-quantitatively determined due to microcrystalline intergrowths and alteration. Minerals: Qtz (quartz); Fs tot {total feldspars, including Afs (alkali feldspars), Pl (plagioclase); \* (sericitized), \*\* (albitized)}; Cpx (clinopyroxene); Am (amphibole), PB (phlogopite, biotite); Opq (opaques); Ap (apatite); Chl (chlorite); Cal (calcite and other carbonates); "other" (microcrystalline intergrowths of post-magmatic minerals, e.g., epidotes, sheet silicates, titanite; in sample 350 also prehnite and grossularite; in sample 492A also pumpellyite and prehnite). Other abbreviations: fel (sum of light-coloured minerals, i.e., Q + Fs tot + Ap); M' (colour index, calculated as  $M' = 100 - fel$ ). Locations are as follows: KJWDS (Karpacz-Janowice Wielkie Dyke Swarm), ISB (Intra-Sudetic Basin), GSB (Góry Sowie Block), GDS (Gniewosów Dyke Swarm), ZSDS (Złoty Stok Dyke Swarm). Rock type abbreviations are as follows: rm (richterite minette), m (minette), v (vogesite), k (kersantite), s (spessartite), mn (monzonite), mmd (micromonzodiorite)

the quartz monzodiorite to monzodiorite fields. Taking into account the textural characteristics, these rocks are classified as microcrystalline monzodiorites (micromonzodiorites).

In some of the strongly altered rocks, a reliable determination of the original magmatic mineralogy is all but impossible. The most altered, problematic rocks were classified using a general terminology, e.g., "altered mica lamprophyre" or "altered mafic rock". In addition, whole-rock chemistry, including immobile trace element geochemistry, was used to compare the fresher and the more altered specimens and to help better constrain the affinities of some of the altered rocks.

There follows a regional overview of the petrographic characteristics based on the freshest samples of Sudetes lamprophyres and associated mafic rocks (minettes and other lamprophyres, monzonites and micromonzodiorites) as they crop out from NW to SE. Mineral species from the clinopyroxene, amphibole, epidote, carbonate, and Fe-Ti oxide groups, among others, were identified using electron microprobe (EMP) determinations. Feldspars

were also identified via EMP, but without a determination of their structural state.

## KARPACZ-JANOWICE WIELKIE DYKE SWARM (KJWDS)

### Minettes

The minettes of the Karpacz-Janowice Wielkie Dyke Swarm (KJWDS) comprise two main types: richterite minettes and "common" minettes. A specific textural variety of the latter is represented by spheroidal minettes.

Fresh richterite minettes were sampled from a dyke near the village of Bukowiec (locality 6, App. 1). Strongly altered but chemically equivalent rocks of this type were also found further south, near Kowary. The fresh specimens (Fig. 6A) represent porphyritic mesocratic rocks with abundant phenocrysts of dark mica (mainly phlogopite, minor biotite), up to 3 mm long. In places, the subparallel alignment of dark micas defines a flow foliation. Rarely, chlorite pseudomorphs after (?) olivine phenocrysts are observed. The groundmass is microcrystalline

to fine-grained, sometimes poikilitic, and consists of alkali feldspars (mainly sanidine, very minor albite), amphiboles (mainly richterite), dark micas (phlogopite), ilmenite, clinopyroxene (augite/diopside, partly chloritized), titanite, quartz and apatite.

The dark micas form euhedral to subhedral platy crystals with a distinctive zoning. Usually, the light brown cores are phlogopitic in composition, while the thin, dark brown zones at the rims are gradational towards phlogopite/biotite (normal zoning). A few phenocrysts per thin section show characteristic brown, variably corroded biotite cores, overgrown by pale-brown phlogopite (reverse zoning).

The dominant groundmass mineral is K-feldspar (nearly pure orthoclase in composition), which usually forms small plates. There are also much larger (up to 3 mm) subhedral crystals that poikilitically enclose the other rock components and sometimes also contain irregular intergrowths of Na-K-feldspar. The K-feldspars are strongly stained with hematite and contain small patches of chlorite, smectite and albite 0.01–0.02 mm in size. Albite occurs also in the interstices of the groundmass.

Amphiboles are confined to the groundmass where they form prismatic crystals. There are also aggregates of amphiboles with titanite and quartz, the latter mineral filling miarolitic interstices between euhedral amphiboles and titanites. The amphiboles are strongly zoned. In most crystals the light greenish to olive-coloured cores and mantles of richterite composition grade into pale-coloured rims of winchyste. Some crystals show incomplete overgrowths, patchy intergrowths, and contain veins of the blue amphiboles ferriwinchyste-riebeckite. In addition, the blue amphiboles are locally overgrown by acicular, greenish actinolite (Fig. 6B).

The “common” minettes crop out in several dykes. These rocks show the main textural features and modal composition as the richterite minettes, as well as similar chemical composition and zoning of the dark micas. Distinctive features of the “common minettes”, compared to the richterite minettes, are the following: the phenocryst assemblages are more variable and, apart from the dark micas, include diopside and chlorite pseudomorphs after olivine (Fig. 6C); several samples contain quartz xenocrysts with clinopyroxene reaction rims (partly chloritized); the microcrystalline groundmass is devoid of amphiboles but does occasionally contain fan-shaped to spherulitic aggregates of alkali feldspars; and the groundmass dark micas and clinopyroxenes show a stronger enrichment in Fe.

The spheroidal minettes crop out between Mysłakowice and Bukowiec, south-east of Jelenia Góra (localities 35, 36). These rocks are similar to the minettes described above, but contain abundant leucocratic domains characterized by a spherical shape having a diameter up to 5 mm (Fig. 3E). These domains consist mainly of K-rich sanidine (Or > 90%) and show felsitic to spherulitic textures. These minettes also contain prismatic apatite phenocrysts, up to 1 mm long, as well as quartz xenocrysts. Anhedral aggregates of pumpellyite associated with chlorite were identified in the groundmass in one specimen.

### Vogesites

The KJWDS vogesites are mesocratic rocks that usually show fine-grained and inequigranular textures, with the main minerals ranging from ~0.5 to 1 mm in size (Fig. 6D). Poikilitic textures, in which 2–3 mm long alkali feldspar poikilocrysts enclose euhedral prismatic amphiboles and other minerals, are common. Some specimens are strongly porphyritic (Fig. 6E) and contain abundant phenocrysts of brown amphiboles and minor amounts of chloritized dark mica. The phenocrysts are up to 2 mm long and the groundmass is microcrystalline. In well exposed dykes near Mysłakowice, south of Jelenia Góra, porphyritic textures are found in thin (cm–dm wide) vogesite veins, whereas poikilitic textures tend to occur in dykes that are a few metres thick and composite in nature.

The brown amphibole is the dominant ferromagnesian mineral. It is usually strongly zoned with compositions varying from kaersutite to titanian pargasite or magnesiohastingsite. Along the margins, there are overgrowths of magnesiohornblende and actinolite. Other ferromagnesian minerals include partly chloritized phlogopite and minor clinopyroxene (augite/diopside). In several specimens, there are only abundant chlorite pseudomorphs after these micas or clinopyroxenes, as deduced from the relict platy or prismatic habits, respectively. Some of the chloritic pseudomorphs may be after olivine.

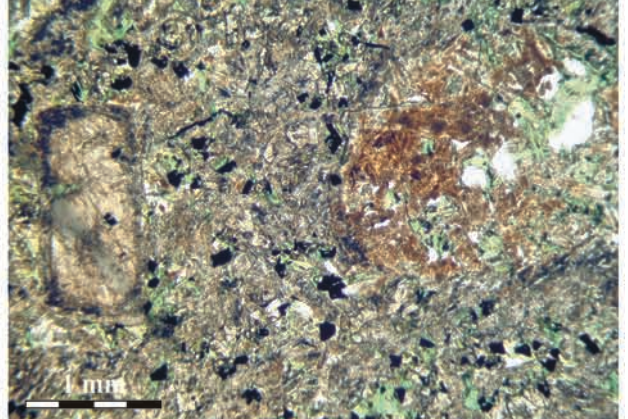
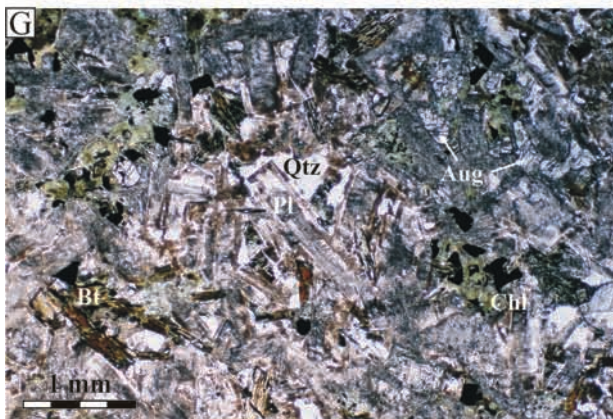
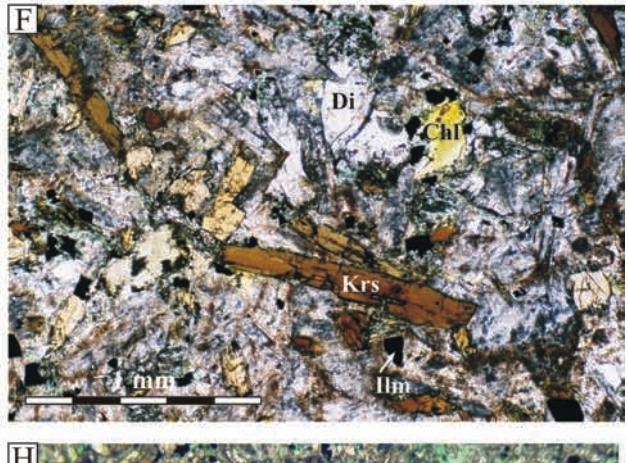
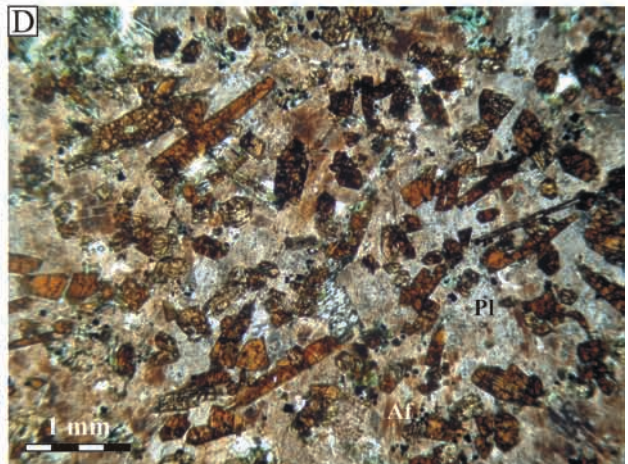
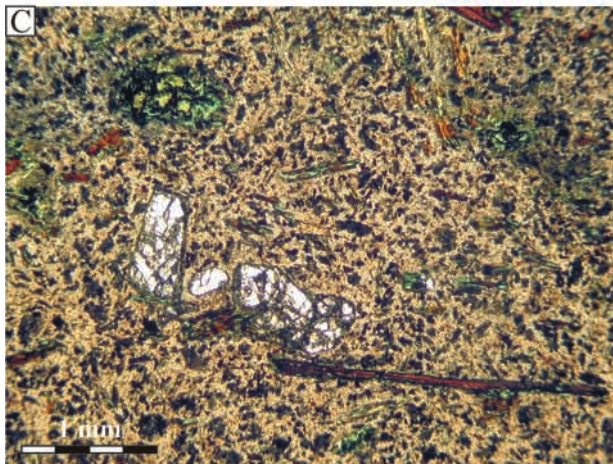
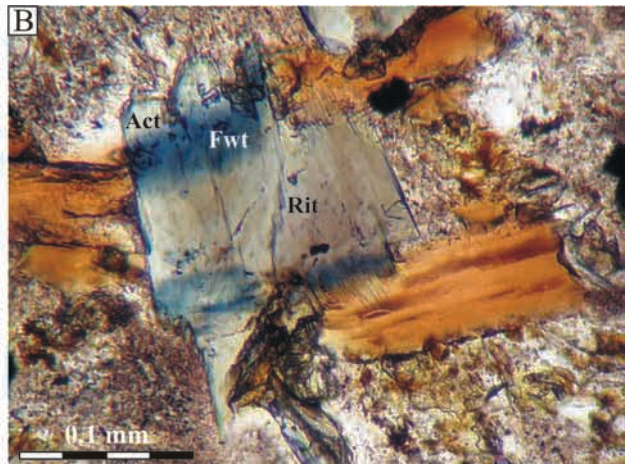
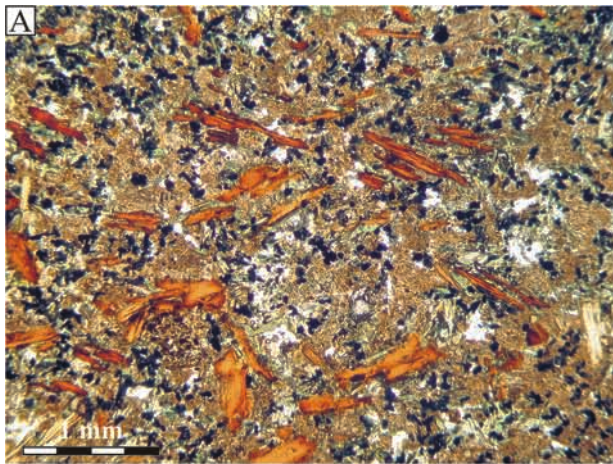
Plagioclase is a common groundmass component, forming subhedral, platy crystals that are very strongly to totally sericitized and that sometimes reveal relics of K-rich oligoclase. The volumetrically predominant alkali feldspars (mainly sanidine, more rarely albite) vary widely in form and comprise plates of variable size, larger poikilocrystals, as well as overgrowths on plagioclase and anhedral interstitial crystals.

The other mineral components of the vogesites are small, equant to elongated magnetite and ilmenite crystals, anhedral, interstitial quartz and calcite, and acicular apatite. Small grains of epidote and titanite are found in chlorite pseudomorphs and in the groundmass. Some specimens show quartz xenocrysts with reaction rims composed of clinopyroxene and opaques.

### Spessartites

The spessartites (Fig. 6F) are mesocratic rocks characterized by microcrystalline to fine-grained, weakly porphyritic textures. The rare phenocrysts are up to 2 mm long and comprise brown amphiboles and clinopyroxenes. The modal composition and the main textural features of these rocks are similar to those found in the vogesites, but the spessartites can be distinguished by the predominance of altered plagioclase over alkali feldspars; by more abundant clinopyroxene and less common dark mica, which is the reverse of that seen in the vogesites; and by more abundant and variable post-magmatic mineral assemblages.

The amphiboles form prismatic, brown crystals in which kaersutite cores grade to rims of magnesiohastingsite, magnesiohornblende and actinolite. Small biotite flakes can occur at amphibole rims. Clinopyroxenes form thick prismatic crystals and range from augite to diopside



in composition. Some crystals show embayments and oscillatory zoning. The amphiboles, pyroxenes and biotite are partly replaced by chlorite. Samples containing relatively fresh amphiboles and pyroxenes also show abundant chlorite pseudomorphs (which include intergrowths with other minerals), probably after olivine.

Feldspars form platy, euhedral crystals as well as anhedral, interstitial grains. The platy crystals are of strongly sericitized plagioclase that contain relics of andesine. In one specimen, relatively fresh crystals display a normal zonation from labradorite cores to oligoclase rims, and occasionally one observes platy crystals of albite or albite intergrown with K-feldspar. The interstitial alkali feldspars comprise albite and sanidine, both showing variable proportions of the albite and orthoclase end-members. Quartz forms anhedral, interstitial grains in the groundmass.

The minor minerals of the spessartites include Ti-magnetite, ilmenite and apatite. Common post-magmatic minerals – found in pseudomorphs, in the groundmass, and often as very fine-grained aggregates of several phases – include chlorite, calcite, titanite, epidote-group minerals and actinolite. In addition, pumpellyite was detected in three specimens of spessartite, and prehnite and garnet (grossularite–andradite) in two others.

#### Monzonites and micromonzodiorites

Monzonites and micromonzodiorites form numerous dykes in the KJWDS. The textures of these rock types range from medium- or fine-grained to microcrystalline and from inequigranular to porphyritic. Porphyritic textures typically characterise the micromonzodiorites, but such textures also occur in the chilled margins of monzonite dykes. The characteristic features that distinguish the monzonites and micromonzodiorites from the lamprophyres are the presence of feldspar phenocrysts and a lack of dark mica or amphibole phenocrysts.

The monzonites (Fig. 6G) are usually fine-grained, mesocratic to leucocratic rocks. Their main components are feldspars. Plagioclase forms both platy and lath-shaped crystals that are strongly sericitized, with rare relics of an-

desine–oligoclase composition. Platy plagioclases may have K-rich sanidine overgrowths, and K-rich sanidine itself may occur as fine-grained, interstitial micrographic and granophyric intergrowths with quartz.

The ferromagnesian silicates comprise biotite and augite, usually partly altered. Augite is mainly replaced with chlorite and acicular amphiboles (magnesiohornblende to ferroactinolite) that occur along crystal margins and within cracks. Biotite is partly replaced along its cleavage planes by chlorite associated with Ca–Fe garnet (grossularite–andradite) and prehnite (Fig. 20D). Other common minerals are ilmenite and apatite.

The micromonzodiorites (Fig. 6H) are mesocratic rocks usually characterized by porphyritic textures and a microcrystalline groundmass. The phenocrysts are up to 2 mm long and comprise altered plagioclase, augite and chlorite pseudomorphs, probably after olivine. The altered plagioclase and augite are also the main groundmass components where they form smaller, euhedral to subhedral, prismatic crystals 0.5–0.1 mm long. Leucocratic enclaves (ocellae) composed mainly of subhedral to anhedral alkali feldspars are found in many specimens (Fig. 6H).

Plagioclase is strongly replaced by sericite accompanied by very fine-grained aggregates of prehnite and (?)titanite. Rare relics of magmatic plagioclase reveal a composition of labradorite or oligoclase/albite. Alkali feldspars of variable composition (sanidine, albite) overgrow the altered plagioclase and form interstitial aggregates. Augite comprises small, relatively homogeneous grains, but the larger crystals display sieve textures and small intergrowths of amphiboles (Mg-hornblende, actinolite and ferroactinolite) in the cores, and oscillatory and sector zoning in the outer parts. Other groundmass components are sanidine, quartz, ilmenite, titanite, chlorite, calcite, clinozoisite and, rarely, brown amphiboles. In addition, small crystals of prehnite and post-magmatic Ca–Fe garnets (grossularite–andradite) are found in the groundmass feldspars and in some chlorite pseudomorphs (Fig. 20B).

Many micromonzodiorite specimens contain inclusions (Fig. 3F and G). Very common are glomerocrystals and fine-grained magmatic enclaves (Fig. 7A) that are composed of tens to hundreds of augite crystals, strongly

**Fig. 6.** Photomicrographs of lamprophyres and other mafic rocks of the Karpacz–Janowice Wielkie Dyke Swarm. All photos are in plane-polarized light. (A) Richterite minette with phenocrysts of phlogopite in a groundmass mostly of K-feldspar, richterite, opaques and quartz. (B) Zoned amphibole crystal (Rit – richterite; Fwt – ferriwinchyte; Act – actinolite) in the groundmass of the richterite minette. Same specimen as (A). (C) Minette with phenocrysts of red-brown phlogopite/biotite (partly chloritized), diopside and chlorite pseudomorphs (after ?olivine). The groundmass mainly consists of alkali feldspars, opaques and chlorite pseudomorphs. (D) Fine grained to microcrystalline vogesite composed of euhedral, brown amphiboles (mainly kaersutite), alkali feldspars (Af) and sericitized plagioclase (Pl). The texture is inequigranular and in places poikilitic, with larger alkali feldspar poikilocrystals enclosing the other minerals. (E) A group of euhedral, brown-coloured amphibole phenocrysts (kaersutite to pargasite to magnesiohastingsite) in a vogesite. The microcrystalline groundmass consists of alkali feldspars, chlorite, opaques and minor quartz. (F) Spessartite composed of larger, euhedral kaersutite (Krs) crystals in a groundmass of feldspars (sericitized plagioclase, minor alkali feldspars), diopside (Di), chlorite pseudomorphs (Chl) and ilmenite (Ilm). (G) Monzonite. The main minerals visible are strongly sericitized plagioclase laths (Pl) with thick overgrowths of alkali feldspars; quartz (Qtz); augite (Aug); partly altered biotite (Bt) with intergrowths of chlorite, prehnite and garnet (cf. Fig. 20D); chlorite pseudomorphs (Chl); and opaques. (H) Micromonzodiorite with a phenocryst of sericitized plagioclase (left side of photo) in a groundmass of the smaller altered plagioclase laths with less abundant augite, chlorite, alkali feldspars and opaques. A small ocellus composed of haematite-stained alkali feldspars, chlorite and quartz is seen on the right side of photo. See Fig. 20B for a detailed back scattered electron (BSE) image of the groundmass.

sericitized feldspar with relics of oligoclase to albite composition, and chlorite pseudomorphs after, presumably, olivine. The modal composition of these enclaves is equivalent to the phenocryst assemblage of the micromonzodiorites.

Rarely encountered enclave types include fine-grained, felsitic enclaves, which are texturally and modally variable. One felsitic enclave, cm–dm in size, is strongly folded and partly mingled with the host (Fig. 3F). This enclave shows a leucogranitic/rhyolitic composition and comprises subhedral quartz, alkali feldspars and plagioclase. These minerals are rimmed/separated by thin zones

of haematite-stained microcrystalline alkali feldspar and quartz (Fig. 7B). Another small enclave, ~10 mm in diameter (Fig. 7C), is composed mainly of Na-rich feldspar (anorthoclase) which, toward the central part of the enclave, becomes poikilitic and contains patches with numerous inclusions of sillimanite, biotite and Al-rich spinel (hercynite). Minor sericite and chlorite aggregates may represent pseudomorphs after some other mineral phases.

## INTRA-SUDETIC BASIN (ISB)

### Minettes

The minettes of the Intra-Sudetic Basin (ISB; Fig. 8A) are mesocratic rocks characterized by porphyritic textures and fine-grained to microcrystalline groundmass. The phenocrysts are mainly dark mica plates, up to 5 mm long, but, more rarely, can be carbonates and chlorites pseudomorphing ferromagnesian silicates. Dark micas, carbonate–chlorite pseudomorphs, alkali feldspars and plagioclase are the main components of the groundmass, with smaller amounts of ilmenite, magnetite and apatite.

The dark mica phenocrysts form euhedral to subhedral, sometimes corroded plates displaying a normal zoning of pale-brown to orange phlogopitic cores overgrown by thin zones of deep-brown biotite (Fig. 8A). Interestingly, the phlogopites often reveal polysynthetic twinning similar to that found in the tetraferriphlogopites of lamproites: the twin planes are parallel to the (001) cleavage planes of mica, and the adjacent lamellae are distinguished due to slightly different pleochroic colours (cf. Mitchell, 1997). In addition, some dark micas show reverse zoning of rounded, brown-coloured biotitic cores overgrown by pale-brown phlogopite that itself is rimmed by a darker biotite (Fig. 8B).

The carbonate–chlorite pseudomorphs after ferromagnesian silicates vary in size, habit, fracture patterns and the mutual arrangements of the component minerals. Some of them contain chromite inclusions. The pseudomorphs probably formed at the expense of olivine and

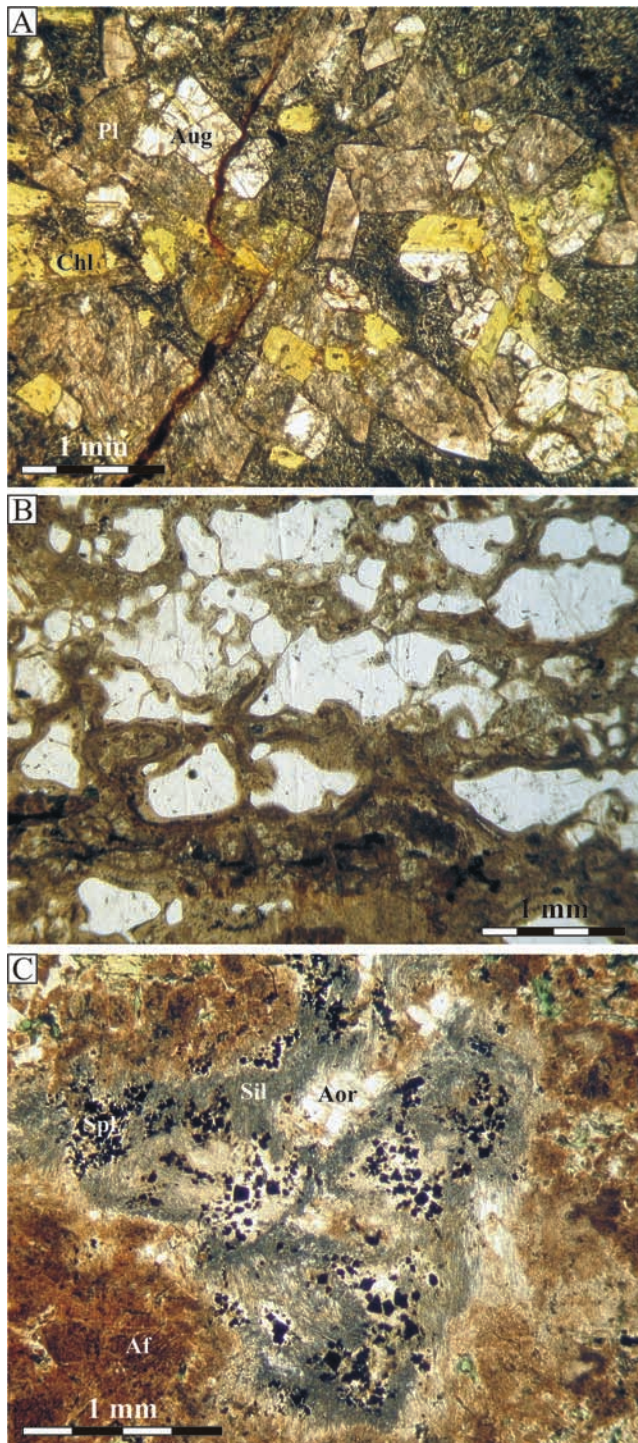
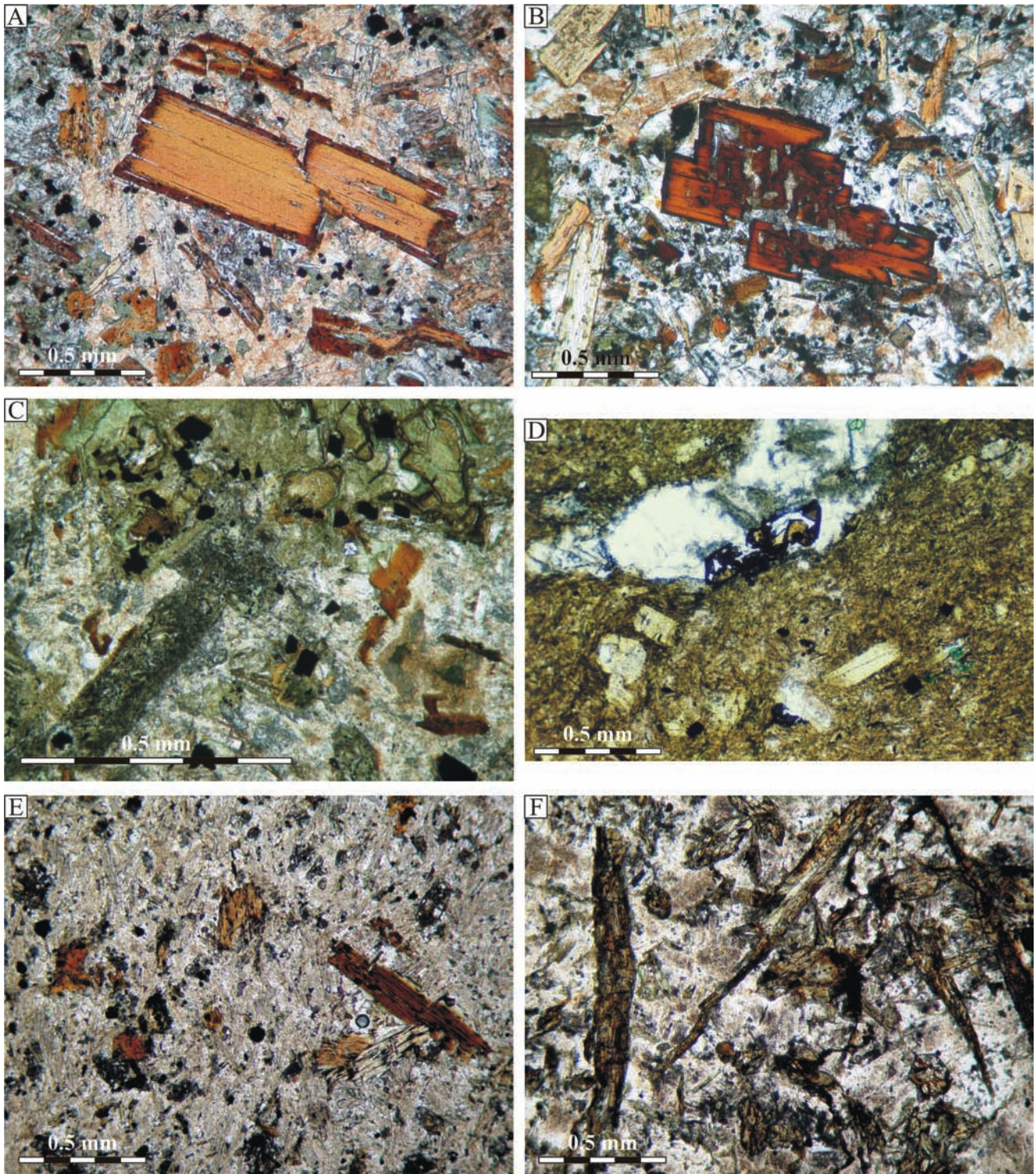


Fig. 7. Plane-polarised light photomicrographs of enclaves from the micromonzodiorites in the Karpacz–Janowice Wielkie Dyke Swarm. (A) Cognate enclave, composed of altered plagioclase (Pl), chlorite pseudomorphs (Chl) and fresh augite (Aug). To the right, the enclave grades into a glomerocrystic aggregate with a more loose packing of crystals and with a more abundant, quench-textured, opaque-rich, microcrystalline groundmass. A similar enclave is shown near the lower right corner of Fig. 3G. (B) Marginal part of the felsic flow-folded enclave shown in Fig. 3F. The enclave consists of embayed, clear quartz crystals surrounded by bands of haematite-stained, microcrystalline alkali feldspars, and less abundant sericitized plagioclase. (C) A small restitic enclave with a concentric structure. The outer part is mainly composed of haematite-stained alkali feldspars (Af), and the inner part consists of a more clear, poikilitic anorthoclase (Aor) with numerous needles of sillimanite (Sil), abundant spinel inclusions (Spl), and, though not well seen in this photo, small biotite flakes and abundant sericite.



**Fig. 8.** Photomicrographs of lamprophyres and altered mafic rocks from the Intra-Sudetic Basin (A-D) and from the Góry Sowie Block (E, F). (A) Minette showing euhedral phlogopite phenocryst with thin overgrowth of darker biotite. The groundmass of this minette is composed of smaller dark micas, alkali feldspars, plagioclase (andesine), carbonates, chlorites, opaques and apatite. (B) The same minette as (A), showing a corroded and complexly zoned dark mica phenocryst that has a biotitic core mantled by phlogopite and rimmed by biotite. (C) Altered mica lamprophyre composed of carbonate–chlorite pseudomorphs after Fe–Mg silicates, opaques and biotite in a matrix of alkali feldspars, carbonates and apatite. (D) Altered mafic rock. Chlorite pseudomorphs after ferromagnesian mineral phenocrysts are set in a carbonate–chlorite–albite groundmass with small opaque grains. A big irregular amygdale in the upper part of this photo is filled with calcite and quartz with a larger, skeletal, crystal of a  $\text{TiO}_2$  polymorph (?anatase). (E) Kersantite composed of dark mica phenocrysts, intermediate between phlogopite and biotite in composition, set in a groundmass of altered plagioclase, alkali feldspars, partly chloritized augite and opaques. (F) Spessartite composed of prismatic, partly altered amphiboles, altered plagioclase, alkali feldspars, quartz and opaques.

possibly amphibole and pyroxene, but no relics of these primary phases are found.

The feldspars vary in their habit and composition. Plagioclase of andesine composition forms plates and laths and displays weak normal zoning. Similar euhedral laths are also characteristic of Na-K feldspar (sodic sanidine). Both andesine and sodic sanidine laths are overgrown by Na-rich alkali feldspar (anorthoclase), and the anhedral, interstitial feldspars comprise sanidine and albite. Plagioclase is subordinate with respect to the alkali feldspars. In more strongly altered minettes, plagioclase laths are partly albitized.

In some specimens, there are quartz xenocrysts with reaction rims composed of chlorites and opaques. The two latter minerals most likely replace the original clinopyroxene. There are also two types of rare enclaves (<3 cm in size). First, there are fine grained, ultramafic magmatic enclaves that grade into glomerocrysts and are composed of phlogopites and of carbonate-chlorite pseudomorphs after olivine and/or pyroxene. The phlogopites are homogeneous to normally zoned and equivalent in composition to the dominant phenocrysts in the minettes. Second, there are fine-grained, leucocratic magmatic enclaves of a trachytic composition, which mainly consist of radiating aggregates of sodic sanidine laths and minor amounts of interstitial anhedral albite, quartz, small biotite flakes and opaque grains.

#### Altered mica lamprophyres and other mafic rocks

The altered mica lamprophyres form a short dyke close to the rhyodacites of the Chełmiec laccolith, west of Wałbrzych. These rocks (Fig. 8C) are characterized by an almost complete alteration of their primary igneous phases, with only rare relics of biotite, chromite and, possibly, some alkali feldspars. All other components are pseudomorphed.

These rocks show inequigranular to porphyritic textures and a fine-grained groundmass. The largest pseudomorphs (phenocrysts) after Fe-Mg silicates are up to 5 mm long, but usually do not exceed 1 mm. These pseudomorphs are of carbonates (calcite and ankerite) and chlorites with small inclusions of opaques, including Fe-Ti oxides and chromite. The variable textures and secondary mineral proportions of these pseudomorphs suggest they formed at the expense of olivine (e.g. Fig. 20F), but also of other Fe-Mg minerals. Brown-coloured biotite is mainly found in the groundmass where it forms euhedral to subhedral plates. The groundmass also contains lath-shaped and anhedral alkali feldspars (albite to sanidine). Some feldspar laths are probably albitized plagioclase. Another component of these rocks is apatite, which occurs as thin prismatic crystals up to 0.7 mm long. There are also numerous opaques, usually inhomogeneous and composed of ilmenite intergrown with a TiO<sub>2</sub> phase (?brookite or anatase). The groundmass contains small carbonate grains (mainly ankerite), quartz grains and chlorite flakes.

The ISB altered mica lamprophyres were previously classified as kersantites (Bossowski & Czerski, 1985). In fact, very similar petrographic and geochemical characteristics are found in less altered kersantites described herein

from the Gniewosów Dyke Swarm. However, the ISB altered mica lamprophyres also show some similarities to minettes from the vicinity of Kamienna Góra: similar pseudomorphs after the Fe-Mg minerals and some geochemical characteristics. Due to the unclear petrographic affinity of these rocks, the term "altered mica lamprophyre" is used here.

The altered mafic rocks, sampled from a few dykes in the sedimentary rocks of the Intra-Sudetic Basin and the Bardo Unit (localities 44, 45, 46, 51) are almost devoid of any original igneous minerals and are composed of various types of pseudomorphs (e.g., Fig. 8D). All the altered mafic rocks are porphyritic with a microcrystalline groundmass. The phenocrysts are now chlorite-carbonate pseudomorphs, up to 2 mm long, with a variable habit and internal textures. These pseudomorphs possibly formed from olivine and other Fe-Mg silicates. Some of the altered mafic rocks contain completely albitized and strongly corroded phenocrysts (and xenocrysts?) of feldspars, and some samples show amygdaloidal textures and contain aligned to irregular vesicles filled with carbonates, chlorites and quartz. The groundmass of the altered mafic rocks consists of albite laths with interstitial alkali feldspars, carbonates, chlorites, opaques and quartz. A characteristic component of some pseudomorphs and amygdaloids in the mafic rocks from Koczan hill (locality 44) are relatively big (0.5 mm long) euhedral TiO<sub>2</sub> crystals (?anatase; Fig. 8D).

The geological setting and some of the geochemical characteristics of the altered mafic rocks from the area west of Wałbrzych suggest links with some Carboniferous volcanic rocks of the Intra-Sudetic Basin, namely, the Borówno basaltic andesites and the Nagórnik andesites (Awdankiewicz, 1999a). Nevertheless, these latter andesitic rocks contain abundant plagioclase phenocrysts, which are rather exceptional in the altered mafic rocks described above. The altered mafic rocks from the eastern part of the Intra-Sudetic Basin can, however, be correlated with the kersantites of the Góry Sowie Block, mainly based on geochemical similarities. The mafic rocks discussed here might be gradational between lamprophyres and their volatile-poor equivalents (like andesitic or shoshonitic rocks), but detailed petrographic classification is hampered by the very strong alteration.

## GÓRY SOWIE BLOCK

### Kersantites and spessartites

The kersantites of the Góry Sowie Block are meso- to leucocratic rocks having a colour index of 40 to 29%, which straddles the lower limit for lamprophyres (33%). However, except for the lower colour index, the more leucocratic samples show very similar petrographic, mineralogical and geochemical features as those of the more mafic samples.

The more mafic kersantites (Fig. 8E) are moderately to weakly porphyritic with a microcrystalline groundmass. The phenocrysts are up to 1.5 mm long, and the main groundmass components are ~0.1–0.2 mm in size.

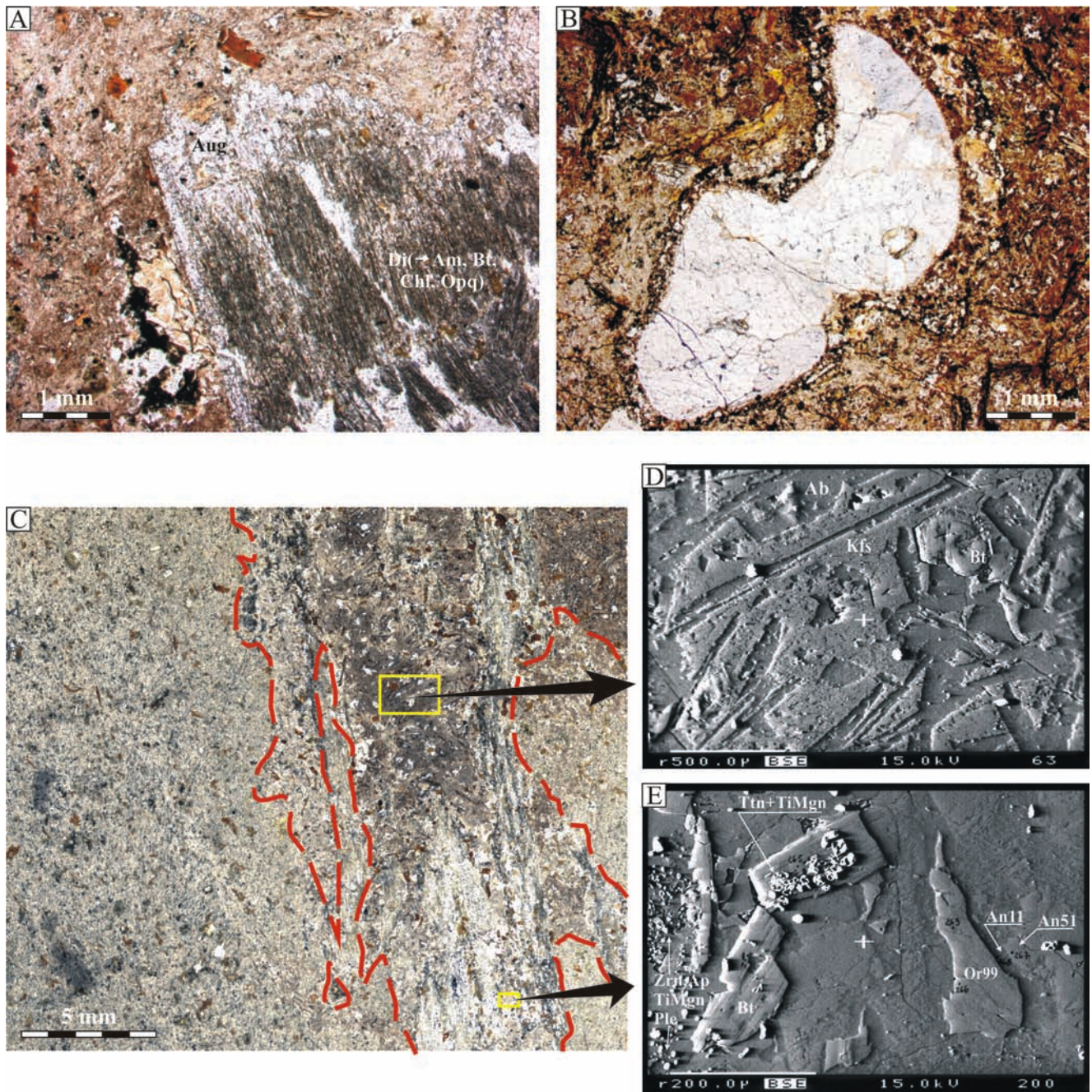


**Fig. 9.** Examples of inclusions from the kersantites of Ostrzew Hill in the Góry Sowie Block at locality 52. (A) Fragment of a clinopyroxene macrocryst ( $\sim 10$  mm in total size) with a strongly altered core which consists of diopside (Di) intergrown with amphiboles (Am), biotite (Bt), chlorite (Chl) and opaques (Opq), and a more clear rim of augite (Aug) composition. Photomicrograph, plane polarized light. (B) Embayed quartz xenocryst with a reaction rim of a microcrystalline intergrowth of augite, biotite, amphiboles, chlorite and opaques. Photomicrograph, plane polarized light. (C) A composite, banded enclave with an irregular outline (highlighted with red broken line) partly mingled with the kersantite host. Scanned thin section, transmitted light; the enclave comprises various domains illustrated in the back scattered electron (BSE) images of (D) and (E). (D) BSE image of a domain with trachytic/microsyenitic composition and containing abundant albite laths (Ab), anhedral K-feldspar (Kfs), minor biotite (Bt) and, locally, quartz. (E) BSE image of a domain of microdioritic/andesitic composition, which consists of corroded, sieve textured and variably zoned plagioclase (An11-51), corroded K-feldspar (Or99), and biotite (Bt). Some biotites and feldspars represent poikilocrystals containing numerous inclusions of zircon, apatite, Ti-magnetite, pleonast, titanite (Zrn, Ap, TiMgn, Ple, Ttn, respectively) and other minerals.

The phenocrysts are mainly of dark mica, transitional in composition between biotite and phlogopite. More rarely, there are phenocrysts of clinopyroxene (diopside to augite), amphibole (brown-coloured titanian magnesiohastingsite to edenite, with rims of magnesiohornblende and actinolite) and chlorite pseudomorphs, probably after olivine. The dark micas, amphiboles and clinopyroxenes, which are chloritized to varying degrees, also occur also in the groundmass; however, the main groundmass components are feldspars. These are, mainly, strongly albitized and sericitized plagioclase laths, with locally preserved relics of original andesine–oligoclase and some indistinct zoning. Anhedral interstitial alkali feldspars, and alkali feldspar intergrowths in altered plagioclase laths, vary in composition from pure albite to pure orthoclase. The other, less abundant components of the kersantites comprise quartz, opaques (ilmenite and magnetite), apatite, titanite, carbonates and clay minerals (?smectites). At some localities (56–58, App. 1), the kersantites are strongly altered: the plagioclase is completely albitized, the Fe–Mg silicates are replaced by chlorite, and euhedral pyrite occurs in the groundmass.

Felsic kersantites are found in the Fore-Sudetic part of the Góry Sowie Block (localities 59, 60, App. 1). These rocks are distinguished by larger biotite phenocrysts (5–10 mm), strong sericitization of plagioclase and, in some specimens, plagioclase phenocrysts. The felsic composition and the rare feldspar phenocrysts indicate a gradation into microdioritic/andesitic rocks.

The kersantites cropping out at the Ostrzew Hill (locality 52, App. 1) represent the more mafic type and are rich in inclusions, which range from single crystals (macrocrysts) through crystal aggregates to small enclaves (Fig. 9). Usually several inclusion types are found in a single rock sample. Some macrocrysts are up to 15 mm long and some enclaves are up to 50 mm in size. The macrocrysts display embayments, reaction rims and sieve textures – evidence of disequilibrium with the host kersantite. Enclaves are often inhomogeneous with respect to their texture and composition (e.g., banded) and are partly disintegrated and mingled with the host kersantites. The most characteristic types of inclusions are as follows: macrocrysts of diopside that are partly resorbed, are strongly intergrown with biotite, amphiboles and chlorites, and are rimmed by augite (Fig. 9A); macrocrysts of feldspars, which are oval-shaped, inhomogeneous, sieve-textured and composed of intergrown andesine and sodic to potassic feldspars; xenocrysts and polycrystalline aggregates of embayed quartz with reaction rims of clinopyroxene, amphibole and other minerals (Fig. 9B); felsitic enclaves (ocellae) of microsyenite/trachyte composition, some with reaction rims similar to those around quartz xenocrysts; and compound enclaves with domains or bands of distinctive composition and textures, including corroded, sieve textured and poikilitic feldspars and biotites, and Al-spinel inclusions (Fig. 9C, D, E).

Spessartite samples were collected north of Rościszów (locality 61 App. 1). These spessartites (Fig. 8F) are characterized by a sparsely porphyritic texture with a micro-crystalline groundmass. Rare, brown hornblende pheno-

crysts are up to 2 mm long. Along the rims and cracks, hornblende is partly replaced by chlorite, opaques, and greenish acicular actinolitic amphiboles. The groundmass consists mainly of plates and laths of plagioclase, which is strongly albitized, sericitized and stained with a hematite pigment. In addition, the groundmass contains small prismatic hornblende crystals, strongly chloritized plates of biotite, anhedral alkali feldspars, anhedral quartz, fine grains of opaques, acicular apatite and fine-grained aggregates of post-magmatic minerals, possibly epidote-group minerals, carbonates and titanite. These petrographic characteristics closely resemble the spessartites from the Złoty Stok Dyke Swarm.

## ZŁOTY STOK DYKE SWARM (ZSDS)

### Vogesites

The vogesites of the Złoty Stok Dyke Swarm (ZSDS) are mesocratic rocks. Two characteristic types that can be distinguished are the coarsely porphyritic vogesites (Fig. 10A), and the finely porphyritic vogesites (Fig. 10B). The coarsely porphyritic vogesites contain abundant phenocrysts of amphiboles and clinopyroxenes, up to 3 mm long, and they also contain quartz and biotite xenocrysts. The finely porphyritic vogesites contain smaller (<2 mm), sparse phenocrysts of amphibole, clinopyroxene and pseudomorphs after (?)olivine. The groundmass in both types is similar and consists mainly of amphiboles and alkali feldspars. The alkali feldspars form small laths as well as anhedral crystals and comprise K-rich sanidine, anorthoclase and albite. Some sericite–albite laths represent pseudomorphs after plagioclase. In addition, there are small crystals of Fe–Ti oxides (Ti-magnetite, chromite), apatite and small amounts of interstitial quartz.

The amphibole phenocrysts of the coarsely porphyritic vogesites are euhedral and distinctly zoned. These phenocrysts consist of large, rounded, olive-green cores (mainly tschermakite to magnesiohastingsite) with pale-greenish overgrowths (magnesiohastingsite enriched in Mg). Groundmass amphiboles have the same composition as the rims of the phenocrysts. Amphiboles in the finely porphyritic vogesites are euhedral magnesiohastingsites that pass into rims of magnesiohornblende or pargasite; in places, these amphiboles contain thin intergrowths of actinolite.

Clinopyroxenes in both vogesite types are Ca-rich augites that grade to diopside. Clinopyroxene phenocrysts in the coarsely porphyritic vogesites often show sieve-textured cores containing groundmass inclusions, while the rims are more homogeneous. Clinopyroxene phenocrysts in the finely porphyritic vogesites are partly altered and replaced by carbonates along the rims and internal cracks.

Biotite xenocrysts in the coarsely porphyritic vogesites are euhedral to subhedral and brown-coloured. These crystals show rounded edges, corrosional embayments, thin opaque-rich marginal zones, and are partly chloritized along the cleavage planes and rims (Fig. 10A). Many crystals also contain thick intergrowths of prehnite. There is probably a reverse zoning expressed by a rimward gra-

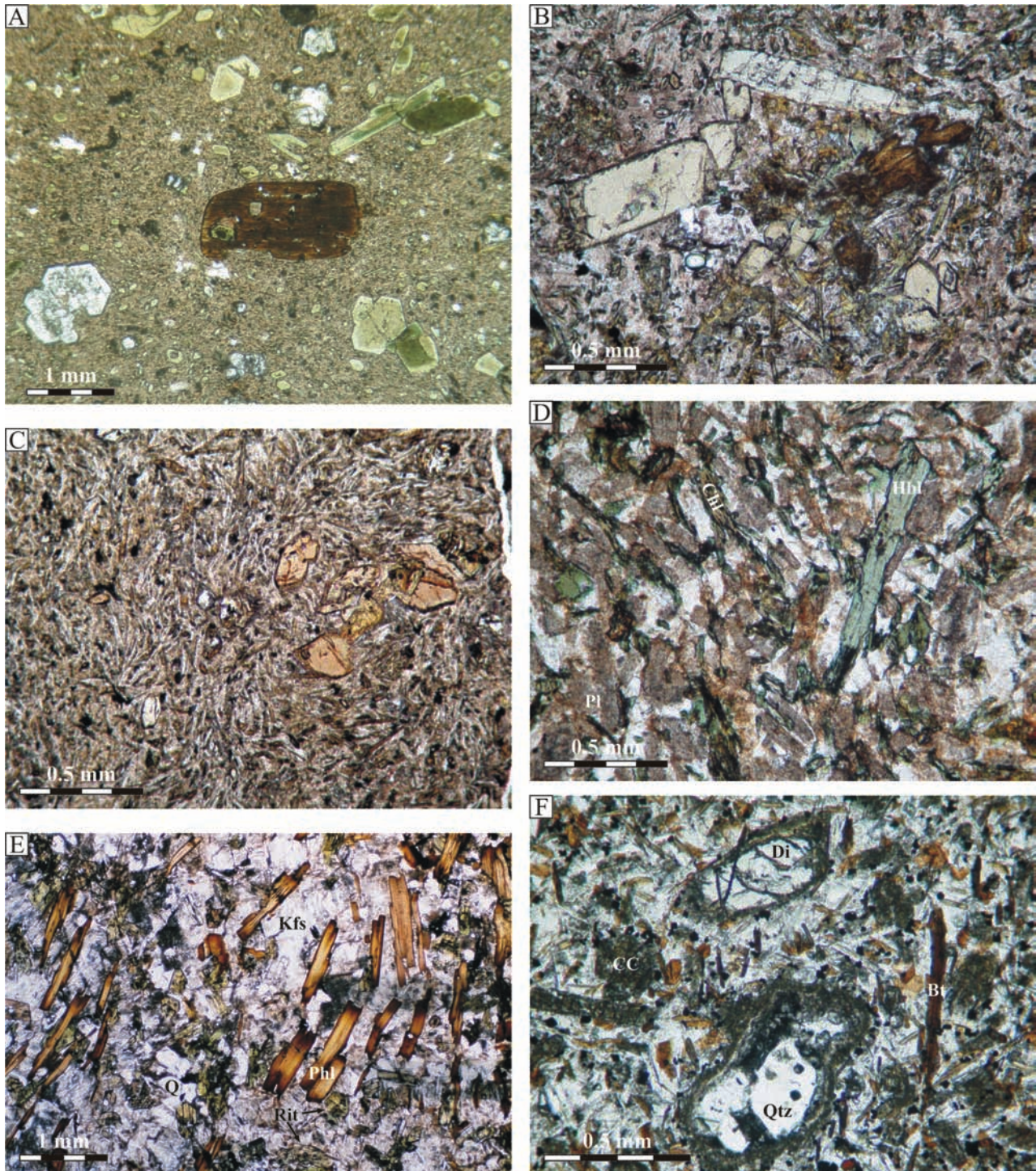


**Fig. 10.** Plane-polarized light photomicrographs of the mafic rocks from the Złoty Stok Dyke Swarm (A-D) and from the Gniezów Dyke Swarm (E and F). (A) Coarsely porphyritic vogesite with phenocrysts of zoned, green coloured amphiboles (magnesiohastingsite, tschermakite), augite (near the lower left corner, corroded) and rounded, partly chloritized biotite xenocryst (centre of photo). The microcrystalline groundmass consists of alkali feldspars and small amphiboles and clinopyroxenes. (B) Amphibole phenocrysts (magnesiohastingsite) and a chlorite-pumpellyite pseudomorph after (?)olivine in the finely porphyritic vogesite. The groundmass is composed mainly of alkali feldspars and amphiboles. (C) Spessartite with amphibole phenocrysts (magnesiohastingsite) in a groundmass of the same mineral and alkali feldspars. (D) Micromonzodiorite composed of sericitized plagioclase (Pl) laths with relics of oligoclase composition; green magnesiohornblende (Hbl); chloritized biotite (Chl); and interstitial, anhedral alkali feldspars and quartz. (E) Richterite minette. Numerous euhedral phlogopite (Phl) crystals, which are zoned to biotite near the rims, are set in K-feldspar (Kfs). There are also abundant smaller, prismatic richterite (Rit) crystals and, locally, quartz (Q). The texture of this minette is poikilitic: the area shown is occupied by 4–5 large K-feldspar crystals that enclose all the other minerals. (F) Kersantite with phenocrysts of biotite (Bt) and diopside (Di), and with embayed quartz (Qtz) xenocryst, in a groundmass of smaller plagioclase laths, biotite plates, isometric opaques and anhedral alkali feldspars and quartz. Abundant chlorites and carbonates, usually in intimate intergrowths (CC), are found in the groundmass, along the rims and cracks in the diopside phenocryst, and along the margins of the quartz xenocryst.

dation into phlogopite, but this is partly obscured due to the more intense chloritization near the rims. Quartz xenocrysts in these vogesites are oval and embayed, with thin reaction rims of numerous prismatic clinopyroxene crystals. There are also small (a few mm in size), fine-grained magmatic enclaves, composed of quartz, alkali feldspar, altered interstitial glass(?) and clinopyroxene crystals concentrated near the enclave margins. Both vogesite types contain pseudomorphs after a ferromagnesian mineral, probably olivine, of chlorites or very fine-grained aggregates of other minerals. Pumpellyite was found in one pseudomorph in the finely porphyritic vogesite.

### Spessartites

The spessartites (Fig. 10C) are mesocratic rocks that show porphyritic to nearly aphyric textures and a microcrystalline groundmass. The phenocrysts are mainly amphiboles and, more rarely, clinopyroxenes; the groundmass is of amphiboles and altered plagioclase. In terms of textures, modal composition and mineral chemistry, the spessartites of the ZSDS are similar to the finely porphyritic vogesites described above. The main difference is the much higher abundance of altered plagioclase in the groundmass.

The amphiboles, both phenocrysts and smaller groundmass crystals, are represented by pale-brown to greenish magnesiohastingsite or tschermakite. Some crystals show weak zoning and contain intergrowths and overgrowths of magnesiohornblende and actinolite. The clinopyroxenes are Ca-rich augites that grade to diopside. The main groundmass feldspar is plagioclase, and this is strongly sericitized and/or albitized. Plagioclase relics from one sample were analyzed as labradorite. Interstitial alkali feldspars comprise albite as well as sanidine. The groundmass also contains anhedral interstitial quartz. In addition, spinels of various compositions (Ti-magnetite, Al-spinel, chromite) occur as small inclusions in phenocrysts and in the groundmass. There are also post-magmatic minerals which are developed along the rims and cracks of amphiboles and pyroxenes, and occur also as groundmass aggregates. Calcite, chlorites and epidote-group minerals are the most common; pumpellyite and prehnite are less so.

Some spessartite specimens contain minor phenocrysts of altered plagioclase in addition to the amphibole and clinopyroxene phenocrysts. This indicates a petrographic gradation into micromonzodiorite/andesite. However, the mineralogical and the whole-rock chemical characteristics are essentially the same, irrespective of the presence or absence of these plagioclase phenocrysts. Both the mineralogical and geochemical characteristics of the spessartites are different from the typical micromonzodiorites described below.

### Micromonzodiorites

The micromonzodiorites (Fig. 10D) are meso- to leucocratic rocks with the colour index of ~30%. They are porphyritic to aphyric, and fine-grained to microcrystalline. Where present, the phenocrysts are up to 2 mm long and are of plagioclase, magnesiohornblende and biotite. In

some micromonzodiorites, these latter minerals form glomerocrysts and small enclaves. Plagioclase is strongly sericitized, but relics of oligoclase are preserved. The amphiboles and dark micas are variably chloritized. Sericitized plagioclase laths, small magnesiohornblende prisms and biotite plates are the main groundmass components, together with minor amounts of interstitial K-feldspar and quartz, and small crystals of Fe-Ti oxides, titanite and apatite.

## GNIEWOSZÓW DYKE SWARM (GDS)

### Minettes

Similar to the KJWDS, the minettes of the Gniewoszów Dyke Swarm (GDS) comprise richterite minettes, as well as the more common, richterite-free types. The richterite minettes from the vicinity of Gniewoszów (localities 67 and 70, App. 1) are mesocratic porphyritic rocks with dark mica phenocrysts, up to 3 mm long, in a microcrystalline to fine-grained groundmass. The main groundmass components are smaller plates of phlogopite, as well as amphiboles and K-feldspars. Several of the minettes are medium-grained and characterized by well developed K-feldspar poikilocrysts up to 5 mm long. These large K-feldspars enclose smaller, aligned crystals of phlogopite and richterite (Fig. 10E).

The mica phenocrysts are pale brown phlogopites that get strongly zoned near their rims, where they pass into a dark-brown biotite. Other, rarer phenocrysts, are pseudomorphs (after olivines or pyroxenes) of carbonates and talc that contain inclusions of chromite-magnesiochromite. The amphiboles form thick prismatic groundmass crystals of richterite, with pleochroic colours ranging from pale yellowish-green to pinkish-brown. The cores of many amphiboles enclose small, oval pseudomorphs of talc; near the margins richterite grades into winchytite; locally, there are overgrowths of actinolite. The groundmass K-feldspar is K-rich sanidine, many crystals of which are inhomogeneous and, apart from haematite-stained patches, contain micropertthites ~1–2 microns wide and patches and veinlets of albite. Other components of the GDS minettes are euhedral to subhedral, up to 1 mm long, crystals of ilmenite, titanite, apatite and anhedral, interstitial albite and quartz.

Similar richterite minettes also crop out near Darnków, east of Kudowa Zdrój, and near Łądek Zdrój (localities 62 and 94). The richterite minettes from Darnków are fine-grained phlogopite-phyric rocks distinguished by acicular and skeletal groundmass amphiboles (potassic richterite and potassic eckermanite). The richterite minettes from Łądek Zdrój show similar petrographic characteristics to the Gniewoszów minettes, but also contain groundmass diopside (Wierzchołowski, 1979).

The richterite-free minettes of the GDS possess a more felsic modal composition and a more common post-magmatic alteration. This alteration is mainly expressed by a variable replacement of phlogopite by chlorite and opaques.

### Kersantites and spessartites

The kersantites are found at one locality (72, App. 1) ~10 km east of the main outcrops of the GDS. These meso- to melanocratic rocks are rich in ferromagnesian minerals and pseudomorphs after these minerals (colour index ~65%), and are porphyritic with phenocrysts up to 2 mm long and with a microcrystalline groundmass (Fig. 10F). The phenocrysts are pseudomorphs after olivine (composed of carbonates with inclusions of chromite), diopside partly replaced by carbonates, and dark mica that grades between biotite and phlogopite. There are also rare quartz xenocrysts with reaction rims of clinopyroxenes that themselves are partly replaced by carbonates. Diopside and dark micas are also abundant in the groundmass.

The main light-coloured mineral in the groundmass is plagioclase. It forms lath-shaped crystals that are normally zoned from labradorite cores to andesine rims. Plagioclase laths are overgrown by K–Na alkali feldspars (anorthoclase to sodic sanidine). Anhedronal alkali feldspars with quartz also occur interstitially. Minor components of the kersantites are acicular apatites and small grains of Fe–Ti oxides.

Only one spessartite specimen was collected from within the GDS (locality 69, App. 1). This spessartite shows similar petrographic characteristics to the spessartites of the ZSDS, but it is strongly altered: the ferromagnesian minerals are chloritized, and the plagioclase is sericitized.

## MINERAL CHEMISTRY

### DARK MICAS

The dark micas represent the main Fe–Mg silicates in the Sudetic minettes and kersantites, where they form both phenocrysts and groundmass crystals. Other mafic rock types of this study contain only small amounts of dark mica, usually in the groundmass. In total, 263 analyses of dark micas were obtained. Representative analyses are given in Appendix 2 and the general chemical variation is shown in Figure 11.

The micas that were analyzed are phlogopites and biotites, and their relatively wide ranges of Mg, Fe and Al ratios (Fig. 11A) are similar to the values found in lamprophyre micas worldwide (Fig. 4.5f in Rock, 1991). The phlogopite and biotite micas contain significant F substitution, which decreases with falling Mg/(Mg + Fe<sup>2+</sup>) ratio from ~0.94 anions per formula unit (a.p.f.u.) in the phlogopites to nearly 0 in the biotites. Often present in significant amounts are Ti and Na, up to ~1 and 0.3 cations per formula unit (c.p.f.u.), respectively. These substitutions do not correlate well with the Mg/(Mg + Fe<sup>2+</sup>) ratios of the micas, but show some regional variation, e.g., the highest Ti and Na contents in the micas are found in the minettes and altered mica lamprophyres of the Intra-Sudetic Basin; the lowest Ti and Na contents are in the minettes of the GDS; other rocks have intermediate values.

A comparison between the dark mica compositions in the different igneous rocks of this study is shown in Figures 11B–E. The phlogopites and biotites in the minettes of the KJWDS and the Intra-Sudetic Basin (ISB) are very similar in terms of their Al–Fe–Mg proportions and are plotted with the same symbol in Figure 11B. These micas show the widest range of chemical variation and display various zoning styles, which account for the significant overlap in Figure 11B of phenocryst core and mantle compositions with phenocryst rim and groundmass compositions. Volumetrically, however, it is the phlogopites that are the predominant mica; biotite analyses are overrepresented. The groundmass micas of the KJWDS and ISB minettes usually straddle the phlogopite/biotite boundary.

Groundmass micas in the vogesites of the KJWDS are phlogopites similar to those of the minettes. Groundmass micas of the spessartites and monzonites, however, are biotites (Fig. 11C). Dark micas of the kersantites (Fig. 11D) plot close to the phlogopite/biotite boundary, largely on the phlogopite side; Fe-rich biotites are rare. Dark micas in the enclaves from the kersantites in the Góry Sowie Block (Ostrzew Hill) show a similar composition as the phenocrysts in the host kersantites, but tend to be enriched in Fe and Al. Groundmass micas in the altered mica lamprophyre of the ISB are biotites with variable Fe–Mg ratios and Al contents similar to those in the kersantites. Micas in the minettes of the GDS (Fig. 11E) are phlogopites with very low Al contents, zoned to phlogopite/biotite near the rims. The vogesites of the ZSDS contain partly resorbed biotite xenocrysts, possibly grading towards phlogopite near their rims. Chloritization largely obscures this zoning.

The most characteristic textures and zoning styles in the mica phenocrysts of the minettes are compared in Figure 12. The minettes of the KJWDS and the ISB contain two main populations of phenocrysts. The dominant population comprises euhedral phlogopites that grade rimwards into biotite (Fig. 12A). This normal zoning is mainly expressed by the rimward increase in Fe and a corresponding decrease in Mg; the variation of other major components (e.g., Al, Ti) is relatively weak. Phlogopites of the main KJWDS and ISB mica phenocryst population are accompanied by a minor, second population of strongly embayed/rounded (corroded), variably zoned biotites. In many cases the corroded biotitic cores are mantled by phlogopite, and thin zones at the margins grade back towards biotite (Fig. 12B). Other corroded biotites range from relatively homogeneous to oscillatory zoned, but the zoning patterns are partly obscured by chloritization which is much more intense in the biotites than in the phlogopites.

By contrast, the minettes of the GDS contain only one type of dark mica phenocryst. These micas are euhedral to partly embayed phlogopites, rich in Mg and poor in Al, with a homogeneous composition inside the crystals

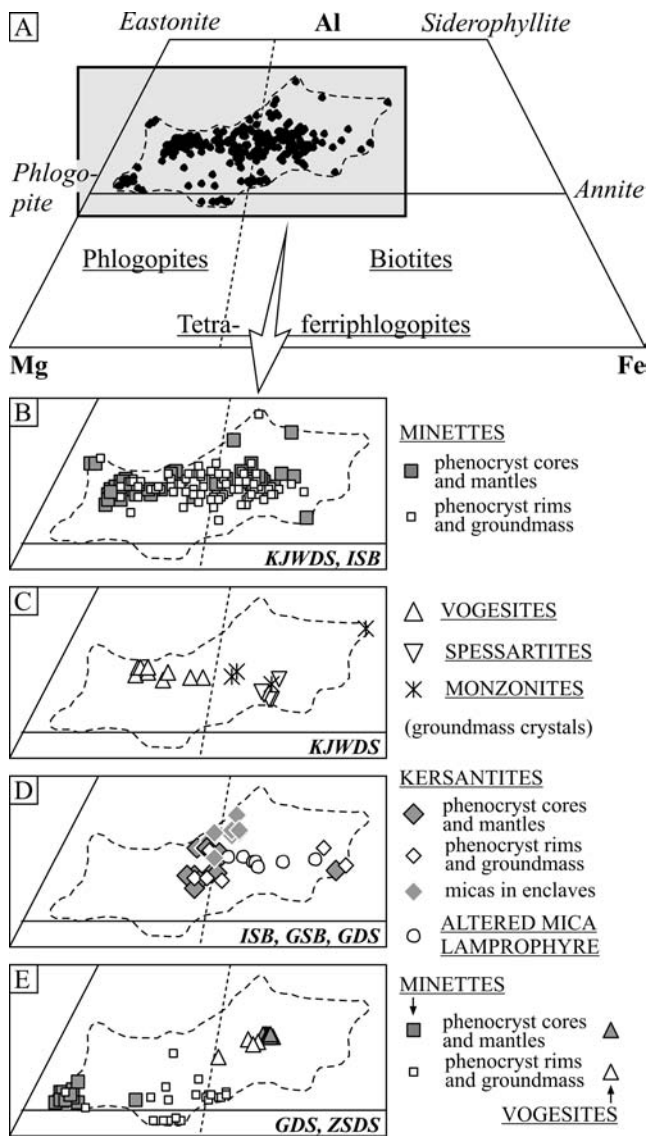


Fig. 11. The chemical variation of dark micas in the Mg–Al–Fe plot, after Rock (1991). Total Fe as  $\text{Fe}^{2+}$ . (A) Plot for all analyses. (B) to (E) Plots for samples grouped according to rock type and geographic location: KJWDS (Karpacz–Janowice Wielkie Dyke Swarm), GDS (Gniewosów Dyke Swarm), ZSDS (Złoty Stok Dyke Swarm), ISB (Intra-Sudetic Basin), GSB (Góry Sowie Block).

and a strong normal zoning only in the thin zones close to margins and embayments (Fig. 12C). These marginal, Fe-rich zones grade to magnesian biotite and, in one specimen, the outermost overgrowths (the last two points in zoning profile shown in Fig. 12C; also App. 2) show a more peculiar composition: a depletion in Al below 2 c.p.f.u., as well as some excess in Si at over 6 c.p.f.u. Possibly, these micas contain some  $\text{Fe}^{3+}$  in tetrahedral sites and grade towards the tetraferriophlogopite end-member. Alternatively, the high Si may suggest some  $\text{Li}^+$  substitution in the octahedral site and a gradation towards zinnwaldite.

The chemical variation of the dark micas illustrated in Figure 11 B–E indicates that the composition of these micas varies depending on the host-rock type and, further-

more, correlates with the bulk-rock chemical composition. For example, the lower limit of the Fe/Mg ratio in the micas tends to increase with the host-rock enrichment in Fe in the general sequence minettes–vogesites–kersantites–spessartites/monzonites. Similarly, the Al content of the phlogopite phenocrysts in the minettes correlates with the bulk-rock Al content, both being lowest in the minettes of the GDS and highest in the minettes of the ISB.

## AMPHIBOLES

Amphiboles are widespread in the mafic rocks of this study. In total, 521 analyses of amphiboles in 21 rock samples were obtained. The amphiboles vary widely in composition and were classified (following Leake *et al.*, 1997) into 12 main species: magnesiohastingsite (42% of the analyses), kaersutite (14%), tschermakite (9%), magnesiohornblende (9%), actinolite (8%), pargasite (7%), richterite (5%), edenite (3%) and winchytite (2%), with only a single occurrence of barroisite, riebeckite and eckermanite. A similar range of amphibole compositions is reported by Rock (1991) for lamprophyres worldwide, although the presence of kaersutite typifies alkaline lamprophyres, while richterite typifies lamproites (Rock, 1991). Selected analyses are shown in Appendix 3, and the overall chemical variation of the amphiboles is illustrated in Figure 13.

Four main amphibole groups were distinguished based on the B Na vs. T Si plot (groups 1 to 4 in Fig. 13A). Most of the analyzed amphiboles belong to the calcic amphiboles ( $\text{B Na} < 0.5$  c.p.f.u.) and these comprise groups 1–3 which are characterized by specific ranges of T Si:  $\sim 5.8$ – $6.6$  (group 1);  $7.3$ – $7.6$  (group 2); and  $7.7$ – $8.0$  (group 3). Groups 2 and 3 differ also in their B Na contents, which are lower in group 3. Group 4 comprises sodic-calcic to sodic amphiboles with B Na and T Si ranges of  $0.56$ – $1.83$  and  $7.55$ – $7.95$ , respectively. Although the four groups can be discriminated using parameters such as A ( $\text{Na} + \text{K}$ ), C Ti or  $\text{Mg\#} = \text{Mg}^{2+}/(\text{Mg}^{2+} + \text{Fe}^{2+})$ , some ranges of these parameters partly overlap (Fig. 13B–D). Almost all of the amphiboles show high Mg#, exceeding 0.5.

Group 1 amphiboles are the main Fe–Mg silicates of the vogesites and spessartites where they form the phenocryst and groundmass crystals. Such amphiboles are also found in the kersantites of the Góry Sowie Block. Within group 1, there are significant regional differences in amphibole compositions, and less distinctive differences between rock types (vogesites vs. spessartites vs. kersantites). Amphiboles in the lamprophyres of the KJWDS show lower T Si, higher C Ti and, in most cases, lower Mg#, as well as higher A ( $\text{Na} + \text{K}$ ), compared to amphiboles from the GDS. Amphiboles in the kersantites of the Góry Sowie Block, however, show distinctive chemical characteristics: their T Si contents are similar to those in the lamprophyres of the GDS, but their A ( $\text{Na} + \text{K}$ ) and C Ti values are higher.

The amphiboles in the vogesites and spessartites of the KJWDS are kaersutite, titanian magnesiohastingsite and, more rarely, titanian pargasite. The Si-poor and Ti-rich,

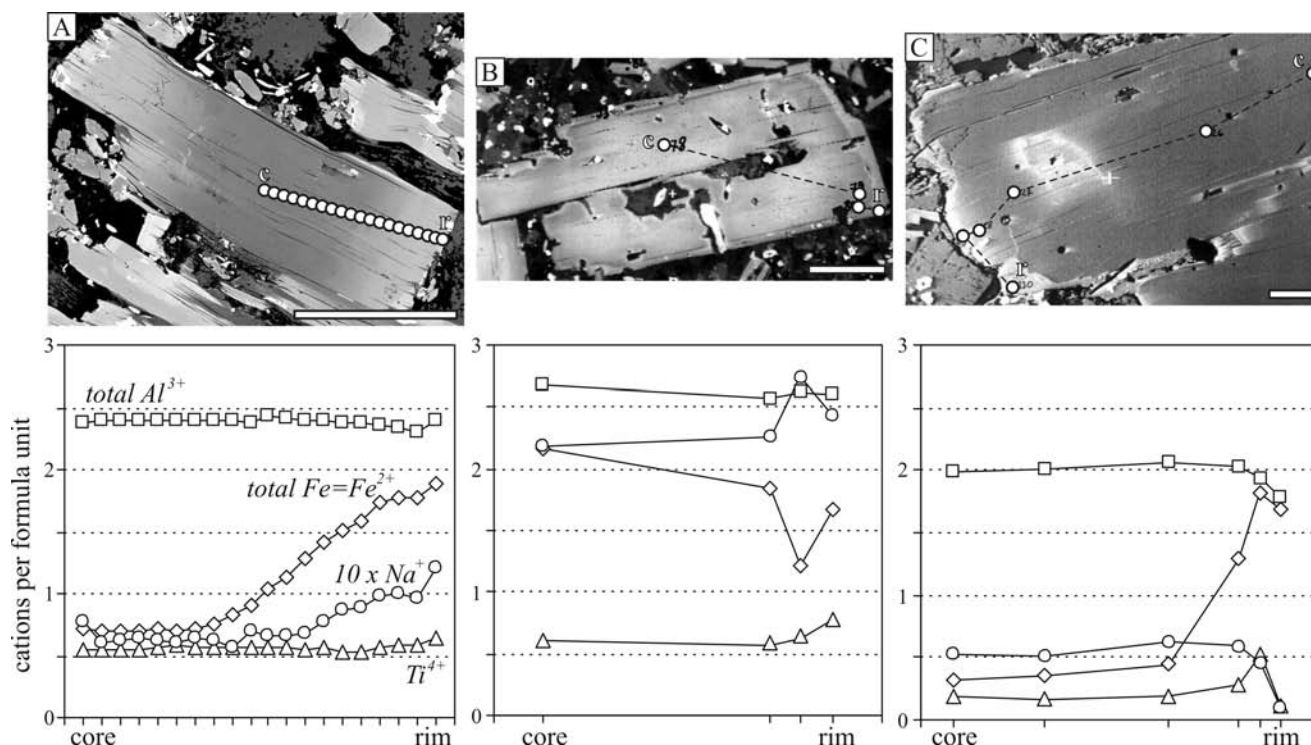


**Fig. 12.** Selected back scattered electron (BSE) images and zoning patterns of the dark mica phenocrysts from the minettes. White circles in the BSE images show the location of microprobe analysis spots, and the diagrams below show the chemical variation for selected elements. The mica analyses were recalculated to 22 O, total Fe as  $\text{Fe}^{2+}$ . (A) Normally zoned mica, with phlogopite composition in the core and mantle, and biotite composition near the margins (sample 626, KJWDS). (B) Corroded and reversely zoned mica (sample 508B, ISB). The large, partly resorbed core is biotitic in the centre but phlogopitic in its outer part. The thin, light grey overgrowth represents biotite. (C) Nearly homogeneous phlogopite phenocryst (sample 465M, GDS). Only near the margins and embayments, there are thin, normally zoned overgrowths that have a composition transitional between phlogopite and biotite and are also locally depleted in Al. Scale bar in all images is 0.2 mm long.

kaersutitic compositions are most characteristic of the vogesites. Amphiboles in vogesite and spessartite samples from the GDS represent magnesiohastingsite and tschermakite with gradations towards edenite and magnesiohornblende (Si-poor magnesiohornblende, in contrast with Si-rich magnesiohornblende of the group 2). These amphiboles are often "titanian" with C Ti usually from 0.25 to 0.5. The tschermakitic compositions with A ( $\text{Na} + \text{K}$ ) < 0.5 are most characteristic of the spessartites. Amphiboles in the kersantites of the Góry Sowie Block are titanian edenite and titanian magnesiohastingsite.

The group 1 amphiboles of titanian magnesiohastingsite and magnesiohornblende are also found in minor amounts in the groundmass of some monzonites and micromonzodiorites, though the Si-rich amphiboles of groups 2 and 3 are more common in these latter two rock types. Group 2 amphiboles of magnesiohornblendes grading to Si-poor actinolites are found in all lamprophyres (except minettes) as well as in the other mafic rocks. In contrast with group 1, no regional variation was found. In the lamprophyres, the group 2 magnesiohornblendes form local, discontinuous overgrowths on group 1 phenocrysts, and in the other mafic rocks group 2 amphiboles are found in the groundmass as prismatic to subhedral crystals.

Group 3 amphibole is actinolite and, in a manner sim-

ilar to group 2, is found in all of the analyzed rock types, irrespective of their geological location. These actinolites form acicular crystals that occur as the outermost overgrowths on, and also intergrowths within, other amphiboles and clinopyroxenes. They are also common in microcrystalline groundmass aggregates and in pseudomorphs after ferromagnesian minerals.

The sodic-calcic to sodic amphiboles of group 4 are characteristic of the richterite minettes where they form euhedral to subhedral groundmass crystals. Most of these amphiboles are richterite, locally overgrown by actinolite. But in one richterite minette from the KJWDS, a more complex zoning was observed: olive-green richterite crystals grading rimward into winchyste, and partly overgrown, or replaced along cracks, by blue-coloured amphiboles that ranged from ferriwinchyste to riebeckite. The outermost, almost colourless to greenish, overgrowths are actinolite. In addition, in one specimen from the GDS there are groundmass eckermanites, but the microprobe analyses were of poor quality (low totals) due to the very small width of the acicular and skeletal crystals.

The group 1 amphiboles show variable textures and zoning patterns, and representative examples are shown in Figure 14. Amphibole phenocrysts in the vogesites from the KJWDS (Fig. 14A) are often characterized by the pres-

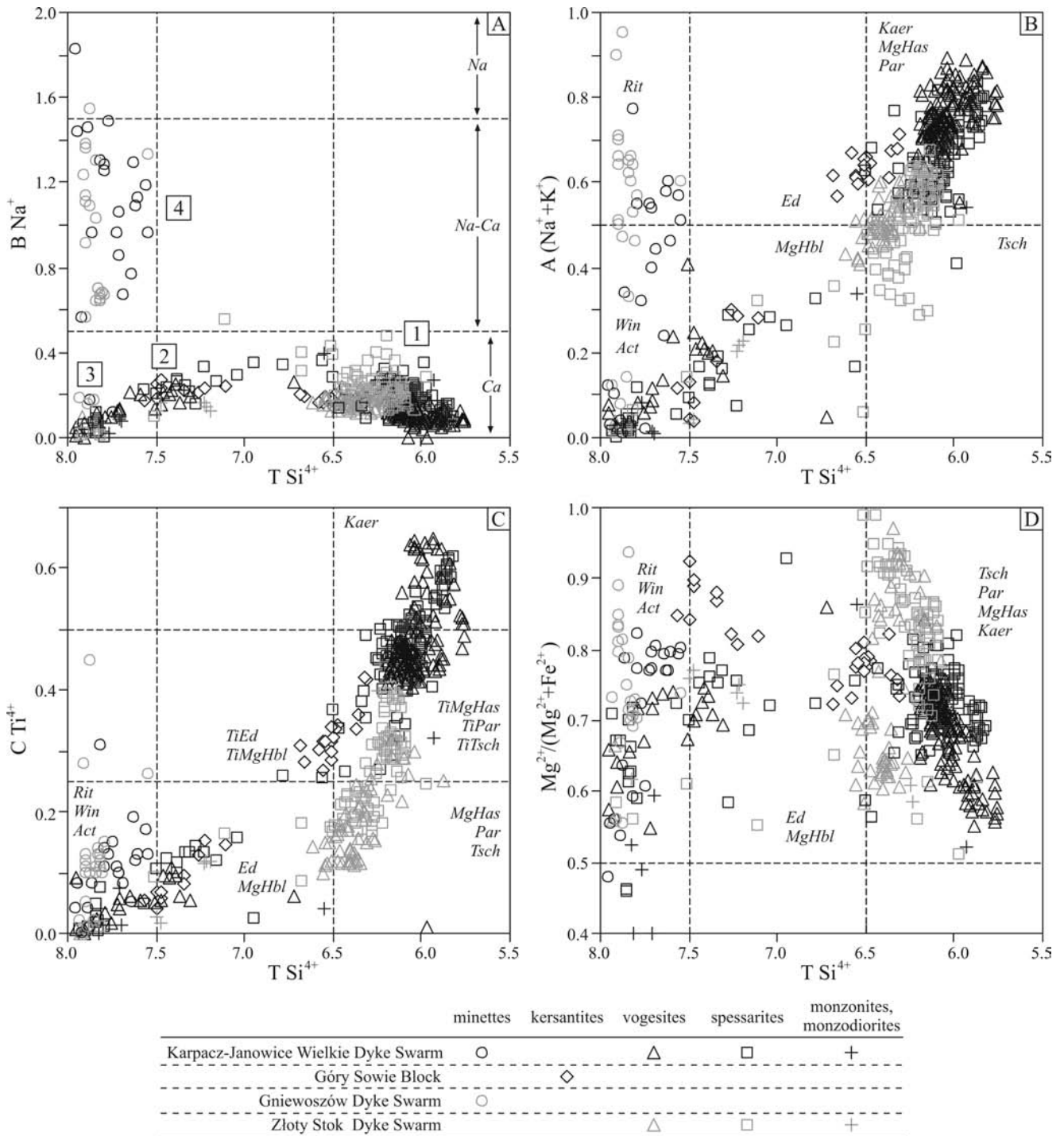


**Fig. 13.** The chemical variation of amphiboles plotted on a variety of compositional diagrams. All values in cations per formula unit recalculated to 23 O and 13 CNK (13 CNK – total cations except Ca, Na and K = 13). The four amphibole groups (1–4) discussed in the text are indicated in the B Na–T Si plot (A) together with the general classification of amphiboles: Ca (calcic), Na–Ca (sodic–calcic), Na (sodic). Amphiboles are abbreviated as follows: Act (actinolite), Ed (edenite), Kaer (kaersutite), MgHbl (magnesiohornblende), MgHas (magnesiohastingsite), Par (pargasite), Rit (richterite), Tsch (tschermakite), Win (winchyste). The prefix “Ti” in Fig. 13C indicates a titanian variety, e.g., Ti–Ed (titanian edenite).

ence of anhedral to subhedral, compositionally distinctive, internally zoned cores. In the example shown, the core composition ranges from titanian pargasite to kaersutite. The zoning of the core is truncated by its irregular outer surface and, along the core/mantle boundary, there are

abrupt changes in composition: the Mg# (and MgO) increase, while A (Na + K), Ti, total Al (and total Fe) decrease, and the composition grades to titanian magnesiohastingsite (locally also titanian pargasite). The mantle and rims of this crystal show oscillatory zoning in which the

amplitude of the chemical variations is generally smaller than that at the core/mantle boundary. The thicker, main zones of the crystal in Figure 14A are further highlighted by an inhomogeneous distribution of inclusions: apatite (very small prismatic crystals); Fe-Ti oxides (larger sub-hedral crystals); and groundmass inclusions (dark patches of various size). Other amphibole crystals in the vogesites of the KJWDS show similar features, but often the cores are less distinctive whereas the oscillatory zoning of the mantle and rims is more pronounced.

Less complex zoning of amphibole phenocrysts occurs in the vogesites of the ZSDS (Fig. 14B). In most specimens these phenocrysts contain large, relatively homogeneous, partly rounded cores and compositionally distinctive, relatively thin, euhedral overgrowths. Both the core and the overgrowth are magnesiohastingsite. Some oscillatory variation (not well reflected in the back scattered electron image) is marked by variations in alumina and alkalis, and, locally, the composition can change to edenite, magnesiohornblende or tschermakite. Notably, the magnesiohornblendes in these phenocrysts represent compositional group 1 (Si-poor) and not group 2 (Si-rich, Fig. 13) amphiboles. The outer core of the phenocrysts contains some inclusions of Fe-Ti oxides. Across the boundary of the core and the overgrowth, the compositional change is mainly expressed by the rapid increase in Mg# (and MgO), less pronounced enrichment in alkalis, and a depletion in total Fe. The overgrowths of the phenocrysts show the same composition as the groundmass amphibole crystals.

In contrast with the vogesites, zoning in amphibole phenocryst in the spessartites is weaker (Fig. 14C and D). Compositionally distinctive cores are absent and stronger chemical changes are found mainly near the rims of the crystals where the Si-poor amphiboles (magnesiohastingsite, kaersutite or tschermakite) are overgrown by the Si-enriched amphiboles (magnesiohornblende or actinolite). The amphibole phenocrysts in some spessartites of the ZSDS are characterized by the presence of anhedral pseudomorphs of chlorite near their cores (Fig. 14D).

## CLINOPYROXENES

Representative clinopyroxene analyses (from a total of 248) are given in Appendix 4, and the variations in clinopyroxene composition are shown in Figures 15 and 16. Following the classification system of Morimoto (1989), the clinopyroxenes belong to the quadrilateral (QUAD) group and are, mainly, Mg-rich diopsides and augites. Similar clinopyroxene compositions are found in calc-alkaline lamprophyres worldwide (Figure 4.3C in Rock, 1991).

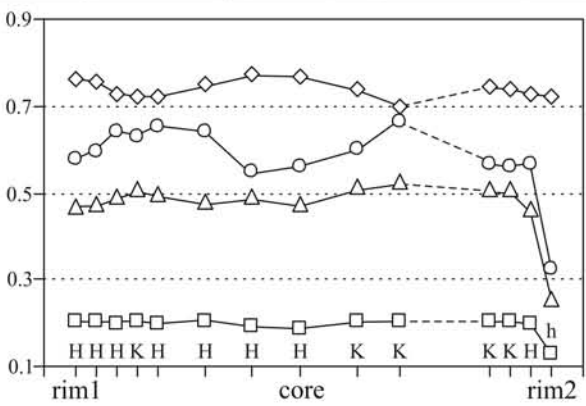
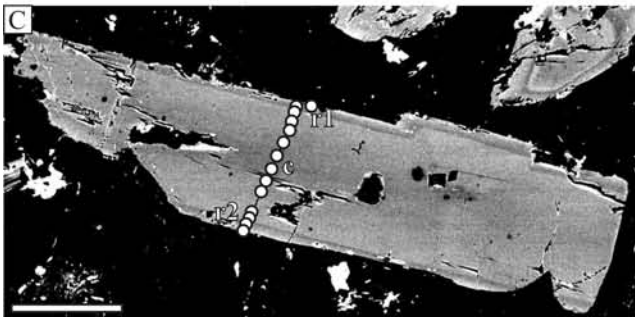
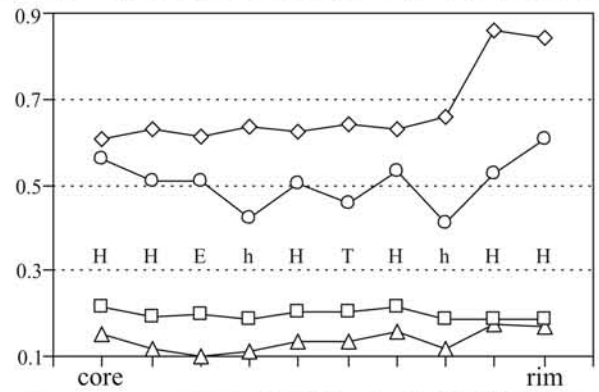
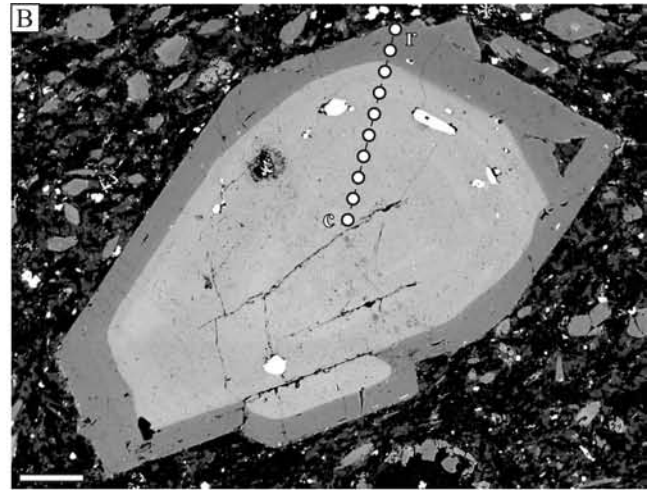
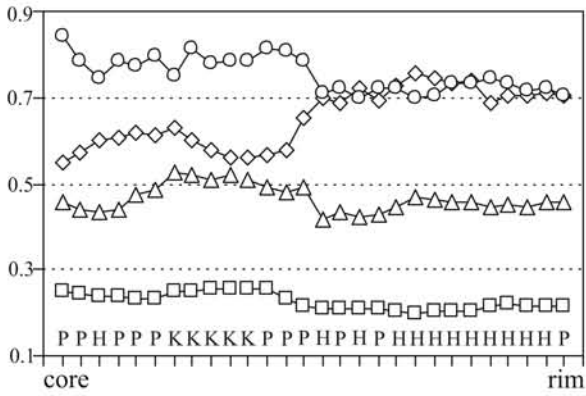
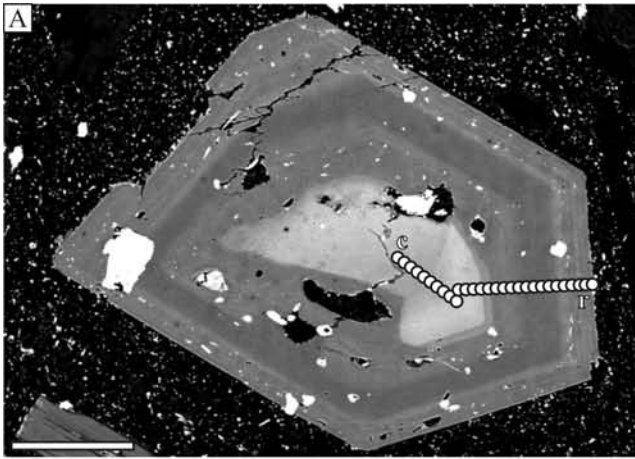
Clinopyroxenes from the Sudetic lamprophyres often straddle the augite/diopside boundary in the clinopyroxene quadrilateral at generally low ferrosilite contents; only a few analyses show a significant Fe enrichment and extend into Mg-rich hedenbergite (Fig. 15A). Some 70% of the analyzed clinopyroxenes show elevated Al contents ( $0.1 < \text{Al} < 0.35$  c.p.f.u.) and represent aluminian diopsides and augites (Fig. 16). Although low-Al clinopyroxenes ( $\text{Al} < 0.1$  c.p.f.u.) characterize the minettes in the

Karpacz-Janowice Wielkie Dyke Swarm (KJWDS), they also occur in other rock types in the groundmass or in phenocryst rims. A minority of clinopyroxenes (~23% of analyses) show a slight enrichment in Cr ( $0.01 < \text{Cr} < 0.025$  c.p.f.u.), and could be termed chromian diopsides and augites. The highest Cr contents are found in the Mg-rich clinopyroxenes of the spessartites, kersantites and vogesites, Cr decreasing rapidly with falling Mg#. The Al vs. Mg# variation is more complex. In particular, most clinopyroxenes of the monzonites and micromonzodiorites in the KJWDS show relatively high Al at moderate Mg# (Fig. 16).

The general composition of the clinopyroxenes correlates with their host rock types. In the KJWDS (Fig. 15B-D), there is a gradual shift in clinopyroxene compositions from Mg-rich diopside to Fe-enriched augite (i.e., gradual enrichment in ferrosilite and depletion in wollastonite components) in the following sequence: minettes (mostly diopside) – vogesites and spessartites (predominantly diopside, partly augite) – monzonites and micromonzodiorites (augite). Clinopyroxene phenocrysts in these rocks tend to show an overall normal zoning (depletion in enstatite and enrichment in ferrosilite components at rims). However, in many crystals, there are more complex patterns due to the presence of compositionally distinct cores, oscillatory zoning, sieve textures and embayments (Fig. 17A and B). These complex variations are reflected in the significant overlap between the core and mantle compositions (filled/heavy symbols) and the rim and groundmass compositions (open/light symbols), as shown in Figures 15B-D. In addition, Fe-enriched diopsides and augites that grade into hedenbergite are found as thin overgrowths or patchy intergrowths within some clinopyroxene crystals, and as euhedral crystals associated with quartz in miarolitic cavities in the groundmass. The data for the KJWDS include clinopyroxene analyses from a cognate enclave in a micromonzodiorite (Fig. 15E). These latter clinopyroxenes show a similar compositional range as those in the host micromonzodiorites, although the wollastonite content tend to be relatively low in augites of the enclave.

Clinopyroxenes of the kersantites (the Góry Sowie Block and the GDS) are similar in composition to those of the lamprophyres of the KJWDS (Fig. 15F). Pheno- and megacryst cores are diopsidic in composition, whereas the rims and the associated groundmass crystals vary from diopside to augite. The diopsidic cores in the phenocrysts in the Góry Sowie Block are often sieve-textured and variably altered, while those in the GDS do not show these features.

The vogesites and spessartites of the ZSDS are characterized by the presence of augites, in contrast with the largely diopsidic clinopyroxenes in the vogesites and spessartites of the KJWDS. The lowest ferrosilite contents are found in vogesite augites, whereas spessartite augites show some enrichment in ferrosilite. The phenocrysts in both rock types usually show some normal to oscillatory zoning, and rim compositions overlap core-mantle compositions. Some augite phenocrysts in the vogesites (Fig. 17C) are characterized by partial resorption in the central part, as well as patches and overgrowths enriched in Fe.



◇  $Mg^{2+}/(Mg^{2+}+Fe^{2+})$  Values in cations  
 ○  $A(Na^{+}+K^{+})$  per formula unit,  
 △  $C Ti^{2+}$  normalized to  
 □  $(^{IV}Al^{3+}+^{VI}Al^{3+})/10$  23 O and 13 CNK.  
 E - edenite, H - magnesiohastingsite, h - magnesio-  
 hornblende, K - kaersutite, P - pargasite, T - tscher-  
 makite.

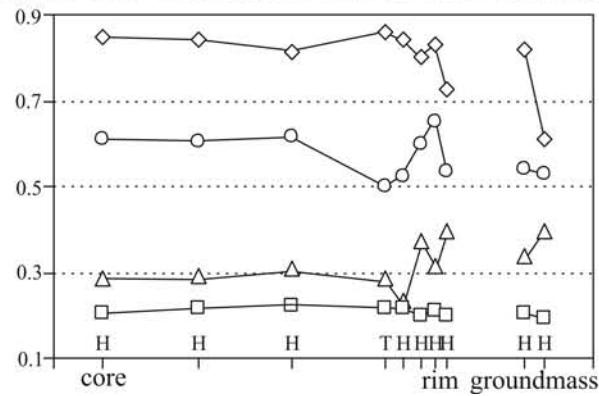
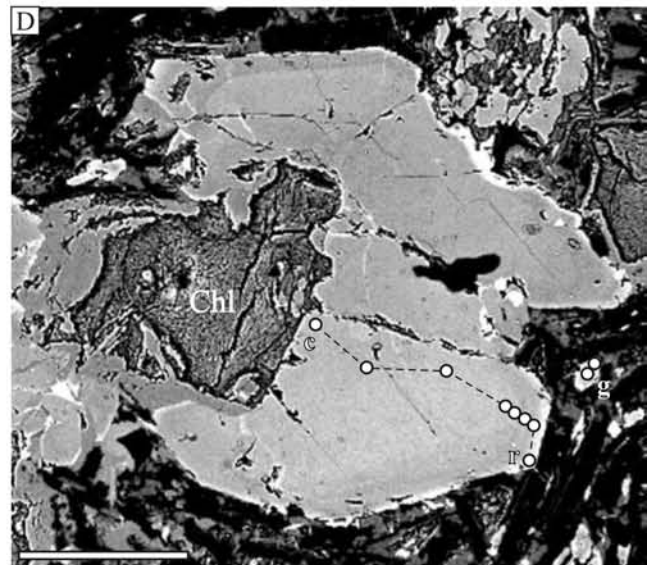


**Fig. 14.** Selected backscattered electron (BSE) images and zoning patterns of amphibole phenocrysts in the lamprophyres. White circles in the BSE images show the location of microprobe analysis spots (c – core; r – rim; g – groundmass), and the diagrams below show the variation for selected elements together with amphibole classification at each spot. (A) and (B) Strongly zoned amphiboles with distinct cores from the vogesites (A – sample 629A, KJWDS; B – sample 536B, ZSDS). (C) and (D) Weakly zoned amphiboles from the spessartites (C – sample 351, KJWDS; D – sample 484, ZSDS). Scale bar 0.1mm long.

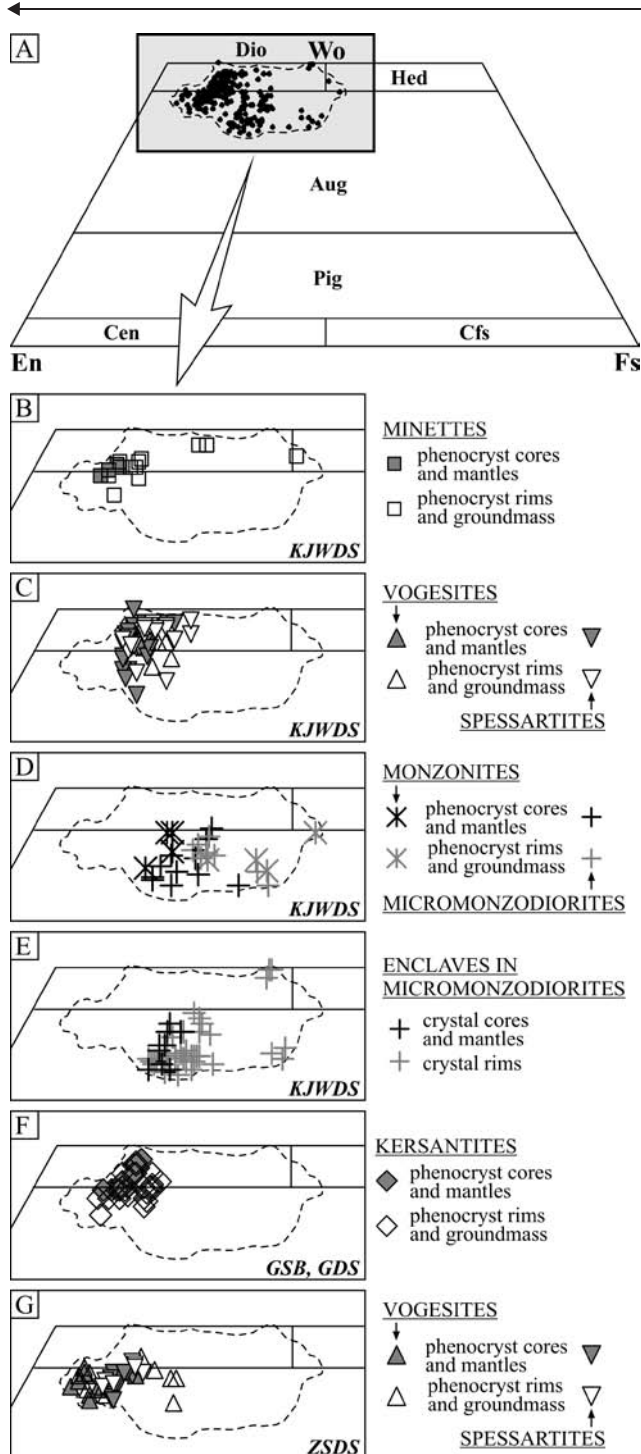


**Fig. 15.** Composition of pyroxenes from the mafic rocks in the wollastonite (Wo)–enstatite (En)–ferrosilite (Fs) diagram. (A) Plot for all analyses. (B) to (G) Diagrams for samples grouped according to rock type and geographic location: KJWDS (Karpacz–Janowice Wielkie Dyke Swarm), GDS (Gniewosów Dyke Swarm), ZSDS (Złoty Stok Dyke Swarm), ISB (Intra-Sudetic Basin), GSB (Góry Sowie Block).

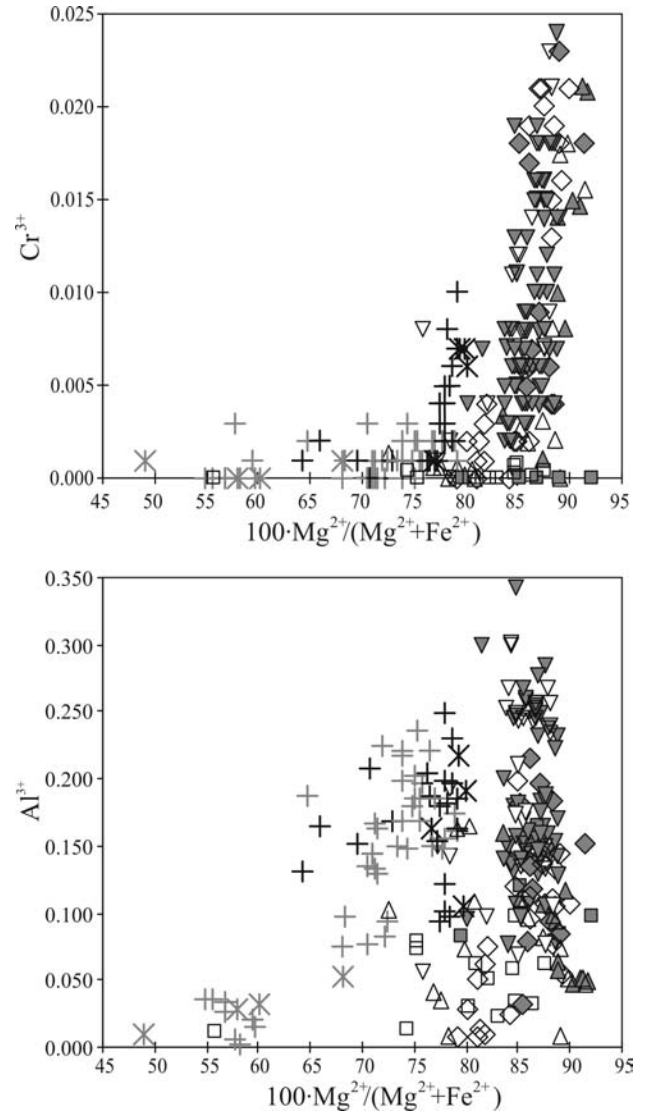


**Fig. 16.** Chemistry of clinopyroxenes from the mafic rocks plotted on Cr and Al vs. Mg# diagrams. Values in cations per formula unit recalculated to 6 O. Symbols as in Figure 15.

## FELDSPARS

Feldspars are typically found in the groundmass of the lamprophyres and as phenocrysts and groundmass crystals in the other mafic rocks of this study. Representative analyses from a total of 337 feldspar analyses are given in Appendix 5. Feldspar nomenclature is based on chemistry and plotting the end-member proportions in the albite–anorthite–orthoclase triangle for disordered feldspars (Fig. 18, after Deer *et al.*, 1992). As the fine-grained to microcrystalline textures reflect high cooling rates, the assump-

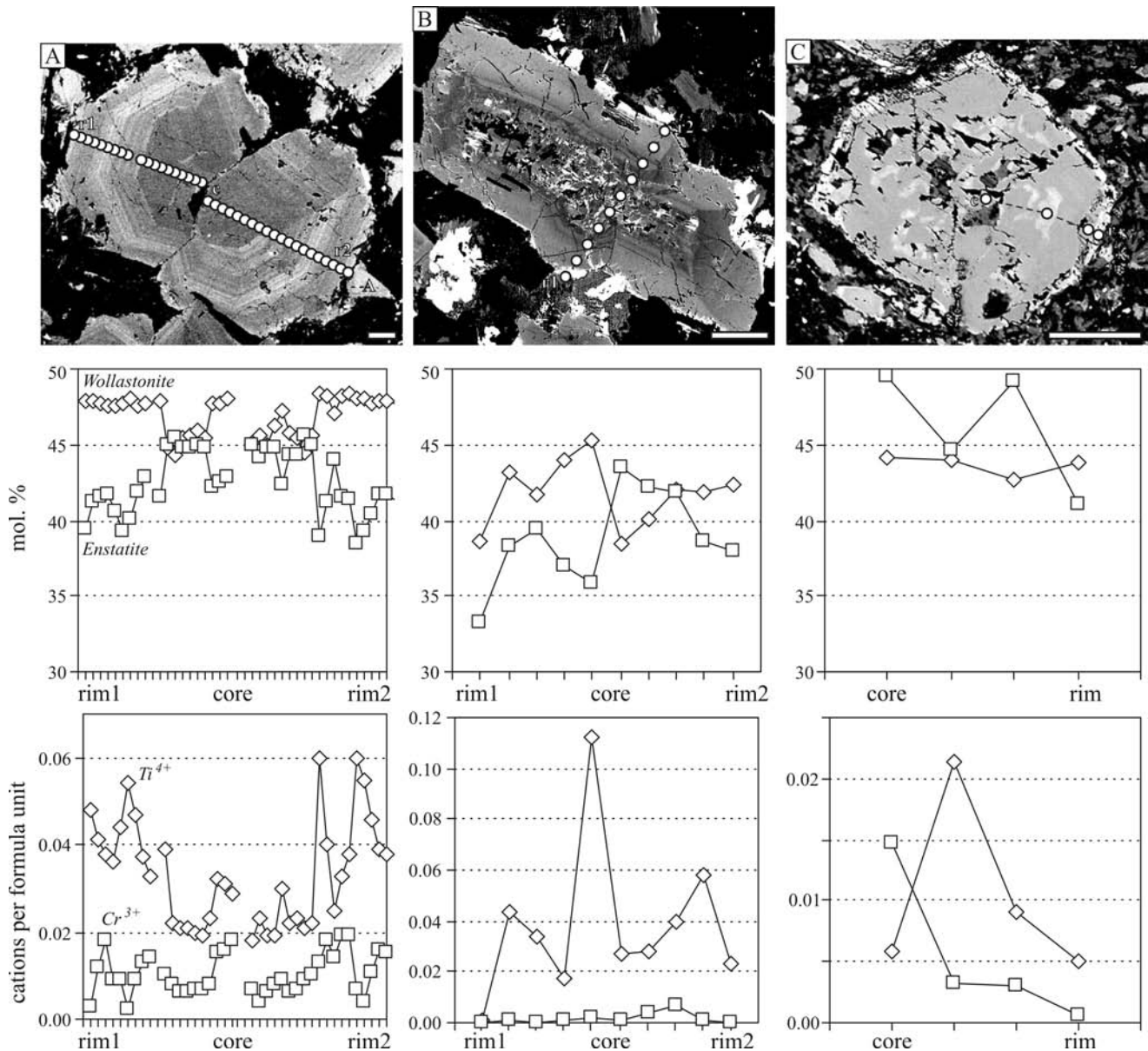


Fig. 17. Selected back scattered electron (BSE) images and zoning patterns of clinopyroxene phenocrysts. White circles in the BSE images show the location of microprobe analysis spots (c – core; r – rim), and the diagrams below show the variation for selected components. Analyses recalculated to 6 O. (A) Diopside with a homogeneous core and oscillatory zoned mantle and rim (spessartite, sample 318B, KJWDS). (B) Oscillatory- and sector-zoned augite with a sieve-textured core (micromonzodiorite, sample 328B, KJWDS). (C) Augite with partly corroded core, showing also patches and an overgrowth depleted in the enstatite molecule (vogesite, sample 536B, ZSDS). Scale bar in all images 0.1mm long.

tion of a generally low degree of structural ordering seems justified at least for the primary, magmatic feldspars.

A bimodal distribution of feldspar composition is characteristic of most minettes and vogesites. In these rocks, the dominant feldspar is K-rich sanidine (typically Or > 88), with minor albite and rare Na-K alkali feldspars. Some K-rich sanidines (Or 95–90) in the minettes of the GDS contain very thin ( $\sim 1 \mu\text{m}$ ) lamellae of Na-enriched sanidine ( $\sim \text{Or } 71$ , though difficult to measure due to small thickness), as well as thicker, irregular intergrowths of albite. Similar patches of albite are also charac-

teristic of the sanidines in the richterite minettes of the KJWDS. However, the minettes of the Intra-Sudetic Basin contain groundmass Na-sanidine as well as normally zoned plagioclase (andesine-oligoclase) overgrown by anorthoclase. Common to several vogesite samples are pseudomorphs after plagioclase that are composed of albite densely intergrown with sericite.

The strongest variation of feldspar composition is found in the kersantites and spessartites. The dominant feldspar of these rocks is plagioclase, but this is usually strongly albitized and sericitized. Relics of labradorite-

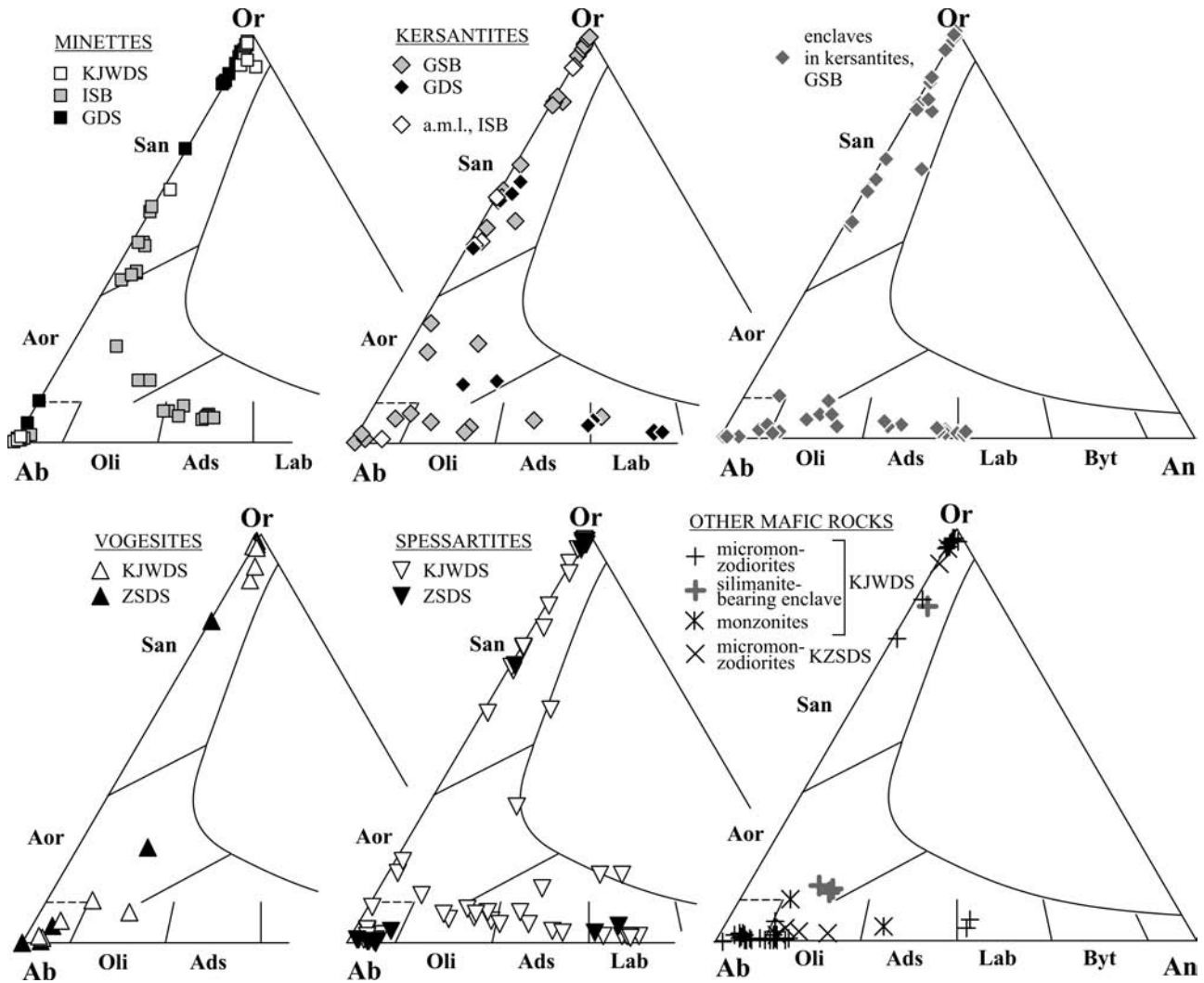


Fig. 18. Composition of feldspars from the mafic rocks in the albite (Ab)-anorthite (An)-orthoclase (Or) triangle. Feldspars are abbreviated as follows: Sa (sanidine), Aor (anorthoclase), Oli (oligoclase), Ads (andesine), Lab (labradorite), Byt (bytownite). KJWDS (Karpacz-Janowice Wielkie Dyke Swarm); GDS (Gniewosów Dyke Swarm); ZSDS (Złoty Stok Dyke Swarm); ISB (Intra-Sudetic Basin); GSB (Góry Sowie Block).

oligoclase are found in some pseudomorphs, and in some less altered crystals there is a normal zoning in the labradorite-oligoclase range. Alkali feldspars form overgrowths on plagioclase and intergrowths within plagioclase, and occur as anhedral interstitial crystals. Overall, alkali feldspar compositions in these rocks cover an almost continuous spectrum from pure albite to pure orthoclase. Feldspars from enclaves in the kersantites from the Ostrzew Hill in the Góry Sowie Block have a composition that compares well with that in the host kersantites.

There is a relatively wide range of plagioclase and alkali feldspar compositions in the monzonites and micromonzodiorites. However, relics of original Ca-rich plagioclase (labradorite) are rare in these rocks due to pronounced albitization and sericitization. Alkali feldspar compositions tend to show a bimodal distribution, being either Na- or K-rich (albite-anorthoclase or K-rich sanidine). A sillimanite-rich enclave in one micromonzodiorite contains abundant anorthoclase, close to oligoclase in composition, as well as minor sanidine.

## CHLORITES AND TALC

In the mafic rocks, chlorites are widespread post-magmatic minerals that formed at the expense of primary igneous ferromagnesian silicates or that crystallized in vesicles and cracks. Chlorites are found in almost all the thin sections studied. Representative examples from a total of 155 chlorite analyses from 26 samples are given in Appendix 6; chemical variation is illustrated in Figure 19.

The chlorites show a moderate chemical variation and, in the Hey (1954) diagram, they plot mainly in the fields of pycnochlorite and diabantite, less commonly in the fields of brunsvigite and talc-chlorite. Chlorites of the monzonites and micromonzodiorites show relatively high Fe and low Si contents and are mostly brunsvigite. Nevertheless, pycnochlorite and diabantite were also found, as was one example of ripidolite/daphnite. Chlorites relatively rich in Fe are characteristic of the minettes but, compared with those of the monzonites and micromonzodiorites, they usually show higher Si and slightly lower Fe

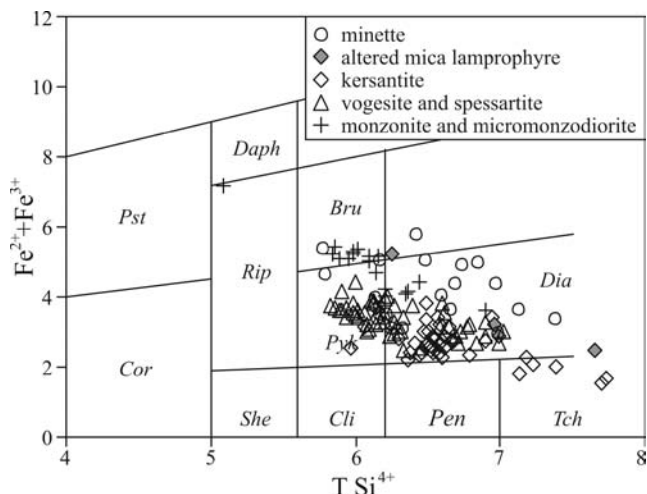


Fig. 19. The chemical composition of chlorites from the mafic rocks plotted on the Hey (1954) diagram. Abbreviations are as follows: Bru (brunsvigite), Cli (clinocllore), Cor (corundophilite), Daph (daphnite), Dia (diabantite), Pen (penninite), Pst (pseudothuringite), Pyc (pynochlorite), Rip (ripidolite), She (sheridanite), Tch (talc-chlorite).

contents and are diabantite. Similar chlorites were found in the altered mica lamprophyre. The vogesites and spessartites contain mainly pynochlorite, but many analyses were of diabantite. The latter is the main chlorite type in the kersantites, although these rocks contain also talc-chlorites that are characterized by the highest Si and lowest Fe contents in the entire data set.

Chlorites from the various rocks analyzed show similar, overlapping Si and Fe ranges. Despite some systematic differences, there appears to be no simple correlation between bulk rock composition and chlorite composition, e.g., chlorites with the highest Fe contents are found both in Fe-rich rocks (monzonites, micromonzodiorites) and in Fe-poor rocks (minettes). Similarly, within individual specimens, no clear relationships are observed between the composition of chlorites and their textural position.

Talc occurs in one richterite minette sample from the GDS. This talc forms oval pseudomorphs after an uniden-

tified mineral in the cores of some richterite crystals. Compared with the ideal formula of talc, the analyzed mineral contains a significant amount of iron, most probably substituting as  $\text{Fe}^{2+}$  for  $\text{Mg}^{2+}$ . In three analyses, this substitution ranges from  $\sim 0.12$  to  $0.42$  c.p.f.u., which represents up to 14% of the available octahedral sites.

### ACCESSORY AND SECONDARY SILICATES (TITANITE, EPIDOTE GROUP MINERALS, GARNETS, PREHNITE, PUMPELLYITE)

The silicates discussed herein generally represent post-magmatic components. They are found as replacement products and pseudomorphs after magmatic Fe-Mg silicates, or as fine-grained groundmass grains and aggregates in various combinations with chlorites and carbonates. However, some euhedral titanites in the groundmass of some minettes could have crystallized at a late-magmatic stage. Representative analyses of these minerals are given in Appendices 7 to 9.

Titanite is the most widespread minor silicate and occurs in nearly every rock type. The epidote-group minerals are less common. Garnet, prehnite and pumpellyite were analyzed from 3, 6 and 7 rock samples, respectively. These three minerals are most characteristic of mafic rocks rich in strongly altered plagioclase (e.g., spessartites, micromonzodiorites, monzonites) and are rare in alkali-feldspar rich mafic rocks (minettes, vogesites). Selected BSE images (Fig. 20) illustrate some most characteristic textural patterns of the minor silicates and of other common post-magmatic minerals.

Titanite compositions (Fig. 21) are variable and usually depart from the ideal formula  $\text{CaTiSiO}_5$ . The main differences include lowered Ti and Ca contents, which are below the ideal of 1 c.p.f.u. each and fall to  $\sim 0.6$  and  $0.8$ , respectively; and significant Al, Fe and Mg contents, which range up to  $\sim 0.35$ ,  $0.22$  ( $\text{Fe}^{3+}$ ) and  $0.21$  c.p.f.u., respectively. In addition, there is usually some excess in Si, up to 1.1 c.p.f.u. The relationships between the elements (Fig. 21) suggest that  $\text{Ti}^{4+}$  is being substituted by  $\text{Al}^{3+}$  and  $\text{Fe}^{3+}$ , charge being balanced by some excess  $\text{Si}^{4+}$ . Also,

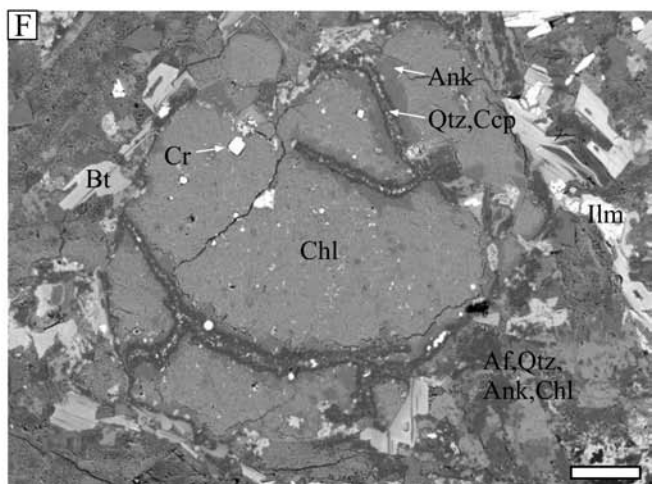
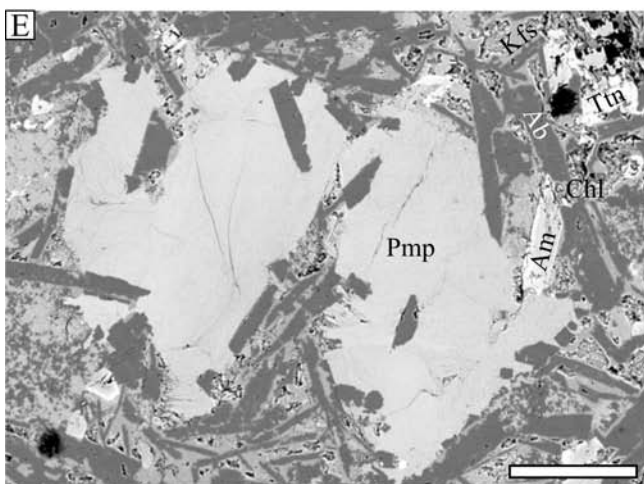
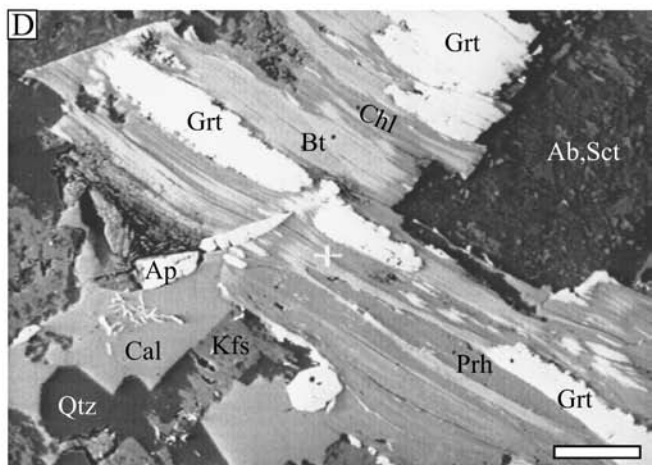
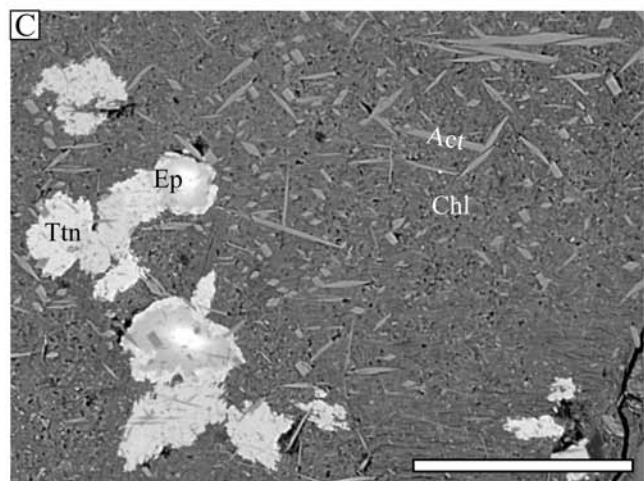
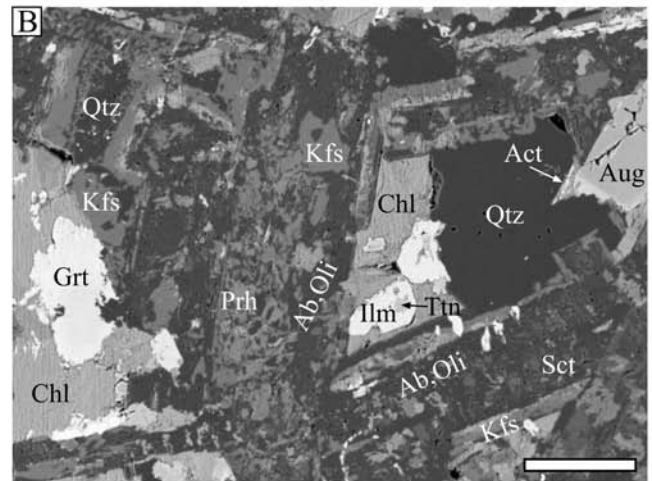
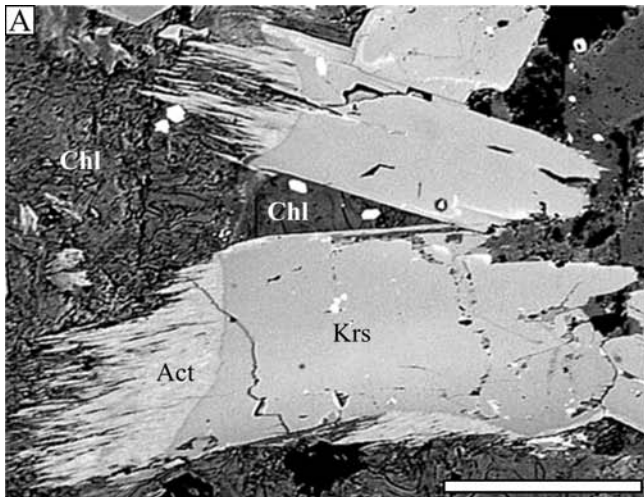
Fig. 20. Back scattered electron (BSE) images illustrating characteristic post-magmatic minerals in the mafic rocks of the study area. (A) Actinolite overgrowths on kaersutite in a chlorite matrix in a vogesite. (B) The groundmass of a micromonzodiorite, the same specimen as in Fig. 6H, composed of altered plagioclase laths, with relics of oligoclase composition, densely intergrown and overgrown with albite, K-feldspar, prehnite and sericite. In the left part of the image there is also garnet and chlorite, and augite with small actinolite overgrowths is seen in the right side. Other minerals illustrated include ilmenite, titanite and quartz. (C) Chlorite pseudomorph after a ferromagnesian mineral in a spessartite, with numerous intergrowths of actinolite and also titanite and epidote-group minerals. The latter are zoned from allanite at cores (bright in the BSE image) to epidote at rims. (D) Partly altered biotite in a monzonite, intergrown with chlorite, garnet and prehnite. Other minerals seen in this image include quartz, K-feldspar, apatite, calcite, and albitized and sericitized plagioclase. (E) Pumpellyite aggregate filling a miarolitic cavity in the groundmass of a vogesite composed of albite, K-feldspar, amphiboles, chlorite and titanite. (F) Pseudomorph after olivine in an altered mica lamprophyre, composed of chlorite with veins of ankerite and of quartz with minute chalcopyrite inclusions. The pseudomorph also contains small chromite inclusions. Adjacent to this pseudomorph are numerous biotite plates, and, locally, ilmenite. The groundmass consists of various intergrowths of alkali feldspars, quartz, ankerite and chlorite. Mineral abbreviations are as follows: Ab (albite); Act (actinolite); Af (alkali feldspar); Am (amphibole); Ank (ankerite); Ap (apatite); Aug (augite); Bt (biotite); Cal (calcite); Chl (chlorite); Ccp (chalcopyrite); Chr (chromite); Ep (the epidote-group minerals allanite and epidote); Grt (the garnet range grossularite-andradite); Ilm (ilmenite); Kfs (K-feldspar); Oli (oligoclase); Prh (prehnite); Pmp (pumpellyite); Qtz (quartz); Sct (sericite); Ttn (titanite). Scale bar is 0.1mm long in all images.

$\text{Ca}^{2+}$  is being partly substituted by  $\text{Mg}^{2+}$ . The largest Al, Fe and Mg substitutions are most characteristic of titanites from the kersantites and spessartites, but to a lesser extent are found elsewhere. In addition, energy dispersive spectrometry (EDS) shows that some minette titanites contain significant Zr substitutions.

The epidote group minerals are characterized by having high  $\text{Fe}^{3+}/(\text{Fe}^{3+} + \text{VIAl}^{3+})$  ratios that range from  $\sim 0.3$  to 0.35 (Fig. 22), signifying epidote with some gradation

towards clinozoisite. Some epidotes possess low contents of  $\text{Ca}^{2+}$  in the X sites, down to  $\sim 1.4$  c.p.f.u. Rare earth element analyses in two low-Ca grains within chloritic pseudomorphs in vogesites indicate significant contents of the light rare earth elements, mainly La and Ce, up to  $\sim 0.6$  c.p.f.u. These low-Ca epidotes represent allanite. In addition, some of the allanite-epidote grains are zoned (Fig. 20C), with LREE contents decreasing rimwards.

The garnets are Ca- and Fe-rich, with variable Ti sub-



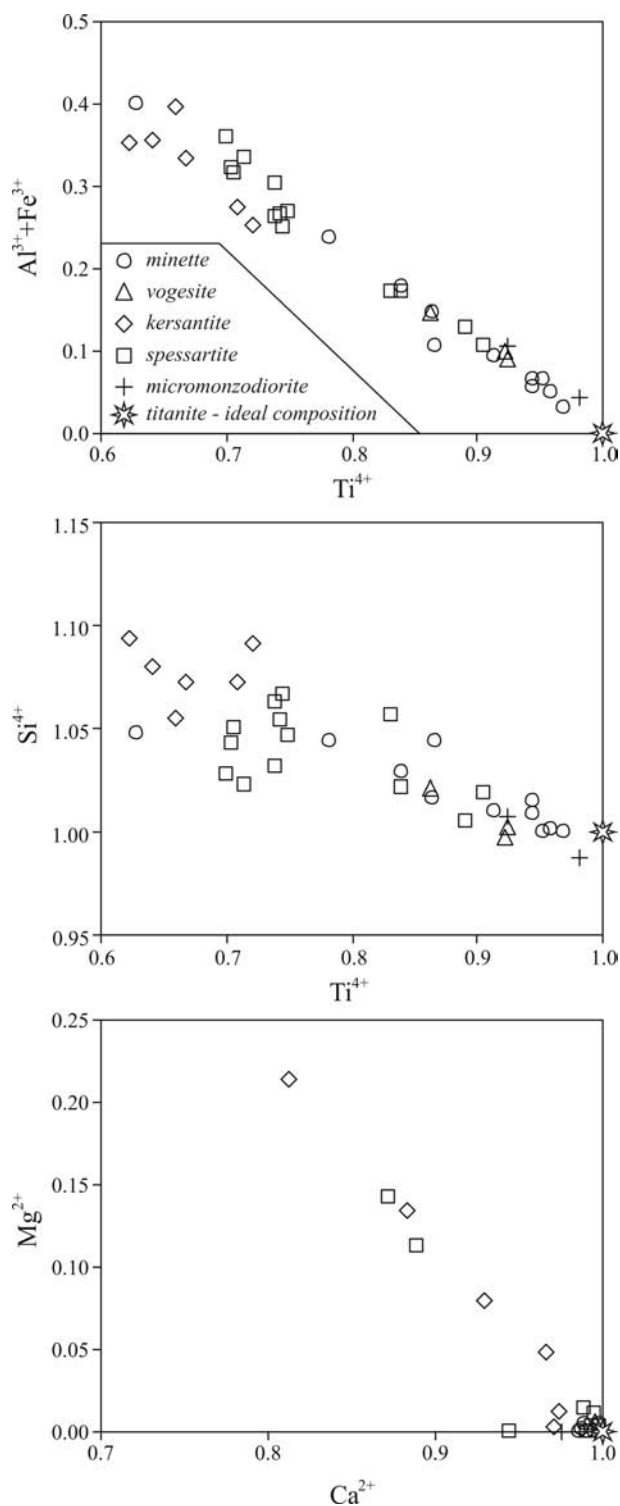


**Fig. 21.** Variation of titanite composition in the mafic rocks studied. The element contents given in cations per formula unit recalculated for 5 O and total Fe = Fe<sup>3+</sup>.

stitution (up to 2.4% TiO<sub>2</sub>, App. 8) and belong to the grandite series. The crystallochemical formulas in Appendix 8 were normalized to 8 cations assuming total Fe = Fe<sup>3+</sup> (when FeO was recalculated into Fe<sup>3+</sup> and Fe<sup>2+</sup> assuming charge balance, negative Fe<sup>2+</sup> was obtained). The

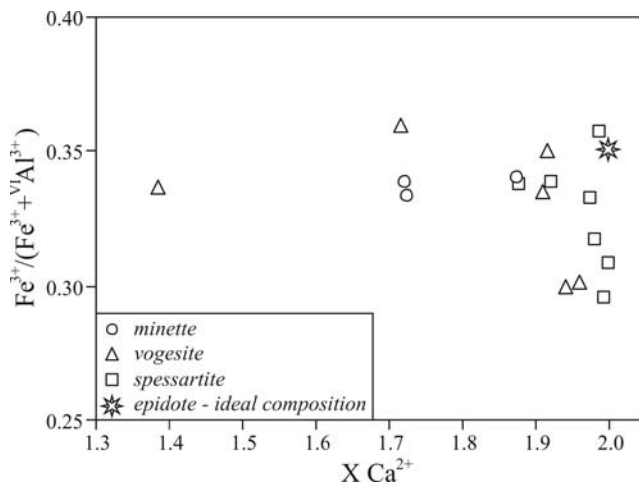


**Fig. 22.** Figure 22. Composition of epidote-group minerals in the Fe<sup>3+</sup> / (Fe<sup>3+</sup> + Al<sup>3+</sup>) vs. X Ca<sup>2+</sup> plot. Values in cations per formula unit calculated for 12.5 O, total Fe = Fe<sup>3+</sup>.

simplified recalculation applied here gives oxide totals close to 100%, as well as reasonable cation proportions (App. 8). End-member calculations show that the garnets are grossularite–andradite solid solutions that are dominated by andradite (Adr 49–63% in 12 out of 16 analyses, more rarely Adr 71–82%); that have substantial Ti-garnet substitution (up to 0.15 Ti c.p.f.u.); and that have very limited pyrope, spessartine and uvarovite substitutions (< 2 mol. % in total).

It is possible that the analyzed garnets contain some hydrogarnet substitution, as is found in similar occurrences elsewhere (e.g., Freiberger *et al.*, 2001). However, a reliable hydrogarnet recalculation, as well as a calculation of the titanian end-members morimotoite and schorlomite, would require confirming the presence of [OH] in the structure and/or additional X-ray diffraction data on site occupancy (Armbruster *et al.*, 1998). A tentative recalculation was, however, attempted, using the following assumptions: First, the cation sum in the octahedral and dodecahedral sites equals 10; second, there are no vacancies in the structure; third, all Ti and Al is allocated to the octahedral site; and fourth, [OH] is in the tetrahedral site only (Armbruster *et al.*, 1998). From these assumptions only, there may be up to 10 % hydrograndite (hydrogrossularite + hydroandradite) and up to 7.5 % of the Ti-garnet morimotoite in addition to the predominant andradite and grossularite end-members.

The composition of prehnite is close to the ideal formula. The main difference is a significant substitution of Fe<sup>3+</sup> for Al<sup>3+</sup> of up to ~0.6 c.p.f.u. in the octahedral sites, which corresponds to ~30% octahedral site occupancy.

Pumpellyites have a variable composition, especially with respect to the Mg<sup>2+</sup> and Fe<sup>2+</sup> (App. 9). Pumpellyites from the KJWDS are usually characterized by very low Mg contents, down to nearly 0, while their Fe<sup>2+</sup> contents are high and range from 0.9 to 1.6 c.p.f.u. By contrast, pumpellyites from the ZSDS usually show higher Mg<sup>2+</sup> of 0.6–0.7 c.p.f.u. and a lower Fe<sup>2+</sup> of below 0.7 c.p.f.u.

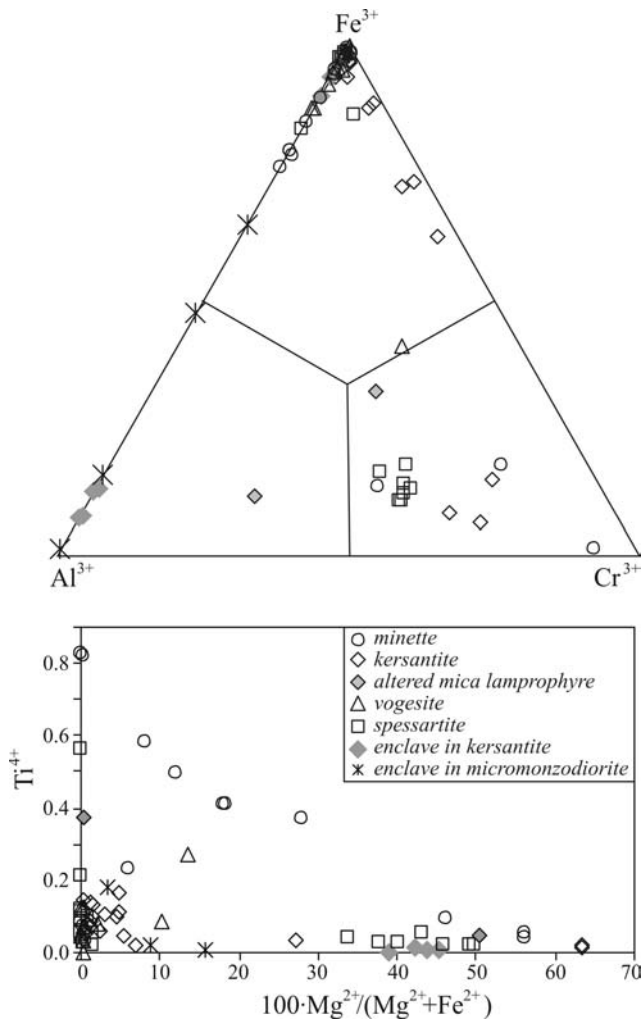


Fig. 23. Composition diagrams for the spinels. Values in cations per formula units, analyses recalculated to 4 O.  $Fe^{3+}$  calculated assuming cation sum = 3.

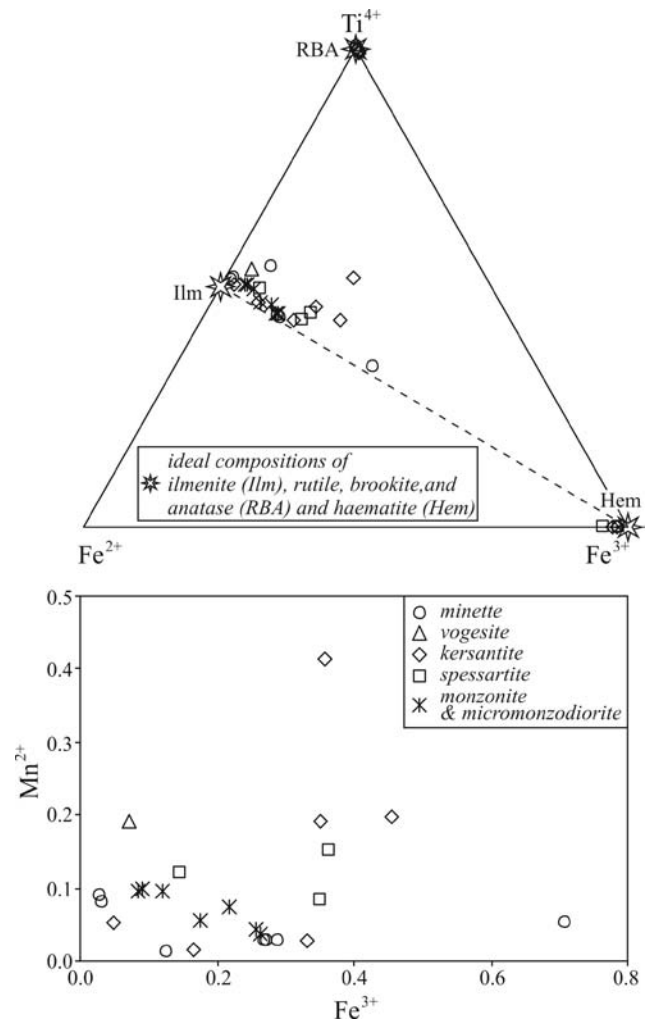


Fig. 24. Composition of ilmenite and haematite in the  $Fe^{2+}$ - $Fe^{3+}$ - $Ti^{4+}$  plot. Analyses recalculated to 3 O,  $Fe^{3+}$  calculated assuming cation sum = 2.

## OXIDES (SPINELS, ILMENITE, HAEMATITE, Ti OXIDES)

Oxides are common minerals in the lamprophyres and related rocks of the Sudetes and occur in small quantities as inclusions in phenocrysts, as inclusions in pseudomorphs, and as fine groundmass grains. In total, 107 analyses of oxides were obtained. Spinel, ilmenite, haematite and titanium oxide(s) were identified in the lamprophyres. However, only ilmenite and haematite were found in the associated mafic rocks. Representative analyses are given in Appendix 10 and general chemical variations are illustrated in Figures 23 and 24.

Most of the analyzed spinels belong to the magnetite series and represent magnetite with small substitutions of Ti, Mg, Al or Cr. Such compositions plot close to the  $Fe^{3+}$  corner in the Al-Fe-Cr triangle (Fig. 23) and characterize the spessartites and vogesites. Magnetites in the minettes show very low Cr and relatively high contents of Ti, Mg and Al, plotting along a trend towards the Al corner, whereas magnetites in the Góry Sowie kersantites show

low Al and Ti but a variable Mg and Cr enrichment, trending towards the Cr corner in the Al-Fe-Cr plot.

Chromite series spinels, though less common, are typically found in a variety of lamprophyres as small inclusions in pseudomorphs after Fe-Mg minerals (mostly after olivine) and in amphibole and pyroxene phenocrysts. Chromite inclusions in the minettes and kersantites of the GDS are mainly magnesiocromite; Mg-rich chromite occurs in the spessartites. Chromites with significant substitutions of Al, Mg,  $Fe^{3+}$  and Ti occur in the altered mica lamprophyres.

In addition, Al-rich spinels of the common spinel series were analyzed in two enclaves in the mafic rocks. In a monzodioritic enclave in the kersantite from Ostrzew Hill (the Góry Sowie Block) the Al spinels are pleonaste, relatively rich in Mg. In a leucocratic, restitic enclave in the micromonzodiorite from the KJWDS, hercynite, ferric hercynite and aluminian magnetite were found.

The composition of the ilmenites tended to depart from the ideal formula of  $FeTiO_3$ . In the  $Fe^{2+}$ - $Fe^{3+}$ - $Ti^{4+}$  diagram (Fig. 24), the analyses plot along the ilmenite-

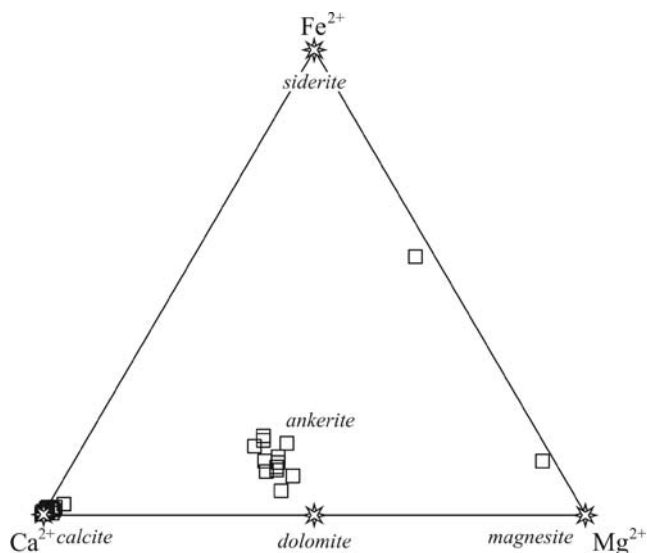


Fig. 25. Composition of carbonates in the Ca-Fe-Mg plot. Stars: ideal compositions of calcite, dolomite, magnesite and siderite. Squares: compositions measured in the rocks studied.

haematite join and represent ilmenite-dominated solid solution of these two end-members. As well as containing up to  $\sim 0.7$   $\text{Fe}^{3+}$  c.p.f.u, these oxides contain up to  $\sim 0.4$   $\text{Mn}^{2+}$  cations and, thus, can be classified as manganese ferri-ilmenites. Only a few haematites were analyzed, and

these show recalculated compositions close to the ideal formula, although low totals may suggest the presence of iron hydroxides.

Titanium oxides were analyzed in five specimens and represent nearly pure  $\text{TiO}_2$ . These are probably brookite and/or anatase and/or some amorphous phases, but detailed identification is hampered by their very fine grain size.

## CARBONATES

Carbonates represent common alteration products in the mafic rocks and occur in various pseudomorphs and as dispersed groundmass grains or vesicle fill. In total, 35 analyses from 16 samples were obtained; representative results are given in Appendix 11. The chemical variations illustrated in Figure 25 show that most of the carbonates are calcite (21 analyses) or ankerite (12 analyses), while two others are Ca-poor carbonates (magnesite-siderite). Most of these carbonates show minor Mn substitution (typically  $< 0.05$ , and in one analysis  $\sim 0.09$  c.p.f.u.). In many of the lamprophyres both calcite and ankerite are found. The widest range of carbonate composition occurred in a kersantite sample from the GDS, which contains calcite, ankerite, magnesite and magnesite-siderite, all within a single quartz-carbonate pseudomorph, probably after olivine.

## BULK-ROCK CHEMISTRY

### GENERAL GEOCHEMICAL AFFINITIES, POST-MAGMATIC ALTERATION AND ELEMENT MOBILITY

Selected bulk rock chemical characteristics of the Sudetic lamprophyres and related mafic rocks are illustrated in Figure 26. Mean minette, kersantite, vogesite and spessartite compositions (from Rock, 1991) are plotted for comparison. Most of the studied samples are intermediate in composition, with moderate contents of alkalis, but some samples are silica-rich and represent acidic compositions. In the total alkali silica (TAS) diagram (Fig. 26A), the samples straddle the boundary between the alkaline and subalkaline series and plot in the fields of basaltic trachyandesites, trachyandesites and trachytes, with a small scatter into adjacent fields. The minettes and vogesites tend to show higher content of alkalis and hence more pronounced alkaline affinities, while other mafic rocks, especially the monzonites and micromonzodiorites, are poorer in alkalis and rather show subalkaline affinities. All the samples plot in the calc-alkaline field of the AFM diagram (not shown here).

Samples classified purely petrographically show relatively little scatter in the TAS plot, despite their degree of alteration. For instance, all fresh to moderately altered minettes of the KJWDS plot in the trachyandesite field, whereas the fresh to moderately altered KJWDS vogesites

and spessartites plot close to the boundary between the basaltic trachyandesite and trachyandesite fields. This suggests that the silica and alkalis, which potentially represent the more mobile major components, were not strongly affected during any post-magmatic alteration processes. However, a few specimens do show more significant chemical changes. In particular, two minette samples and one altered mica lamprophyre sample from the Intra-Sudetic Basin have  $\text{SiO}_2$  contents  $< 50\%$  (the lowest in the whole data set) and probably suffered some depletion in silica. This is consistent with the extensive replacement of silicate igneous minerals by post-magmatic carbonates that is observed in the thin sections. Also, some alkali loss probably occurred in one sample of altered mafic rock that had  $\text{Na}_2\text{O} + \text{K}_2\text{O} < 5\%$ , which is  $\sim 3\%$  lower than in other specimens of these rocks.

The  $\text{K}_2\text{O}$ - $\text{Na}_2\text{O}$  plot (Fig. 26B) shows that many of the rocks studied have a  $\text{K}_2\text{O}/\text{Na}_2\text{O}$  ratio close to 1 and range from mildly sodic (most typical) to mildly potassic. However, nearly all the minettes and several of the vogesites show a distinctive predominance of  $\text{K}_2\text{O}$  over  $\text{Na}_2\text{O}$  and represent potassic rocks. Following the criteria of Foley *et al.* (1987;  $\text{MgO} > 3\%$ ,  $\text{K}_2\text{O} > 3\%$ ,  $\text{K}_2\text{O}/\text{Na}_2\text{O} > 2$ ), all the richterite minettes and some of the other lamprophyres could be classified as ultrapotassic. This ultrapotassic to potassic affinity is a primary igneous feature, as indicated by the modal composition of these

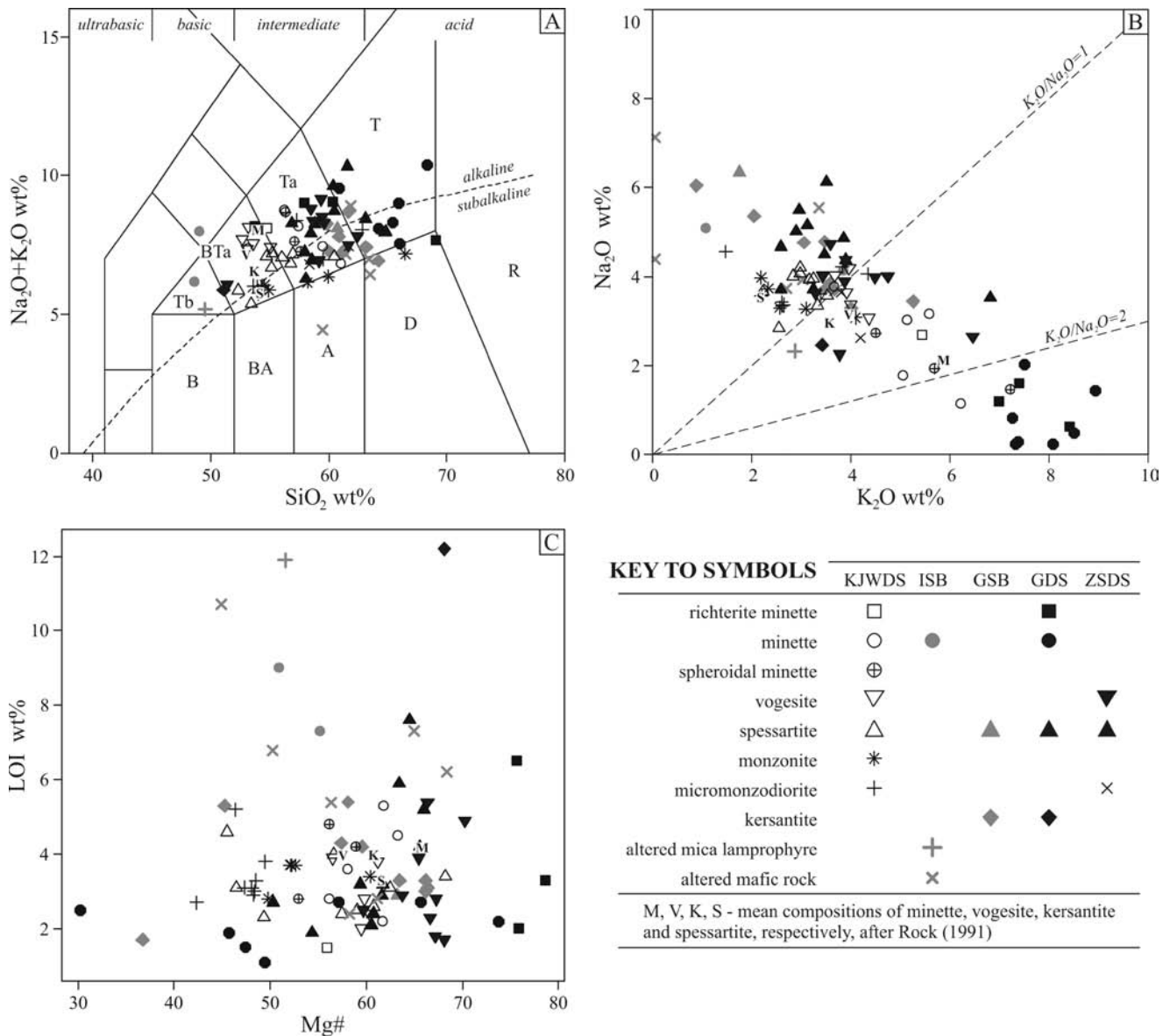


**Fig. 26.** General geochemical characteristics of the lamprophyres and the other mafic rocks. The mean compositions of minette, vogesite, kersantite and spessartite (from Rock, 1991) are plotted for comparison. All major element data in wt%, recalculated to 100% on a loss on ignition (LOI)-free basis. (A) The Le Maitre *et al.* (2002) total alkali versus silica (TAS) diagram, with selected fields annotated: *A* (andesites), *B* (basalts), *BA* (basaltic andesites), *BTa* (basaltic trachyandesites), *D* (dacites), *R* (rhyolites), *T* (trachytes), *Ta* (trachyandesites), *Tb* (trachybasalts). The boundary between the alkaline and subalkaline series is after Irvine & Baragar (1971). (B) Plot of  $\text{Na}_2\text{O}$  vs.  $\text{K}_2\text{O}$ . (C) Plot of LOI vs.  $\text{Mg\#}$  ( $\text{Mg\#} = 100 \times \text{MgO}/(\text{MgO} + \text{FeO})$ ), molar proportions with total Fe as FeO.

rocks, rich in magmatic phlogopite and K-feldspars. However, a few specimens from the Intra-Sudetic Basin (ISB) and from the Góry Sowie Block (GSB) show a strong enrichment in  $\text{Na}_2\text{O}$  (>4%) and depletion in  $\text{K}_2\text{O}$  (<2%). These latter specimens represent strongly altered rocks characterized by a complete replacement of the igneous minerals by, mainly, albite, carbonates and chlorite. Their strongly “sodic” affinities are very likely related to post-magmatic metasomatic alteration.

Figure 26C shows that the magnesium numbers [ $\text{Mg\#} = 100 \times \text{MgO}/(\text{MgO} + \text{FeO})$ , molar proportions with total Fe as FeO] and loss on ignition (LOI) values of the samples studied are high and mostly fall in the ranges of ~45–70 and 1–6%, respectively. Both these parameters gener-

ally reflect the abundance of primary hydrous Mg-rich silicates (dark micas, amphiboles) in the samples studied, though the LOI values could be high if abundant post-magmatic carbonates or chlorites were present: in specimens with the highest LOI (up to ~12%) carbonatization and chloritization was indeed confirmed from thin-sections. These include the altered mafic rocks, altered mica lamprophyre and minettes from the ISB, and kersantite from the GDS. Nevertheless, in these high LOI minette and kersantite samples the alteration is highly selective: pseudomorphs after olivine are abundant, but dark mica and plagioclase remain unaltered.

The geochemical relationships above indicate that the lamprophyres and related igneous rocks of the Sudetes are

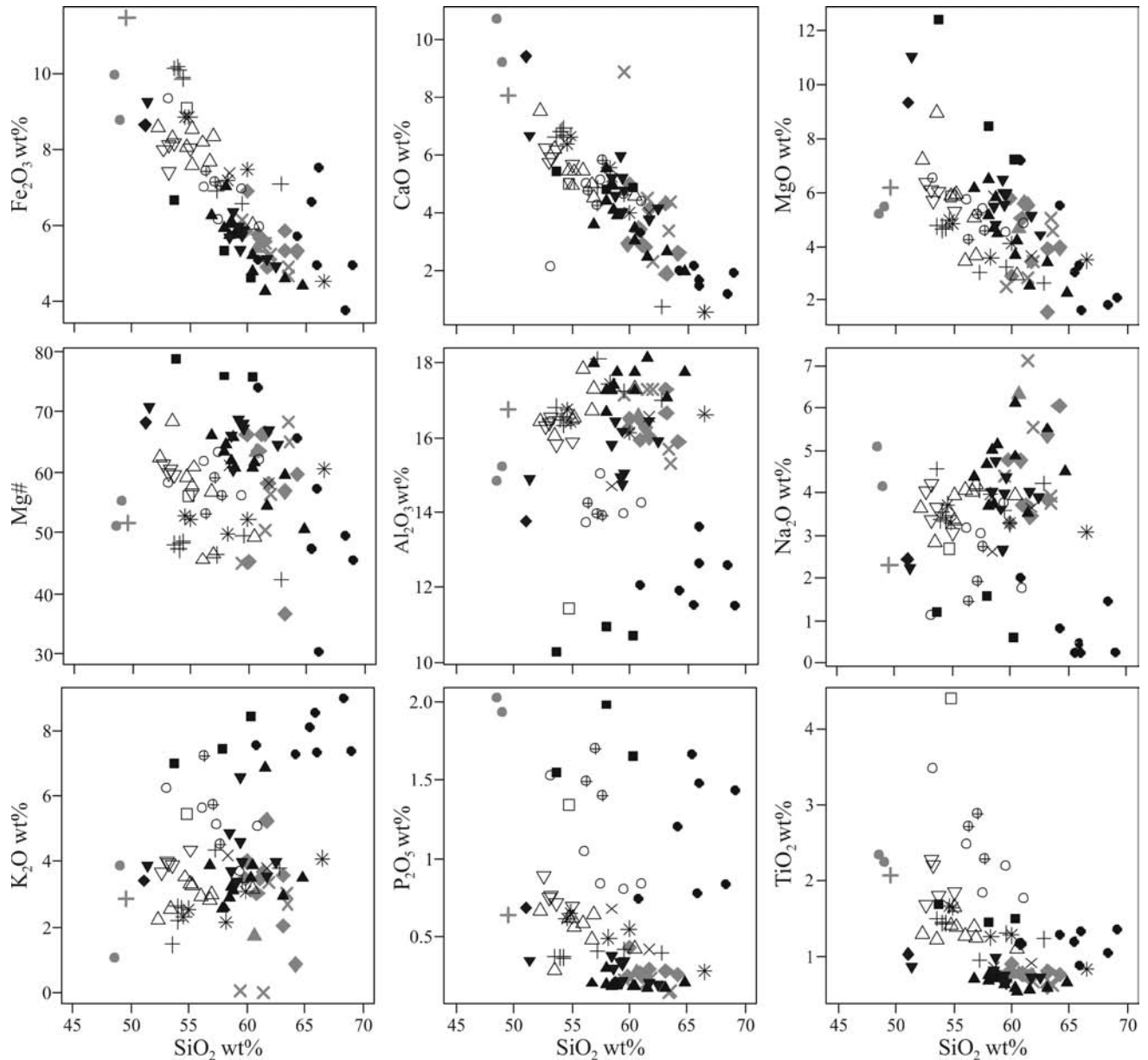


Fig. 27. Major element variation in the lamprophyres and other mafic rocks plotted against  $\text{SiO}_2$ . All values in wt% recalculated on loss on ignition (LOI)-free basis. Symbols as in Fig. 26.

intermediate to acidic, mildly alkaline to subalkaline (calc-alkaline), magnesium rich, and volatile rich. The minettes range from ultrapotassic to potassic, and the other mafic rocks range from potassic to sodic. These characteristics compare well with the general features of lamprophyres, although the Sudetic samples tend to be enriched in silica and alkalis compared to the mean composition of minette, kersantite, spessartite and vogesite given by Rock (1991). The whole-rock chemical compositions of the samples reflect the original magmatic characteristics. Strong chemical changes related to post-magmatic processes are apparent in a relatively few specimens, which are characterized by both petrographic and chemical evidence of strong alteration, including abundant car-

bonates and chlorites, very high LOI and  $\text{Na}_2\text{O}$ , and very low  $\text{K}_2\text{O}$ . Such specimens mainly come from dykes emplaced within the sedimentary rocks of the Central Sudetes.

### MAJOR ELEMENT AND TRACE ELEMENT CHARACTERISTICS

Figure 27 shows the variation of major elements against silica (Harker diagrams) for all the samples analyzed. One can see that  $\text{CaO}$ ,  $\text{Fe}_2\text{O}_3$  (total Fe as  $\text{Fe}_2\text{O}_3$ ) and  $\text{MgO}$  negatively correlate with  $\text{SiO}_2$ , whereas the variations of  $\text{Mg\#}$  and the other elements are less regular. The

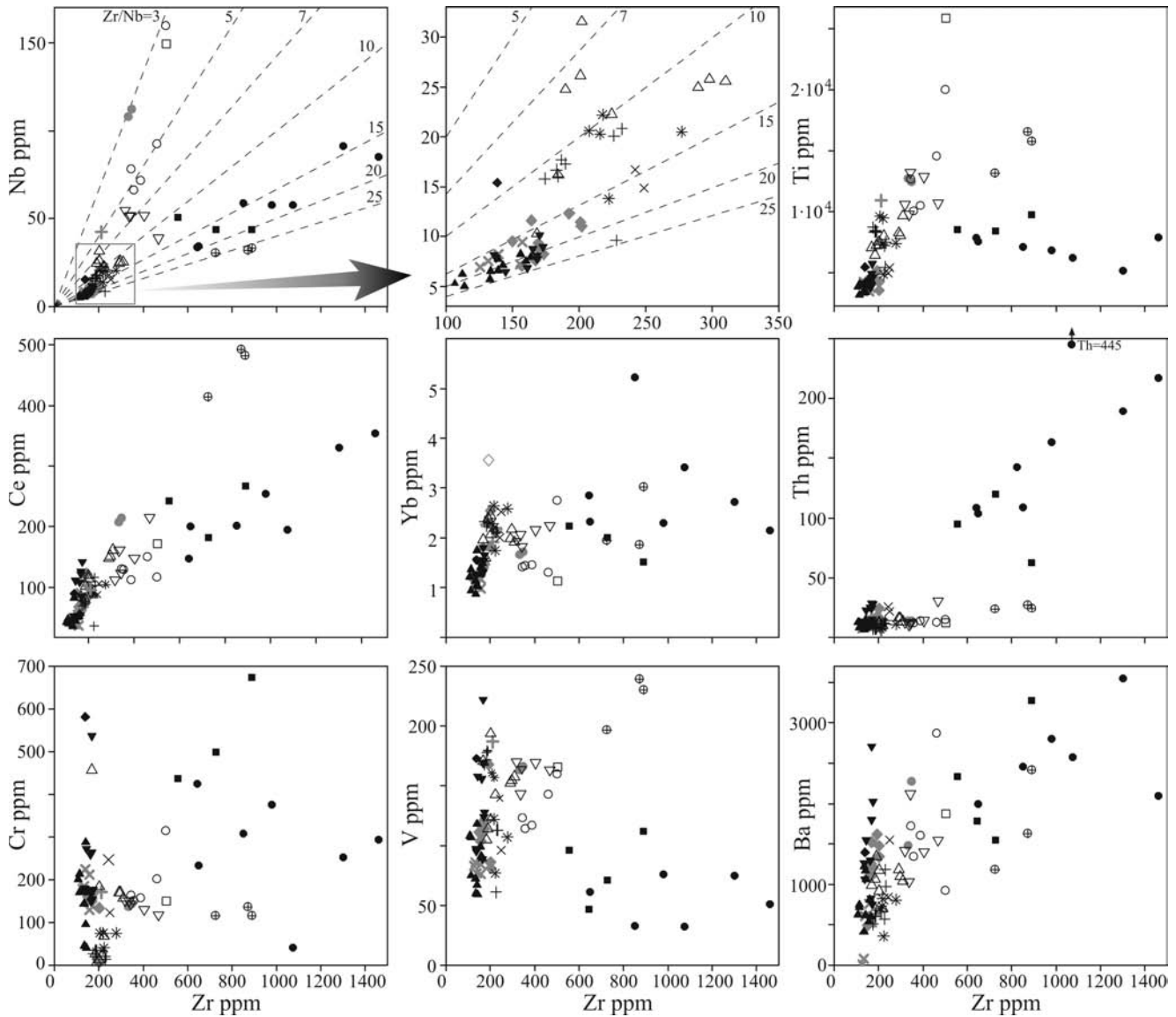


Fig. 28. Variation of selected trace elements against Zr. Symbols as in Fig. 26. Broken lines in the Nb–Zr plots are constant Zr/Nb ratio lines (values given near each line).

plots of CaO, Fe<sub>2</sub>O<sub>3</sub>, MgO and Mg# vs. SiO<sub>2</sub> highlight some regional compositional differences of the mafic rocks. In particular, the mafic rocks from the KJWDS show lower SiO<sub>2</sub>, MgO and Mg#, but higher CaO and Fe<sub>2</sub>O<sub>3</sub> compared to the mafic rocks from the ZSDS and GDS. The mafic rocks from the Central Sudetes area, between the KJWDS to the north-west and the GDS and ZSDS in the south-east, are characterized by a type of transitional, variable composition. The minette and altered mica lamprophyre rocks from the western-central parts of the Intra-Sudetic Basin show strong similarities to the KJWDS mafic rocks, whereas altered mafic rocks of the central and eastern parts of the Intra-Sudetic Basin together with the kersantites of the Góry Sowie Block show affinities to the mafic rocks from the ZSDS and GDS.

The other geochemical plots mainly highlight the compositional distinctiveness of the minettes. Compared to the other mafic rock types, the minettes are character-

ized by lower Al<sub>2</sub>O<sub>3</sub> and Na<sub>2</sub>O, but higher K<sub>2</sub>O and P<sub>2</sub>O<sub>5</sub> contents. There are also some regional differences: the minettes of the KJWDS are characterized by the strongest enrichment in TiO<sub>2</sub>, while the minettes of the GDS show the strongest enrichment in K<sub>2</sub>O and also the lowest Al<sub>2</sub>O<sub>3</sub> contents. Chemical differences also exist between the vogesites and the spessartites, in particular the higher Al<sub>2</sub>O<sub>3</sub> content of the spessartites.

Figure 28 illustrates the variation of selected trace and minor elements plotted against Zr. In all these plots, the minettes are distinguished by their high and strongly variable contents of Zr (~300–1500 ppm) and by significant variations of the other elements. There is also a notable contrast between the geochemical characteristics of minettes from the KJWDS and those of the GDS, e.g., there are lower Zr but higher contents of Nb, Ti and V in the KJWDS minettes; there are higher Zr contents and also high but variable contents of Th, Ba, Ce, Cr in the GDS

minettes. The other mafic rocks show relatively low abundances of Zr, usually between 100 and 300 ppm, and plot in relatively tight, aligned clusters, close to the origin of the diagrams. Several elements show rather scattered variation, but well defined linear trends can be discerned in the Ce–Zr, Ti–Zr and, in particular, the Nb–Zr diagrams. In the Nb–Zr diagram, all rock types from the ZSDS and GDS (except kersantite) plot along a flat-lying trend – trend I – characterized by high Zr/Nb ratios of 10–20 in the minettes and 15–25 in the micromonzodiorites, spessartites and vogesites. Along this trend, the Zr content shows a bimodal distribution, with the high-Zr group represented by the minettes (500–1500 ppm Zr) and the low-Zr group represented by micromonzodiorites, spessartites and vogesites (100–250 ppm Zr). Another trend – trend II – is defined by the rocks from the KJWDS (except the spheroidal minettes) together with minette and altered mica lamprophyres from the western part of the Intra-Sudetic Basin. These rocks plot along a steep line with the Zr contents decreasing continuously from ~500 to 170 ppm and the Zr/Nb ratios increasing from 3 to 6 in the minettes, 6 to 12 in the vogesites, 7 to 12 in the spessartites, and up to 25 in the monzonites and micromonzodiorites. Compared with the well-aligned samples of the spessartites and vogesites of the ZSDS, the mafic rocks that define trend II show a more scattered distribution.

The two trends described above also group the rocks according to geographically and geologically related locations: trend I from the SE, and trend II from the NW parts of the study area, respectively. There are, however, some anomalies. The kersantite sample from the GDS has a relatively low Zr/Nb ratio of ~9 and, thus, shows some affinities with rocks cropping out in the NW (trend II), despite its SE location. Similarly, the spheroidal minettes of the KJWDS show some geochemical affinities to rocks of the GDS (high Zr of ~800 ppm, Zr/Nb ~25) although their other features (e.g., the Ce–Zr and Ti–Zr plots) point to characteristics that are in part gradational between trends I and II. Furthermore, the similar Zr ranges and Zr/Nb ratios of the altered mafic rocks of the Intra-Sudetic Basin and of the kersantites of the Góry Sowie Block suggest strong affinities to the vogesites and spessartites of the ZSDS.

The trace element characteristics of the mafic rocks are further illustrated in the mantle-normalized multi-element ‘spiderdiagrams’ and chondrite-normalized rare earth element (REE) plots (Fig. 29). The samples are grouped according to their geological locations. The samples are considered representative of the data set, and most were analyzed for Sr and Nd isotopes. In addition, selected trace element ratios are plotted against the Zr/Nb ratio to highlight certain characteristics of the various rock types (Fig. 30).

All the normalized patterns share some characteristic features, like the enrichment in the large ion lithophile elements (LILE) and light rare earth elements (LREE) over Zr, Y and the heavy rare earth elements (HREE). Most patterns show a relative depletion in Ta, Nb and Ti. Nevertheless, some mica lamprophyres lack these anomalies and may even show enrichment in these elements. A nega-

tive Sr anomaly occurs in most patterns. The normalized REE patterns are usually smooth, with indistinct to small Eu anomalies. In detail, however, there are the significant regional differences and trends.

In the mantle-normalized diagrams, the richterite minettes of the KJWDS (Fig. 29A) are distinguished from nearly all other mafic rocks of the region by their enrichment in Nb and Ta over the LILEs and the LREEs. Compared to the other rocks from the KJWDS (except the spheroidal minettes, discussed below), the richterite minettes show the highest contents of several high field strength (HFS) elements and LREEs, but the lowest content of Y. The LILE contents also tend to be highest in the richterite minettes, although the normalized patterns in the Cs–K segment partly overlap or cross-cut (in contrast with subparallel patterns in the Ta–Ce segment), and this may be due to some LILE mobility during the post-magmatic alteration. Consistent with trend II illustrated in the Nb–Zr plot (Fig. 28) and with falling Nb and Ta contents from the richterite minettes through minettes, vogesites, spessartites to monzonites and micromonzodiorites, the Zr/Nb ratios increase, the normalized patterns become flatter, and the negative Ta–Nb anomaly becomes more pronounced. This geochemical gradation from the richterite minettes to the micromonzodiorites is equally well displayed in the normalized REE plots (Fig. 29B). The richterite minette element pattern is steepest, showing the highest LREE and the lowest HREE contents. However, the other patterns become progressively flatter due to a coupled decrease of the LREE and an increase in the HREE, which reaches the lowest and the highest levels, respectively, in the micromonzodiorites. This effect may be described as an ‘anticlockwise rotation’ of the REE patterns around an ‘axis’ located at Gd, which shows very similar contents in all the samples. The trends of decreasing La/Yb and increasing La/Nb normalized ratios with increasing Zr/Nb ratio, from the richterite minettes to the micromonzodiorites, is well seen in Figure 30A and B. In addition, Figure 30C demonstrates that nearly all minettes and most other lamprophyres of the KJWDS show small positive Eu anomalies (Eu/Eu\* up to ~1.15), whereas the other mafic rocks (monzonites–micromonzodiorites) show small negative Eu anomalies (Eu/Eu\* down to nearly 0.7).

The spheroidal minettes are distinct from the other minettes of the KJWDS due to very high LREE, HFSE and LILE contents, as well as a strong negative Ta–Nb anomaly. Their specific characteristics are further revealed by very high La/Yb and La/Nb normalized ratios and by a high Zr/Nb ratio (Fig. 30A and B).

Samples from the GDS and the ZSDS reveal different types of relationships (Fig. 29C and D). In the mantle normalized plot, the richterite minette of the GDS is characterized by high and comparable levels of Ta, Nb, Nd, Hf and Zr, resulting in almost subhorizontal central segment of the normalized pattern. However, Th and U show a strong positive anomaly relative to the HFSE, whereas the LILE (Cs, Rb, Ba, K) and the LREE (La, Ce) show much smaller degrees of enrichment. The negative Ta–Nb anomaly is small, but there are pronounced Sr and Ti neg-

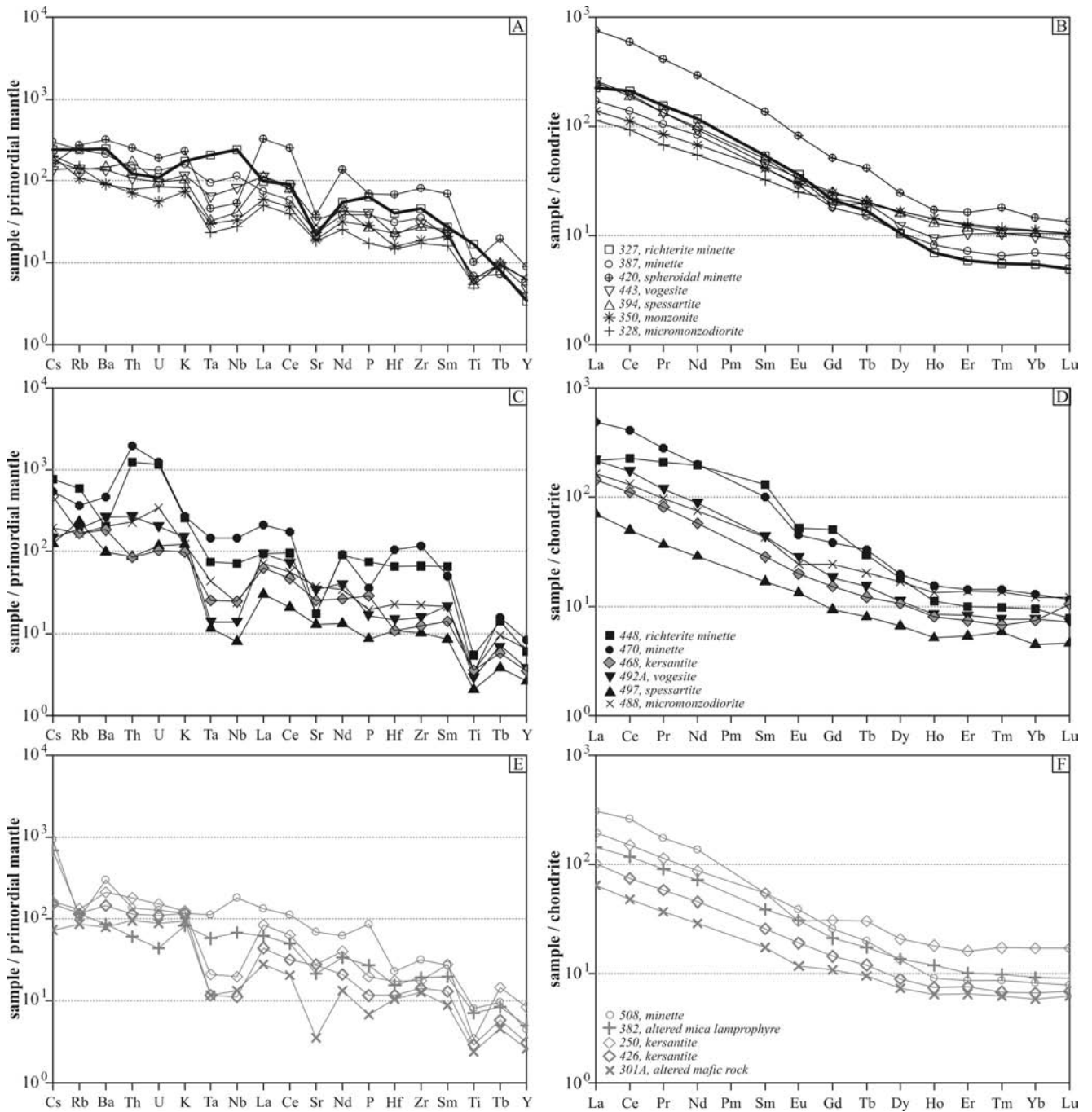


**Fig. 29.** Primordial mantle-normalized trace element patterns (after Wood *et al.*, 1979) and chondrite-normalized rare earth element (REE) patterns of the mafic rocks (after Boynton, 1984). (A) and (B) Patterns from the Karpacz-Janowice Wielkie Dyke Swarm. (C) and (D) Patterns from the Gniewoszów and Złoty Stok Dyke Swarms. (E) and (F) Patterns from the Intra-Sudetic Basin and the Góry Sowie Block. Sample numbers in A to F refer to Appendix 12.

ative anomalies, and the Y content is much lower than the contents of the other HFSE. The richterite-free minette sample shows essentially the same characteristics as the richterite minette but is distinguished by a higher abundance of several trace elements (Th, Ta, Nb, La, Ce, Zr, Hf, Y) as well as by a negative P anomaly. The normalized REE patterns of the minettes display a moderate to strong LREE enrichment relative to the HREE, and also negative Eu anomalies ( $\text{Eu}/\text{Eu}^* = 0.55\text{--}0.73$ ). In addition, the

‘common’ minette shows enrichment in the LREE and HREE but depletion in the middle rare earth elements (MREE) relative to the richterite minette.

The mantle-normalized patterns of the other mafic rocks of the GDS and the ZSDS – vogesites, spessartites, kersantite, micromonzodiorites – display several similarities to each other, and also share the flat Ta–Nb–Hf–Zr pattern (reflected also in the high Zr/Nb ratio, Fig. 30) with the minettes. However, there are several differences

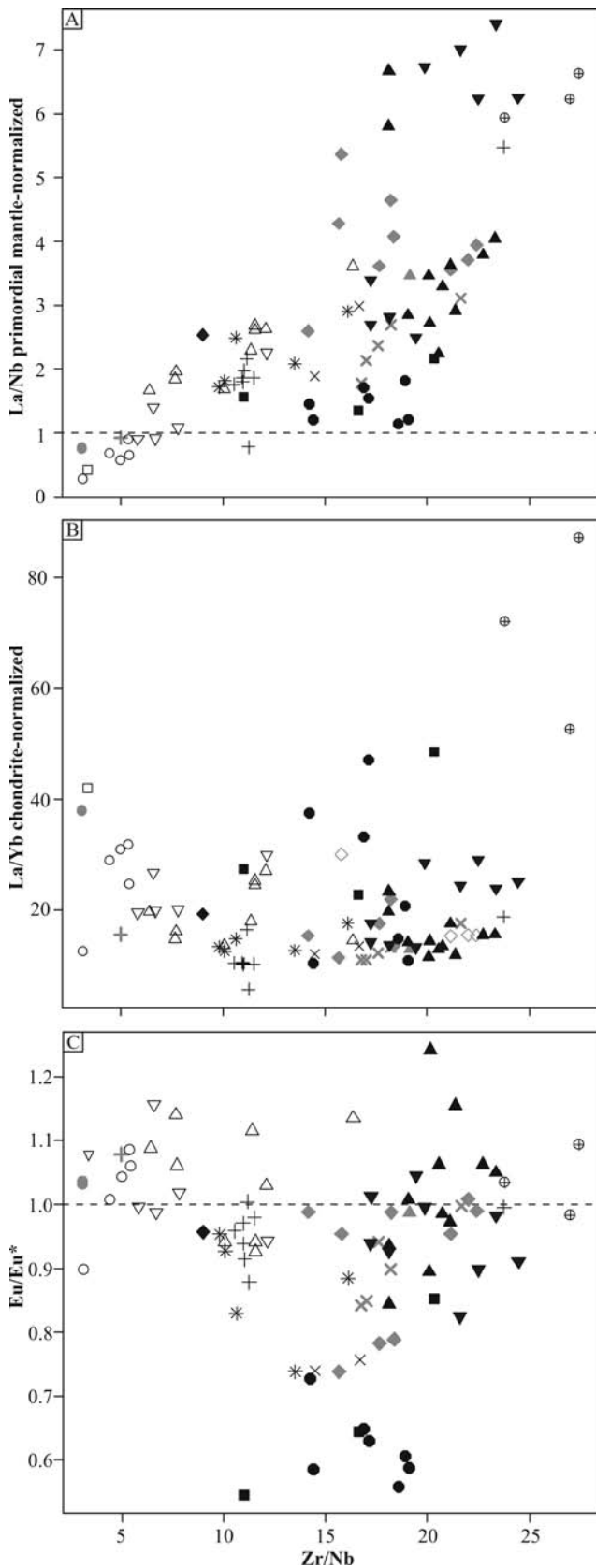


Fig. 30. Ratios of selected trace elements in the mafic rocks plotted against Zr/Nb ratio. (A) Primordial mantle-normalized La/Nb ratio (after Wood *et al.*, 1979). (B) Chondrite-normalized La/Yb (after Boynton, 1984). (C) The  $\text{Eu}/\text{Eu}^*$  ratio ( $= \text{Eu}/(\text{Sm} \cdot \text{Gd})^{1/2}$ ). Symbols as in Fig. 26.

between the mafic rocks of the GDS and ZSDS mentioned above and the minettes: generally lower abundances of most trace elements; a lack of a Th-U positive anomaly; a much more pronounced negative Ta-Nb anomaly; and only small, negative to positive Eu anomalies. The strong negative Ta-Nb anomaly in these rocks mainly results from a stronger LREE/HFSE enrichment (e.g., very high La/Nb ratios in some vogesites and spessartites, Fig. 30A) compared to the minettes. The vogesites differ from the spessartites mainly in their higher contents of most trace elements and in their stronger LREE enrichment (higher La/Nb and La/Yb ratios, Fig. 30A and B). Nevertheless, their geochemical characteristic do partly overlap. The kersantite sample resembles the vogesites, except for its low Zr/Nb ratio which is similar to that of the KJWDS rocks.

The mafic rocks of the Intra-Sudetic Basin and the Góry Sowie Block show a diverse set of trace element characteristics (Fig. 29E and F). The normalized patterns of the minettes and the altered mica lamprophyre from the western part of the Intra-Sudetic Basin show many similarities to the minettes of the KJWDS, in particular a slight enrichment in Ta and Nb over the REE and other HFSE as well as similar degrees of LREE enrichment relative to HREE. However, the kersantites of the Góry Sowie Block and the altered mafic rocks from the Intra-Sudetic Basin show similar affinities as the vogesites and spessartites of the ZSDS, including the negative Ta-Nb anomaly.

## Sr AND Nd ISOTOPE GEOCHEMISTRY

The results of Sr and Nd isotopic determinations are shown in Table 3. The initial Sr and Nd ratios and the  $\epsilon\text{Nd}$  were calculated for 300 Ma, which approximates the upper age limit of the mafic magmatism. Recalculation for 330 Ma, the possible lower age limit of this magmatism, yields very similar results: the  $\epsilon\text{Nd}$  values are higher by less than 0.5  $\epsilon\text{Nd}$  units, and the  $^{87}\text{Sr}/^{86}\text{Sr}$  ratios are lower by less than 0.0005 (less than 0.0015 in the GDS minettes). These differences result in only a small general shift of the whole data set towards the upper left in the  $\epsilon\text{Nd}$ - $^{87}\text{Sr}/^{86}\text{Sr}$  plot (Fig. 31), but the relative positions of the individual points remain almost the same.

The  $^{87}\text{Sr}/^{86}\text{Sr}$  and  $\epsilon\text{Nd}$  values in the mafic rocks studied show a wide variation and a strong negative correlation (Fig. 31). The highest  $\epsilon\text{Nd}$  (about +1.9) and lowest  $^{87}\text{Sr}/^{86}\text{Sr}$  (0.7037) are found in the richterite minette sample from the KJWDS. The richterite minettes from the GDS, at the opposite end of the isotopic trend, show the lowest  $\epsilon\text{Nd}$  (-8.3) and highest  $^{87}\text{Sr}/^{86}\text{Sr}$  (0.7145). The Sr and Nd isotopic characteristics of all other samples fall between these extreme values yet also show distinct regional variations. Samples from the KJWDS, the Intra-Sudetic Basin and the Góry Sowie Block are characterized by higher  $\epsilon\text{Nd}$  ( $> -3$ ) and lower  $^{87}\text{Sr}/^{86}\text{Sr}$  ( $< 0.707$ ), whereas samples from the ZSDS and GDS (except the GDS kersantite) show lower  $\epsilon\text{Nd}$  ( $< -4$ ) and higher  $^{87}\text{Sr}/^{86}\text{Sr}$  ( $> 0.708$ ).

Table 3

Rb–Sr and Sm–Nd isotopic data of the lamprophyres and other mafic rocks

sample	rock	Sm	Nd	$^{147}\text{Sm}/^{144}\text{Nd}$	$^{143}\text{Nd}/^{144}\text{Nd}$	$\pm 2s$	$(^{143}\text{Nd}/^{144}\text{Nd})_i$	$\epsilon\text{Nd}_i$	Rb	Sr	$^{87}\text{Rb}/^{86}\text{Sr}$	$^{87}\text{Sr}/^{86}\text{Sr}$	$\pm 2s$	$(^{87}\text{Sr}/^{86}\text{Sr})_i$
327	rm	10.50	71.20	0.089000	0.512526	3	0.512351	1.9	210	503	1.21	0.708893	6	0.703728
387	m	8.10	49.80	0.098000	0.512471	3	0.512279	0.5	207	530	1.13	0.709472	6	0.704648
420	sm	26.80	177.00	0.092000	0.512292	3	0.512111	-2.7	237	895	0.77	0.710281	8	0.706994
394	s	9.80	59.60	0.099000	0.512320	3	0.512126	-2.5	117	582	0.58	0.708865	6	0.706389
351	s	6.00	35.90	0.101000	0.512381	3	0.512183	-1.3	117	616	0.55	0.708296	8	0.705948
328	mmd	6.30	33.00	0.115000	0.512362	3	0.512136	-2.3	127	429	0.86	0.709860	6	0.706189
382	al	7.60	43.60	0.105000	0.512486	4	0.512280	0.5	98	493	0.58	0.707080	8	0.704604
250	k	4.99	27.20	0.097000	0.512366	4	0.512175	-1.5	101	631	0.46	0.708621	6	0.706657
305	k	5.28	29.10	0.110000	0.512371	4	0.512155	-1.9	95	723	0.38	0.708179	8	0.706557
448	rm	25.20	117.00	0.130000	0.512085	3	0.511830	-8.2	512	405	3.67	0.730160	8	0.714492
465M	rm	35.20	152.00	0.140000	0.512102	3	0.511827	-8.3	634	572	3.21	0.726209	8	0.712505
470	m	19.40	120.00	0.098000	0.512075	3	0.511883	-7.2	314	407	2.24	0.721759	9	0.712196
468	k	5.50	34.40	0.097000	0.512384	4	0.512193	-1.1	144	588	0.71	0.709197	9	0.706166
497	v	8.50	52.90	0.097000	0.512228	4	0.512037	-4.2	164	797	0.60	0.710692	8	0.708131
492A	s	3.30	17.20	0.116000	0.512238	4	0.512010	-4.7	202	298	1.96	0.716844	9	0.708477
488	mmd	8.30	44.70	0.112000	0.512217	4	0.511997	-5.0	143	879	0.47	0.710070	6	0.708064

The concentrations of Sm, Nd, Rb and Sr are in ppm. Standard errors on the mean (2s) are quoted at 95% confidence level. The values of  $(^{143}\text{Nd}/^{144}\text{Nd})_i$ ,  $\epsilon\text{Nd}_i$  and  $(^{87}\text{Sr}/^{86}\text{Sr})_i$  calculated for 300 Ma. Rock abbreviations are as follows: rm (richterite minette), m (minette), sm (spheroidal minette), v (vogesite), k (kersantite), s (spessartite), al (altered mica lamprophyre), mmd (micromonzodiorite)

The Sr–Nd isotopic characteristics of the mafic rocks of the KJWDS change systematically from the richterite minettes and minettes (which possess radiogenic Nd isotope ratios and non-radiogenic Sr isotope ratios that are similar to oceanic island basalts and the bulk-earth) towards the spessartites and micromonzodiorites (which possess less radiogenic Nd isotope ratios and more radiogenic Sr isotope ratios that are similar to crustal values). This trend compares well with the systematic trace element variations characterized above and, although the isotopic ratios of the vogesites and the monzonites were not determined in this study, these rocks would be expected to fall within the described  $\epsilon\text{Nd}$ – $^{87}\text{Sr}/^{86}\text{Sr}$  trend. Consistent with their specific trace element characteristics, the spheroidal minettes have the lowest  $\epsilon\text{Nd}$  and the highest  $^{87}\text{Sr}/^{86}\text{Sr}$  in the KJWDS.

Different, much more crustal-like, Sr and Nd isotopic characteristics are typical of the mafic rocks of the Złoty Stok and Gniewosów Dyke Swarms (except the GDS kersantite). The Sr and Nd isotopic ratios show a bimodal distribution and, as with the Zr–Nb systematics, clearly separate the richterite minettes and the normal minettes of the KJWDS from the vogesites, spessartites and micromonzodiorites of the ZSDS. The ranges of isotopic variation are particularly narrow in the mafic rocks of the ZSDS. Consistent with its trace element data, the kersantite of the GDS displays distinctive isotopic characteristics and plots within the trend of the mafic rocks from the KJWDS.

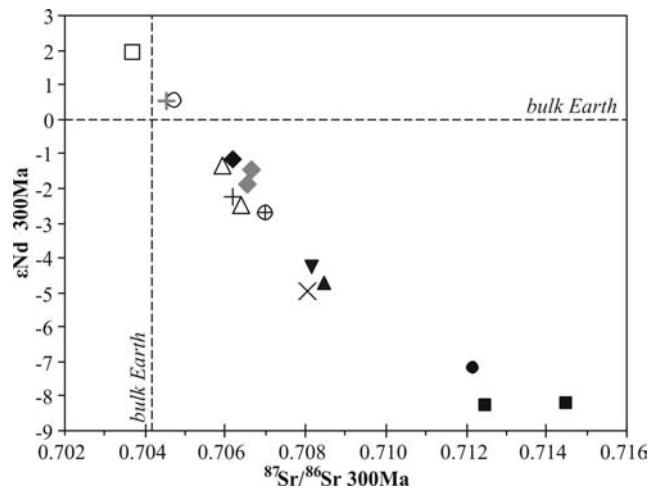


Fig. 31. The  $\epsilon\text{Nd}$ – $(^{87}\text{Sr}/^{86}\text{Sr})$  plot for the mafic rocks. Initial isotopic ratios calculated for 300 Ma. Bulk Earth values calculated for present-day  $(^{143}\text{Nd}/^{144}\text{Nd})_{\text{CHUR}} = 0.512638$  and  $(^{87}\text{Sr}/^{86}\text{Sr})_{\text{UR}} = 0.7045$  (DePaolo, 1988). Symbols as in Fig. 26.

The Sr and Nd isotopic ratios of the mafic rocks of the Intra-Sudetic Basin and the Góry Sowie Block compare well with those of the KJWDS. The altered mica lamprophyre is similar to the minettes and its isotopic ratios are close to bulk Earth values. The kersantites of the Góry Sowie compare well with the spessartites and micromonzodiorites of the KJWDS and also with the kersantite of the GDS.

## ORIGIN, DIFFERENTIATION AND CRYSTALLIZATION OF THE LAMPROPHYRE AND RELATED MAFIC MAGMAS – INTERPRETATION AND DISCUSSION

### MAGMATIC SYSTEMS AND EMPLACEMENT OF THE DYKES

The geological relationships of the lamprophyres and associated mafic dykes in the Sudetes constrain the origin, differentiation and emplacement of these mafic magmas. Because of their localised nature, specific geological position and distinctive rock assemblages, the three dyke swarms distinguished in this paper are interpreted as separate centres of mafic hypabyssal magmatism. All the dyke swarms, as well as the more scattered veins, occur adjacent to some major regional sutures or strike-slip zones. The mafic intrusions postdate the main phases of tectonic displacement, and the sutures and dislocations acted mainly as weakened zones, facilitating and “channelling” the rise and emplacement of magmas within the local crust. The two largest mafic dyke swarms of the Karpacz–Janowice Wielkie Dyke Swarm (KJWDS) and the Złoty Stok Dyke Swarm (ZSDS) show a close association with the Karkonosze and Kłodzko–Złoty Stok granitoid massifs, respectively. A significant role of mantle-derived mafic magmas in the formation and differentiation of the granitoid magmas, due to magma mixing and mingling, is well recognized in both the Kłodzko–Złoty Stok massif (Lorenc, 1994) and, especially, in the Karkonosze massif (Słaby & Martin, 2008). In the Karkonosze massif the mafic, mantle-derived magmatism probably occurred over prolonged periods of time (several millions years) and was involved in the triggering of crustal melting and in the resultant magma mixing processes. This significantly contributed to the formation of the granitic magmas and continued after the consolidation of the Karkonosze pluton (Słaby & Martin, 2008). Notably, both the KJWDS and the ZSDS are characterized by a strong petrographic variation that suggests that magmas were still evolving after the consolidation of the granitoids. In contrast, the smaller Gniewoszów Dyke Swarm (GDS) was emplaced away from granitoid intrusions and shows only limited petrographic variation, reflecting the lack of a long-lived evolving magmatic system in that area. The other mafic dykes in the central Sudetes may show some genetic links with the associated intermediate to acidic volcanic rocks, but these relationships are currently unclear.

The association of the main dyke swarms with the granitoid intrusions also constrains the location of related magmatic systems within the crust. The Karkonosze and Kłodzko–Złoty Stok intrusions were emplaced at mid- to shallow crustal levels (Wojciechowska, 1975; Wierzchołowski, 1976; Mierzejewski & Oberc-Dziedzic, 1990), and field structural data show that the mafic dykes of the KJWDS and the ZSDS were mostly emplaced after the crystallization, consolidation and cooling of their host granitoids. Only a minority of dykes show bending or interdigitation with the granitoids, and these structures indicate emplacement into early fractures when the host granites were still not fully consolidated (see Fig 10 in

Barbarin, 2005). In general, the host granitoid massifs acted as country rocks for the intruding mafic dykes and, therefore, any differentiation processes that affected the mafic magmas occurred below the granitoid plutons, at lower to mid-crustal levels.

The petrographic homogeneity of the great majority of dykes indicates that they represent batches of compositionally uniform magma. However, a composite minette–vogesite dyke in the KJWDS points to a local coexistence and roughly contemporaneous emplacement of two compositionally distinct lamprophyre melts of minette and vogesite composition. The smaller-scale modal banding in this composite dyke probably reflects flow-related segregation of crystals and magma during the dyke emplacement. In addition, local networks of leucocratic veins at some minette and altered mica lamprophyre localities (KJWDS, Intra-Sudetic Basin, GDS) probably formed due to late-stage, post-emplacement segregation of residual, evolved melts into contraction fractures within the dykes.

### PETROGRAPHIC CONSTRAINTS ON THE MAGMATIC AND POST-MAGMATIC PROCESSES

The modal composition of the lamprophyres from the Sudetes falls into the ranges given for calc-alkaline lamprophyres (Table 3.2 in Rock, 1991). The petrographic data presented in this paper document a gradation from mica lamprophyres, through amphibole lamprophyres, towards the associated monzonitic-monzodioritic rocks. This gradation is expressed in two ways: first, a general decrease of the colour index from ~65–60 in some minettes and kersantites through 55 to 35 in most other lamprophyre samples down to 30–20 in some felsic lamprophyres and micromonzodiorites; and second, the change from more hydrous, phlogopite- and biotite-dominated phenocryst assemblages in the minettes and kersantites, through amphibole-dominated assemblages in the vogesites and spessartites, to anhydrous clinopyroxene–plagioclase assemblages in the monzonites and micromonzodiorites. In some spessartites that are transitional between the lamprophyres and the monzonites-micromonzodiorites, plagioclase phenocrysts began to appear.

This variation in modal compositions and phenocryst assemblages can mainly be linked with crystallization from magmas of changing bulk compositions and of variable water contents. As discussed by several authors (e.g., Sisson & Groove, 1993; Johnson *et al.*, 1994; Carmichael *et al.*, 1996; Feldstein & Lange, 1999), dissolved water lowers the liquidus temperatures of magmas, stabilizes hydrous silicates and suppresses plagioclase crystallization due to the depolymerization of the melt. At high water fugacity (> 3–5 wt % of dissolved H<sub>2</sub>O in the melt), dark micas and amphiboles crystallize first; even at modest water fugacities, the crystallization of anhydrous Fe–Mg silicates, like

olivine and clinopyroxene, as well as the Fe-Ti oxides, is enhanced relative to feldspar.

Based on these relationships, the petrographic variation from the mica lamprophyres through the amphibole lamprophyres to the monzonites and micromonzodiorites generally reflects crystallization from more and more evolved and drier magmas. In addition, following the arguments discussed by Wilson (1989) for amphiboles in island arc- and active continental margin-related volcanic and plutonic suites, the abundance of euhedral amphiboles in the Sudetic lamprophyres indicates an early crystallization of these minerals and at some depth in the crust. The lack of opacite rims is consistent with moderate pressure of final cooling under subvolcanic conditions, in contrast to volcanic suites in which low-pressure amphibole instability results in extensive decomposition of amphiboles to opacite. A similar reasoning can account for the common occurrence of euhedral dark micas, without opacite rims, in the minettes and kersantites.

The abundance of crystal and rock fragment inclusions in lamprophyres has long been recognized (Rock, 1991), and the origin of such inclusions relative to their host rocks vary from wholly accidental (xenocrystic) to closely related (comagmatic, cognate). Granite xenoliths and feldspar and quartz xenocrysts are common within the KJWDS and were apparently derived from the Karkonosze granite during the late stages of dyke emplacement. Several other inclusion types in the KJWDS, and at some other localities (e.g., Ostrzew Hill), probably formed as a result of specific crystallization and differentiation processes that affected individual lamprophyre magmas, such as interaction with crustal materials.

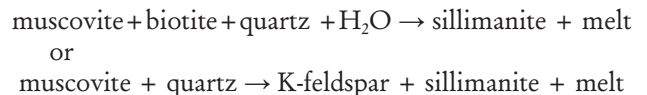
Relatively common inclusions in the minettes of the KJWDS and the Intra-Sudetic Basin are rounded, embayed quartz crystals with clinopyroxene reaction rims. These crystals possibly originated due to mixing lamprophyre and silicic magmas. The influence of mixing and mingling processes is further supported by the presence of the leucocratic enclaves and spheroidal textures in some minettes, suggesting dispersal of more viscous felsic melt in a less viscous mafic host. Almost identical "globular" textures are common in, and similar interpretations have also been proposed for, the minettes from the Fränkisch-Thüringisches Schiefergebirge in south-east Germany (von Seckendorff *et al.*, 2004). The minettes of the Intra-Sudetic Basin also contain phlogopite glomerocrysts and small enclaves. Similar dark mica enclaves are encountered in the minettes of the GDS. Such enclaves most likely represent cognate crystal aggregates (autoliths) and may be indicative of fractional crystallization processes.

The vogesites and spessartites in the Sudetes generally lack any specific inclusions, except the coarsely porphyritic vogesites of the ZSDS. The distinctive, heterogeneous pheno- and xenocryst assemblage – phenocrysts of amphibole; xenocrysts of biotite, quartz and titanite – of these latter rocks points to an influence of magma mixing processes in the evolution of these vogesite magmas.

In the micromonzodiorites of the KJWDS are oval, leucocratic, quartz- and alkali feldspar-rich ocellae that can be interpreted as the products of decompression-related

segregation of siliceous fluids (cf. Mauger, 1988; Rock, 1991). However, there are also fine-grained magmatic enclaves and glomerocrysts composed mostly of altered plagioclase and clinopyroxene (Fig. 7A). Strong modal and mineralogical affinities with the host micromonzodiorites support the interpretation of these inclusions as comagmatic enclaves (autoliths) that originated as crystal aggregates (cumulates) during a pre-emplacement crystallization of the micromonzodiorite magma. The presence of these enclaves argues for the operation of fractional crystallization processes, and the abundance of such enclaves further suggests that these processes were regionally influential in the micromonzodiorites of the KJWDS. Cognate enclaves composed of hornblende, biotite and plagioclase also occur in the micromonzodiorites of the ZSDS, and these enclaves may also be related to fractional crystallization processes.

Other enclaves in the micromonzodiorites of the KJWDS, however, indicate that contamination with partly melted crustal rocks was also involved in the differentiation of the micromonzodiorite melts. The modal composition and texture of the leucocratic fine-grained enclave illustrated in Figures 3F and 7B are almost identical to the partly melted gneisses described by Mehnert *et al.* (Fig. 2, 1973). This enclave can be interpreted as a crustal xenolith partly melted, mingled with, and assimilated in, the host micromonzodiorite. Similarly, the sillimanite-bearing enclave illustrated in Fig. 7C texturally resembles a fragment of flecky gneiss (Fig. 20 in Mehnert, 1971) and its modal composition suggests a formation resulting from melting reactions such as those discussed by Thompson (1982) and Yardley (1989):



The enclave is therefore interpreted as restite after partial melting/migmatization of some metapelitic rock, becoming incorporated at a deep level within the micromonzodiorite magmatic system. The cognate and migmatization-related enclaves suggest that the micromonzodioritic magmas evolved from assimilation-fractional crystallization processes.

Inclusions are also abundant in the kersantites of Ostrzew Hill in the Góry Sowie Block. Some quartz and feldspar macrocrysts may represent xenocrysts derived from adjacent country rocks, at the emplacement level of the intrusions. Overall, however, the diversity of inclusions at this locality indicates that several processes from deeper parts of the magmatic system were involved. Modally and texturally variable enclaves; sieve-textured, partly resorbed diopside macrocrysts; poikilitic to sieve-textured plagioclase and biotite in some enclaves; and partly restitic mineralogy (Al-spinel inclusions) all suggest a mixing and interaction of melts of various compositions, partial melting of some crystals, and possibly the remelting of early crystallization products. The presence of quartz and feldspar-rich ocellae further indicates a rapid segregation of siliceous fluids (Mauger, 1988).

The petrographic characteristics of the analyzed Sudetic rocks point to a widespread occurrence of post-magmatic mineral assemblages variably overprinting the igneous assemblages. The alteration may have occurred due to the influence of post-magmatic fluids during the late cooling stages of the dykes, but could equally be due to some younger fluid–rock interaction episodes unrelated to the magmatic processes. A pronounced alteration and the very rare preservation of magmatic minerals is characteristic of the dykes emplaced in the sedimentary rocks in the Central Sudetes. The most characteristic post-magmatic minerals at these locations are chlorites, carbonates, quartz and albite. In contrast, dykes emplaced within the crystalline basement rocks are generally less altered, and the post-magmatic mineral assemblages are more variable, including sericite, epidote-group minerals, actinolite, prehnite, pumpellyite and grandite garnets. The differences in the degree and style of alteration reflect different post-emplacment histories, and/or different conditions of fluid–rock interactions of the dykes in their different host rocks. The sedimentary host rocks of the Central Sudetic locations may have given rise to a relatively pronounced alteration of the subvolcanic rocks during diagenesis, whereas dykes emplaced in the crystalline basement were much less affected, or not affected at all, by such processes.

#### MINERALOGICAL CONSTRAINTS ON THE MAGMATIC AND POST-MAGMATIC PROCESSES

The dark micas, amphiboles and clinopyroxenes in the analyzed Sudetic rocks exhibit wide compositional variations, and the composition of these minerals changes systematically with their host rock. These relationships reflect a general control of bulk magma composition on mineral chemistry and the influence of crystallization conditions. However, the intensive variables of temperature, pressure and oxygen fugacity during crystallization of the various minerals cannot easily be quantified. For example, Ba and Ti partitioning between phlogopite and the coexisting melt may be used to calculate the pressures and temperatures of crystallization, but the melt composition must be independently known, either from additional groundmass analysis or from recalculation of bulk-rock chemical data and phenocryst modal and compositional data (Righter & Carmichael, 1996). Separate groundmass analyses are not available for the rocks studied, and any recalculation seems unreliable because of the complex zoning in the phenocrysts. Similarly, crystallization pressure estimates using the Al-in-hornblende geobarometer (e.g., Féménias *et al.*, 2006) are not possible because of inappropriate phenocryst assemblages: there are no plagioclase phenocrysts associated with the amphibole phenocrysts. Potentially, crystallization pressures can be calculated using the clinopyroxene geobarometer, but this method requires an independent, accurate estimate of temperature (Nimis, 1999). Because of these limitations, the quantitative approach is here avoided. Furthermore, a detailed analysis of the post-magmatic mineral assemblages and

their crystallization conditions is beyond the scope of this study. However, the mineral chemistry and zoning patterns do provide important qualitative constraints on the petrogenesis of the lamprophyres and the other rocks studied, and these aspects are discussed below.

The textures and compositions of the phlogopite and biotite phenocrysts place constraints on the differentiation processes operating in the mica lamprophyre magmas (Figs. 11 and 12). Data for the minettes of the KJWDS and the Intra-Sudetic Basin lead to three conclusions: First, the mica phenocryst assemblages in these rocks are heterogeneous and comprise crystals that initially formed at different conditions, crystallizing from magmas of various composition and/or at different P–T conditions; second, phenocrysts of different origins were assembled together due to magma mixing; third, the mixing of magmas and related changes in the P–T–X conditions (X = melt composition) resulted in the partial resorption and chemical zoning of phenocrysts. The presence of two main mica phenocryst populations, and the large compositional contrast between the cores of normally zoned phlogopites and the reversely zoned biotites, show that these latter three processes could have occurred due to an interaction of two major end-members: a volumetrically dominant, primitive, mantle-derived magma carrying phlogopite phenocrysts and a volumetrically subordinate, more evolved melt of, likely, crustal origin, containing biotite phenocrysts. These melts could have interacted during the passage of the primitive magmas through the continental crust. Given that both populations of phenocrysts in the minettes seem to include some sub-populations characterized by more subtle differences in composition, zoning and resorption textures, it is possible that the mixing processes occurred at distinct stages within more complex, evolving magmatic systems (e.g., recharged with primitive melts from the mantle, with variably evolved magmas developed, stored and interacting at different levels), and that some crystals underwent ‘recycling’ within this system. The magma that was finally emplaced as the minette dykes, although dominated with the mantle-derived end-member, could represent a hybrid of various melts aggregated during the tapping and draining of the whole magmatic system.

Similar mica compositions and zoning styles are found in the minettes and kersantites of Northern England, among other sites (Meyer *et al.*, 1994). According to Meyer *et al.* (1994), the minettes of Northern England carried heterogeneous phlogopite phenocryst assemblages and formed due to magma mixing in a continuously replenished, fractionating magma chamber. The model proposed for the KJWDS minettes is similar, but the presence of two distinctive phenocryst populations argues for a more significant role of two end member mixing processes.

By contrast, the minettes of the GDS contain a homogeneous population of phlogopite phenocrysts that show normal zoning at the rims and only scarce evidence of magmatic corrosion. The evolution of these minette magmas was apparently different, without a significant influence of magma mixing processes. The normal zoning of the phlogopite rims probably reflects crystallization from

residual, more fractionated melts, during enhanced cooling, following the emplacement of the minette magma in the dykes. However, the phlogopite zoning could also have depended on more than one intensive parameter, including temperature, oxygen fugacity and/or water fugacity (Wones & Eugster, 1965).

The dark micas are also important components of the kersantites. Compared to the micas in the minettes, the relatively Fe-rich compositions of the kersantite micas (Fig. 11D) are consistent with crystallization from Fe-enriched melts. The lack of significant chemical variation and zoning of these micas suggest a more stable P-T-X conditions of their crystallization compared with the minettes of the KJWDS and the Intra-Sudetic Basin. On the other hand, the inclusions and enclaves suggest a strong influence of disequilibrium/open system processes in the Góry Sowie Block kersantites. The Al- and Fe-enrichment trend defined by the mica phenocrysts and by the micas from the enclaves (Fig. 11D) may have resulted from the contamination of a more primitive, Al-poor melt with a more evolved, Al-rich crustal component. Possibly, the relatively Fe-rich and homogeneous dark mica phenocrysts in the kersantites crystallized relatively late and from already contaminated melts.

The evolution of the vogesite and spessartite magmas is constrained by the mineral chemistry and textures of the amphiboles (Figs. 13 and 14). The wide chemical variation of the amphiboles (from groups 1 to 4) together with their textural variations, reflect a multiplicity of origins. Amphiboles of the first group are apparently magmatic in origin. The regional variation (KJWDS vs. Góry Sowie Block vs. KZSDS) in amphibole composition may largely reflect differences in melt compositions in the separate magmatic systems that were tapped during the emplacement of the different dyke swarms. In the vogesites of both the KJWDS and the ZSDS, the distinctive phenocryst textures and zoning patterns indicate a history of two or more growth stages, partial resorption of the early formed phenocryst cores, and a resumption of crystallization under new conditions. The rapid enrichment in magnesium at the transition from the resorbed cores into the outer shells of the phenocrysts strongly suggest that resorption was followed by crystallization at a higher T and/or from more magnesian melts. These features may reflect mixing of magmas with various compositions and temperatures, possibly due to the replenishment of magmatic systems where crystallization of phenocryst cores took place within more primitive, Mg-rich, hotter melts. The influence of magma mixing in the vogesites of the ZSDS is also supported by the presence of partly resorbed (and possibly reversely zoned) biotite xenocrysts. It can also be suggested that the more complex oscillatory zoning in the KJWDS amphibole phenocrysts reflects a prolonged crystallization at unstable conditions due to further, smaller-scale changes of melt chemistry, or repeated episodes of mixing. The texturally less complex ZSDS amphibole phenocrysts imply a more rapid sequence of events, with a mixing event immediately preceding, and possibly even causing, the final rapid magma emplacement into the dykes.

In contrast to those in the vogesites, amphibole phenocrysts of the spessartites are only weakly zoned, implying crystallization under relatively stable conditions. However, zoning in amphiboles from the spessartites of the KJWDS tends to be stronger and suggestive of a more complex/prolonged crystallization, compared to similar amphiboles from the ZSDS. In both groups of spessartites the stronger zoning near the rims of the phenocrysts probably reflects disequilibrium crystallization related to the emplacement and rapid cooling of the magmas in the dykes. Similarly, relatively weak zoning is also characteristic of the group 1 amphiboles in the kersantites of the Góry Sowie Block.

The amphiboles of groups 2 and 4 represent mainly late-magmatic to early post-magmatic crystallization products, as indicated by their textural positions as groundmass crystals or as overgrowths on other amphiboles. Magnesiohornblende (group 2) is widespread in many common igneous rock types (e.g., granitoids, dioritoids), but the occurrence of the Na-Ca to Na igneous amphiboles (group 4) is relatively rare and typical of alkaline rocks of a specific composition, e.g., some syenites or riebeckite granites (Deer *et al.*, 1992). Richterite is a characteristic mineral of richterite-phlogopite lamproites (Mitchell, 1997; Le Maitre *et al.*, 2002). However, richterites in lamproites show extremely high contents of TiO<sub>2</sub> (>3% wt.) and K<sub>2</sub>O (>4%), but those in this study showed lower percentages in these components: <2.8% and <3.7%, respectively. Nevertheless, some gradation towards lamproitic affinities in the richterite minettes of the Sudetes is apparent.

The actinolites of group 3, as well as blue Na-Ca to Na amphiboles (ferriwinchyste-riebeckite), represent post-magmatic amphiboles. The actinolites are characteristically associated with chlorites, epidote-group minerals, carbonates and other minerals that replace the primary, igneous phases. In general, these replacement minerals must have formed at conditions similar to those of the greenschist facies, due to the hydrothermal/autometasomatic processes that affected the rocks at the late cooling stages and that partly overprinted and obscured the magmatic mineral assemblages. This style of alteration is very common in lamprophyres (Rock, 1991). However, the blue amphiboles must have formed under quite specific conditions, possibly related to bulk chemistry of the host minette and/or a more unusual chemistry of the post-magmatic fluids.

The regional variation in clinopyroxene compositions, as well as the differences between various rocks within individual dyke swarms (Fig. 15), are very probably related to differences in the magma compositions from which the clinopyroxenes crystallized. The widest clinopyroxene variations are from the KJWDS, where the gradual changes in clinopyroxene composition from the Mg- and Cr-rich diopsides in the lamprophyres to the Fe-enriched augites in the monzonites and micromonzodiorites may reflect crystallization from progressively more evolved melts. The Al enrichment in the clinopyroxenes of the monzonites and micromonzodiorites (Fig. 16) and the petrographic data suggests that there was an interac-

tion of these latter magmas with Al-rich components of crustal origin (e.g., partial melts). The textural diversity and zoning patterns of the clinopyroxene phenocrysts probably resulted from both differentiation-related processes and emplacement-related processes. Compositionally distinct or sieve-textured cores in the clinopyroxenes suggest changes in magma composition, as might be expected from magma mixing or contamination (O'Brien *et al.*, 1988). The oscillatory and sector zoning, which are characteristic of rapidly cooled volcanic rocks (Dowty, 1976; Shelley, 1993) can be linked with crystal growth during enhanced cooling of the magma within the dykes. In addition, the strongly Fe-enriched hedenbergite, and similar compositions, reflect late-stage crystallization and possible interactions with evolved, residual melts. Similar interpretations can be applied to the kersantites in the Góry Sowie Block and to the vogesites of the ZSDS: partial resorption of early phenocrysts induced by changes in magma chemistry due to contamination or magma mixing. The more homogeneous clinopyroxenes in the kersantite from the GDS, however, seem to have crystallized under much more stable conditions.

The observed diversity of feldspar composition in the rocks studied (Fig.18) is related to both magmatic and post-magmatic processes. The switch in feldspar compositions from K- and Na-rich alkali feldspars in the minettes and vogesites to dominantly Ca- and Al-rich plagioclase in the other lamprophyres and mafic rocks reflects general changes in the composition of the magmas from which these feldspars crystallized. Following the intrusive, subvolcanic emplacement, the various magmas crystallized rapidly in relatively thin dykes. Under such conditions, exsolution textures in alkali feldspars formed only rarely in some of the thicker and more slowly cooled dykes, such as the 10 m thick richterite minette dyke near Gniewosów. Even there, however, the perthitic lamellae are only micrometres thick (microperthite), and the compositional difference between the host K-feldspar and the exsolved Na-K feldspar is small (~20% Or), which indicates "freezing" of the system at an early stage of exsolution. Similarly, the high cooling rates account for the normal zoning of groundmass plagioclase laths observed in some specimens. Nevertheless, one must remember that plagioclase compositions and zoning patterns are strongly obscured by the widespread post-magmatic alteration. Apart from sericite, the ubiquitous component of the pseudomorphs after plagioclase is albite: this mineral also forms metasomatic perthites (as patchy intergrowths) in the K-feldspar of some minettes. And although the post-magmatic origin of most albite in the rocks studied is unambiguous, some vogesite samples contain groundmass euhedral K-feldspar laths and similar albite laths: a magmatic or post-magmatic origin for these albite laths is more equivocal.

Garnets, prehnite and pumpellyite have not, prior to this study, been recognized in the lamprophyres and related mafic rocks of the Sudetes. These minerals might be very widespread, but they are not easy to recognize because they occur as indistinct, microcrystalline groundmass aggregates. Prehnite, pumpellyite and epidote-group

minerals are characteristic components in mafic igneous rocks affected by very low to low-grade metamorphism (prehnite-pumpellyite facies). These minerals, together with grandite-series garnets are also subsolidus autometasomatic alteration products in plutonic rocks of granitic and syenitic to dioritic composition (Freiberger *et al.* 2001). The minerals mentioned above, in the mafic rocks of the Sudetes formed due to hydrothermal/autometasomatic alteration processes during the subsolidus cooling of the dyke rocks. The garnets, prehnite and pumpellyite preferentially formed in mafic rocks rich in plagioclase, where the hydrothermal decomposition of coexisting igneous Fe-Mg silicates (dark micas, pyroxenes) and Ca-rich plagioclase provided the necessary components for the crystallization of the post-magmatic Mg-Fe-Ca-Al silicates, at conditions corresponding to the sub-greenschist facies. However, the post-magmatic mineral assemblages in many samples are highly variable and also include chlorites, actinolite, albite and others that probably formed at greenschist facies. Therefore, four conclusions can be derived from the low-grade mineralogy: First, the subsolidus alteration processes generally occurred over a relatively wide range of conditions, spanning the greenschist and sub-greenschist facies; second, the mineral assemblages that developed in various dykes were partly controlled by bulk-rock modal and chemical composition; third, other local controls, like cooling rates or the abundance of fluids, influenced the intensity and style of alteration; and fourth, the various mineral assemblages observed in individual samples reflect specific fluid-rock interaction histories, including distinctive T(P) intervals over which the alteration processes were most effective.

## PRIMITIVE ROCKS, PRIMARY MAGMAS AND THE MANTLE SOURCES OF MAGMAS

A critical problem in the petrogenetic interpretation of mafic igneous suites is the identification of the least evolved or near-primary compositions because these can constrain the mantle sources of magmas. Magmatic differentiation at shallower lithospheric levels, subsequent to magma segregation from the mantle source rocks, may modify the primary magma characteristics and even strongly obscure source characteristics if there was extensive interaction with continental crustal components. Based on the results of Roeder and Emslie (1970) and of Yoder (1976), Wilson (1989) considered that primary basaltic melts in equilibrium with typical upper mantle peridotites (olivine + orthopyroxene + clinopyroxene ± garnet ± spinel) should have  $\text{SiO}_2 < 50\%$ ,  $\text{Mg\#} > 68-75$ ,  $\text{Ni} > 400-500\text{ppm}$  and  $\text{Cr} > 1000\text{ppm}$ . Lower values of Mg# (63-67) and Ni (235-400 ppm) are suggested for primary melts by Wallace and Carmichael (1989) based on the results of Green (1971) and Sato (1977) studies. As strictly primary magmas may be rare in some igneous provinces, often the least evolved basaltic rocks (*sensu lato*) are used to constrain the characteristics of magma sources in the mantle. For instance, Wilson and Downes (2006) consider that  $\text{SiO}_2 < 55\%$  and  $\text{MgO} > 6\%$  discriminate primitive from

evolved mafic rocks in the Tertiary–Quaternary Central European Volcanic Province, while Upton *et al.* (2004) argue that Carboniferous and Permian volcanic rocks of Scotland with MgO >4% represent primitive compositions, not influenced by interaction with crustal rocks. As discussed by Wallace and Carmichel (1989) and Wilson (1989), the above criteria were developed in the context of oceanic basalt genesis (Mid Ocean Ridge Basalt (MORB)–Ocean Island Basalt (OIB)) and if olivine is not the residual phase during partial melting of mantle rocks then the Mg# and Ni are not buffered and the geochemical criteria cannot be applied. Melting of phlogopite pyroxenites or strongly metasomatized lherzolites (as at continental rift or subduction-related settings) can give rise to melts that range from low-silica and strongly alkaline or extremely potassic, to higher-silica and that are basaltic andesite to andesite in composition (Wyllie, 1982; Wyllie & Sekine, 1982; Sekine & Wyllie, 1983; Lloyd *et al.*, 1985; Wilson, 1989). More recent experimental studies (Conceição & Green, 2004, and references therein) demonstrate that melting of phlogopite lherzolites at ~3 GPa and at high contents of carbon dioxide and fluorine gives rise to variably silica undersaturated nephelinitic, leucititic and lamproitic melts; whereas melting at ~1 GPa of metasomatized, variably hydrated lherzolites containing small amounts of phlogopite and pargasite produces melts of basaltic andesite to trachyandesite composition with shoshonitic characteristics (SiO<sub>2</sub> up to 58%; K<sub>2</sub>O/Na<sub>2</sub>O = 1.3–1.4; Mg# = 76–80). The above short overview shows that primary, mantle derived magmas may vary widely in composition with respect to silica, alkalis, magnesium numbers and Cr and Ni contents. Noteworthy here is that silica-enriched, intermediate-composition primary magmas form if mantle melting involves hydrated peridotites or pyroxenitic lithologies.

The Sudetic mafic rocks studied here apparently range from primitive to variably evolved. Several samples that are characterized by high Mg# (>60) and high Cr and Ni contents (>100–200 ppm) probably represent primitive mantle-derived magmas (and in some cases possibly even near-primary). The Ni and Cr contents are highly sensitive to an early olivine and spinel fractional crystallization, and drop significantly if even small amounts of differentiation are involved. As further argued below, even some rocks with lower Mg# (50–60) largely retain mantle-related characteristics despite some degree of differentiation.

Geochemical and isotopic characteristics of three samples of primitive, high-Mg# mafic rocks are compared in Figure 32. These mica lamprophyres (two richterite minettes and a kersantite) are considered here as representative of the primitive mafic rocks included in this study: the three samples span the whole range of the measured Sr–Nd isotopic ratios and display the most characteristic trace element patterns. Taking account of results discussed by Conceição & Green (2004) and Wilson (1989, chapter 12) there are four key characteristics of these mica lamprophyres: 1) high Mg# at relatively high SiO<sub>2</sub>; 2) potassic to ultrapotassic affinity; 3) enrichment in several incompatible trace elements relative to the primitive mantle; 4) hy-

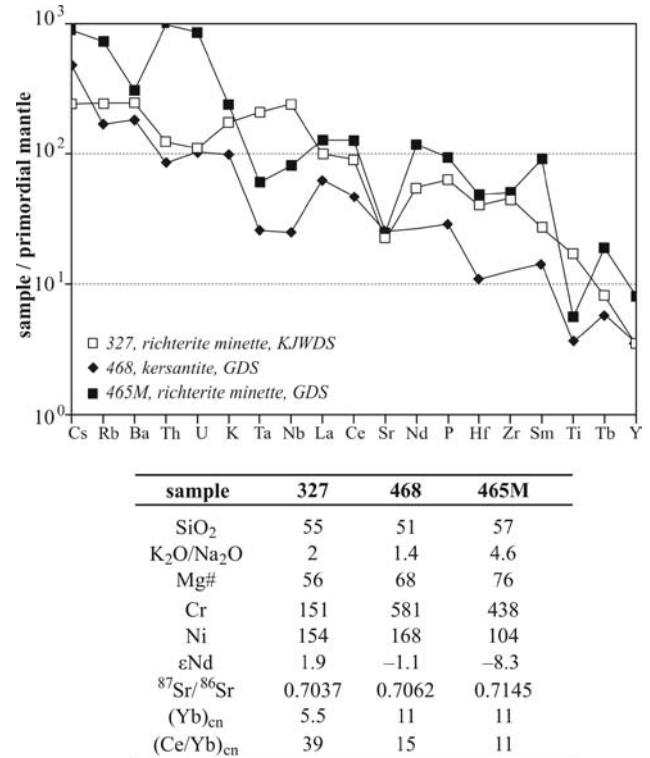


Fig. 32. A comparison of primordial mantle-normalized patterns (after Wood *et al.*, 1979) and selected geochemical and isotopic data of three samples of primitive mafic rocks. Major element contents and ratios given on wt% LOI-free basis, Cr and Ni in ppm. εNd and Sr isotopic ratios calculated for 300Ma. (Yb)<sub>CN</sub> and (Ce/Yb)<sub>CN</sub> are chondrite-normalized values (after Boynton, 1984).

drous phenocryst assemblages. These characteristics together indicate that the mantle-derived magma for these lamprophyres originated by relatively low degrees of melting of hydrated, phlogopite and/or amphibole-bearing peridotites, at relatively low pressures and at a high H<sub>2</sub>O/CO<sub>2</sub> ratio. The lack of K-depletion in the spidergrams indicates that the hydrous K-rich phase(s) in the mantle preferentially melted out during the magma formation and were not present in the residuum during magma segregation. The variable trace element and isotopic characteristics require, however, that geochemically different mantle sources and, possibly, some differences in melting processes (depth, degree, residual mineralogy, or other) were involved.

The richterite minette from the KJWDS (sample 327) has lower Mg# and Cr values than the other two samples (Fig. 32), which reflect some degree of differentiation. The petrographic characteristics of this richterite minette confirm some mixing with an acidic magma of crustal origin; however, the most distinctive geochemical features – including the enrichment in Nb and Ta relative to Th, K, La and Ce; and the low Sr isotopic ratios and high εNd (+1.9) – strongly argue against intense shallow-level interaction with the continental crustal rocks. If such interaction was influential, a depletion in Ta, Nb and Ti, and a strong shift in Sr–Nd isotopic ratios towards typical crustal values

(e.g., negative  $\epsilon\text{Nd}$ ) would occur. As this is not the case, the interaction with crustal components was very limited, so preserving several key source-related characteristics. Nevertheless, it is possible that some enrichment in Cs, Rb and Ba over Th and U in the mantle-normalized pattern of this richterite minette do represent the effect of contamination by enriched crustal material and that the primary  $\epsilon\text{Nd}$  of the richterite minette magma was originally slightly higher than the calculated value of +1.9.

The trace element and Sr–Nd isotopic characteristics of the KJWDS richterite minette compare well with the within-plate basalts and suggest a derivation from a mildly depleted, but later re-enriched, mantle source. The ‘within-plate style’ of this enrichment – the Nb and Ta spidergram peaks – likely reflect the infiltration and solidification of small-volume silicate melts enriched in incompatible elements in the mantle source (Pearce, 1983; Wilson, 1989). This enrichment event must have taken place shortly before the formation of the richterite minette magma, because a long interval between enrichment and melting would have resulted in the evolution of the higher Sr isotopic ratios and lower  $\epsilon\text{Nd}$  values. However, some trace element ratios do reach high values (e.g., Th/Yb = 10.4 and Ta/Yb = 7.9) and are above those that are typical of the most strongly enriched within-plate basalts (Pearce, 1983). Furthermore, the hydrous phenocryst assemblage, strongly potassic characteristics ( $\text{K}_2\text{O}/\text{Na}_2\text{O} > 2$ ) and relatively high silica content of the richterite minette are very different from those of within-plate basalts. These differences may reflect some specific source characteristics and partial melting conditions, such as the low degrees of melting of a phlogopite- or amphibole-bearing lherzolite and high  $\text{H}_2\text{O}/\text{CO}_2$  ratios. Furthermore, the LREE enrichment ( $\text{Ce}/\text{Yb}_{\text{CN}} = 39$ ; CN = chondrite normalized, after Boynton, 1984) and relatively low HREE abundances ( $\text{Yb}_{\text{CN}} = 5.5$ , the lowest in the whole data set) are suggestive of deep melting, within the stability field of garnet lherzolites (or possibly in the transition zone from spinel to garnet lherzolites). This conclusion is supported by the low Y content and high Ce/Y ratio of the richterite minette (Fig. 32). In contrast to the other primitive lamprophyres discussed in this study, the richterite minette from the KJWDS, and its mantle source, lack subduction-related signatures. Based on the evidence given above, the source of the richterite minette might be the asthenospheric mantle.

Although similar in modal mineral composition, the richterite minettes from the GDS show markedly different trace element and isotopic characteristics (Fig. 32). The high Mg# values and Cr and Ni contents of these rocks compare well with very primitive basic magmas: Mg# = 79, Ni = 460 and Cr = 670 in one specimen suggests a near-primary composition. The lack of xenoliths or xenocrysts and the presence of almost homogenous phlogopite phenocrysts, are consistent with a negligible to small degree of shallow-level differentiation. The high silica contents (54–60%) and the  $\text{K}_2\text{O}/\text{Na}_2\text{O}$  ratios (4.6–13.6) indicate (ultra)potassic affinity and a derivation from a hydrated, phlogopite or amphibole-bearing mantle source undergoing low degrees of partial melting at relatively low

pressures and high  $\text{H}_2\text{O}/\text{CO}_2$  ratios. The high HREE abundance and only moderate LREE enrichment in sample 465M (Fig. 32) suggest partial melting at relatively shallow mantle depths, within the spinel peridotite stability field. However, the sample of the most primitive GDS richterite minette, mentioned above, showed a low HREE abundance and a strong LREE enrichment ( $\text{Yb}_{\text{CN}} = 7$ ,  $\text{Ce}/\text{Yb}_{\text{CN}} = 46$ ) suggestive of the partial melting of a garnet-bearing peridotite. The GDS richterite minettes apparently segregated from their mantle sources at different depths, possibly spanning the transition zone between the garnet and spinel peridotites. But it is also possible that these richterite minettes derived from variable degrees of partial melting, with garnet being eliminated from the residual mineral assemblage at the higher degrees of melting.

The Ta, Nb and Ti depletions in the normalized trace element patterns of the richterite minettes from the GDS, as well as their Sr and Nd isotopic ratios, indicate an input from evolved continental crustal rocks. However, similar isotopic characteristics have been found in mantle-derived lamproites and micaceous kimberlites (Wilson, 1989, fig. 12.21). Because of the primitive geochemical characteristics of the GDS richterite minettes, their isotopic characteristics cannot be attributed to shallow-level magma contamination within the crust but must be inherited from the mantle. The radiogenic Sr and unradiogenic Nd isotopic ratios point to a contamination of the mantle source of the magmas by evolved, Rb and LREE enriched, crustal material. This contamination either occurred long before the richterite magma formed (long enough for the ‘incubation’ of the observed isotopic ratios) or it occurred shortly before the magma formation via the incorporation of geologically old crustal materials. Such mantle contamination may be the result of either subduction of crustal rocks into the mantle, or veining of the mantle by silicate melts and fluids derived from subducted crustal rocks, or some combination of these processes.

The crustal contribution to the mantle source of the richterite minettes from the GDS is further supported by the pronounced Sr and Eu depletion anomalies in these rocks. Such anomalies often characterise evolved igneous rocks such as andesites or granitoids, where they result from fractional crystallization of plagioclase (e.g., Wilson 1989). Depletion of Sr and Eu also occurs in sedimentary rocks, such as the North American Shale Composite (NASC) (Gromet *et al.*, 1984) that have originated from hypergenic reworking of older, evolved crustal rocks. However, the GDS richterite minettes were not affected by fractional crystallization of plagioclase (alkali feldspars are only late-stage groundmass components in these rocks) and, thus, their Eu and Sr anomalies are probably inherited from the mantle. The very strong enrichment in Th and U in these rocks requires not only a low degree of partial melting but also unusually high contents of these elements in the mantle source. High Th and U abundances are generally found in crustal rocks, or partial melts derived from crustal rocks. Therefore, both the isotopic Sr–Nd and trace element characteristics point to the richterite minette mantle source being contaminated by

some crustal components, either directly in the form of subducted crustal rocks, or indirectly by siliceous partial melts derived from crustal rocks. Considering the contaminated nature and relatively shallow depths of melting, the mantle source of the richterite minettes of the GDS can be tentatively linked with the lithospheric mantle.

The third primitive sample in Figure 32 is the kersantite from the GDS. Similar to the associated richterite minettes, the geochemical and petrographic features point to a very low degree of differentiation of the kersantite magma. The geochemical and isotopic characteristics may, thus, mainly reflect those in the mantle source of the magma. Compared with the minettes, the kersantite shows lower abundances of nearly all incompatible trace elements and a pronounced depletion in Ta, Nb and Ti. There are also significant petrographic and major-element differences, including abundant plagioclase and high CaO and Al<sub>2</sub>O<sub>3</sub> contents of this kersantite. The Sr and Nd isotopic ratios of the kersantite are intermediate between the KJWDS and GDS richterite minettes discussed above, suggestive of a mildly Rb- and Sm-enriched (and LREE-enriched) source. The characteristics of this GDS kersantite are, in part, comparable to subduction-related, calc-alkaline, plagioclase-rich mafic rocks, like basaltic andesites or andesites.

Although the isotopic ratios of the GDS kersantite could potentially be linked with the melting of a mixed mantle source (i.e., melting of a heterogeneous source containing distinct geochemical domains, corresponding to the KJWDS and GDS minettes), the melting of such a source cannot explain the major and trace element characteristics of the kersantite. A more specific mantle source is required. By analogy with subduction-related rocks, the mantle source of the kersantite magma may represent a metasomatized peridotite that was modified from the infiltration of subduction-related hydrous fluids and melts. The specific characteristics of the kersantite (abundant dark mica, lack of plagioclase phenocrysts, high K<sub>2</sub>O/Na<sub>2</sub>O) are different from those of common subduction-related andesitic rocks and may be explained by specific melting conditions: low degrees of melting at relatively low pressures and high H<sub>2</sub>O/CO<sub>2</sub> ratio in the magma source. In addition, the relatively high contents of the HREE (Yb<sub>CN</sub> = 11) and less pronounced LREE enrichment in the kersantites compared to the minettes (Ce/Yb<sub>CN</sub> = 15) suggest melting within the spinel lherzolite stability field, possibly in the lithospheric mantle.

In summary, the geochemical and isotopic variation of the primitive mafic rocks requires melting of three distinct mantle sources, abbreviated herein as S1, S2 and S3. The richterite minettes of the KJWDS originated from the S1 source, which showed within-plate characteristics. The richterite minettes of the GDS were derived from the S2 source, which showed evidence of crustal contamination. The kersantite from the GDS tapped the metasomatized S3 source. The S1 source could have been located in the asthenosphere, while the S2 and S3 sources were situated in the lithosphere. Some interactions between these three sources, or between melts derived from these sources, may also have occurred. For example, some magmas could

have originated from the aggregation of several melt batches coming from the S1 and S2 sources, while other melts could have been produced by melting of heterogeneous sources, composed of domains with S2 and S3 characteristics.

## MAGMATIC EVOLUTION

### Karpacz-Janowice Wielkie Dyke Swarm

The Karpacz-Janowice Wielkie Dyke Swarm (KJWDS) is the largest of the Sudetic mafic dyke swarms and is characterized by the strongest petrographic and geochemical variations. Nevertheless, there are strong genetic links between the different rock types in this swarm, as revealed from the close association of compositionally distinct dykes in space and time; from the gradations in modal compositions, in the phenocryst assemblages and in the mineral chemistries; and from the continuous geochemical variation between the minettes and the micromonzodiorites. The high Mg# and the Ni and Cr contents of the lamprophyres document their primitive characteristics and a strong (probably predominant) contribution by mantle-derived melts into the bulk composition of these rocks. The lower Mg# and Ni and Cr contents of the monzonites and the micromonzodiorites point to a more evolved character of these rocks. However, the wide range in incompatible trace element ratios (e.g., Zr/Nb, LREE/HREE) and in the Sr and Nd isotopic ratios show that the various lamprophyre types, monzonites and micromonzodiorites do not represent a suite of comagmatic rocks derived by fractional crystallization from a single parental magma. Although fractional crystallization probably occurred during the ascent of these magmas, partial melting of heterogeneous magma sources and open-system differentiation processes, including interactions of mantle-derived melts with crustal components, must have been involved.

The geochemical trends and characteristics of the KJWDS show that the richterite minettes belong to the least evolved members of the suite, ones that were derived from an asthenospheric, within-plate type source (S1). Several other minette, vogesite and spessartite samples of the KJWDS show high-Mg# geochemical characteristics (Mg# ~ 55–60, Ni ~ 100, Cr ~ 200), and one spessartite sample from an isolated dyke in the Izera gneisses in the cover of the Karkonosze granite shows pronounced primitive characteristics (Mg# = 68, Ni = 122ppm, Cr = 458ppm). However, in contrast with the richterite minettes, these other lamprophyres usually exhibit more crustal-like trace element and Sr–Nd isotopic signatures, such as Ta, Nb and Ti depletion or negative εNd. These features possibly reflect an increased contribution of continental crustal components related to shallow-level differentiation processes but, considering the relatively primitive geochemical characteristics, may also reflect some heterogeneity in the mantle sources of these rocks. Such interpretation is supported by the Nb–Zr, Ti–Zr and Y–Zr diagrams (Fig. 28) where the spheroidal minettes and some of the vogesites plot along distinct trends, similar to the richterite minette

samples from the GDS (derived from the contaminated lithospheric source, S2). Therefore, some of the primitive lamprophyre magmas in the KJWDS may have originated from heterogeneous sources, dominated by the S1 component but with some influence of the S2 component. A more complex model, with additional contribution of the metasomatized S3 source is possible, but cannot easily be proved, as the expected effects could be similar to the results of crustal contamination.

The nature of the differentiation processes that affected the KJWDS magmas is not only constrained by the geochemical data, but also by various structural, textural and mineralogical evidence. For example, the KJWDS lamprophyres show the following: 1) composite, minette-vogesite dykes; 2) felsitic bands and globular textures in some minettes; 3) quartz xenocrysts in some lamprophyres; 4) mixed populations of dark mica phenocrysts in the minettes, including euhedral, normally zoned phlogopites, and variably resorbed, reversely zoned biotites; 5) resorption and reverse zoning of amphibole phenocrysts in the vogesites. These features imply that the chemical evolution of the KJWDS lamprophyre magmas was affected by mixing of mafic and felsic melts. The richterite minette approximates well the mafic, mantle-derived end-member, although even in this rock the mixed populations of dark mica phenocrysts document a small (few %) admixture of a felsic melt. The composition of this felsic end-member is constrained by quartz and biotite xenocrysts and by alkali feldspar-rich bands and globules in the minettes, which suggest a rhyolitic/trachytic affinity. The geochemical trends of the lamprophyres point towards the origin in several trace element diagrams (Nb–Zr, Ti–Zr, Ce/Zr and others), and indicate very low contents of HFSE in the felsic end-member. The specific changes in the REE patterns (Fig. 29B) require mixing of the richterite minette magma with a LREE-poor and HREE-enriched component. These characteristics suggest that the felsic end-member could have been a LREE-poor partial melt derived from continental crustal rocks having characteristics similar to average lower continental crust (very low HFSE, low Th and LILE; Weaver & Tarney, 1984).

The mixing processes were probably accompanied by some degree of fractional crystallization, as suggested by abundant phenocrysts of phlogopite and less common clinopyroxene and altered olivine. In addition, the outcrop- and sample-scale structures related to magma mixing (points 1 and 2 in the preceding paragraph) are rare, and those observed at the thin section to single crystal-scale (points 3, 4 and 5) are much more common. These relationships suggest that the mixing processes resulted in almost complete hybridisation of the mafic and felsic end-members, with only some resorbed xenocrysts left as the witness to this mixing. Incomplete homogenisation/magma mingling was rare. In addition, the complex zoning of some dark mica and amphibole phenocrysts suggest that mixing occurred in separate stages within an evolving magmatic system undergoing replenishment.

The differentiation of the monzonite–monzodiorite magmas and their interaction with crustal rocks probably occurred due to a different set of processes. Clino-

pyroxene–plagioclase glomerocrysts and small cognate enclaves in the micromonzodiorites reflect fractional crystallization of these magmas. Fractional crystallization of plagioclase is consistent with the Eu depletion in these rocks (Fig. 30C). In addition, clinopyroxenes of both the host rocks and the enclaves show a distinctive enrichment in Al, which may indicate contamination of the fractionating magmas by Al-rich components derived from crustal rocks. The possibility of assimilation of partially melted, felsitic crustal material is also supported by the migmatitic and restitic enclaves encountered in the KJWDS suite. Furthermore, abundant inherited zircons derived from older crustal rocks were identified in one micromonzodiorite specimen. The ages of the inherited zircons range from Proterozoic to Neoproterozoic/Cambrian and compare well to other SHRIMP data from the crystalline complexes in this part of the Variscan Belt (Awdankiewicz *et al.*, 2007a). These inherited zircons provide evidence for a distinct crustal contribution in the micromonzodiorite magma. However, no zircons, either magmatic or inherited, were found in the KJWDS richterite minette and spessartite samples, which supports the model whereby there is a lack of significant crust-derived component in these lamprophyres.

The geochemical trends in the monzonite–micromonzodiorite samples follow the trends defined by the lamprophyres towards the origin of Nb–Zr, Ti–Zr, Th–Zr and other interelement diagrams. The geochemical characteristics of the most evolved lamprophyres partly overlap with the characteristics of the monzonites and micromonzodiorites. Similar overlapping relations are suggested by the Sr–Nd isotopic data for these rock types. Thus, the geochemical characteristics of the contaminant of the monzodiorite magmas were very similar to the felsic end-member that was involved in the mixing processes with the lamprophyre magmas. The geological relationships support the idea of magma differentiation at lower crustal levels and a lower-crustal derivation of contaminated partial melts.

A general model for the formation and differentiation of the KJWDS magmas can, thus, be constructed. The lamprophyre magmas originated from heterogeneous mantle sources. The richterite minettes originated from an asthenospheric mantle that had within-plate characteristics (the S1 source); the vogesites and spessartites had some contribution from a contaminated and/or metasomatized lithospheric mantle (the S2 and S3 sources). These magmas underwent weak to moderate differentiation within the lower crust. Differentiation was dominated by magma mixing ( $\pm$  fractional crystallization of phlogopite, amphiboles, clinopyroxenes, or olivine) in the less evolved lamprophyric compositions. Differentiation was dominated by assimilation and fractional crystallization, with significant amounts of plagioclase and clinopyroxene crystallization, in the more evolved, monzonitic–monzodioritic compositions.

Recently Słaby and Martin (2008) showed that mixing with lamprophyre melts strongly influenced the evolution of the Karkonosze granite magma. The results of Słaby and Martin (2008), together with the results of this study,

suggest that magma mixing was an important differentiation process in most magma types produced and emplaced within the Karkonosze magmatic system. However, a more detailed discussion of these problems has not been included here because the Słaby and Martin (2008) paper was issued when this publication was in press.

#### Gniewosów Dyke Swarm

The Gniewosów Dyke Swarm (GDS) is distinguished from the other swarms by the abundant richterite minette and minette dykes, but only very few occurrences kersantite or spessartite. The richterite minettes are interpreted as primitive to near-primary melts that originated from a contaminated, lithospheric mantle source (S2), possibly at a range of depths. The higher SiO<sub>2</sub> and lower Mg# of the non-richterite minettes indicate that they are more evolved and that they are possibly related to the richterite minettes by fractional crystallization. The co-variation of several major and trace elements (e.g., MgO, Al<sub>2</sub>O<sub>3</sub>, TiO<sub>2</sub> vs. SiO<sub>2</sub>; Nb, Ce and Th vs Zr) can be explained by fractional crystallization of phlogopite. The P<sub>2</sub>O<sub>5</sub> and CaO depletion with increasing SiO<sub>2</sub>, together with MREE-depletion in the more evolved minettes (Fig. 29D) are consistent with fractional crystallization of apatite. Differentiation in a closed system is supported by the petrographic and mineralogical characteristics of the minettes: a lack of xenoliths or xenocrysts, and a single population of nearly homogeneous phlogopite phenocrysts. A cognate phlogopite enclave in one of the richterite minette samples may represent a cumulate that is related to fractional crystallization processes, while pegmatite veins may represent segregated residual melts. However, some pairs of major and trace elements (e.g., Fe<sub>2</sub>O<sub>3</sub>-SiO<sub>2</sub>, Cr-Zr, Y-Zr) show considerable scatter instead of regular trends. And the Sr isotopic ratios and εNd values are not quite uniform, as would be expected in case of ideal, closed-system fractional crystallization. Even the most evolved minettes (with low MgO, high Zr) show relatively high Ni contents, similar to some of the richterite minettes. This cannot be easily reconciled with fractional crystallization of phlogopite, because Ni is compatible in phlogopite (Tischendorf *et al.*, 2001) and should be strongly depleted in the evolved minettes. These complex relationships suggest that the geochemical characteristics of the minettes reflect fractional crystallization trends superimposed over magma source-related variation (i.e., source heterogeneity combined with variable depths and degrees of melting). Similarly, the significant petrographic, geochemical and isotopic differences between the minettes and the kersantites and spessartites show that these latter lamprophyres cannot be related to the minettes by any shallow-level differentiation processes and must have originated from different mantle sources. Overall, the dominant control on the petrological characteristics of the GDS lamprophyres seems to be source-related.

#### Złoty Stok Dyke Swarm

The Złoty Stok Dyke Swarm (ZSDS) comprises spessartites and vogesites with less common micromonzodiorites. In terms of magnesium numbers (Mg#), the vogesites show the most primitive characteristics (Mg#

mostly 70–65), while the spessartites and micromonzodiorites are more evolved (Mg# usually from 65 to 60, but ~60 is the micromonzodiorites). The high Mg compositions must reflect mantle source characteristics. All the rocks show very similar Sr isotopic ratios, εNd values and many similarities in their trace element patterns, which point to a common mantle magmatic source. Considering the isotopic and trace element relationships between the ZSDS rocks and the GDS richterite minettes and kersantites, a heterogeneous lithospheric mantle, with contributions from both the metasomatized S3 source and the contaminated S2 source in the ZSDS magmas seems likely. The melting conditions were probably similar to those proposed for the kersantites and the richterite minettes (i.e., low degrees of melting, at relatively low pressure, in the spinel-peridotite stability field).

Some of the primitive vogesites show a more pronounced enrichment in the light and middle rare earth elements, revealed by more steeply inclined normalized REE patterns and high La/Yb and La/Nb ratios (Fig. 29D; Fig. 30A and B). The fan-shaped, rather than subparallel, arrangement of the REE patterns suggest that variable degrees of partial melting – lower for the strongly LREE enriched vogesites – contributed to this trace element variation. The process of magma mixing is indicated by the quartz and biotite xenocrysts and reverse zoning in amphibole phenocrysts in some LREE-enriched, coarsely porphyritic vogesites. However, an open-system process like magma mixing cannot be easily reconciled with the isotopic evidence for closed system differentiation. Thus, the evidence suggests the following: first, magma mixing occurred at the early stage of magmatic evolution and affected only the more primitive compositions, which represented the parental melts for other, more evolved magmas; second, the amount of mixing was not large, and the isotopic ratios of the interacting magmas were, by chance, not much different, so the resulting shift in the isotopic compositions of the vogesites was very small.

The mafic rocks of the ZSDS exhibit a considerable diversity in magnesium numbers and in their quantities of SiO<sub>2</sub>, Al<sub>2</sub>O<sub>3</sub>, Cr, Ni, Zr, Nb. This is due to shallow-level differentiation processes, with the vogesite magmas (highest Mg#) representing the parental melts. The very similar Sr and Nd isotopic ratios in the three analyzed specimens argue for a closed-system process such as fractional crystallization. In fact, the restricted range of Zr and Nb variation, the almost constant Zr/Nb ratios, and the depletion in both elements in the spessartites relative to vogesites, are consistent with fractional crystallization of mineral assemblages dominated by hornblende (with minor clinopyroxene) from a vogesite magma. The observed Zr and Nb variation was reproduced by simple numerical modelling (not shown here), using the basic equation for fractional crystallization (e.g., Rollinson, 1993), and the Zr-Nb trend reflects moderate compatibility and very similar values of partition coefficients for both Zr and Nb in hornblende in intermediate-composition melts (1.3 for Nb, 1.4 for Zr, *vide* Rollinson, 1993). Such simple models of hornblende-dominated fractional crystallization also explain the HREE variation. However, the fractional

crystallization that probably produced micromonzodiorite from vogesite would require quite different mineral assemblages from those seen. This latter geochemical trend can be explained by plagioclase-dominated fractional crystallization, with small amounts of amphiboles and/or clinopyroxenes. Zirconium and Nb remain incompatible in plagioclase-dominated fractionating assemblages and this leads to the enrichment in Zr and Nb in the daughter melts, which is consistent with the observed trend. Fractional crystallization of plagioclase is also consistent with the negative Eu anomalies in the micromonzodiorites ( $\text{Eu}/\text{Eu}^* = 0.85$ ). Significantly, plagioclase phenocrysts are not found in the vogesites, occur sparsely in some transitional spessartites and are common in the micromonzodiorites. As the crystallization sequence of amphibole vs. plagioclase strongly depends on the water content of magmas, the various crystallisation paths inferred from geochemical data may be explained by the variation in water content of the parental magmas; hornblende-dominated assemblages crystallizing from water-rich melts, and plagioclase-dominated assemblages crystallizing from water-depleted melts. The variable water contents can, in turn, be linked back to variable degrees of decompression and related volatile loss from several successive magma batches rising to different heights within the general magmatic system.

#### Mafic veins in the Central Sudetes

The mafic rocks of the Intra-Sudetic Basin and the Góry Sowie Block discussed herein show considerable geochemical variation, with some rocks having affinities to the KJWDS, and others to the GDS and the ZSDS. The petrological diversity requires that both source-related and shallow-level differentiation processes were involved. Melting of various mantle sources across the area agrees well with the geological relationships, because the dykes do not form a coherent group but are scattered over a relatively large area of the Central Sudetes.

The minettes and altered mica lamprophyres cropping out in the western to central part of the Intra-Sudetic Basin are characterized by high Mg# (51–55) and contents of Cr (140–170 ppm) and Ni (90–120 ppm), all indicative of a relatively primitive composition. The trace element and isotopic patterns of these rocks, and the mixed populations of dark mica phenocrysts in the Intra-Sudetic minettes, are comparable to the minettes of the KJWDS. These features point to a similar origin for all these minettes: a derivation from magmas from the within-plate type asthenospheric source (S1) with subsequent modification due to mixing with acidic melts of lower crustal provenance. However, the abundant plagioclase and relatively high P and Ce bulk-rock contents the minettes of the Intra-Sudetic Basin, together with several chemical analogies between the altered mica lamprophyre and the kersantite from the GDS, probably reflect magma source heterogeneity underneath the western part of the Intra-Sudetic Basin, with some contributions from the S2 and/or S3 sources to the dominant S1 source.

The altered mafic rocks and the kersantites crop out in the central and eastern part of the Intra-Sudetic Basin

and in the Góry Sowie Block. The close petrographic and geochemical analogies between the kersantites from the Góry Sowie and those from the GDS – similar modal composition; generally low incompatible trace element abundances; Ta, Nb and Ti depletion; and very similar Sr and Nd isotopic ratios – suggest a similar origin. The altered mafic rocks may largely represent equivalents of the Góry Sowie Block kersantites or their differentiates.

Several specimens of altered mafic rocks and kersantites from the Intra-Sudetic Basin and the Góry Sowie Block show high Mg# (>60) and are relatively rich in Cr (~150 ppm) and Ni (>100 ppm). The most primitive characteristics are found in the mafic rocks from Koczan Hill (Mg#, Cr and Ni up to 68, 225 ppm and 184 ppm, respectively). The trace element and isotopic compositions of such primitive rocks indicate a similar source to that of the GDS kersantite, i.e., metasomatized mantle source S3. Some differences in the trace element patterns may reflect a regional geochemical variation of this source and/or some variation in partial melting conditions.

There is also evidence of shallow level differentiation processes. Felsic kersantites from the Fore-Sudetic part of the Góry Sowie Block have low Mg# (down to 37) and very low Cr and Ni contents (almost zero), indicating an evolved composition. These kersantites are also characterized by the enrichment in Zr, Nb and REE, and a depletion in Sr, P and Eu. These latter characteristics are generally consistent with the formation of the evolved kersantite magma being due to fractional crystallization of biotite, clinopyroxene, apatite and, possibly, plagioclase.

However, some kersantites of the Góry Sowie Block (Ostrzew Hill) contain abundant inclusions (clinopyroxene macrocrysts, quartz xenocrysts, various magmatic enclaves), implying complex differentiation processes in a crustal magma chamber. A SHRIMP zircon study of one of these kersantite specimens (Marek Awdankiewicz and Ryszard Kryza, unpublished) revealed abundant inherited zircons of largely Neoproterozoic and Early Ordovician ages, comparable to ages found in the crystalline basement rocks of the Sudetes. These inherited zircons possibly come from the lower crustal rocks that contributed to the kersantite magma in the assimilation-fractional crystallization processes. It should be stressed however, that the trace element patterns and the isotopic ratios of these more evolved and contaminated kersantites from the Góry Sowie Block and the primitive kersantites from the GDS are very similar. Apparently, the crustal-like geochemical signatures of the Góry Sowie kersantites, inherited from the mantle, were relatively insensitive to moderate degrees of assimilation-fractional crystallization within the continental crust.

#### A PETROGENETIC MODEL OF THE LAMPROPHYRIC MAGMATISM IN THE SUDETES

A tentative petrogenetic model is illustrated in Figure 33. The dyke swarms distinguished in this paper represent separate centres of hypabyssal mafic magmatism in the

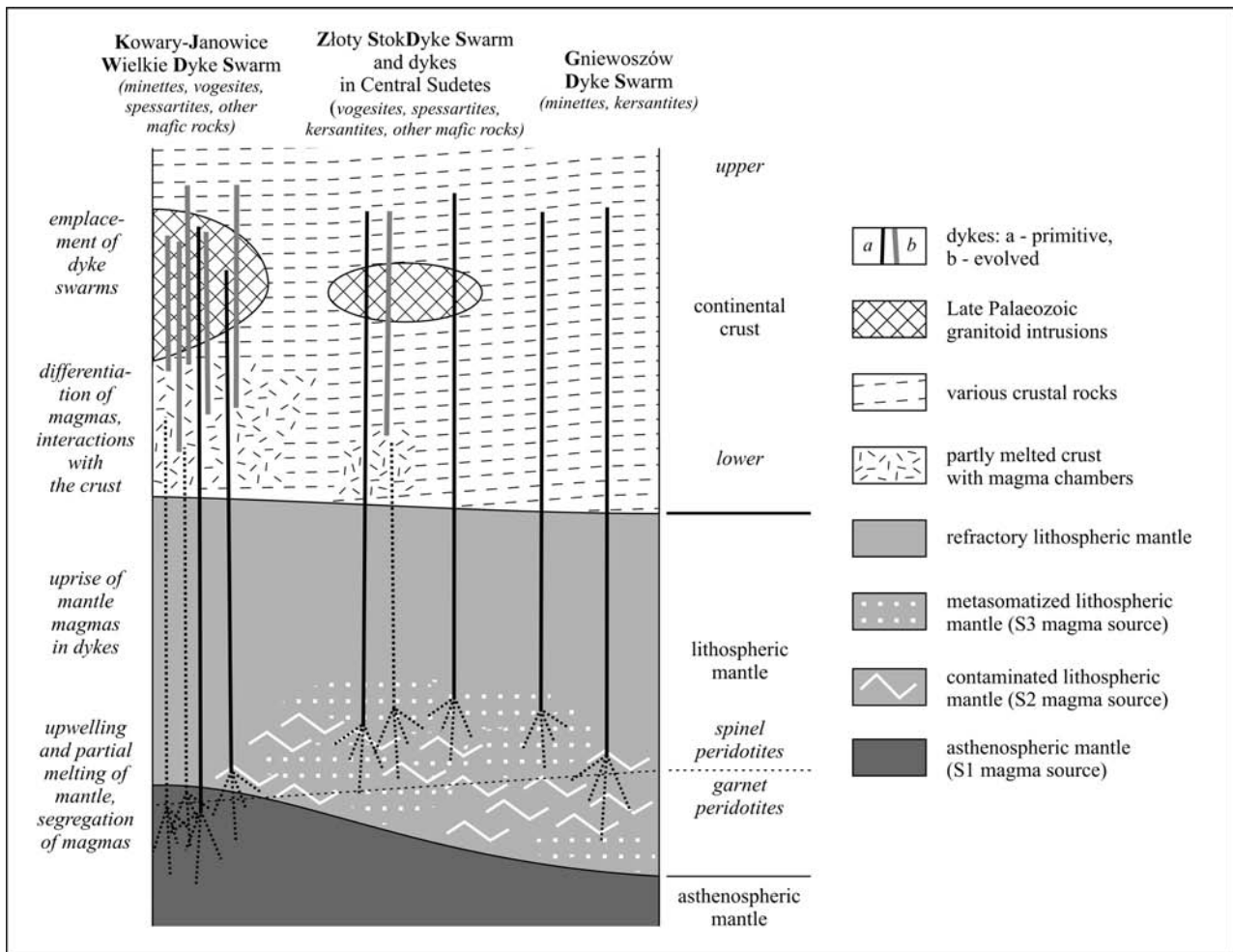


**Fig. 33.** Tentative petrogenetic model illustrating the magma sources and the main magmatic processes involved in the formation of lamprophyre dykes in the Sudetes during the Late Palaeozoic. The heterogeneous upper mantle melted at various depths; the resulting primitive magmas were either directly emplaced into the shallow crust or variably evolved at lower crustal levels due to magma mixing, contamination and fractional crystallization. Both source-related and shallow-level processes contributed to the distinctive subvolcanic rock assemblages and the specific petrological characteristics at different locations in the area.

Sudetes. Each centre was characterized by distinctive mantle sources of magmas, specific composition of the parental melts, and specific differentiation paths of the daughter magmas within the crustal magmatic systems. The two largest dyke swarms of the KJWDS and the ZSDS are associated with granitoid massifs and show the strongest geochemical and petrographic variation due to the advanced evolution of their magmas in lower-crustal chambers. The KJWDS and ZSDS mafic magmatism probably occurred over a prolonged period of time (?several million years). At the early stages, the mafic magmas contributed to the formation of granitoid magmas, which themselves show evidence of magma mixing and mingling (Słaby & Martin 2008). When the granitoid plutons consolidated, the mafic dyke swarms were emplaced. In the KJWDS, the parental magmas mainly originated from the asthenospheric S1 source; the variation from richterite minettes to minettes, vogesites and spessartites resulted predominantly from the mixing of mantle-derived magmas with felsic melts of crustal origin. The minettes of the western part of the Intra-Sudetic Basin are of a similar origin. Further evolu-

tion to monzonites and micromonzodiorites occurred as a result of the fractional crystallization and assimilation of crustal rocks. In the ZSDS, the vogesite magma originated from a heterogeneous lithospheric source that had S2 and S3 domains, the magma being partly affected by mixing processes. The parental magmas rose to different levels within the magmatic system, decompression leading to variable loss of volatiles. Hornblende-dominated fractional crystallization of wet magmas led to spessartitic compositions, while plagioclase-dominated fractional crystallization from volatile-depleted magma batches resulted in the formation of monzodioritic magmas. In contrast, the smallest of the lamprophyre swarms, the GDS, was emplaced away from granitoid massifs and within metamorphic basement rocks. The GDS is characterized by a very limited geochemical and petrographic variation, indicating that the magmatic system was not long-lived. The richterite minette magmas of the GDS originated from the lithospheric S2 source, possibly at various depths and/or degrees of partial melting, and evolved via fractional crystallization. The isolated kersantite and

spessartite dykes of the GDS swarm require melting of distinctive sources: an S3 source and a mixed, S2/S3 source, respectively. The S3 source is probably responsible for the kersantites and related mafic rocks in the Góry Sowie Block and adjacent parts of the Intra-Sudetic Basin. However, variable amounts of shallow-level differentiation and interaction with the crust were involved in these latter areas.

## TOWARDS A GENERAL MODEL OF THE FORMATION AND DIFFERENTIATION OF CALC-ALKALINE LAMPROPHYRE MAGMAS

The petrographic and geochemical characteristics of the Sudetic lamprophyre suites compare well to analogous suites (Rock, 1991). Nevertheless, the Sudetic suite does have characteristics of its own. In particular, the range of Sr and Nd isotopic ratios reported here for the Sudetic lamprophyres is very wide and exceeds the range reported by Hegner *et al.* (1998) for lamprophyres in a traverse extending along the Variscan Belt from Massif Central and Armorica to the Bohemian Massif. This suggests a particularly strong mantle heterogeneity beneath the Sudetes during the Late Palaeozoic. The trace element and Sr–Nd isotope geochemistry of the Sudetic rocks studied supports the widely accepted view that lamprophyre magmas are typically derived from metasomatized/subduction-modified mantle sources. However, this study revealed that minettes with a very similar modal composition can originate from quite different mantle sources (the GDS vs.

KJWDS minettes) and that the presence of a subducted sedimentary component in a mantle source (Turpin *et al.*, 1988; Hegner *et al.*, 1998; von Seckendorff *et al.*, 2004) may not be a prerequisite to the formation of minette magma. Although the genetic links between lamprophyre types are much debated (see the introductory sections of this paper), this study suggests the following relationships: minettes reveal characteristics that are dominated by mantle sources; kersantites and vogesites have mantle source characteristics variably overprinted by shallow-level processes; spessartites represent mantle magmas variably modified by shallow-level differentiation processes and are often transitional to the associated monzonitic-monzodioritic rocks. The strongest geochemical and petrographic variation in the lamprophyre dyke swarms developed at sites of more intense, voluminous and prolonged production of magma in the mantle. This magma fed long-term magmatic systems that spanned extensive sections of the upper mantle and the crust, from the asthenosphere up to the middle/upper crust. In such systems, various combinations of magma mixing, magma mingling, fractional crystallization and the assimilation of crustal components contribute to the diversity of daughter magmas. However, restricted and episodic mantle melting inhibited the development of evolving magmatic systems and resulted in the emplacement of petrologically uniform dyke swarms with a weak overprint by shallow-level differentiation processes. The calc-alkaline lamprophyres may represent a polygenetic rock group and the formulation of a general model for this type of magmatism would require a detailed comparison of several lamprophyre magmatic systems in the Variscan Belt and elsewhere.

## CONCLUSION

This paper is the first comprehensive synthesis of the lamprophyres and related mafic hypabyssal rocks in the Sudetes. The key conclusions on the petrogenesis of these rocks can be summarized in the following points:

1) Lamprophyres (minettes, vogesites, kersantites, spessartites) and associated mafic rocks (monzonites and micromonzodiorites) in the Sudetes were emplaced as small dyke swarms and scattered veins during the Carboniferous as a result of post-collisional extensional processes in the eastern part of the European Variscides.

2) The two largest dyke swarms are associated with the Karkonosze and Kłodzko–Złoty Stok granitoid massifs and show the greatest geochemical and petrographic variation. The small dyke swarm in the SW part of the Orlica–Śnieżnik Dome is hosted in metamorphic basement rocks, is unrelated to granites, and shows only limited geochemical variations. The scattered veins in the Central Sudetes, which are mostly hosted in Carboniferous sedimentary rocks (the Intra-Sudetic Basin and the Góry Sowie Block) display only moderate variations in their petrography and geochemistry.

3) The dyke swarms represent distinctive magmatic centres located adjacent to structural discontinuities (dislo-

cations, sutures) in the crust, and characterized by specific mantle sources and differentiation processes that were involved in their magmatic evolution.

4) Three types of mantle sources for the lamprophyre magmas are inferred: an asthenospheric source and two lithospheric sources, one of which was metasomatized and the other was contaminated by subducted crustal rocks. Primitive lamprophyre magmas originated from low degrees of partial melting of phlogopite- and/or amphibole-bearing peridotites that also contained garnet or spinel. The geochemical and isotopic variation of the minettes, vogesites and kersantites resulted primarily from source heterogeneity, source mixing and variable depths of melting, with relatively weak overprinting by shallow-level differentiation processes.

5) Episodic melting of the mantle led to the emplacement of small dyke swarms of very limited geochemical and petrographic variation due to closed system differentiation (e.g., the Gniewosów Dyke Swarm). Prolonged mantle melting led to more voluminous magmatism, development of long-lived, lower-crustal magmatic systems, and the intrusion of granitoid plutons followed by the emplacement of lamprophyre dyke swarms (e.g., the

Karpacz-Janowice Wielkie and Złoty Stok Dyke Swarms). The significant geochemical and petrographic variations resulted from open-system differentiation, whereby lamprophyre magmas were mixed with crustal melts and the more evolved magmas assimilated crustal rocks. Open system processes were accompanied by fractional crystallization.

6) The interpretation of the lamprophyric rocks and their magma sources implies a complex structure and compositional diversification of the mantle and crust, including the presence of subducted crustal materials, underneath the Sudetes region during Carboniferous times.

### Acknowledgments

I am grateful to Prof. Ryszard Kryza and dr Honorata Awdankiewicz for our collaboration during the studies of the lamprophyres in the Sudetes. Many thanks are due to Ula and Wiktor for their patient assistance during the field work. I am grateful to dr Piotr Dzierżanowski (Uniwersytet Warszawski), to dr Jean-Luc Devidal (Université Blaise Pascal, Clermont-Ferrand) and, especially, to dr Heinz-Juergen Bernhardt (Ruhr-Universität Bochum) for their help and assistance during several microprobe

7) Many lamprophyres and associated mafic rocks contain well preserved igneous mineral assemblages, but there is a widespread evidence of intense alteration related to autometamorphic processes during subsolidus cooling. The variable post-magmatic mineral assemblages reflect alteration under greenschist to sub-greenschist facies metamorphic conditions, the variable composition of protoliths and, in case of veins hosted in sedimentary rocks, a strong diagenetic overprint.

analytical sessions. I wish to pass special thanks for dr Arne Wilner with family for their hospitality at Bochum. Dr Honorata Awdankiewicz is gratefully acknowledged for her help in drawing the figures. Helpful reviews of this paper by Prof. Ryszard Kryza and dr Anna Lewandowska are greatly appreciated. The text has benefited significantly from the corrections by Patrick Roycroft. This study has been supported by KBN grant 3 P04D 0255 22.

### REFERENCES

- ALEKSANDROWSKI, P. & MAZUR, S., 2002. Collage tectonics in the northeasternmost part of the Variscan belt: the Sudetes, Bohemian Massif. In: Winchester, J. A., Pharaoh, T. C. & Verniers, J. (Eds.), *Palaeozoic Amalgamation of Central Europe. Geological Society, London, Special Publications*, 201: 237–277.
- ALEKSANDROWSKI, P., KRYZA, R., MAZUR, S. & ŻABA, J., 1998. Kinematic data on major Variscan strike-slip faults and shear zones in the Polish Sudetes, northeast Bohemian Massif. *Geological Magazine*, 134: 727–739.
- ARMBRUSTER, T., BIRRER, J., LIBOWITZKY, E. & BERAN, A., 1998. Crystal chemistry of Ti-bearing andradites. *European Journal of Mineralogy*, 10: 907–921.
- AWDANKIEWICZ, M., 1999a. Volcanism in a late Variscan intra-montane trough: Carboniferous and Permian volcanic centres of the Intra-Sudetic Basin, SW Poland. *Geologia Sudetica*, 32: 13–47.
- AWDANKIEWICZ, M., 1999b. Volcanism in a late Variscan intra-montane trough: the petrology and geochemistry of the Carboniferous and Permian volcanic rocks of the Intra-Sudetic Basin, SW Poland. *Geologia Sudetica*, 32: 83–111.
- AWDANKIEWICZ, M., 2004. Sedimentation, volcanism and subvolcanic intrusions in a late Palaeozoic intramontane trough (the Intra-Sudetic Basin, SW Poland). In: Breitzkreuz, C. & Petford, N. (Eds.), *Physical Geology of High-Level Magmatic Systems. Geological Society, London, Special Publications*, 234: 5–11.
- AWDANKIEWICZ, M., 2006. Fractional crystallization, mafic replenishment and assimilation in crustal magma chambers: geochemical constraints from the Permian post-collisional intermediate-composition volcanic suite of the North-Sudetic Basin (SW Poland). *Geologia Sudetica*, 38: 39–62.
- AWDANKIEWICZ, M., 2007. Lamprophyres of the Orlica-Śnieżnik Dome and the Kłodzko-Złoty Stok Massif – new data on petrology, geochemistry and petrogenesis. In: Rappich, V. and Řidkošil, T. (Eds.), *VENTS 2007. Abstracts and excursion guide. Sborník Museum Českébo Ráje, Acta Musei Turnoviensis*, 2: 7–10.
- AWDANKIEWICZ, M. & AWDANKIEWICZ, H., 2007. Post-magmatic garnet, prehnite and pumpellyite in mafic dykes of the Karkonosze Massif – preliminary data. *Mineralogia Polonica – Special Papers*, 31: 53–56.
- AWDANKIEWICZ, M., AWDANKIEWICZ, H. & KRYZA, R., 2004. Petrography and mineral chemistry of the Góry Sowie kersantites: preliminary results. *Mineralogical Society of Poland – Special Papers*, 24: 65–68.
- AWDANKIEWICZ, M., AWDANKIEWICZ, H. & KRYZA, R., 2005a. Petrology of mafic and felsic dykes from the eastern part of the Karkonosze Massif. *Mineralogical Society of Poland – Special Papers*, 26: 111–114.
- AWDANKIEWICZ, M., AWDANKIEWICZ, H. & KRYZA, R., 2005b. The richterite minette from Bukowiec (the Karkonosze-Izera Block): petrological characteristics. *Mineralogical Society of Poland – Special Papers*, 26: 115–118.
- AWDANKIEWICZ, M., AWDANKIEWICZ, H. & KRYZA, R., 2007b. Petrologia i geochemia lamprofirów regionu sudeckiego. Projekt badawczy 3 P04D 025 22. Raport końcowy. {in Polish only, unpublished report}. 79 pp.
- AWDANKIEWICZ, M., AWDANKIEWICZ, H., KRYZA, R. & RODIONOV, N., 2007a. Preliminary SHRIMP zircon age of the micromonzodiorite dyke from Bukowiec: age constraint for the Karkonosze Granite (Polish Sudetes). *Mineralogia Polonica – Special Papers*, 31: 57–60.
- BACHLIŃSKI, R. & BAGIŃSKI, B., 2007. Kłodzko-Złoty Stok granitoid massif. In: Kozłowski, A. & Wiszniewska, J. (Eds.), *Granitoids in Poland. Archiwum Mineralogiae Monograph*, 1: 261–273.
- BADURA, J. & BOSSOWSKI, A., 1987. *Szczegółowa mapa geologiczna Sudetów 1:25000. Arkusz Lipniki*. {in Polish only}. Wydawnictwa Geologiczne, Warszawa.
- BARBARIN, B., 2005. Mafic magmatic enclaves and mafic rocks associated with some granitoids of the central Sierra Nevada

- batholith, California: nature, origin, and relations with the hosts. *Lithos*, 80: 155–177.
- BEA, F., MONTERO, P. & MOLINA, J. F., 1999. Mafic Precursors, Peraluminous granitoids, and Late Lamprophyres in the Avila Batholith: A model for the generation of Variscan Batholiths in Iberia. *The Journal of Geology*, 107: 399–419.
- BERG, G., 1923. *Der Granit des Riesengebirges und seine Ganggesteine (Petrographische Studien)*. {in German only}. Preußischen Geologischen Landesanstalt, 94 pp.
- BÉZIAT, D., JORON, J-L. & MONCHOUX, P., 1993. Spessartites in the Montagne Noire, France: mineralogical and geochemical data. *European Journal of Mineralogy*, 5: 879–891.
- BORKOWSKA, M., 1966. Petrografia granitu Karkonoszy. [Pétrographie du granite des Karkonosze]. *Geologia Sude-tica*, 2: 7–119.
- BOSSOWSKI, A. & CZERSKI, M., 1985. *Szczegółowa mapa geologiczna Sudetów 1:25000. Arkusz Boguszów*. {in Polish only}. Wydawnictwa Geologiczne, Warszawa.
- BOSSOWSKI, A., CYMERMAN, Z., GROCHOLSKI, A. & IHNATOWICZ, A., 1994. *Szczegółowa mapa geologiczna Sudetów 1:25000. Arkusz Jedlina Zdrój*. {in Polish only}. Wydawnictwo Kartograficzne Polskiej Agencji Ekologicznej S.A., Warszawa.
- BOSSOWSKI, A., SAWICKI, L. & WROŃSKI, J., 1981. *Mapa geologiczna Polski 1:200 000. B – mapa bez utworów czwartorzędowych. Arkusz Wałbrzych*. {in Polish only}. Wydawnictwa Geologiczne, Warszawa.
- BOYNTON, W. R., 1984. Geochemistry of the rare earth elements: meteorite studies. In: Henderson, P. (Ed.), *Rare Earth Element Geochemistry*. Elsevier, Amsterdam, 63–114.
- CARLIER, G., LORAND, J. P., AUDEBAUD, E. & KIENAST, J. R., 1997. Petrology of an unusual orthopyroxene-bearing minette suite from southeastern Peru, Eastern Andean Cordillera: Al-rich lamproites contaminated by peraluminous granites. *Journal of Volcanology and Geothermal Research*, 75: 59–87.
- CARMICHAEL, I. S. E., LANGE, R. A. & LUHR, J. F., 1996. Quaternary minettes and associated volcanic rocks of Mascota, western Mexico: a consequence of plate extension above a subduction modified mantle wedge. *Contributions to Mineralogy and Petrology*, 124: 302–333.
- CLOOS, H., 1925. *Einführung in die tektonische Behandlung magmatischer Erscheinungen, pt 1. Das Riesengebirge in Schleißen*. Gebr. Borntraeger, Berlin, 194 pp.
- CONCEIÇÃO, R. V. & GREEN, D. H., 2004. Derivation of potassic (shoshonitic) magmas by decompression melting of phlogopite + pargasite lherzolite. *Lithos*, 72: 209–229.
- CWOJDZIŃSKI, S., 1976. *Szczegółowa mapa geologiczna Sudetów 1:25000. Arkusz Złoty Stok*. {in Polish only}. Wydawnictwa Geologiczne, Warszawa.
- CWOJDZIŃSKI, S., 1979a. *Szczegółowa mapa geologiczna Sudetów 1:25000. Arkusz Krosnowice*. {in Polish only}. Wydawnictwa Geologiczne, Warszawa.
- CWOJDZIŃSKI, S., 1979b. *Szczegółowa mapa geologiczna Sudetów 1:25000. Arkusz Trzebiezowice*. {in Polish only}. Wydawnictwa Geologiczne, Warszawa.
- CWOJDZIŃSKI, S., 1985. *Szczegółowa mapa geologiczna Sudetów 1:25000. Arkusz Stronie Śląskie*. {in Polish only}. Wydawnictwa Geologiczne, Warszawa.
- CWOJDZIŃSKI, S. & KOZDRÓJ, W., 1995. *Szczegółowa mapa geologiczna Sudetów 1:25000. Arkusz Wojcieszów*. {in Polish only}. Wydawnictwo Kartograficzne Polskiej Agencji Ekologicznej S.A., Warszawa.
- CYMERMAN, Z., 1992. *Szczegółowa mapa geologiczna Sudetów 1:25000. Arkusz Duszniki Zdrój*. {in Polish only}. Wydawnictwa Geologiczne, Warszawa.
- CYMERMAN, Z., 1995. *Szczegółowa mapa geologiczna Sudetów 1:25000. Arkusz Lewin Kłodzki*. {in Polish only}. Wydawnictwo Kartograficzne Polskiej Agencji Ekologicznej S.A., Warszawa.
- CYMERMAN, Z., PIASECKI, M. A. J. & SESTON, R., 1997. Terranes and terrane boundaries in the Sudetes, northeast Bohemian Massif. *Geological Magazine*, 134: 717–725.
- CYMERMAN, Z. & WALCZAK-AUGUSTYNIAK, M., 1988. *Szczegółowa mapa geologiczna Sudetów 1:25000. Arkusz Dzierżoniów*. {in Polish only}. Wydawnictwa Geologiczne, Warszawa.
- DE PAOLO, D. E., 1988. *Neodymium isotope geochemistry*. Springer Verlag, Berlin, 187 pp.
- DE STEFANO, A., LEFEBVRE, N. & KOPYLOVA, M., 2006. Enigmatic diamonds in Archean calc-alkaline lamprophyres of Wawa, southern Ontario, Canada. *Contributions to Mineralogy and Petrology*, 151: 158–173.
- DEER, W. A., HOWIE, R. A. & ZUSSMAN, J., 1992. *An Introduction to the Rock-Forming Minerals*. Longman Scientific & Technical, 696 pp.
- DIDIER, J. & BARBARIN, B., 1991. *Enclaves and Granite Petrology*. Developments in Petrology, vol. 13. Elsevier, Amsterdam, 625 pp.
- DOWTY, E., 1976. Crystal structure and crystal growth: II. Sector zoning in minerals. *American Mineralogist*, 61: 460–469.
- DUMICZ, M., 1964. Budowa geologiczna krystaliniku Gór Bystrzyckich. [Geology of the crystalline massif of the Bystrzyckie Mts]. *Geologia Sude-tica*, 1: 169–206.
- DUTHOU, J. L., COUTURIE, J. P. & MIERZEJEWSKI, M. P., 1991. Oznaczenia wieku granitu Karkonoszy metodą izochronową, rubidowo-strontową, na podstawie całych próbek skalnych. [Next dating of granite sample from the Karkonosze Mountains using Rb-Sr total rock isochrone method]. *Przegląd Geologiczny*, 39, 2: 75–79.
- DZIEDZIC, K., 1996. Two-stage origin of the Hercynian volcanics in the Sudetes, SW Poland. *Neues Jahrbuch für Mineralogie, Geologie und Palaeontologie*, 199: 65–87.
- ELBURG, M. & FODEN, J., 1999. Sources for magmatism in Central Sulawesi: geochemical and Sr-Nd-Pb isotopic constraints. *Chemical Geology*, 1-4: 67–93.
- ESPERANÇA, S. & HOLLOWAY, J. R., 1987. On the origin of some mica-lamprophyres: experimental evidence from a mafic minette. *Contributions to Mineralogy and Petrology*, 95: 207–216.
- FELDSTEIN, S. N. & LANGE, R. A., 1999. Pliocene Potassic Magmas from the Kings River Region, Sierra Nevada, California: Evidence for Melting of a Subduction-Modified Mantle. *Journal of Petrology*, 40: 1301–1320.
- FÉMÉNIAS, O., MERCIER, J-C. C., NKONO, C., DIOT, H., BERZA, T., TATU, M. & DEMAÏFFE D., 2006. Calcic amphibole growth and compositions in calc-alkaline magmas: Evidence from the Motru Dike Swarm (Southern Carpathians, Romania). *American Mineralogist*, 91: 73–81.
- FOLEY, S. F., VENTURELLI, G., GREEN, D. H., & TOSCANI, L., 1987. The ultrapotassic rocks: characteristics, classification and constraints for petrogenetic models. *Earth Science Reviews*, 24, 81–134.
- FRANKE, W. & ŻELAŻNIEWICZ, A., 2002. Structure and evolution of the Bohemian Arc. In: Winchester, J. A., Pharaoh, T. C. & Verniers, J. (Eds.), *Palaeozoic Amalgamation of Central Europe*. Geological Society, London, *Special Publications*, 201: 279–293.
- FRACKIEWICZ, W. & TEISSEYRE, H., 1976. *Szczegółowa mapa geologiczna Sudetów 1:25000. Arkusz Międzygórze*. {in

- Polish only}. Wydawnictwa Geologiczne, Warszawa.
- FREIBERGER, R., HECHT, L., CUNEY, M., & MORTEANI, G., 2001. Secondary Ca-Al silicates in plutonic rocks: implications for their cooling history. *Contributions to Mineralogy and Petrology*, 141: 415–429.
- GALAN, G., PIN, C. & DUTHOU, J. L., 1996. Sr-Nd isotopic record of multi-stage interactions between mantle-derived magmas and crustal components in a collision context. The ultramafic-granitoid association from Vivero (Hercynian belt, NW Spain). *Chemical Geology*, 131: 67–91.
- GAWROŃSKI, O., 1959. *Szczegółowa mapa geologiczna Sudetów 1:25000. Arkusz Jugów*. {in Polish only}. Wydawnictwa Geologiczne, Warszawa.
- GAWROŃSKI, O., 1961. *Szczegółowa mapa geologiczna Sudetów 1:25000. Arkusz Pieszyce*. {in Polish only}. Wydawnictwa Geologiczne, Warszawa.
- GIERWIELANIEC, J., 1971. *Szczegółowa mapa geologiczna Sudetów 1:25000. Arkusz Łądek Zdrój*. {in Polish only}. Wydawnictwa Geologiczne, Warszawa.
- GIERWIELANIEC, J. & RADWAŃSKI, ST., 1958. *Szczegółowa mapa geologiczna Sudetów 1:25000. Arkusz Jeleniów*. {in Polish only}. Wydawnictwa Geologiczne, Warszawa.
- GREEN, D. H., 1971. Composition of basaltic magmas as indicators of conditions of origin: Application to oceanic volcanism. *Philosophical Transactions of the Royal Society of London*, A268: 707–725.
- GROMET, L. P., DYMEK, R. F., HASKIHN, L. A. & KOROTEV, R. L., 1984. The “North American Shale Composite”: its compilation, major and trace element characteristics. *Geochimica et Cosmochimica Acta*, 48: 2469–2482.
- GROVES, D. & EDGAR, A., 1994. Preface. *Mineralogy and Petrology (Special Volume)*, 51: 111–112.
- HEGNER, E., KÖLBL-EBERT, M. & LOESCHKE, J., 1998. Post-collisional Variscan lamprophyres (Black Forest, Germany):  $^{40}\text{Ar}/^{39}\text{Ar}$  phlogopite dating, Nd, Pb, Sr isotope and trace element characteristics. *Lithos*, 45: 395–411.
- HEY, M. H., 1954. A new review of the chlorites. *Mineralogical Magazine*, 30: 277–292.
- HOCH, M., RECHKÄMPER, M. & TOBSCHALL, H. J., 2001. Sr, Nd, Pb and O Isotopes of Minettes from Schirmacher Oasis, East Antarctica: a Case of Mantle Metasomatism involving Subducted Continental Material. *Journal of Petrology*, 42, 7: 1387–1400.
- IRVINE, T. N. & BARAGAR, W. R. A., 1971. A guide to the chemical classification of the common volcanic rocks. *Canadian Journal of Earth Sciences*, 8: 523–548.
- JOHNSON, M. C., ANDERSON, A. T. & RUTHERFORD, M. J., 1994. Pre-eruptive volatile contents of magmas. In: Carroll, M. R. & Holloway, J. R. (Eds.): *Volatiles in magmas. Reviews in Mineralogy*, 30: 281–330.
- JOHNSTON, J. D., TAIT, J. A., OLIVER, G. J. H. & MURPHY, J. C., 1994. Evidence for a Caledonian orogeny in Poland. *Transactions of the Royal Society of Edinburgh, Earth Sciences*, 85: 131–142.
- KASZA, L., 1967. *Szczegółowa mapa geologiczna Sudetów 1:25000. Arkusz Nowa Morawa*. {in Polish only}. Wydawnictwa Geologiczne, Warszawa.
- KODYM, O., FUSÁN, O. & MATĚJKA, A., (Eds.), 1967. Geological Map of Czechoslovakia 1: 500 000, West. Ústřední ústav geologický, Praha.
- KOZDRÓJ, W., 1994a. *Szczegółowa mapa geologiczna Sudetów 1:25000. Arkusz Poręba*. {in Polish only}. Wydawnictwo Kartograficzne Polskiej Agencji Ekologicznej S.A., Warszawa.
- KOZDRÓJ, W., 1994b. *Szczegółowa mapa geologiczna Sudetów 1:25000. Arkusz Lesica*. {in Polish only}. Wydawnictwo Kartograficzne Polskiej Agencji Ekologicznej S.A., Warszawa.
- KOZŁOWSKI, A. & WISZNIEWSKA, J., 2007 (Eds.). *Granitoids in Poland*. Archivum Mineralogiae Monograph, 1: 371 pp.
- KRAMER, W. & SEIFERT, W., 1993. Mica-lamprophyres and related volcanics of the Erzgebirge and metallogenic aspects. In: Seltmann, R., Kämpf, H. & Möller, P. (Eds.), *Metallogeny of collisional orogens*. Czech Geological Survey, Prague, 159–165.
- KRYZA, R., AWDANKIEWICZ, M. & AWDANKIEWICZ, H., 2007. Zircon inheritance masking the magmatic age of a volcanic rock: example from late Variscan rhyolite in the Góry Sowie, Polish Sudetes. *Mineralogia Polonica – Special papers*, 30: 39.
- LE MAITRE, R. W., BATEMAN, P., DUDEK, A., KELLER, J., LAMEYRE, J., LE BAS, M. J., SABINE, P. A., SCHMID, R., SORENSEN, H., STREICKEISEN, A., WOOLEY, A. R. & ZANETTIN, B., 2002. *A classification of volcanic rocks and glossary of terms. Recommendations of the International Union of Geological Sciences Subcommission on the Systematics of Igneous Rocks*. Blackwell, Oxford, 236 pp.
- LEAKE, B. E., WOOLEY, A. R., ARPS, C. E. S., BIRCH, W. D., GILBERT, M. C., GRICE, J. D., HAWTHORNE, F. C., KATO, A., KISCH, H. J., KRIVOVICHEV, V. G., LINTHOUT, K., LAIRD, J., MANDARINO, J. A., MARESCH, V. W., NICKEL, E. H., ROCK, N. M. S., SCHUMACHER, J. C., SMITH, D. C., STEPHENSON, N. C. N., UNGARETTI, L., WHITTAKER, E. J. W. & YOUZHI, G., 1997. Nomenclature of amphiboles: Report of the Subcommittee on Amphiboles of the International Mineralogical Association, Commission on New Minerals and Mineral Names. *American Mineralogist*, 82: 1019–1037.
- LEAT, P. T., THOMPSON, R. N., MORRISON, M. A., HENDRY, G. L. & TRAYHORN, S. C., 1987. Geodynamic significance of post-Variscan intrusive and extrusive potassic magmatism in SW England. *Transactions of the Royal Society of Edinburgh, Earth Sciences*, 77: 349–360.
- LLOYD, F. E., ARIMA, M. & EDGAR, A. D., 1985. Partial melting of a phlogopite-clinopyroxenite nodule from southwest Uganda: An experimental study bearing on the origin of highly potassic continental rift volcanics. *Contributions to Mineralogy and Petrology*, 91: 321–329.
- LORENC, M., 1994. Rola magm zasadowych w ewolucji granitoidów (studium porównawcze wybranych masywów hercyńskich). [The role of basic magmas in granitoid evolution (a comparative study of some Hercynian massifs)]. *Geologia Sudetica*, 28: 1–130.
- ŁAPOT, W., 1986. Petrografia utworów karbonu Gór Sowich. [Petrography of Carboniferous rocks from the Sowie Mts (Sudetes)]. *Geologia Sudetica*, 21: 1–184
- MACDONALD, R., THORPE, R. S., GASKARTH, J. W. & GRINDROD, A. R., 1985. Multi-component origin of Caledonian lamprophyres of northern England. *Mineralogical Magazine*, 49: 485–494.
- MACHOWIAK, K., MUSZYŃSKI, A. & ARMSTRONG, R., 2004. High-level volcanic granodioritic intrusions from Żelaźniak Hill (Kaczawa Mountains, Sudetes, SW Poland). In: Breikreuz, C. & Petford, N. (Eds.), *Physical Geology of High-Level Magmatic Systems*. Geological Society, London, Special Publications, 234: 67–74.
- MAJEROWICZ, A., 1972. Masyw granitowy Strzegom-Sobótka. Studium petrologiczne. [On the petrology of the granite massif of Strzegom-Sobótka]. *Geologia Sudetica*, 6: 7–96.

- MARHEINE, D., KACHLIK, V., MALUSKI, H., PATOČKA, F. & ŽELAŽNIEWICZ, A., 2002. The  $^{40}\text{Ar}$ - $^{39}\text{Ar}$  ages from the West Sudetes (NE Bohemian Massif): constraints on the Variscan polyphase tectonothermal development. In: Winchester, J. A., Pharaoh, T. C. & Verniers, J. (Eds.), *Palaeozoic Amalgamation of Central Europe. Geological Society, London, Special Publications*, 201: 133–155.
- MASTALERZ, K., AWDANKIEWICZ, M. & CYMERMAN, Z., 1995. *Szczegółowa mapa geologiczna Sudetów 1:25000. Arkusz Kamienna Góra*. {in Polish only}. Wydawnictwa Geologiczne, Warszawa.
- MAUGER, R. L., 1988. Ocelli: transient disequilibrium features in a Lower Carboniferous minette near Concord, North Carolina. *Canadian Mineralogist*, 26: 117–131.
- MAZUR, S., ALEKSANDROWSKI, P., KRYZA, R. & OBERC-DZIEDZIC, T., 2006. The Variscan Orogen in Poland. *Geological Quarterly*, 50: 89–118.
- MAZUR, S., ALEKSANDROWSKI, P., TURNIAK, K. & AWDANKIEWICZ, M., 2007. Geology, tectonic evolution and Late Palaeozoic magmatism of Sudetes – an overview. In: Kozłowski, A. & Wiszniewska, J. (Eds.), *Granitoids in Poland. Archivum Mineralogiae Monograph*, 1: 59–87.
- MEHNERT, K. R., 1971. *Migmatites and the origin of granitic rocks*. Elsevier, Amsterdam, 404 pp.
- MEHNERT, K. R., BÜSCH, W. & SCHNEIDER, G., 1973. Initial melting at grain boundaries of quartz and feldspar in gneisses and granulites. *Neues Jahrbuch für Mineralogie Monatshefte*, 4: 165–83.
- MEYER, H. O. A., MITCHELL, R. H. & JAYAGANAPATHY, S., 1994. Phlogopite in calc-alkaline lamprophyres of Northern England. *Mineralogy and Petrology*, 51: 227–237.
- MIERZEJEWSKI, M. P. & OBERC-DZIEDZIC, T., 1990. The Izera-Karkonosze Block and its tectonic development. *Neues Jahrbuch für Geologie und Paläontologie, Abhandlungen*, 179: 197–222.
- MIERZEJEWSKI, M., 2007. A general view on the Karkonosze granite. In: Kozłowski, A. & Wiszniewska, J. (Eds.), *Granitoids in Poland. Archivum Mineralogiae Monograph*, 1: 111–122.
- MILEWICZ, J., SZAŁAMACHA, J. & SZAŁAMACHA, M., 1989. *Mapa geologiczna Polski 1:200 000. B – mapa bez utworów czwartorzędowych. Arkusz Jelenia Góra*. {in Polish only}. Wydawnictwa Geologiczne, Warszawa.
- MITCHELL, R. H., 1994. The lamprophyre facies. *Mineralogy and Petrology*, 51: 137–146.
- MITCHELL, R. H., 1997. *Kimberlites, orangeites, lamproites, melilitites and minettes: a petrographic atlas*. Almaz Press Inc., Canada, 243 pp.
- MORIMOTO, N., 1989. Nomenclature of pyroxenes. *Canadian Mineralogist*, 27: 143–156.
- MÜLLER, A., BREITER, K., SELTMANN, R. & PÉSKAY, Z., 2005. Quartz and feldspar zoning in the eastern Erzgebirge volcano-plutonic complex (Germany, Czech Republic): evidence of multiple magma mixing. *Lithos*, 80: 201–227.
- MÜLLER, D. & GROVES, D. I., 2000. *Potassic Igneous Rocks and Associated Gold-Copper Mineralisation*. Springer Verlag, 252 pp.
- MUSZYŃSKI, A., 1987. Niektóre problemy petrograficzne lamprofirów sowiogórskich. [Some petrographical problems of the Góry Sowie lamprophyres]. *Acta Universitatis Wratislaviensis No 788, Prace Geologiczno-Mineralogiczne*, 10: 137–156.
- NIMIS P., 1999. Clinopyroxene geobarometry for magmatic rocks. Part 2. Structural geobarometers for basic to acid, tholeiitic and mildly alkaline magmatic systems. *Contributions to Mineralogy and Petrology*, 135: 62–74.
- O'BRIEN, H. E., IRVING, A. J. & MCCALLUM, I. S., 1988. Complex zoning and resorption of phenocrysts in mixed potassic mafic magmas of the Highwood Mountains, Montana. *American Mineralogist*, 73: 1007–1024.
- OBERC, J., 1957. *Region Gór Bardzkich (Sudety). Przewodnik dla geologów*. {in Polish only}. Wydawnictwa Geologiczne, Warszawa, 284 pp.
- OBERC, J., BADURA, J., PRZYBYLSKI, B. & JAMROZIK, L., 1994. *Szczegółowa mapa geologiczna Sudetów 1:25000. Arkusz Bardo Śląskie*. {in Polish only}. Wydawnictwo Kartograficzne Polskiej Agencji Ekologicznej S.A., Warszawa.
- OBERC-DZIEDZIC, T., 1999. The geology of the Strzelin granitoids (Fore-Sudetic Block, SW Poland). *Mineralogical Society of Poland - Special Papers*, 14: 22–32.
- PEARCE, J. A., 1983. The role of subcontinental lithosphere in magma genesis at destructive plate margins. In: Hawkesworth, C. J. & Norry, M. J. (Eds.), *Continental basalts and mantle xenoliths*. Nantwich, Shiva, 230–249.
- PETERSON, T. D., ESPERANÇA, S. & LECHEMINANT, A. N., 1994. Geochemistry and origin of the Proterozoic ultrapotassic rocks of the Churchill Province, Canada. *Mineralogy and Petrology*, 51: 251–276.
- PRELEVIĆ, D., FOLEY, S. F., CVETKOVIĆ, V. & ROMER, R. L., 2004. Origin of Minette by Mixing of Lamproite and Dacite Magmas in Veliki Majdan, Serbia. *Journal of Petrology*, 45: 759–792.
- PUZIEWICZ, J., 1988. Plagioclase-pyroxene-biotite rock from the Koźmice quarry, Niemcza Zone (Sudetes, SW Poland): the first occurrence of vaugnerite in Polish Sudetes. *Mineralogical Polonica*, 19: 59–68.
- PUZIEWICZ, J., 1990. Masy granitowy Strzegom-Sobótka. Aktualny stan badań. [Strzegom-Sobótka granitic massif (SW Poland). Summary of recent studies.]. *Archivum Mineralogiczne*, 45: 135–154.
- RIGHTER, K. & CARMICHAEL, J.S.E., 1996. Phase equilibria of phlogopite lamprophyres from western Mexico: biotite-liquid equilibria and P-T estimates for biotite-bearing igneous rocks. *Contributions to Mineralogy and Petrology*, 123: 1–21.
- ROCK, N. M. S., 1991. *Lamprophyres*. Blackie and Son Ltd, Glasgow and London, 285 pp.
- ROEDER, P. L. & EMSLIE, R. F., 1970. Olivine-liquid equilibrium. *Contributions to Mineralogy and Petrology*, 29: 275–289.
- ROLLINSON, H. R., 1993. *Using geochemical data: evaluation, presentation, interpretation*. Longman Scientific & Technical, 352 pp.
- SATO, H., 1977. Nickel content of basaltic magmas: Identification of primary magma and a measure of the degree of olivine fractionation. *Lithos*, 10: 113–120.
- SAWICKI, L., 1959. *Szczegółowa mapa geologiczna Sudetów 1:25000. Arkusz Kamienna*. {in Polish only}. Wydawnictwa Geologiczne, Warszawa.
- SAWICKI, L., 1968. *Szczegółowa mapa geologiczna Sudetów 1:25000. Arkusz Międzyzlesie*. {in Polish only}. Wydawnictwa Geologiczne, Warszawa.
- SAWICKI, L., 1988. *Mapa geologiczna Polski 1:200 000. B – mapa bez utworów czwartorzędowych. Arkusz Kłodzko*. {in Polish only}. Wydawnictwa Geologiczne, Warszawa.
- SEKINE, T. & WYLLIE, P.J., 1983. Experimental simulation of mantle hybridization in subduction zones. *Journal of Geology*, 91: 511–528.
- SHAND, P., GASKARTH, J. W., THIRLWALL, M. F. & ROCK, N. M. S., 1994. Late Caledonian lamprophyre dyke

- swarms of South-Eastern Scotland. *Mineralogy and Petrology*, 51: 277–298.
- SHELLEY, D., 1993. *Igneous and metamorphic rocks under the microscope. Classification, textures, microstructures and mineral preferred orientations*. Chapman & Hall, London, 445 pp.
- SISSON, T. W. & GROVE, T. L., 1993. Experimental investigations of the role of H<sub>2</sub>O in calc-alkaline differentiation and subduction zone magmatism. *Contributions to Mineralogy and Petrology*, 113: 143–166.
- SŁABY, E. & GÖTZE, J., 2004. Feldspar crystallization under magma-mixing conditions shown by cathodoluminescence and geochemical modelling – a case study from the Karkonosze pluton (SW Poland). *Mineralogical Magazine*, 68: 561–577.
- SŁABY, E. & MARTIN, H., 2008. Mafic and Felsic Magma Interaction in Granites: the Hercynian Karkonosze Pluton (Sudetes, Bohemian Massif). *Journal of Petrology*, 49: 353–391.
- SŁABY, E., GALBARCZYK-GĄSIOROWSKA, L., SELTMANN, R. & MÜLLER, A., 2006. Alkali feldspar megacryst growth: Geochemical modelling. *Mineralogy and Petrology*, 89: 1–29.
- SŁABY, E., SELTMANN, R., KOBER, D., MÜLLER, A., GALBARCZYK-GĄSIOROWSKA, L. & JEFFRIES, T., 2007. LREE distribution patterns in zoned alkali feldspar megacrysts from the Karkonosze pluton, Bohemian Massif – implications for parental magma composition. *Mineralogical Magazine*, 71: 193–217.
- STILLE, P., OBERHÄNSLI, R. & WENGER-SCHENK, K., 1989. Hf-Nd and trace element constraints on the genesis of alkaline and calc-alkaline lamprophyres. *Earth and Planetary Science Letters*, 96: 209–219.
- SZAŁAMACHA, J., 1960. *Szczegółowa mapa geologiczna Sudetów 1:25000. Arkusz Kowary*. {in Polish only}. Wydawnictwa Geologiczne, Warszawa.
- SZAŁAMACHA, J., 1972. *Szczegółowa mapa geologiczna Sudetów 1:25000. Arkusz Piechowice*. {in Polish only}. Wydawnictwa Geologiczne, Warszawa.
- SZAŁAMACHA, J., 1973. *Szczegółowa mapa geologiczna Sudetów 1:25000. Arkusz Stara Kamienica*. {in Polish only}. Wydawnictwa Geologiczne, Warszawa.
- SZAŁAMACHA, J. & SZAŁAMACHA, M., 1971. *Szczegółowa mapa geologiczna Sudetów 1:25000. Arkusz Rozdroże Izerskie*. {in Polish only}. Wydawnictwa Geologiczne, Warszawa.
- SZAŁAMACHA, J. & SZAŁAMACHA, M., 1984. *Szczegółowa mapa geologiczna Sudetów 1:25000. Arkusz Świeradów Zdrój*. {in Polish only}. Wydawnictwa Geologiczne, Warszawa.
- SZAŁAMACHA, J. & SZAŁAMACHA, M., 1991. *Szczegółowa mapa geologiczna Sudetów 1:25000. Arkusz Pisarzowice*. {in Polish only}. Wydawnictwa Geologiczne, Warszawa.
- SZAŁAMACHA, J. & TUCHOLSKA, K., 1960. *Szczegółowa mapa geologiczna Sudetów 1:25000. Arkusz Jelenia Góra Wschód*. {in Polish only}. Wydawnictwa Geologiczne, Warszawa.
- SZAŁAMACHA, M., 1960. *Szczegółowa mapa geologiczna Sudetów 1:25000. Arkusz Sosnowka*. {in Polish only}. Wydawnictwa Geologiczne, Warszawa.
- TEISSEYRE, H., 1976. *Szczegółowa mapa geologiczna Sudetów 1:25000. Arkusz Bolków*. {in Polish only}. Wydawnictwa Geologiczne, Warszawa.
- TEISSEYRE, H. & SAWICKI, L., 1958. *Szczegółowa mapa geologiczna Sudetów 1:25000. Arkusz Zagórze Śląskie*. {in Polish only}. Wydawnictwa Geologiczne, Warszawa.
- THOMPSON, A., 1982. Dehydration melting of pelitic rocks and the generation of H<sub>2</sub>O-undersaturated granitic liquids. *American Journal of Science*, 282: 1567–1595.
- TISCHENDORF, G., FÖRSTER, H.-J. & GOTTESMANN, B., 2001. Minor- and trace-element composition of trioctahedral micas: a review. *Mineralogical Magazine*, 65: 249–276.
- TREPKA, S. & GAWROŃSKI, O., 1961. *Szczegółowa mapa geologiczna Sudetów 1:25000. Arkusz Ostroszowice*. {in Polish only}. Wydawnictwa Geologiczne, Warszawa.
- TURPIN, L., VELDE, D. & PINTE, G., 1988. Geochemical comparison between minettes and kersantites from the Western European Hercynian orogen: trace element and Pb-Sr-Nd isotope constraints on their origin. *Earth and Planetary Science Letters*, 87: 73–86.
- ULRYCH, J., PEŠEK, J., ŠTĚPÁNKOVÁ-SVOBODOVA, J., BOSÁK, P., LLOYD, F. E., VON SECKENDORFF, V., LANG, M. & NOVÁK, J. K., 2006. Permo-Carboniferous volcanism in late Variscan continental basins of the Bohemian Massif (Czech Republic) geochemical characteristics. *Chemie der Erde, Geochemistry*, 66: 37–56.
- UPTON, B. G., STEPHENSON, D., SMEDLEY, P. M., WALLIS, S. M. & FITTON, J. G., 2004. Carboniferous and Permian magmatism in Scotland. In: Wilson M., Neumann E.-R., Davies G. R., Timmerman, M. J., Heermans, M. & Larsen, B. T. (Eds.), *Permo-Carboniferous magmatism and rifting in Europe. Geological Society, Special Publications*, 223: 195–218.
- VON SECKENDORFF, V., TIMMERMAN, M. J., KRAMER, W. & WROBEL, P., 2004. New <sup>40</sup>Ar/<sup>39</sup>Ar ages and geochemistry of late Carboniferous-early Permian lamprophyres and related volcanic rocks in the Saxothuringian Zone of the Variscan Orogen (Germany). In: Wilson, M., Neumann, E.-R., Davies, G. R., Timmerman, M. J., Heermans, M. & Larsen, B. T. (Eds.), *Permo-Carboniferous magmatism and rifting in Europe. Geological Society, Special Publications*, 223: 335–360.
- WALCZAK-AUGUSTYNIAK, M. & WROŃSKI, J., 1982. *Szczegółowa mapa geologiczna Sudetów 1:25000. Arkusz Domaszków*. {in Polish only}. Wydawnictwa Geologiczne, Warszawa.
- WALLACE, P. & CARMICHAEL, I. S. E., 1989. Minette lavas and associated leucitites from the Western Front of the Mexican Volcanic Belt: petrology, chemistry and origin. *Contributions to Mineralogy and Petrology*, 103: 470–492.
- WEAVER, B. & TARNEY, J., 1984. Empirical approach to estimating the composition of the continental crust. *Nature*, 310: 575–577.
- WIERZCHOŁOWSKI, B., 1976. Granitoidy kłodzko-złotostockie i ich kontaktowe oddziaływanie na skały osłony. [Granitoids of the Kłodzko-Złoty Stok massif and their contact influence on the country rocks (petrographic characteristics)]. *Geologia Sudetica*, 11: 7–147.
- WIERZCHOŁOWSKI, B., 1977. Skały żyłowe kłodzko-złotostockiego masywu granitoidowego. [Dike rocks of the Kłodzko-Złoty Stok granitoid massif]. *Geologia Sudetica*, 12: 7–28.
- WIERZCHOŁOWSKI, B., 1979. Petrochemiczne studium minetty ze Stójkowa (Sudety Środkowe). [Petrological and chemical study of the minette from Stójków (Middle Sudetes)]. *Archiwum Mineralogiczne*, 35: 67–77.
- WIERZCHOŁOWSKI, B., 2000. Lamprofiry z Łądka Zdroju (Sudety). [Lamprophyres from Łądek Zdrój (Sudetes)]. *Archiwum Mineralogiczne*, 53: 85–108.
- WIERZCHOŁOWSKI, B., 2003. Potassium-rich dyke rock of Rogówek. *Archiwum Mineralogiczne*, 54: 77–97.
- WILSON, M. & DOWNES, H., 2006. Tertiary-Quaternary intra-plate magmatism in Europe and its relationship to

- mantle dynamics. In: Gee, D. G. & Stephenson, R. A. (Eds), *European Lithosphere Dynamics. Geological Society, London, Memoirs*, 32: 147–166.
- WILSON, M., 1989. *Igneous Petrogenesis*. Chapman & Hall, 465 pp.
- WOJCIECHOWSKA, I., 1975. Tektonika kłodzko-złotostockiego masywu granitoidowego i jego osłony. [Tectonics of the Kłodzko-Złoty Stok granitoids massif and its country rocks in the light of mesostructural investigations]. *Geologia Sudetica*, 10, 2: 61–121.
- WONES, D. R. & EUGSTER, H. P., 1965. Stability of biotite: experiment, theory and application. *American Mineralogist*, 50: 1228–1272.
- WOOD, D. A., JORON, J. L., TREUIL, M., NORRY, M. & TARNEY, J., 1979. Elemental and Sr isotope variations in basic lavas from Iceland and the surrounding ocean floor. *Contributions to Mineralogy and Petrology*, 70: 319–339.
- WÓJCIK, L., 1958. *Szczegółowa mapa geologiczna Sudetów 1:25000. Arkusz Nowa Ruda*. {in Polish only}. Wydawnictwa Geologiczne, Warszawa.
- WYLLIE, P. J. & SEKINE, T., 1982: The Formation of Mantle Phlogopite in Subduction Zone Hybridization. *Contributions to Mineralogy and Petrology*, 79: 375–380.
- WYLLIE, P. J. 1982. Subduction products according to experimental prediction. *Bulletin of the Geological Society of America*, 93: 468–476.
- YARDLEY, B., 1989. *An Introduction to Metamorphic Petrology*. Longman Scientific & Technical, Essex, England, 248 pp.
- YODER, H. S., Jr, 1976. *Generation of Basaltic Magma*. National Academy of Science, Washington DC. 265 pp.
- ZAGOŹDŹON, K. & ZAGOŹDŹON, P. P., 2003. Wycieczka 7, stanowisko 6. Wskaźniki kierunku ruchu w skałach żyłowych i następstwo zjawisk tektonicznych w granicie karkonoskim. {in Polish only}. In: Ciężkowski, W., Wojewoda, J. & Żelaźniewicz, A. (Eds.), *Przewodnik do wycieczek LXXIV Zjazdu PTG*. Wrocław, WIND, 46–47.
- ZIEGLER, P. A. & DEZES, P., 2006. Crustal evolution of Western and Central Europe. In: Gee, D. G. & Stephenson, R. A. (Eds), *European Lithosphere Dynamics. Geological Society, London, Memoirs*, 32: 43–56.
- ZIMMERMANN, E. & BERG, G., 1932: *Geologische Karte von Preussen und Benachbarten Deutschen Ländern, 1:25000*. Blatt Kauffung. {in German only}. Preuss. Geol. Landesanst., Berlin.
- ŻELAŹNIEWICZ, A., NOWAK, I., LARIONOW, A. N. & PREYSNAKOV, S., 2006. Syntectonic Lower Ordovician migmatite and post-tectonic Upper Viséan syenite in the western limb of the Orlica-Śnieżnik Dome, West Sudetes: U-Pb SHRIMP data from zircons. *Geologia Sudetica*, 38: 63–80.

## Appendix 1

A list of sampling sites of lamprophyres and related mafic rock. The general location is indicated in Figure 2. X, Y – topographic coordinates (Państwowy Układ Współrzędnych 1965). Site description – main topographic features. Rock type – mafic lithologies exposed or present in blocks (considered to represent subcrops). Samples – samples used for laboratory studies; C – whole-rock chemical analysis; M – mineral microprobe analyses; I – Sr–Nd isotopic analyses.

Locality number	X	Y	Site description	Rock type	Samples	C	M	I
<b>Kowary-Janowice Wielkie Dyke Swarm</b>								
1	645.30	539.55	Trzczańsko, south of the western end of railway tunnel, blocks on top of hill.	micromonzodiorite				
2	647.90	538.36	Janowice Wielkie/Trzczańsko, hill 455.8, old quarry 340 m NNE of top	spessartite	313	+	+	
3	647.44	537.45	Przełęcz Karpnicka, blocks in old quarry NE of parking.	spessartite	318	+	+	
4	644.08	534.10	Between Bukowiec and Krogulec villages, west of road, blocks in scarps of field roads.	micromonzodiorite				
5	644.01	533.80	Between Bukowiec and Krogulec villages, west of road, several small, old quarries along a ridge.	micromonzodiorite	323	+	+	
6	644.1	533.49	Bukowiec, small outcrops in meadows and forests 380 m NNE of hill 474.7.	richterite minette	327	+	+	+
7	643.75	533.28	Bukowiec, 280 m west of hill 474.7, old quarry.	micromonzodiorite	328	+	+	+
				micromonzodiorite	329	+		
8	643.42	532.50	Bukowiec, 850 m SW of hill 474.7, blocks in old granite quarries.	monzonite				
9	643.53	532.50	Bukowiec, 800 m SW of hill 474.7, several small, old quarries	micromonzodiorite	332	+		
10	643.49	532.77	Bukowiec, 600 m SW of hill 474.7, blocks in old shallow quarry on a meadow.	monzonite				
11	643.38	532.16	Kowary/Jeżyny, 650 m north of Góra Brzeźnik, several shallow old quarries.	micromonzodiorite	334	+		
12	643.77	531.79	Kowary, north of the pass between Góra Brzeźnik and Parkowa Góra, blocks in forest.	spessartite	335	+		
13	646.06	531.62	Kowary-Wojków, 500 m west of Skała Skarbczyk, abundant blocks in forest.	minette	339	+		
14	645.55	530.80	Kowary-Wojków, 80 m SE of the top of hill 602.8, blocks in a forest.	minette				
15	644.35	533.14	Bukowiec, 380 m east of hill 474.7, blocks in meadows.	monzonite, micromonzodiorite				
16	644.26	532.76	Bukowiec, 500 m SE of hill 474.7, small quarry and blocks in forest.	spessartite	343	+		
17	645.04	533.27	Between Bukowiec and Gruszków villages, Graniczny Kamień Hill, abundant blocks on the ridge.	monzonite	345	+		
18	645.60	533.22	Gruszków, 400 m north of Góra Czartowiec, old quarries on a ridge.	monzonite	346	+		
				monzonite	348	+		
19	645.72	533.50	Gruszków, 700 m NNE of Góra Czartowiec, old quarries and blocks on a ridge.	monzonite	350	+	+	
				spessartite	351	+	+	+
20	644.70	535.51	Karpniki, hill 500 m SW of castle, edge of forest NW of top, blocks in a scarp.	minette	352	+	+	
21	644.61	535.25	Karpniki, hill 500 m SW of castle, W slope, blocks in forest.	micromonzodiorite				
22	644.69	535.25	Karpniki, hill 500 m SW of castle, S slope, blocks in forest.	minette, micromonzodiorite				
23	644.21	534.70	Krogulec, forested hills west of village, shallow old quarries and blocks in forest.	micromonzodiorite				
24	645.66	535.18	Karpniki, 650 m SE of castle, forested ridge, abundant blocks.	monzonite				

Locality number	X	Y	Site description	Rock type	Samples	C	M	I
<b>Kowary-Janowice Wielkie Dyke Swarm</b>								
26	637.77	529.17	Karpacz, Góra Strzelec, near the top and to the south; abundant blocks.	spessartite	375	+		
27	638.17	528.29	Karpacz, Góra Karpatka, 250 m NNE of top, blocks in a scarp on meadow.	minette				
28	638.37	529.61	Karpacz, Góra Strzelec, 500 m NE of top, blocks in a scarp of forest road.	minette	387	+	+	+
29	638.06	530.79	Miłków, 800 m SE of Góra Czartowiec, shallow quarries and abundant blocks at the edge of forest.	spessartite	394	+	+	+
30	638.51	532.36	Between Głębock and Miłków, a small hill near road crossing, small outcrops.	spessartite				
31	638.60	533.30	Głębock, ridges on meadows east of village, blocks in scarps.	micromonzodiorite	396	+		
				micromonzodiorite	398	+		
32	638.52	533.34	Głębock, ridges on meadows east of village, small quarry and blocks.	spessartite	399	+		
33	639.10	532.84	Miłków, north of village, blocks in small forest on meadows.	vogesite	401	+		
34	639.75	535.45	Mysłakowice, 1.1 km SSE of Krzyżowa Góra, old quarry ("Pod Skarpą").	weathered mafic rock				
35	641.82	533.60	Mysłakowice, 1.1 km south of Góra Mrowiec, small outcrop in a road scarp over Jedlica river.	minette	416	+		
36	641.98	533.65	Mysłakowice, 1.1 km SSE of Góra Mrowiec, old quarry.	minette	418	+		
				spheroidal minette	420	+	+	+
37	642.27	534.27	Between Mysłakowice and Bukowiec, 700 m SE of Góra Mrowiec, blocks in forest.	minette				
38	642.65	535.09	Between Mysłakowice and Bukowiec, 1km NEE of Góra Mrowiec, rocks and small quarry near the edge of forest.	micromonzodiorite	424	+		
39	651.88	532.25	Rędziny, Wlk. Kopa, 1 km NW of top, blocks in forest.	micromonzodiorite	430	+		
40	626.85	545.30	Stara Kamienica, Góra Siekierka, blocks 100 m west of top of hill.	spessartite	434	+		
41	631.42	532.20	Zachęlmie/Przesieka, Przesiecka Góra, W slope, accumulation of blocks on W slopes.	vogesite	443	+		
42	641.08	535.15	Mysłakowice, hill 400.7, old quarry above Jedlica river bank.	minette	626	+	+	
				vogesite	627	+	+	
				vogesite	628	+		
43	641.03	535.18	Mysłakowice, hill 400.7, rocks on W slope above Jedlica river bank.	vogesite	629	+	+	
<b>Intra-Sudetic Basin and Bardo Unit</b>								
44	697.20	505.96	Podlesie, Góra Koczan, rocks on a ridge near the top.	altered mafic rock	300	+		
				altered mafic rock	301	+	+	
45	665.78	530.26	Witków Śląski, meadows NE of village, blocks in a scarp of field road.	altered mafic rock	378	+		
46	665.20	530.61	Witków Śląski, meadows NE of village, blocks in a scarp of field road.	altered mafic rock	380	+		
47	671.46	525.83	Boguszów, old quarry west of 666.5 hill.	altered mica lamprophyre	382	+	+	+
48	657.70	532.03	Dębrznik, hills west of village, small outcrops and blocks in a road at the edge of forest.	minette	507	+	+	
49	656.03	531.15	Antonówka, blocks on meadow NW of village.	minette	508	+	+	
50	656.76	531.28	Antonówka, blocks on meadow north of village.	minette				
51	700.58	489.95	Wojbórz, north of village, hill 492.8, old quarry on W slope.	altered mafic rock	632	+		
<b>Góry Sowie Block</b>								
52	689.72	519.64	Glinno, Ostrzew hill, small exposures 150 m SW of the top.	kersantite	250	+	+	+
				kersantite	251	+		
				kersantite	253		+	

Locality number	X	Y	Site description	Rock type	Samples	C	M	I
<b>Góry Sowie Block</b>								
53	689.60	519.86	Glinno, Ostrzew hill, rocks 250 m NW of the top.	kersantite	254	+		
54	701.29	504.92	Srebrna Przełęcz, rocks in a road scarp north of the pass.	kersantite	255	+		
55	686.33	518.90	Walim, hill 605.5, small rocks near the top.	kersantite	305	+	+	+
56	687.59	524.88	Lubachów, Góra Przygodna, 250 m south of the top, blocks in forest road.	kersantite				
57	687.81	524.80	Lubachów, Góra Przygodna, 400 m SE of the top, small exposures in forest road.	kersantite	307	+	+	
				kersantite	308	+		
58	687.54	525.15	Lubachów, Góra Przygodna, blocks west of the top.	kersantite				
59	706.99	514.47	Przedborowa, Góra Płasza, blocks in the fields north of point 408.0.	kersantite	425	+		
60	706.60	516.54	Piława Grn./Dln., hill 322.6 south of foad, old quarry.	kersantite	426	+		
61	693.85	521.30	Between Rościszów and Piskorzów, 400 m NNW of Góra Cisówka, blocks in forest road.	spessartite	630	+		
<b>Gniewosów Dyke Swarm</b>								
62	677.89	490.66	Darnkowskie Wzgórza, 700 m NW of the top, small outcrop in a scarp.	richterite minette	448	+	+	+
63	675.68	490.17	Krucza Kopa, 1.1 km SWW of the top, blocks in stream valley.	minette				
64	697.44	464.06	Gniewosów, 800 m SSW of the top of Góra Jedlnik, a scarp near the road, with blocks.	minette	456	+		
65	697.49	463.93	Gniewosów, Gniewosów, 950 m SSW of the top of Góra Jedlnik, old quarry near the road.	minette				
66	697.76	463.43	Gniewosów, Gniewosów, 1.5 km SSE of the top of Góra Jedlnik, old quarry in a valley south of village.	minette	458	+	+	
67	697.40	463.61	Gniewosów, 1.3 km SSW of the top of Góra Jedlnik, rocks in a road scarp.	richterite minette				
68	697.44	465.13	Gniewosów, 300 m NW of the top of Góra Jedlnik, small blocks in forest.	minette	462	+		
69	696.81	466.00	Gniewosów, Góra Jedlnik, 1.4 km NW of top, blocks in forest.	spessartite	463	+		
70	699.34	462.69	Gniewosów, south of Szczerba, Castle, big outcrops at the junction of valleys.	richterite minette	465	+	+	+
				richterite minette	466	+		
71	708.69	465.43	Jaworek, between Góra Jeszkowa and Góra Zagajnik, S bank of valley, scarp over a stream.	minette	467	+		
72	710.73	459.32	Trójmorski Wierch, 1km NW of top, abundant blocks in forest.	kersantite	468	+	+	+
73	699.70	460.10	Różanka, hill 594.4, 350 m NE of the top, shallow quarry on the slope.	minette	470	+		+
74	700.16	460.09	Różanka, old quarry in the SE part of village, 750 m NEE of hill 594.4.	minette				
75	699.78	461.38	Różanka, near old quarry 500 m west of the village, blocks in forest.	minette	472	+		
<b>Złoty Stok Dyke Swarm</b>								
76	715.05	490.40	Mąkolno/Hanyszów, 900 m NW of Góra Haniak, blocks on meadows.	spessartite	483	+		
				spessartite	484	+	+	
77	715.33	489.78	Mąkolno/Hanyszów, 500 m SWW of Góra Haniak, blocks in a scarp of forest road.	spessartite				
78	715.15	489.98	Mąkolno/Hanyszów, 650 m west of Góra Haniak, blocks in a scarp of forest road.	spessartite	486	+		
79	714.72	490.31	Mąkolno/Hanyszów, 1.1 km NW of Góra Haniak, blocks in small forest on a hill.	spessartite	487	+	+	
80	711.00	488.37	Laski/Gajek, exposures in a forest road 700 m SW of Góra Sokolec.	micromonzodiorite	488	+	+	+
81	708.79	487.56	Jaszkowa Grn., Góra Starkowiec, 400 m SE of the top, blocks in forest.	spessartite	490	+		
82	709.96	487.47	Jaszkowa Grn., 2.3 km east of church, rocks in forest road and scarp.	spessartite	492	+	+	+

Locality number	X	Y	Site description	Rock type	Samples	C	M	I
<b>Złoty Stok Dyke Swarm</b>								
83	710.74	485.23	Jaszkowa Grn./Droszków, hill 529.0, small rocks on the top.	vogesite	497	+	+	+
84	710.33	485.14	Jaszkowa Grn./Droszków, Góra Stróża, 250 m NE of the top, rocks in a scarp.	spessartite	498	+		
85	710.20	484.99	Jaszkowa Grn./Droszków, Góra Stróża, east of the top, blocks on meadow.	vogesite	500	+		
86	705.40	482.75	Ołdrzychowice/Żelazno, meadows and fields between villages, blocks in scarps.	spessartite				
87	705.24	482.83	Ołdrzychowice/Żelazno, meadows and fields between villages, blocks in scarps.	spessartite				
88	705.32	482.99	Ołdrzychowice/Żelazno, meadows and fields between villages, exposures in a field road.	spessartite	531	+		
				spessartite	532	+		
89	704.93	482.85	Ołdrzychowice/Żelazno, meadows and fields between villages, exposures in a field road.	spessartite				
90	708.18	484.79	Jaszkowa Grn., Góra Brzanka, 1 km east of the top, blocks on meadow.	vogesite	536	+	+	
91	708.20	485.29	Jaszkowa Grn., Góra Brzanka, 1.2 km NE of the top, blocks in a scarp.	vogesite	538	+		
92	708.52	484.82	Jaszkowa Grn., 1.3 km east of Góra Brzanka, near the road to Rogówek, blocks in a field.	vogesite				
93	711.53	485.85	Droszków, Góra Ptaznik, 750 m SW of the top, blocks in forest.	spessartite	542	+		
94	717.20	477.79	Łądek-Stojków, rocks in railway cut 350 m north of station.	richterite minette	600	+		
95	717.32	480.08	Łądek Zdr., Góra Trzykrzyska, 600 m SW of the top, blocks in meadow.	vogesite	601	+		
96	714.33	487.25	Chwalisław, hills SE of village, 400 m SEE of point 575.0, numerous small rocks on slope.	vogesite	603	+		
				spessartite	606	+		
97	713.90	487.32	Chwalisław, ridge SE of village, near point 575.0, blocks in forest.	vogesite	609	+		
98	714.03	486.48	Chwalisław, stream valley 900 m S of point 575.0, rocks in scarp of field road.	micromonzodiorite	610	+		
99	714.36	486.65	Chwalisław, 850 m SSE of point 575.0, small rock in forest.	micromonzodiorite				
100	708.56	482.78	Rogówek, 500 m SSE of village, quarry near the road to Ołdrzychowice.	vogesite				

### Abbreviations used in Appendices 2 to 12:

**Location:** K – Karpacz–Janowice Wielkie Dyke Swarm; I – Intra-Sudetic Basin; S – Góry Sowie Block; G – Gniewosów Dyke Swarm; Z – Złoty Stok Dyke Swarm.

**Rock:** rm – richterite minette; m – minette; sm – spheroidal minette; v – vogesite; k – kersantite; s – spessartite; al – altered mica lamprophyre; mn – monzonite; mmd – micromonzodiorite; am – altered mafic rock.

**Minerals:** the symbols are explained in captions to individual appendices.

**Position:** p – phenocryst; g – groundmass; i – inclusion in another mineral; ps – pseudomorph; e – enclave; c – core; m – mantle; r – rim.

**Other:** “-” – component not determined. FeO – total Fe as FeO; Fe<sub>2</sub>O<sub>3</sub>\* – total Fe as Fe<sub>2</sub>O<sub>3</sub>.

## Appendix 2

## Selected analyses of dark micas

location/ rock	K/rm	K/rm	K/rm	K/m	K/m	K/m	K/sm	K/sm	K/sm	K/sm	K/m	K/m
sample/ anal.	327/35	327/45	327/55	387B/1	387B/16	387B/3	420/102	420/105	420/116	420/117	626/p1-15	626/p1-3
mineral	Phl	Phl	Bt	Phl	Phl	Phl/Bt	Bt	Phl	Phl	Phl	Bt	Phl
position	pc	g	pc	pc	gc	pr	pc	pr	pc	pr	pr	pc
<i>oxides [wt%]</i>												
SiO <sub>2</sub>	38.970	38.180	36.100	37.992	38.402	37.740	35.263	37.340	37.541	37.017	37.685	39.043
TiO <sub>2</sub>	4.700	5.840	6.480	5.050	5.518	5.592	2.750	6.949	7.033	6.998	4.682	4.999
Al <sub>2</sub> O <sub>3</sub>	13.330	12.520	14.570	14.223	14.034	13.288	18.345	13.434	13.145	13.366	13.368	14.304
Cr <sub>2</sub> O <sub>3</sub>	0.160	0.300	0.020	1.203	0.335	0.030	0.041	0.253	0.345	0.000	0.048	0.913
FeO*	5.460	11.620	15.700	6.033	6.480	13.899	18.511	10.156	8.461	11.537	18.140	5.642
MnO	0.070	0.070	0.150	0.000	0.075	0.165	0.292	0.035	0.034	0.078	0.152	0.000
MgO	21.130	16.590	12.970	20.301	20.381	15.503	10.756	16.835	17.682	15.462	13.046	20.132
BaO	-	-	-	0.517	0.343	0.593	0.007	0.020	0.003	0.059	-	-
CaO	0.020	0.100	0.030	0.000	0.000	0.003	0.220	1.195	1.161	1.312	0.111	0.048
Na <sub>2</sub> O	0.330	0.330	0.540	0.265	0.459	0.608	0.448	0.298	0.314	0.324	0.353	0.229
K <sub>2</sub> O	10.090	9.520	9.340	9.774	9.567	8.797	9.182	9.248	9.627	9.174	8.946	9.826
H <sub>2</sub> O*	4.200	4.090	4.010	3.853	3.702	3.339	3.813	3.466	3.383	3.482	3.656	3.676
F	-	-	-	0.634	0.959	1.435	0.322	1.271	1.484	1.177	0.672	1.066
Cl	-	-	-	-	-	-	0.000	0.032	0.026	0.031	-	-
O=F	-	-	-	0.267	0.404	0.604	0.136	0.535	0.625	0.496	0.283	0.449
O=Cl	-	-	-	-	-	-	0.000	0.007	0.006	0.007	-	-
Total	98.460	99.160	99.910	99.578	99.851	100.388	99.815	99.990	99.608	99.515	100.576	99.429
<i>cations [normalized to 22 O]</i>												
Si IV	5.653	5.651	5.409	5.493	5.527	5.583	5.334	5.466	5.489	5.482	5.639	5.605
Al IV	2.279	2.184	2.573	2.424	2.381	2.317	2.666	2.318	2.265	2.333	2.358	2.395
Ti IV	0.068	0.165	0.018	0.083	0.093	0.101	0.000	0.216	0.246	0.185	0.003	0.000
T site	8.000	8.000	8.000	8.000	8.000	8.000	8.000	8.000	8.000	8.000	8.000	8.000
Al VI	0.000	0.000	0.000	0.000	0.000	0.000	0.605	0.000	0.000	0.000	0.000	0.025
Ti VI	0.444	0.485	0.712	0.466	0.505	0.521	0.313	0.549	0.528	0.595	0.524	0.540
Cr	0.018	0.035	0.002	0.138	0.038	0.004	0.005	0.029	0.040	0.000	0.006	0.104
Fe <sup>+2</sup>	0.662	1.438	1.967	0.730	0.780	1.719	2.342	1.243	1.035	1.429	2.270	0.677
Mn	0.009	0.009	0.019	0.000	0.009	0.021	0.037	0.004	0.004	0.010	0.019	0.000
Mg	4.569	3.660	2.897	4.376	4.373	3.419	2.426	3.674	3.854	3.414	2.910	4.309
O site	5.703	5.628	5.597	5.709	5.705	5.683	5.727	5.500	5.461	5.447	5.729	5.654
Ba	-	-	-	0.029	0.019	0.034	0.000	0.001	0.000	0.003	-	-
Ca	0.003	0.016	0.005	0.000	0.000	0.000	0.036	0.187	0.182	0.208	0.018	0.007
Na	0.093	0.095	0.157	0.074	0.128	0.174	0.131	0.085	0.089	0.093	0.102	0.064
K	1.867	1.798	1.785	1.803	1.757	1.660	1.772	1.727	1.796	1.733	1.708	1.800
A site	1.963	1.908	1.947	1.906	1.904	1.869	1.939	2.000	2.067	2.038	1.828	1.871
O	19.936	19.962	19.992	20.000	20.000	20.000	20.000	20.000	20.000	20.000	20.000	20.000
OH	4.064	4.038	4.008	3.710	3.563	3.329	3.846	3.404	3.307	3.441	3.682	3.516
F	-	-	-	0.290	0.437	0.671	0.154	0.588	0.686	0.551	0.318	0.484
Cl	-	-	-	-	-	-	0.000	0.008	0.006	0.008	-	-

Minerals: Phl – phlogopite, Bt – biotite. H<sub>2</sub>O\* – water calculated assuming 20 O and 4(OH, F, Cl).

## Appendix 2 – continued

location/ rock	K/v	K/v	K/s	K/mn	K/mmd	I/m	I/m	I/m	I/m	I/al	I/al
sample/ anal.	627/38	627/39	351/51	350/25	323/76	507B/32	507B/48	508B/82	508B/95	382/13	382/14
mineral	Phl	Phl	Bt	Bt	Bt	Phl	Bt	Phl/Bt	Phl	Bt	Bt
position	gc	gc	gr	g	e	pc	pc	gc	pc	gc	gr
<i>oxides [wt%]</i>											
SiO <sub>2</sub>	36.926	38.019	37.741	36.103	33.485	37.801	35.166	34.977	38.167	36.001	35.482
TiO <sub>2</sub>	5.104	5.189	4.138	4.864	2.226	1.610	4.730	8.372	5.158	7.824	6.736
Al <sub>2</sub> O <sub>3</sub>	13.708	14.093	12.499	14.625	17.969	18.467	14.883	14.915	15.104	13.548	13.593
Cr <sub>2</sub> O <sub>3</sub>	1.039	1.065	0.013	0.012	0.000	0.051	0.039	0.000	0.267	0.000	0.000
FeO	11.303	6.787	18.630	15.420	25.111	2.834	17.447	12.454	6.993	15.835	20.417
MnO	0.130	0.048	0.159	0.102	0.195	0.043	0.365	0.072	0.026	0.190	0.173
MgO	15.843	18.549	12.855	14.250	7.277	24.223	12.955	14.752	20.003	12.533	9.813
BaO	-	-	-	0.035	0.032	-	-	-	-	0.000	0.000
CaO	0.020	0.071	0.059	1.278	0.274	0.155	0.028	0.102	0.045	0.096	0.097
Na <sub>2</sub> O	0.442	0.328	0.240	0.812	0.421	0.918	0.942	0.871	0.601	0.655	0.420
K <sub>2</sub> O	9.038	9.446	8.854	8.246	8.744	9.211	8.606	8.480	9.382	8.520	8.426
H <sub>2</sub> O	3.920	4.025	3.977	3.814	3.825	4.275	3.973	4.067	4.185	4.012	3.931
F	0.336	0.306	-	0.396	0.000	-	-	-	-	-	-
Cl	-	-	-	0.026	0.064	-	-	-	-	-	-
O=F	0.141	0.129	-	0.167	0.000	-	-	-	-	-	-
O=Cl	-	-	-	0.006	0.014	-	-	-	-	-	-
Total	97.668	97.797	99.165	99.811	99.609	99.588	99.134	99.062	99.931	99.214	99.088
<i>cations [normalized to 22 O]</i>											
Si IV	5.549	5.583	5.740	5.401	5.247	5.325	5.356	5.208	5.473	5.426	5.464
Al IV	2.428	2.417	2.241	2.579	2.753	2.675	2.644	2.618	2.527	2.406	2.467
Ti IV	0.023	0.000	0.019	0.020	0.000	0.000	0.000	0.174	0.000	0.168	0.069
T site	8.000	8.000	8.000	8.000	8.000	8.000	8.000	8.000	8.000	8.000	8.000
Al VI	0.000	0.022	0.000	0.000	0.566	0.391	0.027	0.000	0.026	0.000	0.000
Ti VI	0.554	0.573	0.454	0.528	0.262	0.171	0.542	0.763	0.556	0.719	0.711
Cr	0.123	0.124	0.002	0.001	0.000	0.006	0.005	0.000	0.030	0.000	0.000
Fe <sup>+2</sup>	1.421	0.834	2.370	1.929	3.291	0.334	2.222	1.551	0.839	1.996	2.629
Mn	0.017	0.006	0.020	0.013	0.026	0.005	0.047	0.009	0.003	0.024	0.023
Mg	3.549	4.061	2.915	3.178	1.700	5.087	2.941	3.275	4.276	2.816	2.253
O site	5.664	5.620	5.761	5.650	5.845	5.993	5.785	5.598	5.730	5.554	5.616
Ba	-	-	0.000	0.002	0.002	0.000	0.000	0.000	0.000	0.000	0.000
Ca	0.003	0.011	0.010	0.205	0.046	0.023	0.005	0.016	0.007	0.016	0.016
Na	0.129	0.093	0.071	0.236	0.128	0.251	0.278	0.251	0.167	0.191	0.125
K	1.733	1.770	1.718	1.574	1.748	1.655	1.672	1.611	1.716	1.638	1.655
A site	1.865	1.874	1.798	2.016	1.924	1.929	1.955	1.879	1.890	1.845	1.797
O	20.000	20.000	20.000	20.000	20.000	20.000	20.000	20.000	20.000	20.000	20.000
OH	3.840	3.858	4.000	3.806	3.983	4.000	4.000	4.000	4.000	4.000	4.000
F	0.160	0.142	-	0.187	0.000	-	-	-	-	-	-
Cl	-	-	-	0.007	0.017	-	-	-	-	-	-

## Appendix 2 – continued

location/ rock	S/k	S/k	S/k	Z/v	Z/v	G/rm	G/rm	G/rm	G/rm	G/k	G/k
sample/ anal.	250A/158	250D/251	305/393	536B/13	536B/48	458/146	458/147	465A/47	465A/56	468/63	468/64
mineral	Phl	Bt	Phl/Bt	Bt	Bt	Phl	Phl	Bt	Phl	Bt	Phl/Bt
position	pc	e	pc	p	pc	pc	pr	pr	g	gr	gc
<i>oxides [wt%]</i>											
SiO <sub>2</sub>	37.480	34.750	36.710	35.519	36.563	41.548	42.748	39.445	44.023	36.376	35.925
TiO <sub>2</sub>	5.280	5.630	5.560	3.628	3.658	1.750	1.321	4.919	1.410	5.184	5.451
Al <sub>2</sub> O <sub>3</sub>	13.080	17.320	13.560	15.788	15.336	12.208	9.997	11.172	10.186	14.533	14.953
Cr <sub>2</sub> O <sub>3</sub>	0.060	0.040	0.040	0.000	0.000	0.598	0.199	0.044	0.143	0.000	0.009
FeO	12.390	13.380	13.650	16.520	17.842	3.959	13.732	15.388	11.492	20.800	13.933
MnO	0.080	0.180	0.100	0.218	0.183	0.041	0.149	0.099	0.070	0.262	0.087
MgO	16.360	12.970	15.350	14.011	12.291	24.163	18.150	14.812	19.871	9.318	14.873
BaO	1.500	1.410	1.650	-	-	0.000	0.084	0.090	0.357	-	-
CaO	0.010	0.020	0.050	0.020	0.032	0.239	0.000	0.652	0.068	0.116	0.063
Na <sub>2</sub> O	0.790	0.520	0.650	0.328	0.426	0.202	0.081	0.051	0.014	0.879	0.662
K <sub>2</sub> O	8.330	8.960	8.330	7.592	8.948	10.358	8.836	9.394	8.149	8.796	9.043
H <sub>2</sub> O	3.710	4.016	3.768	3.964	3.956	3.328	3.458	3.768	3.582	3.926	4.044
F	0.680	0.000	0.500	0.143	0.069	1.842	1.304	0.510	1.194	-	-
Cl	-	-	-	-	-	0.000	0.016	0.027	0.011	-	-
O=F	0.286	0.000	0.211	0.060	0.029	0.776	0.549	0.215	0.503	-	-
O=Cl	-	-	-	-	-	0.000	0.004	0.006	0.002	-	-
Total	99.464	99.196	99.708	97.671	99.275	99.461	99.523	100.150	100.065	100.190	99.043
<i>cations [normalized to 22 O]</i>											
Si IV	5.587	5.233	5.500	5.409	5.536	5.918	6.278	5.867	6.328	5.545	5.381
Al IV	2.298	2.767	2.395	2.591	2.464	2.050	1.722	1.959	1.672	2.455	2.619
Ti IV	0.115	0.000	0.105	0.000	0.000	0.032	0.000	0.174	0.000	0.000	0.000
T site	8.000	8.000	8.000	8.000	8.000	8.000	8.000	8.000	8.000	8.000	8.000
Al VI	0.000	0.306	0.000	0.242	0.273	0.000	0.008	0.000	0.053	0.155	0.021
Ti VI	0.476	0.638	0.521	0.415	0.417	0.155	0.146	0.376	0.152	0.594	0.614
Cr	0.007	0.005	0.005	0.000	0.000	0.067	0.023	0.005	0.016	-	-
Fe <sup>+2</sup>	1.544	1.685	1.710	2.104	2.259	0.472	1.686	1.914	1.381	2.651	1.745
Mn	0.010	0.023	0.013	0.028	0.023	0.005	0.019	0.012	0.009	0.034	0.011
Mg	3.635	2.911	3.429	3.181	2.774	5.131	3.974	3.285	4.258	2.117	3.321
O site	5.674	5.568	5.678	5.970	5.747	5.830	5.856	5.593	5.869	5.552	5.714
Ba	0.088	0.083	0.097	-	-	0.000	0.005	0.005	0.020	0.000	0.000
Ca	0.002	0.003	0.008	0.003	0.005	0.036	0.000	0.104	0.010	0.019	0.010
Na	0.228	0.152	0.189	0.097	0.125	0.056	0.023	0.015	0.004	0.260	0.192
K	1.584	1.721	1.592	1.475	1.728	1.882	1.655	1.783	1.494	1.710	1.728
A site	1.902	1.959	1.886	1.575	1.859	1.975	1.683	1.907	1.529	1.989	1.930
O	20.000	20.000	20.000	20.000	20.000	20.000	20.000	20.000	20.000	20.000	20.000
OH	3.679	4.000	3.763	3.931	3.967	3.170	3.390	3.753	3.455	4.000	4.000
F	0.321	0.000	0.237	0.069	0.033	0.830	0.606	0.240	0.543	-	-
Cl	-	-	-	-	-	0.000	0.004	0.007	0.003	-	-

**Appendix 3**  
Selected analyses of amphiboles

location/ rock	K/rm	K/rm	K/rm	K/rm	K/v	K/v	K/v	K/v	K/s	K/s
sample/anal.	327/44	327/49	327/75	327/79	497/25	627/p2-3	629A/p4-2	629A/p7-5	351/135	351/73
mineral	Win	FeWin	Rit	Rbk	MgHbl	Krs	Prg	MgHas	MgHbl	Krs
position	gc	gm	gc	gm	pr	pc	pc	pc	pr	gc
<i>oxides [wt%]</i>										
SiO <sub>2</sub>	53.510	54.330	52.670	53.940	42.724	38.956	38.784	41.460	49.922	40.995
TiO <sub>2</sub>	0.730	0.770	1.140	0.370	2.103	4.489	3.860	4.082	1.209	4.655
Al <sub>2</sub> O <sub>3</sub>	1.560	0.880	1.460	0.460	11.809	13.069	13.695	11.147	4.272	11.833
Cr <sub>2</sub> O <sub>3</sub>	0.110	0.010	-	-	0.010	0.037	0.000	0.012	0.016	0.000
Fe <sub>2</sub> O <sub>3</sub>	4.061	11.540	7.030	14.774	8.064	0.321	1.466	2.876	7.888	3.637
FeO	7.365	12.950	8.009	13.915	3.635	13.247	13.468	8.125	8.080	8.635
MnO	0.150	0.040	0.190	0.030	0.098	0.096	0.274	0.147	0.323	0.097
MgO	16.950	8.990	15.130	7.130	14.964	10.960	10.093	14.148	14.077	13.155
ZnO	-	-	-	-	-	0.000	0.000	0.000	-	-
CaO	8.640	3.360	5.860	1.080	11.391	11.844	11.718	11.677	10.618	11.370
Na <sub>2</sub> O	3.570	5.080	5.410	6.800	2.017	1.953	2.106	2.107	1.184	2.327
K <sub>2</sub> O	0.660	0.140	1.000	0.040	0.879	1.600	1.321	1.316	0.398	0.767
H <sub>2</sub> O*	2.089	2.050	2.075	2.034	2.070	1.888	1.894	1.892	2.072	2.032
F	-	-	-	-	-	0.177	0.164	0.283	-	-
Cl	-	-	-	-	-	0.000	0.000	0.000	-	-
O=F	0.000	0.000	0.000	0.000	0.000	0.075	0.069	0.119	0.000	0.000
O=Cl	0.000	0.000	0.000	0.000	0.000	0.000	0.000	0.000	0.000	0.000
Total	99.395	100.141	99.973	100.573	99.763	98.563	98.773	99.153	100.059	99.503
<i>cations [normalized to 23 O and 13CNK]</i>										
Si IV	7.678	7.944	7.612	7.953	6.190	5.923	5.899	6.135	7.225	6.050
Al IV	0.264	0.056	0.249	0.047	1.810	2.077	2.101	1.865	0.729	1.950
Fe <sup>3+</sup>	0.058	0.000	0.139	0.000	0.000	0.000	0.000	0.000	0.047	0.000
Ti IV	0.000	0.000	0.000	0.000	0.000	0.000	0.000	0.000	0.000	0.000
T site	8.000	8.000	8.000	8.000	8.000	8.000	8.000	8.000	8.000	8.000
Al VI	0.000	0.096	0.000	0.033	0.206	0.265	0.354	0.079	0.000	0.108
Fe <sup>3+</sup>	0.381	1.270	0.625	1.639	0.879	0.037	0.168	0.320	0.812	0.404
Ti	0.079	0.085	0.124	0.041	0.229	0.513	0.441	0.454	0.132	0.517
Cr	0.012	0.001	-	-	0.001	0.004	0.000	0.001	0.002	0.000
Mg	3.626	1.960	3.260	1.567	3.232	2.484	2.288	3.121	3.037	2.894
Fe <sup>2+</sup>	0.884	1.584	0.968	1.716	0.440	1.684	1.713	1.005	0.978	1.066
Zn	0.000	0.000	0.000	0.000	0.000	0.000	0.000	0.000	0.000	0.000
Mn	0.018	0.005	0.023	0.004	0.012	0.012	0.035	0.018	0.040	0.012
Ca	0.000	0.000	0.000	0.000	0.000	0.000	0.000	0.000	0.000	0.000
M1,2,3 sites	5.000	5.000	5.000	5.000	5.000	5.000	5.000	5.000	5.000	5.000
Mg	0.000	0.000	0.000	0.000	0.000	0.000	0.000	0.000	0.000	0.000
Fe <sup>2+</sup>	0.000	0.000	0.000	0.000	0.000	0.000	0.000	0.000	0.000	0.000
Zn	-	-	-	-	-	0.000	0.000	0.000	-	-
Mn	0.000	0.000	0.000	0.000	0.000	0.000	0.000	0.000	0.000	0.000
Ca	1.328	0.526	0.907	0.171	1.768	1.929	1.910	1.851	1.646	1.798
Na	0.672	1.440	1.093	1.829	0.232	0.071	0.090	0.149	0.332	0.202
M4 site	2.000	1.967	2.000	2.000	2.000	2.000	2.000	2.000	1.979	2.000
Ca	0.000	0.000	0.000	0.000	0.000	0.000	0.000	0.000	0.000	0.000
Na	0.322	0.000	0.423	0.115	0.335	0.505	0.531	0.456	0.000	0.464
K	0.121	0.026	0.184	0.008	0.162	0.310	0.256	0.248	0.073	0.144
A site	0.442	0.026	0.608	0.122	0.497	0.815	0.787	0.704	0.073	0.608
O	22.000	22.000	22.000	22.000	22.000	22.000	22.000	22.000	22.000	22.000
OH	2.000	2.000	2.000	2.000	2.000	1.915	1.921	1.868	2.000	2.000
F	-	-	-	-	-	0.085	0.079	0.132	-	-
Cl	-	-	-	-	-	0.000	0.000	0.000	-	-

Minerals: Act – actinolite; Ed – edenite; Fac – ferroactinolite; FeTs – ferritschermakite; FeWin – ferriwinchyte; Krs – kaersutite; KRit – potassic richterite; MgHas – magnesiohastingsite; MgHbl – magnesiohornblende; Prg – pargasite; Rit – richterite; Rbk – riebeckite; Ts – tschermakite; Win – winchyte. H<sub>2</sub>O\* – water calculated assuming 22 O and 2(OH, F, Cl).



## Appendix 3 – continued

location/rock	Z/v	Z/s	Z/s	Z/s	Z/s	Z/mmd	Z/mmd	G/rm	G/rm
sample/anal.	536B/p5-10	492A/40	492A/56	492A/75	492A/84	488/92	488/94	448/25	465A/34
mineral	MgHas	Ts	MgHas	Ts	FeTs	MgHas	MgHbl	KRit	Rit
position	pr	gc	pm	pc	pr	g	pc	g	gc
<i>oxides [wt%]</i>									
SiO <sub>2</sub>	44.260	44.119	44.480	43.607	42.674	41.682	51.923	52.810	53.450
TiO <sub>2</sub>	1.566	2.574	1.816	1.992	2.382	2.540	0.123	2.500	1.150
Al <sub>2</sub> O <sub>3</sub>	10.923	10.906	11.342	11.956	10.624	10.809	3.435	0.200	0.870
Cr <sub>2</sub> O <sub>3</sub>	0.032	0.016	0.180	0.143	0.000	0.263	0.000	0.050	0.020
Fe <sub>2</sub> O <sub>3</sub>	4.884	8.694	5.099	7.630	10.987	5.139	5.401	0.000	0.142
FeO	5.155	2.006	3.032	2.747	5.855	12.208	8.139	16.510	11.499
MnO	0.090	0.160	0.097	0.046	0.130	0.358	0.448	0.350	0.260
MgO	15.652	15.903	16.519	15.573	12.402	10.620	15.423	11.890	15.920
ZnO	0.000	-	-	-	-	-	-	0.000	0.000
CaO	11.787	11.044	11.720	11.518	10.221	11.416	11.824	4.770	8.470
Na <sub>2</sub> O	2.108	2.174	2.235	2.034	2.230	1.941	0.597	4.920	3.310
K <sub>2</sub> O	0.984	0.452	0.507	0.477	0.464	0.971	0.231	3.730	2.060
H <sub>2</sub> O	1.978	2.098	2.086	2.090	2.047	2.001	2.083	1.651	1.626
F	0.193	-	-	-	-	-	-	0.740	0.890
Cl	0.000	-	-	-	-	-	-	0.000	0.020
O=F	0.081	0.000	0.000	0.000	0.000	0.000	0.000	0.312	0.375
O=Cl	0.000	0.000	0.000	0.000	0.000	0.000	0.000	0.000	0.005
Total	99.530	100.147	99.113	99.813	100.016	99.948	99.627	99.809	99.308
<i>cations [normalized to 23 O and 13CNK]</i>									
Si IV	6.412	6.304	6.394	6.257	6.251	6.246	7.475	7.910	7.804
Al IV	1.588	1.696	1.606	1.743	1.749	1.754	0.525	0.035	0.150
Fe <sup>+3</sup>	0.000	0.000	0.000	0.000	0.000	0.000	0.000	0.000	0.016
Ti IV	0.000	0.000	0.000	0.000	0.000	0.000	0.000	0.055	0.030
T site	8.000	8.000	8.000	8.000	8.000	8.000	8.000	8.000	8.000
Al VI	0.277	0.140	0.315	0.279	0.085	0.155	0.057	0.000	0.000
Fe <sup>+3</sup>	0.532	0.935	0.552	0.824	1.211	0.579	0.585	0.000	0.000
Ti	0.171	0.277	0.196	0.215	0.262	0.286	0.013	0.227	0.096
Cr	0.004	0.002	0.020	0.016	0.000	0.031	0.000	0.006	0.002
Mg	3.380	3.387	3.540	3.331	2.708	2.372	3.310	2.655	3.465
Fe <sup>+2</sup>	0.625	0.240	0.364	0.330	0.717	1.530	0.980	2.068	1.404
Zn	0.000	-	-	-	-	-	-	0.000	0.000
Mn	0.011	0.019	0.012	0.006	0.016	0.045	0.055	0.044	0.032
Ca	0.000	0.000	0.000	0.000	0.000	0.000	0.000	0.000	0.000
M1,2,3 sites	5.000	5.000	5.000	5.000	5.000	5.000	5.000	5.000	5.000
Mg	0.000	0.000	0.000	0.000	0.000	0.000	0.000	0.000	0.000
Fe <sup>+2</sup>	0.000	0.000	0.000	0.000	0.000	0.000	0.000	0.000	0.000
Zn	0.000	-	-	-	-	-	-	0.000	0.000
Mn	0.000	0.000	0.000	0.000	0.000	0.000	0.000	0.000	0.000
Ca	1.830	1.691	1.805	1.771	1.604	1.833	1.824	0.765	1.325
Na	0.170	0.309	0.195	0.229	0.396	0.167	0.167	1.235	0.675
M4 site	2.000	2.000	2.000	2.000	2.000	2.000	1.990	2.000	2.000
Ca	0.000	0.000	0.000	0.000	0.000	0.000	0.000	0.000	0.000
Na	0.422	0.293	0.428	0.337	0.237	0.397	0.000	0.194	0.262
K	0.182	0.082	0.093	0.087	0.087	0.186	0.042	0.713	0.384
A site	0.604	0.375	0.521	0.424	0.324	0.582	0.042	0.907	0.646
O	22.000	22.000	22.000	22.000	22.000	22.000	22.000	22.000	22.000
OH	1.912	2.000	2.000	2.000	2.000	2.000	2.000	1.649	1.584
F	0.088	-	-	-	-	-	-	0.351	0.411
Cl	0.000	-	-	-	-	-	-	0.000	0.005

## Appendix 4

## Selected analyses of clinopyroxenes

location/ rock	K/rm	K/m	K/m	K/w	K/s	K/s	K/s	K/mn	K/mn	K/mmd	K/mmd
sample/ anal.	327/59	626/23	352A/3	627/23	318B/175	318B/254	313/34	350/37	350/34	328B/186	328B/178
mineral	Aug	Hd	Di	Aug	Di	Di	Aug	Aug	Aug	Aug	Aug
position	g	g	pc	g	pc	pr	pr	pc	pr	pc	pr
<i>oxides [wt%]</i>											
SiO <sub>2</sub>	53.240	51.471	51.190	52.410	48.806	52.036	50.030	49.799	51.327	49.378	51.803
TiO <sub>2</sub>	1.080	0.192	1.170	0.175	1.318	0.292	1.320	1.100	0.149	1.446	0.033
Al <sub>2</sub> O <sub>3</sub>	0.690	0.251	3.790	1.682	5.955	1.268	3.250	3.679	0.610	4.254	0.765
Cr <sub>2</sub> O <sub>3</sub>	0.000	0.000	0.000	0.006	0.456	0.278	0.000	0.029	0.002	0.251	0.014
Fe <sub>2</sub> O <sub>3</sub>	0.667	4.044	1.161	1.469	2.358	1.683	2.507	2.348	1.839	3.327	1.217
FeO	6.799	12.221	4.225	6.798	4.105	7.118	7.254	7.514	14.362	6.737	15.365
MnO	0.170	0.353	0.130	0.405	0.052	0.615	0.280	0.227	0.766	0.203	0.764
NiO	0.000	0.000	0.000	0.000	0.000	0.000	0.000	0.000	0.081	0.028	0.000
MgO	15.640	8.672	15.800	15.150	14.075	12.590	14.780	14.077	11.127	14.414	11.346
CaO	21.630	21.542	22.020	21.146	22.208	23.436	20.040	20.178	19.337	20.115	18.343
Na <sub>2</sub> O	0.440	1.312	0.330	0.328	0.398	0.491	0.300	0.398	0.360	0.404	0.455
K <sub>2</sub> O	0.010	0.000	0.000	0.000	0.000	0.000	0.020	0.001	0.005	0.012	0.000
Total	100.367	100.058	99.816	99.569	99.731	99.807	99.781	99.349	99.965	100.569	100.105
<i>cations [normalized to 6 O and 4 cations]</i>											
Si IV	1.962	1.979	1.881	1.949	1.808	1.954	1.868	1.869	1.969	1.831	1.981
Al IV	0.030	0.011	0.119	0.051	0.192	0.046	0.132	0.131	0.028	0.169	0.019
T site	1.992	1.991	2.000	2.000	2.000	2.000	2.000	2.000	1.996	2.000	2.000
Al VI	0.000	0.000	0.045	0.023	0.068	0.010	0.011	0.031	0.000	0.017	0.015
Ti	0.030	0.006	0.032	0.005	0.037	0.008	0.037	0.031	0.004	0.040	0.001
Cr	0.000	0.000	0.000	0.000	0.013	0.008	0.000	0.001	0.000	0.007	0.000
Fe <sup>+3</sup>	0.019	0.117	0.032	0.041	0.066	0.048	0.070	0.066	0.053	0.093	0.035
Fe <sup>+2</sup>	0.210	0.393	0.130	0.211	0.127	0.223	0.226	0.236	0.461	0.209	0.491
Mn	0.005	0.011	0.004	0.013	0.002	0.020	0.009	0.007	0.025	0.006	0.025
Ni	0.000	0.000	0.000	0.000	0.000	0.000	0.000	0.000	0.002	0.001	0.000
Mg	0.859	0.497	0.866	0.840	0.777	0.705	0.822	0.787	0.636	0.797	0.647
Ca	0.854	0.887	0.867	0.843	0.881	0.943	0.801	0.811	0.795	0.799	0.752
Na	0.031	0.098	0.024	0.024	0.029	0.036	0.022	0.029	0.027	0.029	0.034
K	0.000	0.000	0.000	0.000	0.000	0.000	0.001	0.000	0.000	0.001	0.000
M1,M2	2.008	2.009	2.000	2.000	2.000	2.000	2.000	2.000	2.004	2.000	2.000
<i>end members [mol%]</i>											
Wo	43.87	46.56	45.67	43.26	47.56	48.65	41.53	42.52	40.35	41.97	38.55
En	44.14	26.08	45.59	43.12	41.94	36.36	42.62	41.27	32.30	41.85	33.18
Fs	11.99	27.36	8.74	13.62	10.50	14.99	15.84	16.21	27.35	16.18	28.27

Minerals: Aug – augite; Di – diopside; Hd – hedenbergite. End-members: Wo – wollastonite; En – enstatite; Fs – ferrosilite

## Appendix 4 – continued

location/rock	K/mmd	K/mmd	S/k	S/k	G/k	Z/w	Z/w	Z/s	Z/s
sample/anal.	328B/217	328B/304	250A/167	305/403	468/43	536B/1	536B/61	484/100	484/33
mineral	Aug	Di	Di	Aug	Di	Aug	Aug	Aug	Aug
position	e	e	pc	g	pc	pc	pr	pc	pr
oxides [wt%]									
SiO <sub>2</sub>	51.231	52.050	50.160	52.060	50.966	53.818	52.004	50.988	49.334
TiO <sub>2</sub>	0.817	0.043	1.150	0.520	0.922	0.210	0.319	0.692	1.086
Al <sub>2</sub> O <sub>3</sub>	2.288	0.119	4.180	1.690	5.028	1.196	2.337	3.618	4.824
Cr <sub>2</sub> O <sub>3</sub>	0.105	0.089	0.610	0.120	0.221	0.509	0.042	0.145	0.376
Fe <sub>2</sub> O <sub>3</sub>	2.121	1.260	1.659	1.775	1.255	0.768	0.604	2.037	2.744
FeO	7.784	12.364	4.377	6.013	4.425	3.137	9.628	4.257	4.694
MnO	0.232	0.582	0.180	0.250	0.152	0.158	0.243	0.107	0.260
NiO	0.021	0.045	0.020	0.040	0.000	0.000	0.000	0.000	0.000
MgO	15.427	9.450	14.170	15.370	15.574	17.720	14.317	16.017	14.921
CaO	19.687	23.796	22.790	21.310	21.668	22.015	19.296	21.108	21.109
Na <sub>2</sub> O	0.266	0.417	0.420	0.350	0.344	0.272	0.496	0.352	0.288
K <sub>2</sub> O	0.000	0.005	0.010	0.030	0.025	0.063	0.018	0.000	0.011
Total	99.978	100.220	99.726	99.528	100.580	99.866	99.304	99.321	99.647
cations [normalized to 6 O and 4 cations]									
Si IV	1.905	1.992	1.860	1.935	1.859	1.962	1.949	1.884	1.831
Al IV	0.095	0.005	0.140	0.065	0.141	0.038	0.051	0.116	0.169
T site	2.000	1.998	2.000	2.000	2.000	2.000	2.000	2.000	2.000
Al VI	0.006	0.000	0.043	0.009	0.075	0.013	0.052	0.042	0.042
Ti	0.023	0.001	0.032	0.015	0.025	0.006	0.009	0.019	0.030
Cr	0.003	0.003	0.018	0.004	0.006	0.015	0.001	0.004	0.011
Fe <sup>+3</sup>	0.059	0.036	0.046	0.050	0.034	0.021	0.017	0.057	0.077
Fe <sup>+2</sup>	0.242	0.396	0.136	0.187	0.135	0.096	0.302	0.132	0.146
Mn	0.007	0.019	0.006	0.008	0.005	0.005	0.008	0.003	0.008
Ni	0.001	0.001	0.001	0.001	0.000	0.000	0.000	0.000	0.000
Mg	0.855	0.539	0.783	0.852	0.847	0.963	0.800	0.882	0.826
Ca	0.784	0.976	0.905	0.849	0.847	0.860	0.775	0.836	0.839
Na	0.019	0.031	0.030	0.025	0.024	0.019	0.036	0.025	0.021
K	0.000	0.000	0.000	0.001	0.001	0.003	0.001	0.000	0.001
M1,M2	2.000	2.002	2.000	2.000	2.000	2.000	2.000	2.000	2.000
end members [mol%]									
Wo	40.26	49.64	48.25	43.64	45.34	44.22	40.75	43.76	44.28
En	43.90	27.43	41.74	43.79	45.34	49.53	42.07	46.21	43.55
Fs	15.85	22.94	10.00	12.57	9.32	6.25	17.17	10.03	12.16

## Appendix 5

## Selected analyses of feldspars

location/ rock	K/rm	K/rm	K/v	K/v	K/s	K/s	K/mn	K/mmd	K/mmd	K/mmd	I/m
sample/ anal.	327/37	327/39	627/5	629A/6	351/24	318B/151	350/17	323/56	328B/263	323/77	508B/103
mineral	Sa	Ab	Oli	Sa	Lab	Sa	Ads	Lab	Ab	Aor	Ads
position	g	g	g	g	gc	g	gc	pc	pr	e	g
<i>oxides [wt%]</i>											
SiO <sub>2</sub>	64.260	68.860	63.055	63.958	52.733	64.245	59.756	55.037	68.160	63.232	57.690
TiO <sub>2</sub>	0.000	0.000	0.057	0.005	0.060	0.000	0.028	0.075	-	0.040	0.090
Al <sub>2</sub> O <sub>3</sub>	18.290	19.640	22.543	18.703	28.812	18.686	25.366	27.677	19.660	22.213	25.736
Fe <sub>2</sub> O <sub>3</sub> *	0.340	0.150	0.311	0.283	0.559	0.016	0.304	0.513	0.570	0.383	0.555
MnO	0.000	0.000	0.000	0.058	0.000	0.071	0.013	0.026	-	0.000	0.008
MgO	0.000	0.000	0.017	0.012	0.070	0.000	0.018	0.058	-	0.025	0.025
CaO	0.000	0.020	3.845	0.530	12.271	0.000	6.809	10.437	0.261	2.959	7.547
Na <sub>2</sub> O	0.200	12.090	8.279	0.554	4.404	0.817	7.262	5.319	11.674	8.108	6.520
K <sub>2</sub> O	16.980	0.080	1.325	15.280	0.271	15.607	0.659	0.582	0.015	2.332	0.981
BaO	-	-	-	-	-	-	0.054	0.082	0.000	0.210	0.000
Total	100.070	100.850	99.432	99.383	99.180	99.442	100.269	99.806	100.340	99.502	99.152
<i>cations [normalized to 8O]</i>											
Si	2.980	2.990	2.811	2.970	2.413	2.982	2.662	2.494	2.974	2.828	2.611
Ti	0.000	0.000	0.002	0.000	0.002	0.000	0.001	0.003	-	0.001	0.003
Al	1.000	1.000	1.185	1.024	1.553	1.021	1.331	1.477	1.010	1.170	1.372
Fe <sup>+3</sup>	0.010	0.000	0.010	0.010	0.019	0.001	0.010	0.017	0.019	0.013	0.019
Mn	0.000	0.000	0.000	0.002	0.000	0.003	0.000	0.001	-	0.000	0.000
Mg	0.000	0.000	0.001	0.001	0.005	0.000	0.001	0.004	-	0.002	0.002
Ca	0.000	0.000	0.184	0.026	0.602	0.000	0.325	0.507	0.012	0.142	0.366
Na	0.020	1.020	0.716	0.050	0.391	0.074	0.627	0.467	0.988	0.703	0.572
K	1.010	0.000	0.075	0.905	0.016	0.924	0.037	0.034	0.001	0.133	0.057
Ba	-	-	-	-	-	-	0.001	0.001	0.000	0.004	0.000
X	3.990	3.990	4.008	4.004	3.987	4.004	4.004	3.991	4.003	4.012	4.005
Z	1.030	1.020	0.976	0.985	1.014	1.001	0.991	1.014	1.001	0.984	0.997
<i>end members [mol%]</i>											
Ab	1.94	100.00	73.42	5.08	38.75	7.41	63.40	46.33	98.70	71.88	57.49
An	0.00	0.00	18.84	2.69	59.66	0.00	32.86	50.30	1.20	14.52	36.78
Or	98.06	0.00	7.73	92.23	1.59	92.59	3.74	3.37	0.10	13.60	5.73

Minerals and end-members: Ab – albite; Ads – andesine; An – anorthite; Aor – anorthoclase; Lab – labradorite; NaSa – sodic sanidine; Oli – oligoclase; Or – orthoclase; Sa – sanidine. All feldspar terminology is based on chemical composition only, the structural states were not determined.

## Appendix 5 – continued

location/rock	I/m	I/m	I/al	S/k	S/k	S/k	S/k	S/k	S/k
sample/anal.	508B/121	508B/136	382/7	250D/337	250B/194	250D/338	250B/214	250D/259	250D/311
mineral	Aor	NaSa	NaSa	Lab	Ab	Aor	Sa	Lab	Ab
position	gr	gr	g	g	g	g	g	e	e
<i>oxides [wt%]</i>									
SiO <sub>2</sub>	62.420	66.369	65.550	53.910	66.730	58.120	64.400	54.110	67.250
TiO <sub>2</sub>	0.028	0.000	0.157	0.060	0.000	0.000	0.000	0.060	0.020
Al <sub>2</sub> O <sub>3</sub>	22.463	18.314	19.151	27.960	21.540	26.180	17.880	27.920	20.190
Fe <sub>2</sub> O <sub>3</sub>	0.410	0.400	0.345	0.730	0.330	1.070	0.140	0.820	0.380
MnO	0.000	0.006	0.030	0.000	0.010	0.100	0.000	0.070	0.050
MgO	0.023	0.005	0.000	0.130	0.130	0.820	0.020	0.050	0.040
CaO	4.406	0.049	0.562	10.050	1.220	2.690	0.060	10.470	0.930
Na <sub>2</sub> O	7.363	4.861	5.460	4.980	9.670	6.300	0.020	5.440	11.110
K <sub>2</sub> O	2.626	10.163	8.655	1.140	1.090	3.880	16.790	0.230	0.120
BaO	0.000	0.000	-	0.160	0.050	0.020	0.040	0.050	0.000
Total	99.739	100.167	99.910	99.120	100.770	99.180	99.350	99.220	100.090
<i>cations [normalized to 8O]</i>									
Si	2.795	3.003	2.962	2.467	2.908	2.634	3.004	2.467	2.946
Ti	0.001	0.000	0.005	0.002	0.000	0.000	0.000	0.002	0.001
Al	1.185	0.976	1.019	1.508	1.106	1.398	0.983	1.500	1.042
Fe <sup>+3</sup>	0.014	0.014	0.012	0.025	0.011	0.036	0.005	0.028	0.013
Mn	0.000	0.000	0.001	0.000	0.000	0.004	0.000	0.003	0.002
Mg	0.002	0.000	0.000	0.009	0.008	0.055	0.001	0.003	0.003
Ca	0.211	0.002	0.027	0.493	0.057	0.131	0.003	0.511	0.044
Na	0.639	0.426	0.478	0.442	0.817	0.554	0.002	0.481	0.944
K	0.150	0.587	0.499	0.067	0.061	0.224	0.999	0.013	0.007
Ba	0.000	0.000	-	0.003	0.001	0.000	0.001	0.001	0.000
X	3.995	3.993	3.998	4.002	4.025	4.069	3.992	3.997	4.002
Z	1.002	1.015	1.005	1.013	0.944	0.968	1.006	1.013	0.998
<i>end members [mol%]</i>									
Ab	63.90	41.97	47.61	44.13	87.42	60.93	0.18	47.82	94.93
An	21.10	0.20	2.69	49.22	6.09	14.38	0.30	50.85	4.39
Or	15.00	57.83	49.70	6.65	6.48	24.69	99.52	1.33	0.67

## Appendix 5 – continued

location/ rock	S/k	S/k	Z/v	Z/v	Z/s	Z/s	Z/mmd	Z/mmd	G/rm	G/rm	G/k
sample/ anal.	250C/231	253/375	497/11	497/18	487/18	484/18	488/85	488/87	458/132	458/135	468/77
mineral	NaSa	Sa	Sa	Ab	Lab	Ab	Oli	Sa	Sa	Aor	Lab
position	e	e	gc	g	g	gr	gr	g	gc	gr	gc
<i>oxides [wt%]</i>											
SiO <sub>2</sub>	65.270	64.620	64.031	68.654	53.675	67.142	63.483	64.532	64.020	67.612	52.149
TiO <sub>2</sub>	0.010	0.000	0.013	0.000	0.048	0.068	0.000	0.025	0.030	0.045	0.115
Al <sub>2</sub> O <sub>3</sub>	18.380	18.340	18.505	19.671	28.952	20.748	23.380	18.309	18.290	19.558	29.668
Fe <sub>2</sub> O <sub>3</sub>	0.520	0.040	0.158	0.127	0.592	0.148	0.291	0.171	0.261	0.227	0.793
MnO	0.000	0.000	0.000	0.000	0.000	0.009	0.000	0.028	0.005	0.000	0.001
MgO	0.030	0.020	0.000	0.003	0.083	0.002	0.000	0.000	0.022	0.038	0.118
CaO	0.240	0.020	0.015	0.024	11.139	1.147	4.658	0.031	0.000	0.003	12.752
Na <sub>2</sub> O	3.950	0.200	0.175	11.990	4.716	11.204	8.779	0.855	1.038	10.296	3.681
K <sub>2</sub> O	10.840	16.540	16.747	0.024	0.700	0.070	0.331	15.563	14.985	1.800	0.530
BaO	0.030	0.030	0.000	0.000	-	-	0.000	0.000	0.660	0.000	-
Total	99.270	99.810	99.644	100.493	99.905	100.538	100.922	99.514	99.311	99.579	99.807
<i>cations [normalized to 8O]</i>											
Si	2.988	2.996	2.981	2.987	2.435	2.929	2.785	2.993	2.985	2.983	2.376
Ti	0.000	0.000	0.000	0.000	0.002	0.002	0.000	0.001	0.001	0.001	0.004
Al	0.992	1.002	1.014	1.008	1.548	1.066	1.208	1.000	1.004	1.016	1.592
Fe <sup>+3</sup>	0.018	0.001	0.006	0.004	0.020	0.005	0.010	0.006	0.009	0.008	0.027
Mn	0.000	0.000	0.000	0.000	0.000	0.000	0.000	0.001	0.000	0.000	0.000
Mg	0.002	0.001	0.000	0.000	0.006	0.000	0.000	0.000	0.002	0.002	0.008
Ca	0.012	0.001	0.001	0.001	0.541	0.054	0.219	0.002	0.000	0.000	0.623
Na	0.351	0.018	0.016	1.011	0.415	0.948	0.747	0.077	0.094	0.881	0.325
K	0.633	0.978	0.995	0.001	0.041	0.004	0.019	0.921	0.891	0.101	0.031
Ba	0.001	0.001	0.000	0.000	-	-	0.000	0.000	0.012	0.000	-
X	3.998	3.999	4.001	3.999	4.005	4.002	4.003	4.000	3.999	4.008	3.999
Z	0.998	0.999	1.012	1.013	1.002	1.006	0.985	1.001	0.999	0.984	0.987
<i>end members [mol%]</i>											
Ab	35.22	1.80	1.58	99.80	41.62	94.23	75.84	7.70	9.54	89.71	33.20
An	1.18	0.10	0.10	0.10	54.32	5.37	22.23	0.20	0.00	0.00	63.64
Or	63.60	98.10	98.32	0.10	4.06	0.40	1.93	92.10	90.46	10.29	3.17

## Appendix 6

## Selected analyses of chlorites and talc

location/rock	K/s	K/mmd	K/mmd	I/m	I/al	S/k	S/k	G/m	G/m
sample/anal.	394/45	323/84	328B/210	507B/52	382/18	250A/136	250A/161	458/125	465A/49
mineral	Pyc	Rip	Bru	Bru	Dia	Dia	TCh	Dia	Tlc
position	i	i	i	ps	ps	i	i	i	ps
<i>oxides [wt%]</i>									
SiO <sub>2</sub>	29.388	22.664	27.839	28.925	35.371	33.310	40.600	32.484	59.822
TiO <sub>2</sub>	0.065	0.087	0.000	0.110	0.093	0.660	0.000	0.002	0.048
Al <sub>2</sub> O <sub>3</sub>	17.946	23.280	16.372	18.471	18.967	13.540	11.260	13.094	0.973
FeO*	20.912	38.259	28.691	28.031	19.730	15.430	9.860	25.187	6.689
MnO	0.299	0.347	0.353	0.260	0.085	0.370	0.190	0.168	0.058
MgO	19.316	3.929	14.709	10.960	13.722	23.830	24.380	17.367	25.741
CaO	0.373	0.035	0.154	0.533	0.450	0.500	1.500	0.525	0.358
Na <sub>2</sub> O	0.077	0.011	0.012	0.023	0.028	0.030	0.040	0.040	0.125
K <sub>2</sub> O	0.000	0.046	0.060	0.119	0.411	0.090	0.020	0.092	0.110
H <sub>2</sub> O*	11.769	10.757	11.293	11.402	12.057	12.092	12.576	11.345	-
F	0.000	0.000	0.000	-	-	0.000	0.000	0.401	0.147
Cl	0.000	0.021	0.000	-	-	-	-	0.039	0.000
O=F	0.000	0.000	0.000	-	-	0.000	0.000	0.169	0.060
O=Cl	0.000	0.005	0.000	-	-	-	-	0.009	0.000
Total	100.145	99.431	99.483	98.834	100.914	99.852	100.426	100.566	94.011
<i>cations [normalized to 28 O for chlorites and to 11 O for talc]</i>									
Si IV	5.980	5.083	5.948	6.166	6.964	6.619	7.706	6.694	3.962
Al IV	2.020	2.917	2.052	1.834	1.036	1.381	0.294	1.306	0.039
T site	8.000	8.000	8.000	8.000	8.000	8.000	8.000	8.000	4.000
Al VI	2.283	3.237	2.070	2.807	3.365	1.790	2.225	1.874	0.038
Ti	0.010	0.015	0.000	0.018	0.014	0.099	0.000	0.000	0.003
Fe <sup>+2</sup>	3.558	7.176	5.126	4.998	3.249	2.564	1.565	4.341	0.371
Mn	0.052	0.066	0.064	0.047	0.014	0.062	0.031	0.029	0.004
Mg	5.859	1.314	4.685	3.483	4.028	7.059	6.899	5.335	2.541
Ca	0.081	0.008	0.035	0.122	0.095	0.106	0.305	0.116	0.026
Na	0.030	0.005	0.005	0.010	0.011	0.012	0.015	0.016	0.016
K	0.000	0.013	0.016	0.032	0.103	0.023	0.005	0.024	0.010
O site	11.874	11.834	12.002	11.516	10.878	11.714	11.044	11.736	3.006
O	20.000	20.000	20.000	20.000	20.000	20.000	20.000	20.000	10.000
OH	16.000	15.992	16.000	16.000	16.000	16.000	16.000	15.725	1.939
F	0.000	0.000	0.000	-	-	0.000	0.000	0.261	0.062
Cl	0.000	0.008	0.000	-	-	-	-	0.014	0.000

Minerals: Bru – brunsvigite, Dia – diabantite, Pyc – pycnochlorite, Rip – ripidolite; TCh – talc-chlorite; Tlc – talc. H<sub>2</sub>O\* – water calculated assuming 20 O and 16(OH, F, Cl).

## Appendix 7

## Selected analyses of titanite and epidote-group minerals

location/ rock	K/m	K/s	K/mmd	S/k	Z/v	location/ rock	K/v	K/v	K/s	K/m
sample/ anal.	387B/12	313/18	328B/229	250D/323	536B/50	sample/anal.	629A/Ep1	627/17	394/58	420/107
mineral	Ttn	Ttn	Ttn	Ttn	Ttn	mineral	Aln	Ep	Ep	Ep
position	g	g	g	i	p	position	g	g	g	g
<i>oxides [wt%]</i>						<i>oxides [wt%]</i>				
SiO <sub>2</sub>	30.804	31.350	30.195	32.580	29.826	SiO <sub>2</sub>	32.646	36.105	37.136	35.753
TiO <sub>2</sub>	33.449	29.860	39.950	25.720	36.665	TiO <sub>2</sub>	0.311	0.115	0.445	0.502
Al <sub>2</sub> O <sub>3</sub>	1.913	5.980	0.160	5.860	1.767	Al <sub>2</sub> O <sub>3</sub>	17.742	20.315	21.996	20.193
Cr <sub>2</sub> O <sub>3</sub>	0.000	0.000	0.000	0.040	0.016	Fe <sub>2</sub> O <sub>3</sub> *	13.720	15.920	15.152	16.313
Fe <sub>2</sub> O <sub>3</sub> *	4.042	2.882	1.498	5.084	1.173	MnO	0.401	0.087	0.163	0.200
MnO	0.027	0.020	0.040	0.080	0.087	MgO	0.349	0.122	0.159	0.073
MgO	0.000	0.300	0.000	2.710	0.000	CaO	14.287	21.512	23.323	20.875
CaO	27.817	28.040	28.394	24.840	28.042	Na <sub>2</sub> O	0.000	0.008	0.007	0.000
Na <sub>2</sub> O	0.100	0.000	0.000	0.050	0.027	La <sub>2</sub> O <sub>3</sub>	8.188	0.971	-	-
K <sub>2</sub> O	0.000	0.010	0.000	0.060	0.010	Ce <sub>2</sub> O <sub>3</sub>	7.666	0.976	-	-
Total	98.152	98.442	100.237	97.024	97.613	Pr <sub>2</sub> O <sub>3</sub>	0.357	0.157	-	-
<i>cations [normalized to 5 O]</i>						Nd <sub>2</sub> O <sub>3</sub>	0.804	0.297	-	-
Si	1.028	1.032	0.987	1.080	0.998	Sm <sub>2</sub> O <sub>3</sub>	0.000	0.000	-	-
Ti	0.840	0.739	0.982	0.641	0.923	Gd <sub>2</sub> O <sub>3</sub>	0.152	0.000	-	-
Al	0.075	0.232	0.006	0.229	0.070	Total	96.623	96.585	98.381	93.909
Cr	0.000	0.000	0.000	0.001	0.000	<i>cations [normalized to 12.5 O]</i>				
Fe <sup>+3</sup>	0.102	0.071	0.037	0.127	0.030	Si	2.952	2.991	2.970	2.999
Mn	0.001	0.001	0.001	0.002	0.002	Ti	0.021	0.007	0.027	0.032
Mg	0.000	0.015	0.000	0.134	0.000	Al	1.891	1.983	2.073	1.996
Ca	0.995	0.989	0.995	0.882	1.005	Fe <sup>+3</sup>	0.934	0.992	0.912	1.030
Na	0.006	0.000	0.000	0.003	0.002	Mn	0.031	0.006	0.011	0.014
K	0.000	0.000	0.000	0.003	0.000	Mg	0.047	0.015	0.019	0.009
Total	3.047	3.078	3.009	3.103	3.030	Ca	1.384	1.909	1.998	1.876
						Na	0.000	0.001	0.001	0.000
						La <sup>+3</sup>	0.273	0.030	-	-
						Ce <sup>+3</sup>	0.254	0.030	-	-
						Pr <sup>+3</sup>	0.012	0.005	-	-
						Nd <sup>+3</sup>	0.026	0.009	-	-
						Sm <sup>+3</sup>	0.000	0.000	-	-
						Gd <sup>+3</sup>	0.005	0.000	-	-
						Total	7.830	7.978	8.011	7.956

Minerals: Aln – allanite; Ep – epidote; Ttn – titanite.

## Appendix 8

## Selected analyses of garnets and phrenite

location/ rock	K/s	K/mn	K/mmd	K/mmd	location/ rock	K/s	K/mo	K/mmd	Z/s	Z/s
sample/ anal.	351/89	350/31	328/200	328/254	sample/ anal.	318B/281	350/29	328B/246	484/27	492A/44
mineral	Grt	Grt	Grt	Grt	mineral	Prh	Prh	Prh	Prh	Prh
position	g	i	i	g	position	i	i	g	g	g
<i>oxides [wt%]</i>					<i>oxides [wt%]</i>					
SiO <sub>2</sub>	36.000	34.431	36.170	35.779	SiO <sub>2</sub>	43.939	42.308	43.771	43.607	43.025
TiO <sub>2</sub>	0.093	2.441	0.244	1.427	TiO <sub>2</sub>	0.047	0.304	0.076	0.105	0.010
Al <sub>2</sub> O <sub>3</sub>	4.068	5.536	10.804	8.807	Al <sub>2</sub> O <sub>3</sub>	19.824	21.236	23.086	21.033	21.575
Cr <sub>2</sub> O <sub>3</sub>	0.000	0.006	0.022	0.016	Cr <sub>2</sub> O <sub>3</sub>	0.000	0.000	0.012	0.022	0.031
Fe <sub>2</sub> O <sub>3</sub> *	26.375	21.710	16.926	18.568	Fe <sub>2</sub> O <sub>3</sub> *	5.592	5.119	2.165	4.871	4.232
MnO	0.000	0.071	0.294	0.214	MnO	0.102	0.000	0.000	0.005	0.000
MgO	0.000	0.105	0.241	0.193	MgO	0.244	0.013	0.000	0.113	0.058
CaO	34.064	34.812	34.556	34.585	CaO	26.086	27.191	26.468	26.573	26.376
Total	100.600	99.112	99.257	99.589	Na <sub>2</sub> O	0.088	0.003	0.065	0.026	0.043
<i>cations [normalized to 8 cations]</i>					K <sub>2</sub> O	0.001	0.023	0.000	0.073	0.011
Si	2.963	2.850	2.909	2.899	Total	95.923	96.197	95.643	96.428	95.361
Ti	0.006	0.152	0.015	0.087	<i>cations [normalized to 22 O]</i>					
Al	0.395	0.540	1.024	0.841	Si	6.126	5.907	6.043	6.041	6.013
Cr	0.000	0.000	0.001	0.001	Al IV	1.874	2.093	1.957	1.959	1.987
Fe <sup>+3</sup>	1.633	1.352	1.024	1.132	T site	8.000	8.000	8.000	8.000	8.000
Mn	0.000	0.005	0.020	0.015	Al VI	1.381	1.399	1.796	1.473	1.564
Mg	0.000	0.013	0.029	0.023	Fe <sup>+3</sup>	0.586	0.537	0.225	0.507	0.445
Ca	3.004	3.087	2.978	3.002	O site	1.967	1.936	2.021	1.980	2.009
Total	8.000	8.000	8.000	8.000	Ti	0.005	0.032	0.008	0.011	0.001
<i>end members [mol%]</i>					Cr	0.000	0.000	0.001	0.002	0.003
Prp	0.00	0.42	0.95	0.77	Mn	0.012	0.000	0.000	0.001	0.000
Alm	0.00	0.00	0.00	0.00	Mg	0.051	0.003	0.000	0.023	0.012
Sps	0.00	0.16	0.66	0.48	Ca	3.897	4.068	3.915	3.944	3.949
Uva	0.00	0.02	0.07	0.05	Na	0.024	0.001	0.017	0.007	0.012
Adr	81.82	71.37	51.91	57.76	K	0.000	0.004	0.000	0.013	0.002
Grs	18.18	28.03	46.41	40.93	A site	3.989	4.108	3.941	4.001	3.979
					Total	13.956	14.044	13.962	13.981	13.988

Minerals: Grt – garnet; Prh – phrenite. End members: Alm – almandine; Adr – andradite; Grs – grossularite; Prp – pyrope; Sps – spessartine; Uva – uvarovite (calculated after Deer *et al.*, 1992).



## Appendix 10

## Selected analyses of oxides

location/ rock	K/s	K/mmd	I/al	S/k	S/k	S/k	Z/v	Z/s	G/rm	G/rm	G/k
sample/ anal.	318B/290	323/83	382/20	250B/228	250D/277	253/363	536B/73	484/129	365A/137	448/21	468/67
mineral	Mag	Spl	Spl	Mag	Spl	Mag	Mag	Chr	Mag	Chr	Chr
position	g	e	i	i	e	i	i	i	g	g	g
<i>oxides [wt%]</i>											
SiO <sub>2</sub>	0.231	0.026	0.044	0.070	0.880	0.080	0.240	0.077	0.096	0.083	0.060
TiO <sub>2</sub>	1.720	0.349	1.927	3.080	0.100	2.000	1.236	0.907	14.251	1.493	0.417
Al <sub>2</sub> O <sub>3</sub>	0.744	59.237	32.113	0.530	54.930	1.430	2.127	18.154	6.235	3.460	12.805
Cr <sub>2</sub> O <sub>3</sub>	0.224	0.037	22.072	0.860	0.280	21.640	0.012	40.960	0.446	64.651	54.239
Fe <sub>2</sub> O <sub>3</sub>	63.348	0.956	9.682	61.143	7.170	41.456	62.853	8.445	37.555	0.922	5.126
FeO	32.624	35.814	20.110	32.463	26.508	31.047	31.982	18.806	33.509	15.740	13.773
MnO	0.000	0.329	0.217	0.490	0.370	1.060	0.327	0.187	0.679	0.280	0.205
MgO	0.002	3.748	11.478	0.210	9.430	0.410	0.061	10.164	7.323	11.305	13.346
CaO	0.116	0.039	0.155	0.300	0.230	0.250	0.123	0.511	0.085	0.095	0.071
NiO	-	-	-	0.150	0.100	0.130	-	-	-	-	-
ZnO	-	-	-	0.150	0.300	0.430	-	-	-	-	-
TOTAL	99.009	100.535	97.798	99.446	100.298	99.933	98.960	98.211	100.179	98.029	100.042
<i>cations [normalized to 4 O and 3 cations]</i>											
Si	0.009	0.001	0.001	0.003	0.024	0.003	0.009	0.002	0.003	0.003	0.002
Ti	0.050	0.007	0.044	0.089	0.002	0.057	0.036	0.022	0.372	0.039	0.010
Al	0.034	1.963	1.154	0.024	1.792	0.063	0.096	0.694	0.255	0.140	0.482
Cr	0.007	0.001	0.532	0.026	0.006	0.644	0.000	1.051	0.012	1.754	1.371
Fe <sup>+3</sup>	1.842	0.020	0.222	1.767	0.149	1.174	1.814	0.206	0.981	0.024	0.123
Fe <sup>+2</sup>	1.054	0.842	0.513	1.042	0.614	0.977	1.026	0.510	0.973	0.452	0.368
Mn	0.000	0.008	0.006	0.016	0.009	0.034	0.011	0.005	0.020	0.008	0.006
Mg	0.000	0.157	0.522	0.012	0.389	0.023	0.003	0.492	0.379	0.578	0.636
Ca	0.005	0.001	0.005	0.012	0.007	0.010	0.005	0.018	0.003	0.003	0.002
Ni	-	-	-	0.005	0.002	0.004	0.000	-	-	-	-
Zn	-	-	-	0.004	0.006	0.012	0.000	-	-	-	-
Total	3.000	3.000	3.000	3.000	3.000	3.000	3.000	3.000	3.000	3.000	3.000

Minerals: Mag – magnetite series; Spl – spinel series; Chr – chromite series; Ilm – ilmenite; Hem – haematite; Tiox – Ti oxide.

## Appendix 10 – continued

location/ rock	K/rm	K/s	K/mn	K/mmd	K/mmd	S/k	S/k	G/rm	I/m	I/am	G/rm
sample/ anal.	327/52	313/16	350/35	328B/274	328B/227	250D/328	250D/353	458/139	507A/5	301A/44	448/26
mineral	Ilm	Hem	Ilm	Ilm	Ilm	Ilm	Ilm	Ilm	Tiox	Tiox	Tiox
position	i	i	g	i	i	g	g	g	i	g	i
<i>oxides [wt%]</i>											
SiO <sub>2</sub>	0.060	1.250	0.021	0.000	0.039	0.940	0.060	0.026	0.603	0.300	0.058
TiO <sub>2</sub>	44.950	0.000	45.258	46.893	50.397	40.560	39.550	51.526	98.199	98.380	97.604
Al <sub>2</sub> O <sub>3</sub>	0.000	0.040	0.180	0.000	0.000	0.120	0.070	0.019	0.283	0.090	0.059
Cr <sub>2</sub> O <sub>3</sub>	0.000	0.020	0.099	0.151	0.000	0.160	0.060	0.044	0.405	0.050	0.034
Fe <sub>2</sub> O <sub>3</sub>	14.293	86.448	13.769	11.420	4.771	18.359	23.289	1.488	0.914	0.844	0.118
FeO	38.884	1.129	38.715	38.619	40.394	16.991	25.899	41.987	0.000	0.000	0.000
MnO	1.340	0.000	1.725	3.471	4.648	18.860	9.010	4.106	0.005	0.020	0.023
MgO	0.040	0.090	0.146	0.018	0.032	0.010	0.300	0.108	0.411	0.040	0.002
CaO	0.140	0.160	0.000	0.000	0.161	1.160	0.060	0.020	0.115	0.100	0.039
Total*	99.706	89.137	99.913	100.573	100.442	97.159	98.298	99.324	100.935	99.824	97.937
<i>cations [Ilm-Hem: normalized to 3 O and 2 cations; Tiox: normalized to 1 cation, Fe=Fe<sup>3+</sup>]</i>											
Si	0.002	0.037	0.001	0.000	0.001	0.024	0.002	0.001	0.008	0.004	0.001
Ti	0.861	0.000	0.864	0.890	0.954	0.792	0.770	0.984	0.965	0.983	0.996
Al	0.000	0.001	0.005	0.000	0.000	0.004	0.002	0.001	0.004	0.001	0.001
Cr	0.000	0.000	0.002	0.003	0.000	0.003	0.001	0.001	0.004	0.001	0.000
Fe <sub>+3</sub>	0.274	1.924	0.263	0.217	0.090	0.359	0.454	0.028	0.009	0.008	0.001
Fe <sub>+2</sub>	0.829	0.028	0.822	0.815	0.850	0.369	0.561	0.892	0.000	0.000	0.000
Mn	0.029	0.000	0.037	0.074	0.099	0.415	0.198	0.088	0.000	0.000	0.000
Mg	0.002	0.004	0.006	0.001	0.001	0.000	0.012	0.004	0.008	0.001	0.000
Ca	0.004	0.005	0.000	0.000	0.004	0.032	0.002	0.001	0.002	0.001	0.001

## Appendix 11

## Selected analyses of carbonates

location/rock	I/m	K/s	G/k	I/al	G/m	G/k
sample/anal.	507A/1	318B/2	468/70	382/5	448/8	468/69
mineral	Cal	Cal	Cal	Ank	Ank	Mgs
position	i	i	ps	i	ps	ps
<i>oxides [wt%]</i>						
CaO	58.332	60.001	57.498	31.360	33.445	1.451
MgO	0.027	0.284	1.325	15.312	17.893	40.757
FeO*	0.374	0.539	1.620	6.792	9.313	9.573
MnO	0.460	0.476	0.817	0.077	0.363	0.037
Total	59.193	61.300	61.260	53.541	61.014	51.818
<i>cations [normalized to 2 cations]</i>						
Ca	1.977	1.961	1.877	1.081	1.015	0.044
Mg	0.001	0.013	0.060	0.734	0.756	1.727
Fe+2	0.010	0.014	0.041	0.183	0.221	0.228
Mn	0.012	0.012	0.021	0.002	0.009	0.001
Total	2.000	2.000	2.000	2.000	2.000	2.000

Minerals: Cal – calcite; Ank – ankerite; Mgs – magnesite.

## Appendix 12

## Selected chemical analyses of rocks

Sample	327	387	420	443	394	351	350	328	508	382	301A
Location	K	K	K	K	K	K	K	K	I	I	I
Rock	rm	m	sm	v	s	s	mn	mmd	m	al	am
<i>major elements [wt %]</i>											
SiO <sub>2</sub>	53.62	54.61	54.72	50.76	53.66	58.96	52.37	52.62	45.22	43.53	59.53
TiO <sub>2</sub>	4.31	1.75	2.63	1.62	1.35	1.08	1.60	1.39	2.07	1.82	0.61
Al <sub>2</sub> O <sub>3</sub>	11.19	14.27	13.81	15.70	16.07	16.88	16.10	15.80	14.02	14.72	14.73
Fe <sub>2</sub> O <sub>3</sub>	8.90	5.84	7.22	7.72	7.37	5.86	8.52	9.56	8.09	10.09	4.36
MnO	0.08	0.08	0.17	0.12	0.12	0.08	0.12	0.13	0.15	0.12	0.06
MgO	5.70	5.08	4.11	6.15	5.76	2.88	4.78	4.52	5.04	5.42	4.75
CaO	4.87	4.84	4.57	6.02	5.26	4.44	6.11	6.72	8.47	7.07	3.15
Na <sub>2</sub> O	2.63	2.87	1.41	3.89	3.84	3.83	3.58	3.23	3.80	2.04	3.70
K <sub>2</sub> O	5.32	4.89	7.01	3.55	3.16	3.08	2.24	2.53	3.55	2.52	2.85
P <sub>2</sub> O <sub>5</sub>	1.32	0.80	1.45	0.86	0.55	0.41	0.59	0.36	1.78	0.56	0.14
LOI	1.50	4.50	2.80	3.80	2.60	2.30	3.70	3.00	7.30	11.90	6.20
Total	99.44	99.53	99.90	100.19	99.74	99.80	99.71	99.86	99.49	99.79	100.08
Mg#	56	63	53	61	61	49	53	48	55	52	68
<i>trace elements [ppm]</i>											
Cr	150.5	157.3	116.3	150.5	171.0	27.4	75.2	34.2	142.6	171.0	225
Ni	154.1	129.8	64.5	103.7	82.6	26.8	53.0	21.8	94.3	122.2	183.5
V	166	117	230	143	155	105	161	179	166	187	77
Sc	10	10	14	16	16	12	18	21	16	20	11.4
Ba	1873.0	1600.5	2419.4	1028.8	1100.7	1071.4	701.5	681.3	2274.3	658.4	607.5
Rb	210.1	206.6	237.1	122.4	117.2	117.1	92.9	127.3	89.2	98.1	74.2
Sr	502.9	529.9	895.3	770.8	581.5	616.1	444.3	428.6	1597.7	492.6	81.7
Cs	4.6	5.7	3.1	2.6	3.4	3.2	3.8	3.9	17.7	13.1	1.4
Th	11.9	13.8	24.4	10.3	16.5	10.3	6.8	7.6	13.3	5.9	9.2
U	3.0	3.6	5.1	2.6	2.6	2.1	1.5	2.3	3.5	1.2	2.4
Pb	9.5	34.8	5.7	18.1	19.3	6.0	7.9	6.9	10.1	2.6	0.0
Zr	504.8	389.6	890.6	336.9	297.9	184.4	207.6	189.8	348.8	210.9	139.4
Hf	14.1	11.0	23.8	7.7	8.1	5.1	5.6	5.2	8.0	5.4	3.7
Nb	149.5	71.8	33.0	51.2	25.8	16.2	20.6	17.3	112.1	42.3	8.2
Ta	9.0	4.1	2.0	2.8	1.4	1.0	1.3	1.0	4.9	2.5	0.5
Y	16.6	19.2	43.9	23.9	30.6	20.8	30.1	31.1	21.7	24.5	12.7
La	70.9	53.2	235.1	81.8	79.2	42.6	42.9	35.6	96.1	44.6	20.0
Ce	171.7	112.4	482.8	160.6	152.2	82.0	91.1	75.2	213.9	95.7	38.9
Pr	18.99	12.86	50.49	16.36	16.44	8.91	10.36	8.26	21.46	11.03	4.53
Nd	71.2	49.8	176.7	56.3	59.6	35.9	40.7	33.0	81.4	43.6	17.3
Sm	10.5	8.1	26.8	8.9	9.8	6.0	8.1	6.3	10.6	7.6	3.4
Eu	2.68	2.13	6.05	2.50	2.44	1.87	2.18	1.83	2.84	2.27	0.86
Gd	5.53	4.66	13.21	4.91	6.41	4.38	6.38	5.64	6.64	5.45	2.82
Tb	0.80	0.71	1.97	0.94	0.97	0.67	0.97	0.93	0.94	0.83	0.45
Dy	3.37	3.44	7.88	4.01	5.18	3.71	5.31	5.30	4.33	4.41	2.37
Ho	0.50	0.59	1.23	0.68	0.93	0.69	1.03	1.02	0.65	0.86	0.46
Er	1.24	1.52	3.40	2.18	2.47	1.76	2.59	2.66	1.82	2.14	1.36
Tm	0.18	0.21	0.58	0.34	0.34	0.26	0.37	0.38	0.28	0.32	0.20
Yb	1.14	1.46	3.02	2.06	2.18	1.59	2.29	2.35	1.71	1.92	1.22
Lu	0.16	0.21	0.43	0.29	0.33	0.24	0.34	0.34	0.25	0.29	0.20

## Appendix 12 – continued

Sample	250	305	426	630	465M	448	470	468	463	497	492A	488
Location	S	S	S	S	G	G	G	G	G	Z	Z	Z
Rock	k	k	k	s	rm	rm	m	k	s	v	s	mmd
major elements [wt %]												
SiO <sub>2</sub>	59.67	58.55	56.93	58.87	56.72	56.38	63.90	44.80	53.69	56.20	58.78	60.21
TiO <sub>2</sub>	0.73	0.75	0.86	0.76	1.42	1.40	0.86	0.91	0.69	0.74	0.53	0.90
Al <sub>2</sub> O <sub>3</sub>	15.80	15.33	15.65	16.08	10.71	10.03	13.20	12.07	15.42	15.09	16.77	16.14
Fe <sub>2</sub> O <sub>3</sub>	5.40	5.54	6.56	5.21	5.23	4.31	4.81	7.59	6.51	5.35	5.04	5.07
MnO	0.11	0.09	0.11	0.09	0.07	0.06	0.10	0.13	0.07	0.07	0.08	0.07
MgO	5.38	4.86	2.74	4.52	8.29	6.75	3.23	8.19	5.98	5.11	4.08	3.57
CaO	2.70	3.30	4.73	3.35	4.67	4.55	1.38	8.26	4.07	4.89	3.32	3.90
Na <sub>2</sub> O	3.59	4.58	3.12	6.15	1.57	0.58	0.46	2.15	3.42	3.78	4.72	3.56
K <sub>2</sub> O	3.57	2.94	3.80	1.70	7.25	7.87	8.26	3.00	2.40	4.56	3.75	3.72
P <sub>2</sub> O <sub>5</sub>	0.24	0.26	0.41	0.27	1.94	1.55	0.75	0.60	0.28	0.34	0.18	0.41
LOI	3.10	3.30	5.30	2.90	2.00	6.50	2.70	12.20	7.60	3.80	2.90	2.40
Total	100.29	99.50	100.21	99.90	99.87	99.98	99.65	99.90	100.13	99.93	100.15	99.95
Mg#	66	63	45	63	76	76	57	68	65	65	62	58
trace elements [ppm]												
Cr	154	151	13.7	162.0	437.8	499.3	253.1	581.4	287.3	171.0	171.0	123.1
Ni	110.4	106.4	2.2	83.1	103.6	122.0	143.2	168.1	149.2	86.5	58.4	33.6
V	104	116	168	122	96	71	75	173	118	126	75	96
Sc	12.4	13.1	18	14	16	13	17	22	15	14	12	13
Ba	1100.0	1260.0	1615.3	518.9	2338.8	1545.6	3549.1	1396.7	1166.9	1996.7	747.9	1550.8
Rb	100.9	95.1	113.8	28.4	634.0	511.6	314.0	144.3	81.8	163.7	201.7	143.4
Sr	630.6	723.2	643.3	169.7	572.2	404.8	406.5	587.8	432.2	796.5	297.9	878.8
Cs	2.9	1.0	3.1	0.2	17.1	14.6	10.3	9.1	2.1	2.8	2.4	3.7
Th	11.1	12.4	17.4	16.2	95.2	119.7	189.1	8.2	14.5	26.1	8.3	22.0
U	3.0	2.5	4.1	3.8	23.3	31.6	33.2	2.8	3.6	5.5	3.2	9.3
Pb	24.7	23.9	9.0	24.5	65.8	61.8	75.5	4.4	1.5	39.9	21.5	29.9
Zr	156.9	164.2	192.5	168.4	555.7	727.5	1301.4	138.5	139.4	173.0	113.6	248.6
Hf	4.1	4.5	6.1	4.4	17.1	22.9	36.9	3.8	4.0	5.2	3.8	8.1
Nb	7.0	11.6	12.3	8.8	50.5	43.8	91.5	15.4	7.7	8.7	5.0	14.9
Ta	0.5	0.6	0.9	0.6	2.6	3.2	6.3	1.1	0.6	0.6	0.5	1.9
Y	14.9	16.1	40.6	20.4	39.1	29.7	41.2	17.2	19.6	18.9	12.8	31.3
La	31.6	34.5	60.3	34.9	90.8	67.5	151.3	44.7	51.2	66.6	21.7	50.9
Ce	60.6	65.9	122.2	76.1	242.5	182.1	330.4	89.7	82.6	138.1	40.3	106.0
Pr	7.10	7.77	13.96	8.87	33.44	25.44	34.21	9.95	10.08	14.45	4.47	11.88
Nd	27.2	29.1	52.3	35.1	152.0	117.2	120.4	34.4	34.8	52.9	17.2	44.7
Sm	5.0	5.3	10.7	6.3	35.2	25.2	19.4	5.5	5.8	8.5	3.3	8.3
Eu	1.40	1.49	2.23	1.64	4.49	3.82	3.30	1.46	1.44	2.05	0.98	1.78
Gd	3.74	4.01	7.97	4.10	18.01	13.03	9.94	3.96	3.82	4.72	2.41	6.22
Tb	0.57	0.59	1.44	0.72	1.87	1.40	1.56	0.58	0.60	0.72	0.38	0.95
Dy	2.88	2.93	6.67	3.75	7.81	5.80	6.24	3.44	2.88	3.59	2.13	5.44
Ho	0.53	0.57	1.30	0.63	1.09	0.80	1.12	0.58	0.60	0.61	0.37	0.97
Er	1.59	1.69	3.39	2.01	2.87	2.10	2.98	1.55	1.76	1.74	1.12	2.91
Tm	0.22	0.24	0.56	0.30	0.35	0.32	0.46	0.22	0.22	0.25	0.19	0.44
Yb	1.38	1.51	3.56	1.81	2.24	2.00	2.72	1.56	1.75	1.61	0.94	2.53
Lu	0.22	0.24	0.55	0.27	0.36	0.25	0.37	0.34	0.21	0.23	0.15	0.39

Samples 250, 305 and 436 were analyzed at Actlabs, all other samples at ACME (see section on analytical methods). Details on sampling sites are given in Appendix 1. LOI – loss on ignition. Mg# (magnesium number) =  $100 \times (\text{MgO}/(\text{MgO} + \text{FeO}))$ , molecular ratio with total Fe as FeO.